Energy, Mines and Resources Canada | Energie, Mines et Ressources Canada

CANMET

Canada Centre for Mineral and Energy Technology | Centre canadien de la technologie des minéraux et de l'énergie

GEOTECHNICAL STUDIES AT WHITESHELL RESEARCH AREA (RA-3)

Edited by

T.J. Katsube and J.P. Hume

March 1987

MINING RESEARCH LABORATORIES
DIVISIONAL REPORT MRL 87-52 (INT) (TR)

ADDRESSES AND AFFILIATIONS OF AUTHORS AND EDITORS

A. Annor
R. Jackson (AECL Secondment)
Energy, Mines and Resources Canada
Canada Centre for Mineral and Energy Technology (CANMET)
555 Booth Street
OTTAWA, Ontario
K1A 0G1

P.J. Chernis (AECL Secondment)
M.J. Drury
P.B. Robertson
Energy, Mines and Resources Canada
Geological Survey of Canada
1 Observatory Crescent
OTTAWA, Ontario
K1A 0Y3

K.L. Harding (AECL Secondment)
P. Lapointe
A.G. Latham
Energy, Mines and Resources Canada
Geological Survey of Canada
Geomagnetic Laboratory
601 Booth Street
OTTAWA, Ontario
K1A 0E8

J.P. Hume (AECL Secondment)
T.J. Katsube
J.B. Percival (AECL Secondment)
Energy, Mines and Resources Canada
Geological Survey of Canada
601 Booth Street
OTTAWA, Ontario
K1A 0E8

W.A. Morris
Morris Magnetics
RR#2
LUCAN, Ontario
MON 2J0

NUCLEAR FUEL WASTE MANAGEMENT PROGRAM

CONCEPT ASSESSMENT DOCUMENT

GEOTECHNICAL STUDIES AT WHITESHELL RESEARCH AREA (RA-3)

ROCK PROPERTIES

March 2, 1987

Edited by: T.J. Katsube and J.P. Hume

TABLE OF CONTENTS

CHAPTER I

INTRODUCTION

INTRODUCTION

The nuclear fuel waste disposal concept chosen for development and assessment in Canada involves the isolation of containers of waste in a vault located at a depth of about 1000 m in plutonic rock (Wuschke et al., 1985). Adequate development of this concept requires the development of the capability to assess what impact the disposal system would have on man and the environment if the concept were implemented. This involves the development of the capability to reliably predict the disposal vault performance, and the rate of radionuclide migration through the host rock with the assumption that radionuclide release from the vault was possible. This implies the capability of predicting the radionuclide isolation capacity of the host rock, the vault stability and its effect on the isolation capacity, and the effect that the heat generated by the waste has on vault stability and isolation capacity. In order to develop these capabilities, a rock property program was established to carry out a generic study of the physical properties of plutonic rocks. As part of this generic study, various rock properties have been measured for core samples from two sites (WN site and URL site) within the Whiteshell Nuclear Research Establishment (WNRE) research area. This research area is located within the boundaries of the Lac du Bonnet batholith which lies approximately 100 km northeast of Winnipeg, Manitoba. The common phase of this batholith is pink, porphyritic granite-granodiorite (McCrank, 1985).

The WNRE rock property study consists of three components: geology, physical properties, and geophysics. The geological component includes petrographical studies, micromorphology studies (using the scanning electron microscope), and geochemical studies. The purpose of these studies is to provide an information base to support the generic physical property studies. The physical property component includes the study of mechanical properties, petrophysics, and thermal properties, for the purpose of providing information for predicting vault stability, the radionuclide isolation capacity and the effect of temperature on the host rock. The geophysical component, which includes the study of magnetic and electrical properties (including interpretation of geophysical logs), provides assistance for determining the distribution of physical properties within the pluton, and for strengthening the effectiveness of geophysics as a method for indirectly determining the physical properties of the pluton.

These studies have been carried out mainly under the auspices of the Department of Energy, Mines and Resources (EMR) component of the Canadian Nuclear Fuel Waste Management Program (CNFWMP). This document summarizes rock property studies related to the WNRE research area that have been carried out over the last 9 years. This document focuses on the relevant physical property ranges, the physical property distribution within the pluton, and the general physical, geophysical and certain geological (mineralogy and micromorphology) characteristics of the rocks from the Lac du Bonnet batholith. Various sample collecting methods have been used by different investigators involved in this rock property study. However, there is a standard set of 70 core samples (Soonawala, et al., 1982) from which specimens were made available to all investigators involved in the rock property program. This has allowed cross correlation studies of most of the rock properties.

REFERENCES

McCrank, G.F.D. 1985. A geological survey of the Lac du Bonnet batholith, Manitoba. Atomic Energy of Canada Limited, Report AECL-7816, p. 63.

Soonawala, N.M., Brown, P.A., and Larocque, G.E. 1982. Geology, Geophysics and Rock Properties Research for the Canadian Nuclear Fuel Waste Management Program. Atomic Energy of Canada Limited Technical Record TR-152, p. 162.

Wuschke, D.M., Gillespie, P.A., and Main, D.E. 1985. Second interim assessment of the Canadian concept for nuclear fuel waste disposal. Volume I: Summary. Atomic Energy of Canada Limited Report AECL-8373-1, p. 45.

CHAPTER II

GEOLOGY AND PETROGRAPHY

1. GENERAL GEOLOGY AND PETROGRAPHY

GENERAL GEOLOGY OF THE LAC DU BONNET BATHOLITH AND PETROGRAPHY OF CORE SAMPLES FROM THE WNRE RESEARCH AREA

P.B. Robertson* and P.J. Chernis**
Geological Survey of Canada
1 Observatory Cr.
Ottawa, Ontario K1A 0Y3

*: Department of Energy, Mines, and Resources, Geological Survey of Canada (GSC), Ottawa K1A 0E8
**: Atomic Energy of Canada Ltd., attached to GSC, Ottawa.

GENERAL GEOLOGY OF THE LAC DU BONNET BATHOLITH AND PETROGRAPHY OF CORE SAMPLES FROM THE WNRE RESEARCH AREA

P.B. Robertson and P.J. Chernis
Geological Survey of Canada (GSC), Ottawa K1A 0E8

INTRODUCTION

This paper provides a brief summary of the geology and petrography of the Lac du Bonnet batholith, from available literature, but largely based on work performed by others in the Canadian nuclear fuel waste management program. It is intended to serve as background for interpretations of rock properties in chapters which follow. More detailed descriptions can be found in the references cited below, particularly in the AECL Geological Research Summary Volume (Brown et al., in prep.).

GENERAL GEOLOGY OF THE LAC DU BONNET BATHOLITH

The Lac du Bonnet Batholith lies entirely within Manitoba, approximately 100 km northeast of Winnipeg (Figure 1). The east-northeasterly elongated body is roughly 75 by 25 km in surface extent. Its northern boundary lies just north of Lac

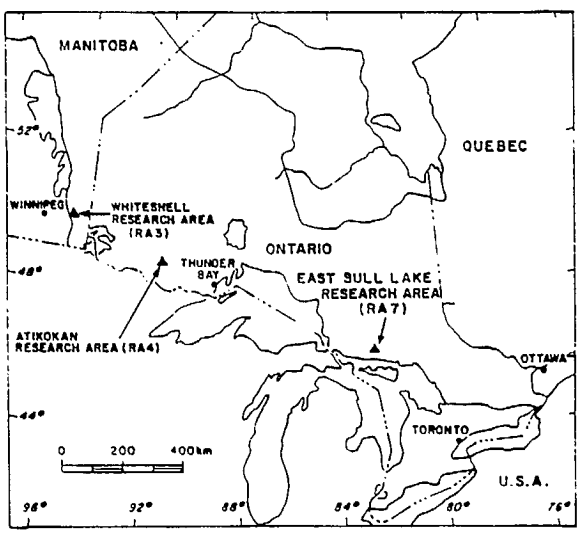

Figure 1. Location of Whiteshell and other AECL Research Areas.

du Bonnet, and the town of Pinawa is located near its southern boundary. The pluton forms part of the Archean age Winnipeg River batholithic belt of the English River Subprovince (Figure 2), a belt comprised of a suite of massive intrusives of granite to granodiorite composition. The batholith has a Rb-Sr whole rock age of 2680 +/- 91 Ma (Farquharson, 1975) and it is considered to postdate the last major orogenic activity in the area (McRitchie, 1971). The northern margin of the pluton east of Lac du Bonnet is a possible fault contact with the metasedimentary and metavolcanic rocks of the Bird River Greenstone Belt, part of the Ear Falls-Manigotagan Gneiss Belt (Beakhouse, 1977; Cherny et al. 1981). The northwestern and southern contacts are gradational, with marginal phases of the batholith interleaved with the tonalitic to granodioritic Early Gneiss Suite up to a kilometre beyond the contact. The northern boundary dips 50-55° north, while the southern boundary is considered to dip steeply southeast (McCrank, 1985). Ordovician sediments – sandstones of the Winnipeg Formation and limestone and dolostone of the Red River Formation – unconformably overlie the batholith in the west. Lacustrine clay, silty clay, sand, gravel and till of the Wisconsin glaciation limit exposure of bedrock in the region (Chagarlamundi, 1971).

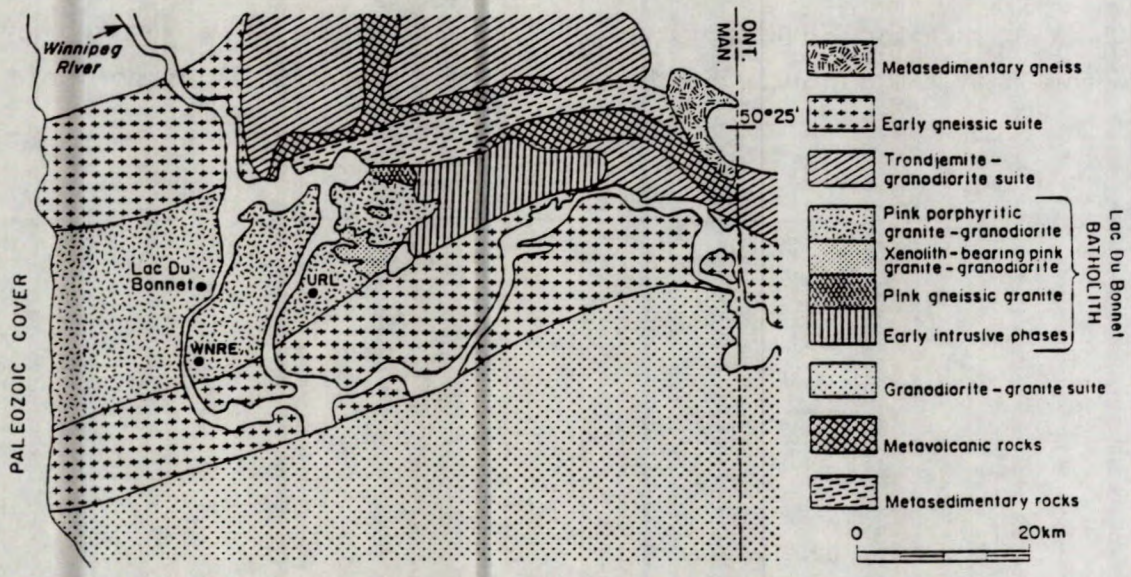

Figure 2. Generalized geology of the Lac du Bonnet Batholith.

The pluton is a relatively undifferentiated body, with the following variations attributed to contamination by assimilation of country rocks, or to stress during intrusion (McCrank, 1985):

(1) Predominantly pink, massive, porphyritic granite to granodiorite subdivided into biotite-rich (>5% biotite) and biotite-poor phases;
(2) Pink hornblende granite to granodiorite;
(3) Grey porphyritic granite to granodiorite, mineralogically and texturally similar to unit 1, but containing fewer fractures;
(4) Xenolith-bearing, pink granite to granodiorite: xenoliths are grey tonalite and amphibolite;
(5) Pink, fine- and coarse-grained granite;
(6) Pink, gneissic granite gradational to unit 1;
(7) Light brown, porphyritic hornblende-biotite granite;
(8) Pink, foliated biotite granite.

Granites and granodiorites of unit 1 make up the bulk of the batholith, with other lithologies occurring as marginal phases or segregations within the body. Unit 4 is thought to represent the roof zone of the batholith as well as heterogeneous, zenolithic layers representing multiple intrusion pulses (Brown et al., 1985, 1987). Units 7 and 8 are restricted to the eastern margin and are believed to be related to older plutons, due to their greater structural complexity. Unit 6, considered to be a synkinematic phase, similarly occurs only near the margins where it is gradational with the massive porphyritic granite of unit 1.

The Whiteshell Nuclear Research Establishment (WNRE) and the Underground Research Laboratory (URL) sites lie within the predominantly granite-granodiorite batholith, approximately 3 km from the southern boundary of the batholith. Units 3 and 4 are present at both locations. Units 2 and 5 are mapped only at the URL site, but are not of sufficient extent to appear on Figure 2. In addition, in the subsurface at the URL, a green-grey phase of the grey granite (unit 3) has been recognized, and occurs between the grey and pink granites (Brown et al. 1985). It is of variable thickness – from 10 to 130 m and possibly as thick as 400 m – and grades into the grey granite.

The pink, massive, medium- to coarse-grained porphyritic granite is relatively uniform in texture and composition over the batholith although locally it displays gneissic banding of grain size variations. The rock is characterized by

plagioclase and microcline feldspar phenocrysts up to 20 mm long in a finer-grained quartz matrix. The biotite-rich variety is enriched also in plagioclase with a reduced microcline content. The grey granite of unit 3 differs from that of unit 1 primarily in its scarcity of fractures and lower degree of alteration. Unit 1 is encountered in the upper few hundred metres of boreholes in the pluton, although discrete zones of red and pink alteration are associated with fracture and fault zones within the grey granite of unit 3, which occurs below unit 1. At the URL site, pink granite occurs predominantly over 260 m (vertical) depth. Xenoliths of tonalite and amphibolite in the pink porphyritic granite typify unit 4, and occur locally in patches several hundred metres in extent. The xenoliths, up to 10 m across, are commonly mantled by biotite selvages and in some cases are stretched in an east-west direction. Internal fabric within unit 1 is primarily east-west and defined by orientation of feldspar, quartz, and biotite grains, and schlieren (McCrank, 1985). Pegmatite and aplite dikes with northeasterly trend form an extensive linear system throughout the batholith, but are most common in unit 4. Unit 4 is restricted to the upper 150 m of boreholes, although other small xenolith-bearing zones occur below that depth.

Fractures of various orientations cut the pluton. The majority strike 30° or 120°, and are sub-vertical (dip greater than 60°), or dip less than 30°. A less prominent sub-vertical set strikes between 150° and 180°. The mean length in outcrop of the sub-vertical fractures is 14 m, and mean spacing varies between 5 and 22 m, whereas the mean length and spacing of the shallow dipping fractures is 18 m and 2 m, respectively (Brown, 1981). At the URL site fracture sets intersected by boreholes have a preference for shallow dips (<25°) (e.g., Lau et al. 1982). Boreholes at the URL intersect 3 major hydrogeologic units (Davison, 1985; Brown et al. 1985). Mean orientation of the shallowest fracture zone (zone 3) is 061/13. It is intersected by borehole URL-6 at approximately 180 m AMSL (above mean sea level). The attitude of the intermediate fracture zone (zone 2) is 035/24, and intersects URL-6 at approximately 0 m AMSL (Brown et al. 1986 – level II geology report). The orientation of the deepest fracture zone has not been reliably determined at all locations. In the north of the URL (25 m depth in hole M13) it's attitude is 060/16, but the strike in the south may be somewhat more northerly (025°, Brown, 1986). There is little evidence of faulting within the batholith, and

all mesoscopic fractures have displacements of less than 10 cm. Fractures that formed during or late in the emplacement of the pluton are filled with quartz, pegmatite, aplite, or hornblende-porphyry. Post-emplacement fractures are filled by epidote, chlorite, calcite, and clay. The Lac du Bonnet Batholith is less fractured than the Eye-Dashwa Lakes Pluton, and the relatively simple fracture-filling mineralogy supports a less complex fracture-filling history.

PETROGRAPHY OF CORE SAMPLES FROM WNRE AND URL

Core samples from the WNRE and URL sites are predominantly pink to grey, coarse-grained, massive, granite to granodiorite of units 1 and 3. The continuously variable size of constituent grains, from microscopic upwards to 20 mm, indicates that inequigranular is a more appropriate textural term than porphyritic. All varieties are comprised of plagioclase (oligoclase), microcline, quartz, biotite, and muscovite, in hypidiomorphic granular texture. Sphene, apatite, calcite, epidote, iron oxides, and allanite are present in accessory amounts. The average composition (with standard deviations) of all WN and URL samples (N=432) that have been examined by Chernis and Robertson (in press) (Figure 3) is: quartz 29.3% +/- 6.1%, plagioclase 36.8% +/- 7.1%, microcline 27.6% +/- 10.4%, and 6.3% accessories. The average composition of 174 samples of medium- to coarse-grained pink and grey granite from borehole URL-2, the longest borehole at the URL site (1200 m) (Chernis, 1985), is similar:

quartz 30.6% +/- 3.9%, plagioclase 37.5% +/- 5.7%,
microcline 27.3% +/- 6.8%, muscovite 0.5% +/- 0.3%,
biotite (includes chlorite) 3.5% +/- 1.5%, opaques 0.4% +/- 0.3%,
and other accessories 0.2% +/- 0.2%.

Most of these URL-2 samples (77%) are classified as monzogranite, and 15% are granodiorite (Figure 3). The larger standard deviations of the entire WN and URL data set reflect the greater diversity of compositions encountered in unit 4. There is no systematic variation of modal composition with depth at a 5 m sampling scale, and the average compositions of pink and grey samples are similar. The pink phases derive their colour from submicroscopic iron-oxide coatings and fillings, deposited from hydrothermal fluids in cleavages and other microcracks in the feldspars, and along grain boundaries. Grey phases lack these iron-oxide

coatings, but are otherwise chemically and mineralogically similar to the pink varieties (see Kamineni et al. 1984). The colour of the green-grey phase derives from the presence of chlorite-filled microfractures and epidotization of plagioclase and biotite, and is thought to be a result of deuteric alteration in proximity to the lower part of the roof zone of the batholith (Brown et al., 1985).

In thin sections, plagioclase (oligoclase) is equant to slightly prismatic, subhedral, usually less than 3.5 mm x 4.5 mm, and exhibits normal zoning. Calcic zones in plagioclase have been deuterically altered to sericite, calcite, epidote, and albite. Microcline is fresh (unaltered) prismatic subhedral, on average less than 5.5 mm x 11 mm but commonly up to 10 mm x 20 mm. It exhibits euhedral plagioclase inclusions, string perthite and Carlsbad and "tartan" twinning.

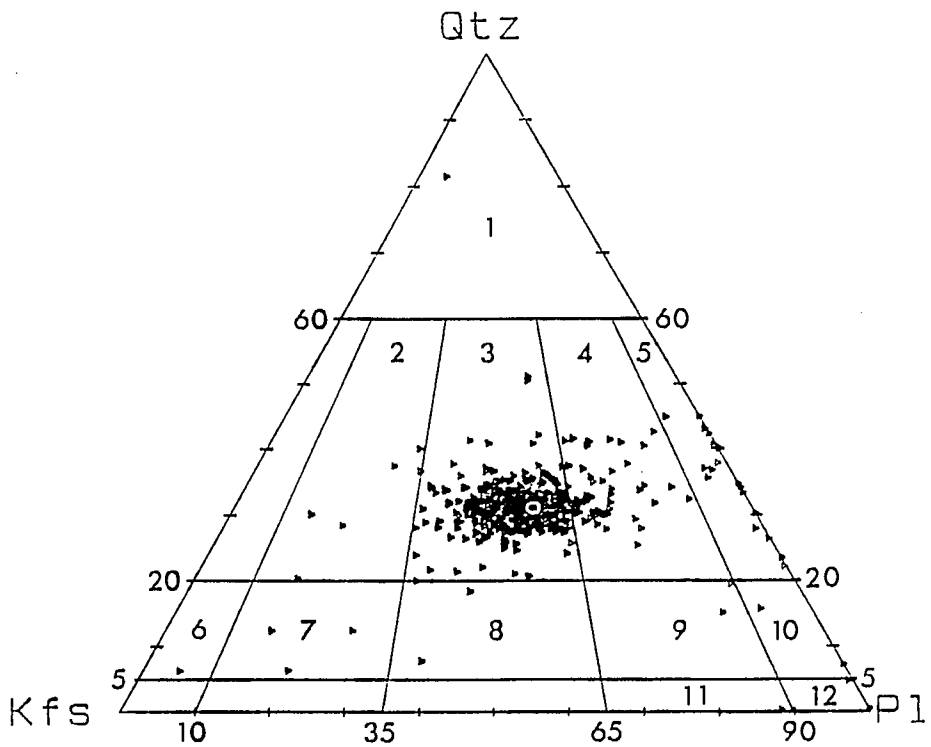

Figure 3. Modal composition of 432 core samples from WN and URL boreholes. The average mode (Qtz + Pl + Kfs normalized to 100%) is: quartz 31.2% +/- 6%, plagioclase 39.8% +/- 10.5%, microcline 29.0% +/- 10.7%.

Myrmekitic intergrowths of quartz in albite occur between oligoclase and microcline grains, and oligoclase or albite rims are common. Quartz occurs as a medium-grained groundmass between feldspar grains, and typically displays undulatory extinction and sutured grain boundaries. Dark brown biotite and colourless muscovite occur as inclusions in the feldspars, but more commonly as sheafs between quartz and feldspar where the muscovite partially rims biotite. Biotite is frequently altered to chlorite.

Two examples of xenolithic material typical of unit 4 were collected as standard samples from borehole WN-2. They are tonalites in composition, and display relict hypidiomorphic-granular texture.

SUMMARY

The Lac du Bonnet Batholith is a post orogenic body comprising 8 units mapped at the surface that are largely of granite composition, and a green-grey alteration phase of the grey granite, encountered only in boreholes. Subordinate granodiorite is also present. Pink granites and granodiorites of unit 1 represent the roof zone and heterogeneous, layered, multiple intrusion pulses, and make up the bulk of the batholith exposed at the surface. At the WNRE and URL sites, the major rock units are, in addition to unit 1, grey granite-to-granodiorite (Unit 3), and xenolith-bearing pink granite-to-granodiorite (Unit 4). The grey granite is mineralogically and texturally identical to pink granite of unit 1, but has fewer fractures and a lower degree of alteration. A green-grey phase of the grey granite (Unit 3) occurs between the grey and pink (Unit 1) granites. The majority of fractures which cut the pluton strike 30° or 120°, and are sub-vertical, or dip less than 30°. Three major subhorizontal hydrogeologic units (fracture zones) occur in boreholes at the URL site. A less prominent sub-vertical fracture set strikes 150°-180°. The Lac du Bonnet batholith is less fractured than the Eye-Dashwa Lakes Pluton, and has a relatively more simple assemblage of fracture-filling minerals.

The average composition of the pluton at the URL site is monzogranite, determined from modal analyses of 432 core samples. There are no systematic mineralogical variations with depth on a 5 m sampling scale and the average compositions of pink and grey samples are similar.

REFERENCES

Beakhouse, G.P. 1977. A subdivision of the Western English River Subprovince. Canadian Journal of Earth Sciences, v. 14, p. 1481-1489.

Brown, A. et al. 1986. Level II geoscience report – geology of the Lac du Bonnet batholith.

Brown, A. 1981. Geoscience research at the Underground Research Laboratory. In, Proceedings of the eleventh information meeting of the Nuclear Fuel Waste Management Program (1981 general meeting), compiled by A.R. Gibson, p. 102-119.

Brown, A., Dugal, J.J.B., Everitt, R.A., Kamineni, D.C., Lau, J.S.O., and McEwen, J.H. 1985. Advances in geology at the URL site (RA 3). In, The Geoscience program – Proceedings of the seventeen information meeting of the Nuclear Fuel Waste Management Program. Atomic Energy of Canada Limited Technical Record TR-299, Volume I, p. 253-264.

Chagarlamundi, P. 1971. Resistivity and seismic refraction surveys over Pleistocene deposits in southern Manitoba, Unpublished M.Sc. thesis, University of Manitoba, 115 p.

Chernis, P.J. 1985. Petrographic analysis of URL-2 and URL-6 special thermal conductivity samples. Department of Energy, Mines, and Resources, Earth Physics Branch Internal report 85-20, 15 p.

Chernis, P.J., and Robertson, P.B. (in press). Summary of modal analyses of WN, URL, ATK, and EBL borehole samples, by the Rock Crack Properties Activity, Nuclear Fuel Waste Management Program. Submitted as an AECL TR-series report, 08-1986.

Cherny, P., Trueman, D.L., Ziehlke, D.V., Goad, B.E., and Paul, B.J. 1981. The Cat Lake-Winnipeg River and the Wekusko Lake pegmatite fields, Manitoba. Manitoba Department of Energy and Mines, Economic Geology Report 80-1, 216 p.

Davison, C.C. 1985. Hydrogeological characterization of the URL site. In, The Geoscience program – Proceedings of the seventeen information meeting of the Nuclear Fuel Waste Management Program. Atomic Energy of Canada Limited Technical Record TR-299, Volume I, p. 231-253.

Farquharson, R.B. 1975. Revised Rb-Sr age of the Lac du Bonnet quartz-monzonite. Canadian Journal of Earth Sciences, v. 12, p. 115-118.

Kamineni, D.C., Dugal, J.J.B., and Ejeckam, R.B. 1984. Geochemical investigations of granitic core samples from boreholes at the Underground Research Laboratory site near Lac du Bonnet, Manitoba. Atomic Energy of Canada Limited, Technical Record TR-221, 61 p.

Lau, J.S.O., Bisson, J.G., and Auger, L.F. 1982. A preliminary report on the URL-2 borehole television survey. Atomic Energy of Canada Limited, Technical Record TR-115-21, 22 p.

McCrank, G.D.F. 1985. A geological survey of the Lac du Bonnet Batholith, Manitoba. Atomic Energy of Canada Limited Report AECL-7816, 63 p.

McRitchie, W.D. 1971. Petrology and environment of the acidic plutonic rocks of the Wanipigow-Winnipeg River region, southeastern Manitoba. In, Geology and Geophysics of the Rice Lake region, southeastern Manitoba (Project Pioneer), W.D. McRitchie and W. Weber, Editors. Manitoba Department of Mines and Natural Resources, Mines Branch Publication 71-1, p. 7-61.

2. MICROMORPHOLOGY

NATURAL AND STRESS-RELIEF MICROCRACKS IN THE LAC DU BONNET GRANITE

P.J. Chernis* and P.B. Robertson**
Geological Survey of Canada
1 Observatory Cr.
Ottawa, Ontario K1A 0Y3

*: Atomic Energy of Canada Limited, attached to GSC, Ottawa
**: Geological Survey of Canada (GSC), 1 Observatory Crescent, Ottawa K1A 0Y3

NATURAL AND STRESS-RELIEF MICROCRACKS IN THE LAC DU BONNET GRANITE

P.J. Chernis and P.B. Robertson
Geological Survey of Canada (GSC), 1 Observatory Crescent, Ottawa K1A 0Y3

INTRODUCTION

Laboratory physical property measurements provide essential data for evaluating the stability and radionuclide release characteristics of a subsurface vault. However, rock samples obtained at depth have been reported to show a change in certain physical properties due to cracking of a stress-relief origin (Simmons and Nur, 1968; Wang and Simmons, 1978; Katsube, 1981; Kowallis and Wang, 1983). Therefore, estimates of in situ conditions of vault stability and radionuclide release characteristics based solely on laboratory results could be erroneous unless these effects are taken into consideration. This paper reviews the work related to stress relief in rock samples obtained from different depths in the Lac du Bonnet batholith, and discusses the structure of natural and stress-relief microcracks observed with the scanning electron microscope. This paper also discusses the effects of tectonic brittle deformation and fracture-controlled alteration on rock properties.

EVIDENCE OF STRESS-RELIEF CRACKING

The possibility of incorrectly interpreting the response of a rock body to stress is particularly well demonstrated by rock property data from the WNRE (Whiteshell Nuclear Research Establishment) research area where, contrary to observations in sedimentary sequences (Athy, 1930; Thomas and Oliver, 1979; Berner, 1980; Hoholick et al., 1984), the porosity of core samples from deep boreholes in the Lac du Bonnet batholith increases with sampling depth. Although properties such as P-wave velocity, uniaxial strength, and permeability of the samples also reflect this trend, geophysical borehole logs do not. This trend of increasing porosity with depth has been observed in other crystalline rocks (Simmons and Nur, 1968; Kowallis and Wang, 1983), and interpreted to be the result of cracking of the core as overburden stress was relieved by drilling (Wang and Simmons, 1978; Katsube, 1981; Kowallis and Wang, 1983). A stress-relief origin for the trend at WNRE is supported by the following:

(1) Compressional wave velocities are restored to "normal" values by the application of confining pressure.
(2) The confining pressure required to restore the velocities increases with sampling depth (Chernis and Stesky, 1984).
(3) Discing of core, which occurs where stresses are high, has been observed in the core from WNRE (Brown, 1982).
(4) High horizontal stresses have been measured in boreholes WN-4 and URL-1 (25 MPa and 30 MPa, respectively; Haimson, 1982).

Therefore, to correctly predict in situ behaviour of crystalline rock it is important to know whether rock samples have been affected during sampling by some process which has artificially increased their porosity.

Core samples from the WNRE research area have been examined with a Scanning Electron Microscope (SEM) to determine the character of their microcrack populations, and to assess the hypothesis that the increase in porosity with depth is related to stress-relaxation cracking during drilling (Chernis et al. 1980; Chernis, 1983; Chernis, 1984a; Chernis, 1984b; Chernis and Stesky, 1984). Measurements of rock properties indicate that the approximate onset depth of stress cracking is 400-450 m (vertical). Samples for SEM analysis were chosen from above this depth (134 m, borehole WN-1), at the onset depth (450 m, borehole WN-4), and below the onset depth (738 m, borehole WN-4). It was found that about 30% of the cracks in the deepest sample are stress cracks, and these cause a doubling of porosity.

OBSERVATIONS OF MICROCRACKS

Microcracks are categorized according to their position in relation to mineral grains. Grain boundary cracks occur between mineral grains, intragranular cracks are those confined within grains, and transgranular cracks cross grain boundaries. Grain boundaries themselves need not have cracks along them. Due to the difficulty sometimes encountered in differentiating between quartz intragranular cracks and quartz grain boundary cracks, these two crack types were treated as one and the same. Natural and stress-relief microcracks are differentiated by their physical characteristics. Natural microcracks in crystalline rocks

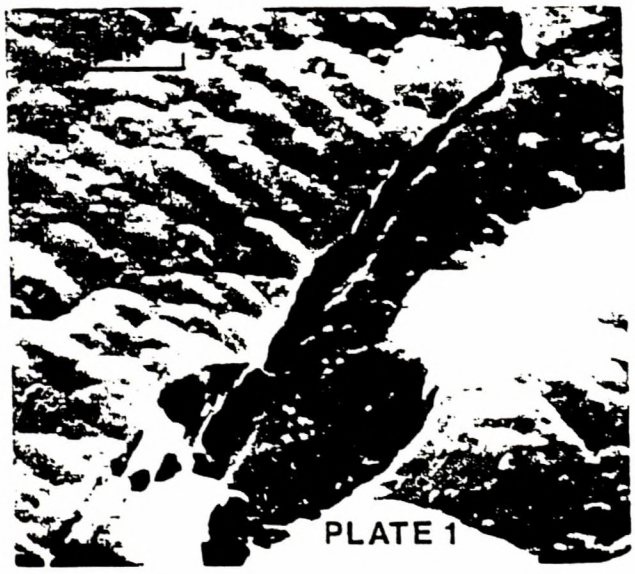

Plate 1. Natural microcracks, such as this microcline intragranular crack, are characterized by rough walls, bridges (B), and blunt terminations (T).

characteristically have rough or irregular walls and/or small infillings (bridges) (Plate 1) (Brace et al. 1972). Newly formed, drill-induced (stress-relaxation) cracks are identified by their smooth, parallel walls which would mate perfectly under compressive stress (suggesting an extensional origin) (Plate 2a), sharp terminations (Plate 2b), and by a lack of infilling or bridging material.

Natural Microcracks

Natural microcracks in samples of the Lac du Bonnet granite which were not affected by drill-induced stress-relief cracking, are less than about 4 μm wide (arithmetic mean = 0.12 μm; geometric mean width = 0.06 μm). Quartz forms a contiguous, fine- to medium-grained network around and between feldspar grains, limiting the area of contact between the volumetrically more abundant feldspars.

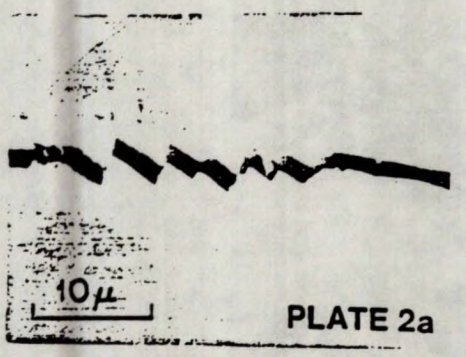

Plate 2. Stress-relief microcracks are characterized by their parallel, well-matching walls (2a), and sharp terminations (2b).

For this reason, the most common grain boundaries and grain boundary cracks are around quartz grains. Cracks around quartz grains may have large amounts of infillings such as calcite, iron oxide, or clay, or may be relatively free of secondary materials. Together they account for 90% of cracks and 93% of the natural crack porosity along grain boundaries, and about 50% of the natural total porosity of the rock (the remaining 50% occurs as intragranular porosity, chiefly in feldspars). Plagioclase typically contains large amounts of pores (up to 2.3% by volume – Sprunt and Brace, 1974) which are less than 5 μm in size, and which may be isolated within grains or intersected by fine intragranular cracks (Plate 3). Many intragranular cracks are so narrow (geometric mean width 0.05 μm) that they themselves do not contribute significantly to the porosity of the samples, but form important linkages to the large amount of pore porosity within plagioclase. Cracks

within plagioclase may be lined with sericite, clay minerals, albite, or iron oxide. In microcline, intragranular basal cleavage cracks are most numerous. They may be straight, narrow features with fairly smooth walls and small amounts of filling materials, or large gaping cracks over 1 μm wide, with irregular walls. The geometric mean crack width of microcline intragranular cracks is 0.07 μm. The density of microcracks is higher within microcline than in plagioclase or at grain boundaries. Cracks at grain boundaries separating feldspars are rare.

Microcracks may be modelled as parallel-walled structures with embayments in their walls (Figure 1). The parallel-walled portions of the cracks (unshaded, Figure 1) defines the porosity of an ideallized smooth-wall crack, or the connecting porosity (Katsube and Hume, this volume). The embayments along the crack walls (shaded, Figure 1) make up the crack wall porosity or pore porosity (Katsube and Hume, this volume). The amounts of connecting and pore porosities are approximately equal in samples which have undergone little or no stress-relief cracking (Chernis, 1984b).

Plate 3. Fine intragranular cracks in plagioclase intersecting micron-sized pores.

Stress-relief microcracks

Stress-relief cracks are most numerous in plagioclase, but the largest cracks have formed at grain boundaries, particularly around quartz, and within microcline grains (Plate 4). Stress-relief microcracks are up to 5.1 μm wide in sample 738 but are an order of magnitude narrower in sample 451, the sample from the approximate onset depth of stress-relief cracking. About 5% of the cracks in sample 451 have stress-crack form. Their narrowness and scarcity indicates that stress-relief cracking has not significantly increased the porosity of sample 451. In sample 738, on the other hand, almost 30% of the observed cracks have stress crack form (23% of grain boundary cracks, 30% of microcline intragranular cracks, and 38% of plagioclase intragranular cracks). Most stress cracks at grain boundaries developed around quartz grains. Stress-relief cracking has increased

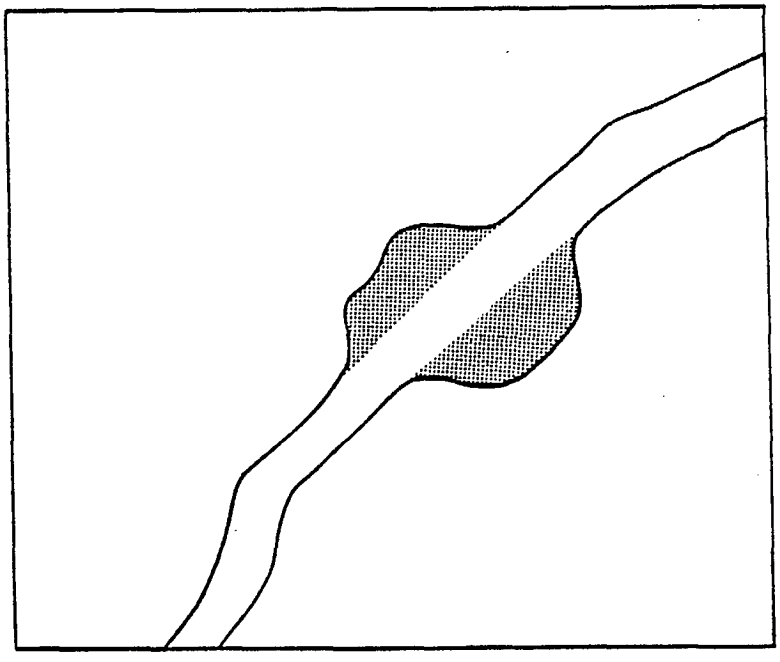

Figure 1. Total crack porosity can be subdivided into smooth-wall crack porosity (or connecting porosity, unshaded), and crack wall porosity (or pore porosity, shaded). See also Katsube and Hume (this volume).

the porosity of sample 738 to 0.6% from the 0.2%-0.4% range measured for samples unaffected by stress cracking (see Wadden, 1979; Drury, 1981). Crack porosity of URL samples, determined from stress-strain curves, also increases approximately 3-fold by the same depth (see Table 4, Katsube and Hume, this vol.). The porosity increase is due principally to the formation of cracks greater than 1 μm in width. These observations indicate that rock properties of samples collected from below about 450 m vertical depth at the WNRE drill site are not representative of the in situ properties, but may be indicative of the range of properties that could be expected in a narrow zone surrounding any excavation below that depth.

Microcracks which are similar in appearance to the drill-related stress-relief cracks in the Lac du Bonnet samples have been observed in samples of the Eye-Dashwa Lakes Pluton (Chernis, 1987). The stress-relief cracks in the Eye-Dashwa Lakes samples, however, show evidence of mineral dissolution and precipitation during hydrothermal alteration: irregular walls, blunt crack tips, and bridges. These are ancient tectonic stress-relief cracks which formed contemporaneously with faults and fractures, during a penetrative brittle deformation. Properties of core samples from the Eye-Dashwa Lakes pluton are dependent on the extent of

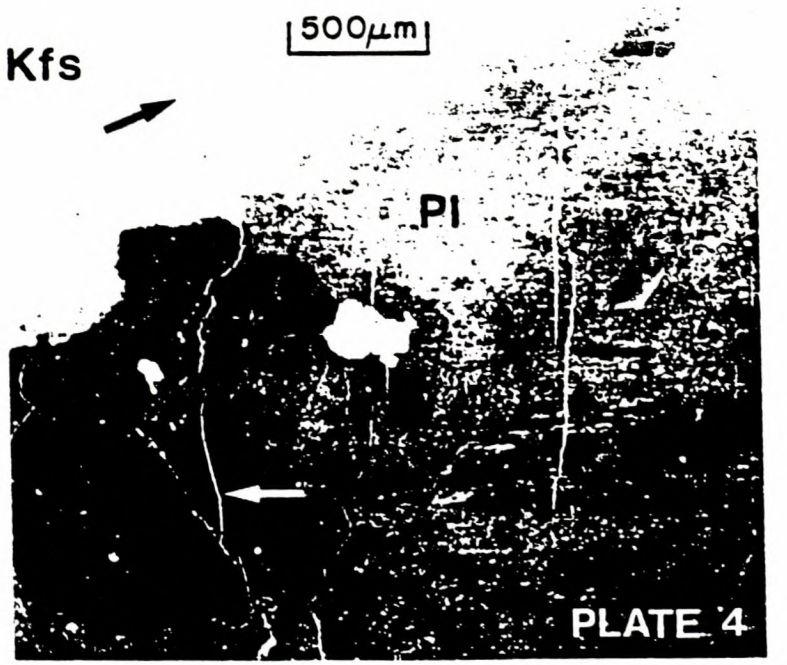

Plate 4. Stress-relief microcracks (arrows) formed at grain boundaries around quartz (Qtz), and within microcline (Kfs) and plagioclase (Pl).

development of tectonic stress cracks, and the level of subsequent fracture-controlled alteration along fractures and accompanying diffusion within the rock matrix.

The effect on the properties plutonic rock, of penetrative fracturing and alteration are well illustrated by a porosity profile across a natural fracture presented in Melnyk and Skeet (1986), and reproduced here in Figure 2. The porosity of the unfractured host rock, approximately 0.4% to 0.5%, is maintained within 60-70 mm from the fracture surface. As the fracture is approached from this distance, the porosity rises steadily to just over 0.7%, at approximately 10 cm from the fracture surface, then falls below 0.7%. The gradual increase in porosity toward the fracture can be attributed to a corresponding increase in the number of tectonic stress-relief microcracks which are contemporaneous with the macrofracture. Alteration profiles across the fracture, and observations of microcracks in thin sections, indicate that the fracture probably formed as the

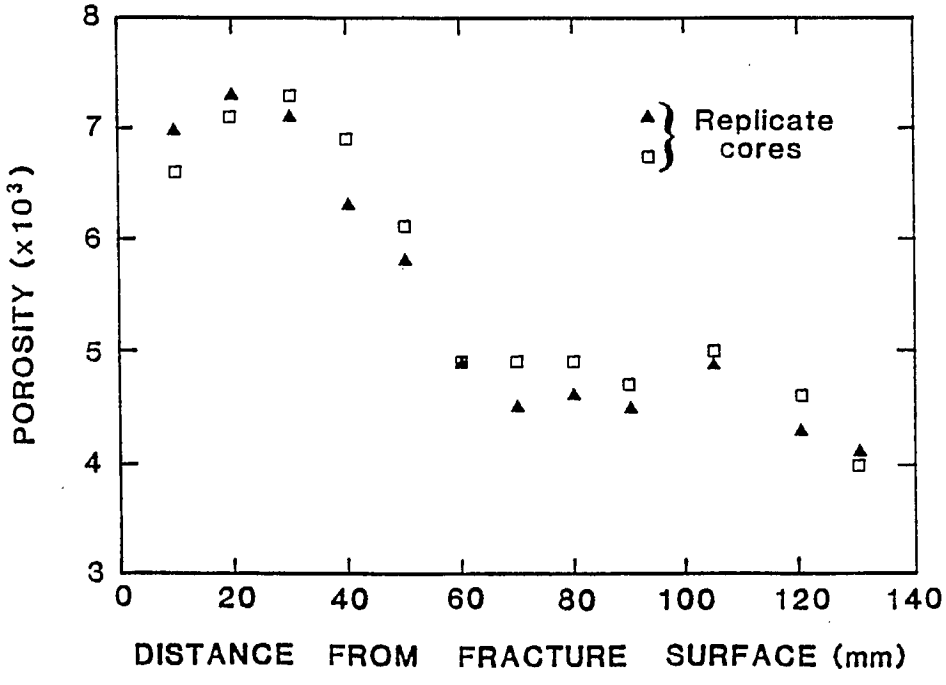

Figure 2. Porosity profile adjacent to a natural surface (from Melnyk and Skeet, 1986).

pluton cooled, and that healing of microcracks (porosity reduction) within 9 mm of the fracture surface occurred during deuteric alteration also associated with the cooling of the pluton (J. Cramer, AECL, personal communication, 1986). The profile illustrates that properties of plutonic rocks are determined by microcrack structures which form in response to penetrative tectonic stresses, and also by subsequent fracture-controlled alteration and accompanying diffusion (crack healing) in the rock matrix.

CONCLUSIONS

The population of natural microcracks in core samples of the Lac du Bonnet granite is equally divided between grain boundary cracks and intragranular cracks. Grain boundary cracks preferentially occur around quartz grains, and account for 50% of the total natural porosity of the samples. Stress cracks are present in core samples collected from depths below approximately 450 m vertical depth at WNRE, and their density increases with depth. They are developed at grain boundaries (particularly around quartz) and within plagioclase and microcline feldspars. In a sample from 738 m, the development of stress cracks typically 1-5 μm in width resulted in doubling of total porosity. This is an excellent illustration that rock properties measured in the laboratory under ambient conditions are not necessarily representative for the rock mass in situ, and also that drilling or excavation may disrupt the rock properties in the near-field region. Predictions of the behaviour of rock surrounding a repository based on measurements of these samples will be valid only for a narrow zone around the excavation. Far-field conditions must be approximated using properties derived from samples devoid of these cracks, determined in the laboratory on samples under simulated in situ conditions, or calculated with allowance for their existence.

The development of stress-relief microcracks is not a simple function of depth, but appears to require the presence of abnormally high horizontal stresses such as measured at WNRE and URL (Underground Research Laboratory) sites. At the Atikokan research area, Chernis (1984c) found no evidence of fresh stress-induced cracks associated with removal from depth as great as 778 m, although ancient tectonic stress-induced microcracks are abundant. This implies that high horizontal stresses are not present at the ATK drill site, possibly due to relaxation of stresses following tectonism, or that the macro- and microfractures in the

pluton effectively diffuse further stress buildup. It has been demonstrated that rock properties of plutonic rocks, in the absence of drill-related stress-relief effects, are dependant on the extent of penetrative tectonic stress-relief cracking, subsequent fracture-controlled alteration and the accompanying diffusion in the rock matrix. The number and size of natural microcracks in candidate plutons may be kept to a minimum by selecting quartz-poor lithologies with low macrofracture and fault densities, and appropriate levels and types of alteration. The relationship between grain size and microcracks has not been fully investigated, but preliminary SEM observations indicate that fine-grained rocks, despite having more grain boundaries, may possess fewer microcracks and may make more favourable repository sites.

REFERENCES

Athy, L.F. 1930. Density, porosity, and compaction of sedimentary rocks. Bulletin of the American Association of Petroleum Geologists, v. 14, p. 1-24.

Berner, R.A. 1980. Early Diagenesis: A Theoretical Approach. Princeton University Press, N.J., 241 p.

Brace, W.F., E. Silver, K. Hadley, and C. Goetze. 1972. Cracks and pores: A closer look. Science, v. 178, p. 162-163.

Brown, A. 1982. Memo to P. Baumgartner (AECL, Pinawa, Manitoba). Re: Discing in URL core, 2 p.

Chernis, P.J. 1983. Notes on the Pore-microfracture structure of some granitic samples from the Whiteshell Nuclear Research Establishment. Atomic Energy of Canada Limited, Technical Record TR-226, 34 p.

Chernis, P.J. 1984a. Comparison of the pore-microcrack structure of shallow and deep samples of the Lac du Bonnet granite. Atomic Energy of Canada Limited, Technical Record TR-223, 20 p.

Chernis, P.J. 1984b. Microcrack structures in plutonic rocks from the Whiteshell Nuclear Research Establishment, Eastern Manitoba, and Atikokan, Northwestern Ontario. Unpublished M.Sc. Thesis, Carleton University, Ottawa, 159 p.

Chernis, P.J. 1984c. The effects of crack healing on the microcrack structure of core samples from borehole ATK-1, in the Eye-Dashwa Lakes Pluton, Northwestern Ontario. Atomic Energy of Canada Limited, Technical Record TR-268, 17 p.

Chernis, P.J. (in preparation). Microcrack structures in the Eye Dashwa Lakes pluton. In The Canadian Nuclear Fuel Waste Management Program: Geotechnical Studies at the Atikokan Research Area, AECL Report 8410-7, p. 13-22.

Chernis, P.J. and R.M. Stesky. 1984. Stress-induced microcracks in core samples from the Lac du Bonnet granite, Manitoba, Presented at the 17th information meeting of the Canadian Nuclear Fuel Waste Management Program – Geoscience, Feb. 21-23, 1984.

Chernis, P.J., D.A. Walker, and A.G. Plant, 1980. Application of scanning electron microscopy to the Canadian radioactive waste disposal program. Microbeam analysis – 1980, D.B. Wittry, Ed., San Francisco Press, p. 136-138.

Drury, M.J. 1981. Thermal conductivity, density, porosity, and mineralogy of core samples from Chalk River, Pinawa, and Atikokan. Energy, Mines, and Resources, Earth Physics Branch, internal report 81-6, 13 p.

Haimson, B.C. 1982. Hydrofracturing in situ stress measurements in the Lac du Bonnet batholith drillholes URL-1 and WN-4. Report to Atomic Energy of Canada Limited, Whiteshell Nuclear Research Establishment, Pinawa, Manitoba, 106 p.

Hoholick, J.D., T. Metarko, and P.E. Potter. 1984. Regional variations of porosity and cement: St. Peter and Mount Simon Sandstones in the Illinois Basin, Bulletin of the American Association of Petroleum Geologists, v. 68, p. 753-764.

Kamineni, D.C., and J.J.B. Dugal. 1981. A preliminary report and interpretation of alteration in the Eye-Dashwa Lakes pluton. Atomic Energy of Canada Limited Technical Record TR-178, 56 p.

Katsube, T.J. 1981. Pore structure and pore parameters that control the radionuclide transport in crystalline rocks. Proceedings of the technical program, International Powder and Bulk Solids Handling and Processing, Rosemount, Ill., p. 394-409.

Katsube, T.J. and J.P. Hume (this volume). Pore structure characteristics of granitic rock samples from Whiteshell Research Area, in, Nuclear Fuel Waste Management Program Concept Assessment Document, Geotechnical Studies at Whiteshell Research Area (RA-3), Rock Properties (T.J. Katsube and J.P. Hume, editors), p. 97-138.

Kowallis, B.J., and H.F. Wang. 1983. Microcrack study of granitic cores from Illinois deep borehole UPH3. Journal of Geophysical Research, v. 88, p. 7373-7380.

Melnyk, T.W. and A.M. Skeet. 1986. An improved technique for the determination of rock porosity. Canadian Journal of Earth Sciences, v. 23, no. 8, p. 1068-1074.

Simmons, G., and A. Nur. 1968. Granites: Relation of properties in situ to laboratory measurements. Science, v. 162, p. 789-791.

Sprunt, E.S., and W.F. Brace. 1974. Direct observation of microcavities in crystalline rocks. International Journal of Rock Mechanics and Mining Sciences, v. 11, p. 139-150.

Thomas, M.B. and T.A. Oliver. 1969. Depth-porosity relationships in the Viking and Cardium Formations of central Alberta. Bulletin of the Canadian Petroleum Geologists, v. 27, p. 209-220.

Wadden, M.M. 1979. Porosity measurements by the immersion technique for WN-1, -2, and CR-6, -7 samples. Geological Survey of Canada internal report TR-7879-D6, 12 p.

Wang, H.F. and G. Simmons. 1978. Microcracks in crystalline rocks from 5.3 km depth in the Michigan Basin. Journal of Geophysicsl Research, v. 83, p. 5849-5856.

3. GEOCHEMISTRY

GEOCHEMICAL ANALYSIS OF STANDARD CORE SAMPLES FROM WHITESHELL RESEARCH AREA

J.B. Percival* and J.P. Hume**
Geological Survey of Canada
601 Booth Street, Ottawa, Ontario, K1A 0E8

*: Carleton University, Ottawa
**: Atomic Energy of Canada Ltd. (on attachment to the Geological Survey of Canada)

GEOCHEMICAL ANALYSIS OF STANDARD CORE SAMPLES FROM WHITESHELL RESEARCH AREA

J.B. Percival and J.P. Hume
Geological Survey of Canada, 601 Booth St., Ottawa, Ontario K1A 0E8

INTRODUCTION

The chemical properties of rocks play an important role in the interpretation of physical rock property data. For this reason, the chemical properties for all of the standard core samples from the Lac du Bonnet batholith have been obtained since 1978, when the Rock Property Activity started under the auspices of the Canadian Nuclear Fuel Waste Management Program. However, this chemical property data has been dispersed in a number of documents which may be hard to obtain. Therefore, it is necessary to compile all such data in one document and add to the data base for standard core samples obtained from the various research areas. Geochemical data presented here has been compiled from Chomyn and Chernis (1980) and Percival (1985). The additional petrographical description of standard samples from boreholes URL-1, 2, 5 and WN-1, 2, 4 that are included in this paper have been compiled from Chernis (1979a, b) and Bilodeau (1984).

SAMPLE SELECTION

URL and WN sites form the WNRE research area which is located within the Lac du Bonnet batholith. This batholith is located in the southern part of the English River subprovince of the Superior Province (McCrank, 1985).

Thirty-six granitic samples were selected from three boreholes at the URL site. The depth ranges of samples from URL-1, -2 and -5 were 46-662 m, 255-1095 m and 16-497 m, respectively. "Depth" implies "down hole length" in this paper. Pink granite predominates in the upper portion (150 m) of borehole URL-1. The suite of URL-2 and URL-5 samples is composed of grey granite.

Thirty-four medium-grained, massive granite samples were chosen from the WN site. Shallow (< 150 m), intermediate (125-460 m), and deep (400-928 m) level samples were taken from boreholes WN-2, WN-1 and WN-4, respectively. The samples are pink to greyish-pink in colour generally grading to gray with depth. This suite of samples also includes two tonalite samples (from WN-2) and one pegmatite specimen (from WN-4).

METHODS OF ANALYSIS

The chemical analysis of the URL and WN series standard samples was carried out by the Analytical Chemistry Laboratory of the Geological Survey of Canada. The samples were analyzed for ten major oxides and P_2O_5, Rb, Zn and Zr using X-ray fluorescence on a 1 g fused disc. Infrared spectrometry was used to determine H_2O, CO_2 and S concentrations. The results are expressed as weight percent oxides. The chemical data was used to calculate the normative mineral composition using the C.I.P.W. norm program based on work done by Hutchison (1975).

RESULTS

The major elemental analysis and the C.I.P.W. normative mineral composition for standard samples from the URL and WN sites is presented in Tables 3 and 4 in the Appendix. The petrographic analysis for URL and WN samples is given in Table 5 in the Appendix. The minimum, maximum, mean and standard deviation of the elemental analyses and C.I.P.W. norm is presented in Tables 1 and 2.

CONCLUSIONS

These results show that the normative composition of the samples from the URL site is predominantly granite with a few granodiorite samples. The samples from the WN site show much less variation in feldspar content but most of them are still classified as granites.

REFERENCES

Bilodeau, B. 1984. Petrographic description of URL-1, -2 and -5 standard P-samples. Nuclear Fuel Waste Management Program, Rock Property Activity, Pore Structure Task, Technical Report 8485-GP2, 16 p. Available from T.J. Katsube (G.S.C.).

Chernis, P.J. 1979a. Petrographical analysis of borehole samples (label-P specimens) from WN-1, WN-2, CR-6 and CR-7. Nuclear Fuel Waste Management Program, Rock Property Activity, Pore Structure Task, Technical Report 7879-T5, 15 p. Available from T.J. Katsube (G.S.C.).

Chernis, P.J. 1979b. Petrographical analysis of borehole samples from WN-4 (label-P specimens). Nuclear Fuel Waste Management Program, Rock Property Activity, Pore Structure Task, Technical Report 7980-T4, 14 p. Available from T.J. Katsube (G.S.C.).

Chomyn, B.A. and Chernis, P.J. 1980. Chemical analyses of samples from boreholes CR-8 and WN-4. Atomic Energy of Canada Limited Project No. 303405, M001/80, Technical Report 8081-T1, 52 p.

Hutchison, C.S. 1975. The norm, its variation, their calculation and relationships. Schweizerische Mineralogische und Petrographische Mitteilungen, v. 55, p. 243-256.

McCrank, G.F.D. 1985. A geological survey of the Lac du Bonnet batholith, Manitoba. Atomic Energy of Canada Limited, Report AECL-7816, 63 p.

Percival, J.B. 1985. Geochemical analyses of standard core samples from the Atikokan and Underground Research Laboratory research areas: Boreholes ATK-1, ATK-5, URL-1, URL-2 and URL-5. Atomic Energy of Canada Limited, TR-330, 39 p.

Table 1. Minimum, maximum, mean and standard deviation of major oxides for the standard samples from the Lac du Bonnet batholith

	SiO_2	TiO_2	Al_2O_3	Fe_2O_3	FeO	MnO	MgO	CaO	Na_2O	K_2O	Oxidation Ratio
URL-1 (n=16)											
min.	70.2	0.10	11.7	0.1	0.6	0.01	0.09	0.35	1.4	3.09	9.09
max.	76.7	0.49	15.5	0.9	2.0	0.05	1.17	2.35	4.6	7.09	50.00
mean	72.2	0.22	14.4	0.5	1.1	0.03	0.46	1.61	3.5	4.55	28.47
std. dev.	1.61	0.098	0.87	0.23	0.41	0.01	0.24	0.422	0.73	0.93	11.85
URL-2 (n=8)											
min.	71.5	0.14	13.7	0.1	0.6	0.02	0.15	1.35	3.4	3.90	8.33
max.	74.3	0.24	15.2	0.7	1.1	0.04	0.51	1.83	4.3	4.70	46.15
mean	72.8	0.19	14.3	0.5	0.9	0.03	0.32	1.57	3.7	4.38	33.76
std. dev.	0.91	0.037	0.53	0.21	0.19	0.006	0.11	0.143	0.35	0.24	11.95
URL-5 (n=12)											
min.	68.1	0.04	13.2	0.1	0.7	0.01	0.03	0.67	2.7	2.99	7.69
max.	74.7	0.45	15.1	0.7	2.5	0.06	1.52	2.48	4.4	4.92	31.25
mean	72.3	0.21	14.3	0.4	1.3	0.03	0.50	1.66	3.6	4.54	19.89
std. dev.	1.73	0.117	0.58	0.20	0.53	0.012	0.35	0.422	0.60	0.96	8.77
WN-1 (n=10)											
min.	70.6	0.13	13.3	0.0	0.5	0.02	0.28	1.01	3.1	4.28	0.00
max.	75.6	0.26	15.8	0.9	3.2	0.04	0.52	1.47	4.2	4.81	64.29
mean	72.4	0.18	14.4	0.6	1.0	0.03	0.36	1.23	3.6	4.6	44.08
std. dev.	1.75	0.044	0.8	0.26	0.8	0.006	0.08	0.17	0.32	0.17	17.42
WN-2 (n=6)											
min.	67.7	0.13	13.7	0.5	0.2	0.02	0.28	1.02	3.2	1.84	28.95
max.	74.6	0.49	15.5	1.2	2.8	0.17	2.58	3.44	3.9	4.84	83.33
mean	71.7	0.26	14.6	1.0	1.3	0.07	1.07	1.88	3.5	3.64	50.85
std. dev.	3.07	0.17	0.77	0.25	1.15	0.07	1.15	1.14	0.26	1.38	22.74
WN-4 (n=18)											
min.	70.0	0.10	13.6	0.0	0.6	0.0	0.17	1.00	3.0	4.56	0.00
max.	74.0	0.30	15.0	1.0	1.4	0.04	0.60	2.00	4.1	9.00	50.00
mean	72.3	0.18	14.3	0.4	1.0	0.02	0.34	1.36	3.7	5.11	27.59
std. dev.	1.27	0.05	0.46	0.29	0.24	0.014	0.103	0.33	0.27	0.99	15.12

Table 2. Minimum, maximum, mean and standard deviation of the C.I.P.W. normative mineral composition for the standard samples from the Lac du Bonnet batholith

	Q	C	OR	AB	AN	MGBI	FEBI	MT	HM	TN	AP	PR	CC	WO
URL-1 (n=16)														
min.	21.77	0.00	13.17	12.04	1.15	0.30	0.74	0.15	0.00	0.22	0.10	0.07	0.00	0.00
max.	41.54	2.24	41.81	39.13	9.38	3.89	4.42	1.32	0.00	1.05	0.41	0.08	0.00	0.07
mean	31.52	1.23	25.34	30.08	6.71	1.55	2.14	0.60	0.00	0.47	0.22	0.08	0.00	0.00
std. dev.	4.06	0.53	6.16	6.19	1.76	0.80	0.97	0.30	0.00	0.21	0.08	0.00	0.00	0.02
URL-2 (n=8)														
min.	27.56	0.78	22.39	29.16	3.94	0.50	0.81	0.15	0.00	0.30	0.12	0.15	0.23	
max.	37.74	1.95	27.35	36.93	6.94	1.70	2.31	1.02	0.00	0.51	0.26	0.17	0.09	
mean	32.13	1.43	24.64	31.85	5.66	1.05	1.44	0.69	0.00	0.39	0.18	0.16	0.37	
std. dev.	3.49	0.44	1.39	2.88	0.86	0.37	0.49	0.31	0.00	0.076	0.044	0.010	0.17	
URL-5 (n=12)														
min.	27.12	0.43	11.48	21.48	3.10	0.10	0.00	0.00	0.00	0.09	0.05	0.02	0.00	
max.	34.66	1.79	41.45	38.02	10.17	5.12	5.31	1.04	0.41	0.97	0.51	0.19	0.23	
mean	31.38	1.02	24.60	30.68	6.90	1.68	2.45	0.47	0.034	0.45	0.22	0.089	0.045	
std. dev.	2.38	0.44	6.89	5.07	1.77	1.19	1.33	0.33	0.12	0.25	0.11	0.042	0.089	
WN-1 (n=10)														
min.	26.74	1.10	21.37	26.79	3.70	0.93	0.29	0.00	0.00	0.28	0.02	0.00	0.00	
max.	37.51	2.52	27.63	35.99	5.85	1.75	7.42	1.32	0.00	0.56	0.19	0.02	0.23	
mean	32.26	1.87	25.80	30.84	4.71	1.21	1.69	0.93	0.00	0.39	0.11	0.002	0.18	
std. dev.	3.46	0.46	1.87	2.82	0.66	0.27	2.06	0.39	0.00	0.095	0.049	0.0063	0.097	
WN-2 (n=6)														
min.	28.20	1.83	1.80	27.25	3.72	0.93	0.00	0.72	0.00	0.28	0.07	0.00	0.23	
max.	37.03	2.97	26.95	33.35	13.49	8.52	5.58	1.74	0.52	1.04	0.45	0.04	0.46	
mean	34.56	2.33	17.99	29.75	7.17	3.55	2.23	1.29	0.087	0.56	0.22	0.0067	0.27	
std. dev.	3.38	0.42	12.29	2.33	4.71	3.81	2.58	0.46	0.21	0.36	0.17	0.016	0.094	
WN-4 (n=18)														
min.	17.75	0.00	25.13	25.71	0.89	0.59	1.21	0.00	0.00	0.21	0.04	0.00	0.00	
max.	34.43	1.67	52.15	35.76	8.20	1.98	2.95	1.45	0.00	0.63	0.24	0.02	0.46	
mean	28.92	0.69	28.64	32.00	5.22	1.15	1.83	0.62	0.00	0.38	0.16	0.0017	0.15	
std. dev.	3.84	0.44	6.01	2.27	1.69	0.35	0.51	0.41	0.00	0.10	0.062	0.0051	0.16	

Q = Quartz
C = Corundum
OR = Orthoclase
AB = Albite
AN = Anorthite

MT = Magnetite
AP = Apatite
PY = Pyrite
CC = Calcite
MGBI = Phlogopite

FEBI = Annite
TN = Sphene
WO = Wolframite
HM = Hematite

APPENDIX

Table 3. Major oxides for all standard samples from the Lac du Bonnet batholith

Sample No.	SiO_2	TiO_2	Al_2O_3	Fe_2O_3	FeO	MnO	MgO	CaO	Na_2O	K_2O	H_2OT	CO_2	P_2O_5	S	Ba*	Rb	Zn	Zr*	Total
URL-1-	46.25	73.1	0.14	14.1	0.5	0.8	0.03	0.43	1.45	3.1	4.82	0.2	0.0	0.09	0.04		0.017	0.007	0.017	98.9
-	68.35	72.1	0.17	14.3	0.5	0.9	0.02	0.48	1.52	3.3	4.64	0.3	0.0	0.09	0.04		0.016	0.008	0.016	98.6
-	100.45	70.2	0.49	14.9	0.9	1.9	0.05	0.81	1.88	3.3	3.43	0.04	0.00	0.14	0.04		0.014	0.006	0.021	100.7
-	131.15	73.6	0.17	14.7	0.4	0.9	0.03	0.42	1.58	3.7	4.58	0.2	0.00	0.08	0.04		0.014	0.006	0.021	100.7
-	176.95	71.7	0.20	14.5	0.4	1.1	0.03	0.33	1.58	3.1	4.94	0.2	0.00	0.07	0.04		0.017	0.006	0.023	98.4
-	230.35	70.8	0.23	15.0	0.7	1.4	0.04	0.52	2.07	3.9	3.64	0.03	0.00	0.11	0.04		0.014	0.006	0.026	98.8
-	259.15	72.8	0.17	14.6	0.1	0.9	0.03	0.38	1.42	3.1	5.37	0.2	0.0	0.08	0.04		0.020	0.006	0.022	99.3
-	302.25	71.3	0.19	15.5	0.4	1.1	0.03	0.41	1.84	4.6	4.02	0.02	0.00	0.10	0.04		0.014	0.009	0.022	99.9
-	357.95	73.4	0.18	13.7	0.6	0.6	0.03	0.30	1.38	3.3	4.85	0.2	0.00	0.06	0.04		0.016	0.006	0.016	98.8
-	397.65	70.9	0.35	15.1	0.2	2.0	0.05	1.17	2.35	4.1	3.09	0.03	0.00	0.17	0.04		0.015	0.008	0.014	100.0
-	443.05	70.4	0.16	15.3	0.9	1.0	0.02	0.33	1.53	4.5	5.15	0.2	0.00	0.08	0.04		0.017	0.007	0.019	99.8
-	496.55	71.6	0.22	14.2	0.2	1.4	0.03	0.44	1.65	3.7	4.61	0.02	0.00	0.09	0.04		0.021	0.006	0.021	98.6
-	577.28	73.3	0.17	14.1	0.3	1.0	0.03	0.39	1.62	3.7	4.38	0.3	0.00	0.06	0.04		0.018	0.006	0.016	99.5
-	592.45	76.7	0.10	11.7	0.3	0.6	0.01	0.09	0.35	1.4	7.09	0.01	0.00	0.04	0.04		0.026	0.003	0.012	98.7
-	615.75	71.4	0.35	14.4	0.5	1.5	0.04	0.55	1.83	3.9	3.71	0.3	0.00	0.11	0.04		0.019	0.007	0.025	98.9
-	662.25	72.5	0.20	14.6	0.3	1.1	0.03	0.36	1.72	3.5	4.53	0.3	0.0	0.08	0.04		0.020	0.008	0.019	99.4
URL-2-	256.3	72.6	0.18	14.4	0.6	0.8	0.03	0.28	1.60	3.5	4.32	0.4	0.2	0.07	0.09		0.020	0.007	0.017	99.3
-	448.3	71.5	0.24	14.9	0.7	1.0	0.03	0.51	1.83	3.8	4.57	0.3	0.1	0.11	0.09		0.021	0.009	0.023	100.0
-	586.2	73.4	0.15	13.8	0.6	0.7	0.02	0.15	1.35	3.4	4.70	1.5	0.3	0.06	0.09		0.021	0.009	0.017	100.4
-	705.9	74.3	0.14	13.7	0.3	0.6	0.02	0.24	1.43	3.4	3.90	0.2	0.1	0.05	0.08		0.017	0.004	0.013	98.6
-	798.9	72.2	0.23	15.2	0.7	1.1	0.04	0.40	1.58	4.2	4.54	0.2	0.1	0.07	0.08		0.019	0.009	0.023	100.8
-	871.8	71.9	0.17	14.4	0.4	0.9	0.03	0.28	1.52	4.3	4.33	0.2	0.2	0.09	0.08		0.019	0.008	0.018	99.1
-	1001.4	73.0	0.21	14.4	0.4	1.0	0.03	0.28	1.64	3.6	4.31	0.2	0.2	0.08	0.08		0.019	0.007	0.019	99.7
-	1095.1	73.3	0.17	13.9	0.1	1.1	0.03	0.38	1.58	3.6	4.40	0.2	0.1	0.08	0.08		0.018	0.006	0.018	99.2
URL-5-	16.6	73.5	0.11	14.1	0.1	0.7	0.02	0.28	1.44	3.8	4.75	0.2	0.1	0.06	0.08		0.014	0.003	0.011	99.4
-	77.1	73.8	0.16	14.2	0.2	1.2	0.03	0.44	1.43	3.3	4.61	0.2	0.1	0.07	0.04		0.018	0.008	0.015	99.9
-	108.7	74.7	0.04	13.2	0.4		0.01	0.03	0.67	2.5	6.92	0.1	0.0	0.02	0.04		0.023	0.001	0.006	98.8
-	127.1	72.0	0.23	14.4	0.4	1.3	0.04	0.54	1.78	3.9	4.06	0.2	0.0	0.11	0.04		0.015	0.007	0.023	99.2
-	157.3	73.7	0.14	14.5	0.1	1.1	0.03	0.42	1.50	3.5	4.79	0.2	0.0	0.08	0.04		0.016	0.008	0.015	100.2
-	199.4	72.7	0.20	14.2	0.4	1.1	0.03	0.50	1.54	3.8	4.59	0.2	0.0	0.09	0.04		0.016	0.008	0.017	99.7
-	246.9	72.4	0.18	15.1	0.1	1.2	0.03	0.50	1.85	3.9	3.76	0.2	0.0	0.09	0.04		0.013	0.008	0.016	99.1
-	289.9	72.7	0.15	14.4	0.3	0.8	0.03	0.38	1.85	3.7	3.90	0.2	0.0	0.06	0.04		0.015	0.009	0.017	98.7
-	334.1	68.1	0.28	15.0	0.4	2.5	0.06	1.52	2.48	4.4	2.99	0.4	0.0	0.21	0.10		0.017	0.011	0.015	98.7
-	370.2	72.0	0.19	15.1	0.5	1.1	0.02	0.36	1.88	4.4	4.09	0.2	0.0	0.07	0.04		0.015	0.007	0.019	100.2
-	451.2	71.7	0.40	13.6	0.7	1.6	0.03	0.45	1.71	2.7	5.08	0.3	0.0	0.01	0.04		0.015	0.007	0.040	98.7
-	497.1	70.6	0.45	14.0	0.6	2.0	0.03	0.61	1.84	3.1	4.95	0.3	0.00	0.13	0.04		0.015	0.008	0.044	98.9
WN-1 -	138.5	71.5	0.25	14.1	0.7	1.1	0.04	0.52	1.31	3.7	4.56	0.0	0.1	0.08	0.01		0.017	0.003		
-	160.8	70.6	0.26	14.9	0.9	0.8	0.04	0.46	1.39	3.9	4.52	0.0	0.1	0.06	0.0		0.017	0.004		
-	223.4	71.2	0.21	15.0	0.7	0.8	0.04	0.33	1.35	3.7	4.66	0.0	0.1	0.05	0.0		0.016	0.003		
-	245.1	70.7	0.17	15.3	0.8	0.7	0.03	0.28	1.37	3.7	4.69	0.0	0.1	0.06	0.0		0.016	0.002		
-	294.4	72.8	0.18	14.1	0.7	0.7	0.03	0.36	1.05	3.1	4.81	0.0	0.1	0.05	0.0		0.016	0.004		
-	303.4	74.6	0.16	13.5	0.5	0.7	0.03	0.38	1.01	3.3	4.76	0.0	0.0	0.04	0.0		0.017	0.002		
-	345.4	75.6	0.14	14.1	0.6	0.5	0.03	0.29	1.10	3.4	4.28	0.0	0.1	0.03	0.0		0.015	0.002		
-	384.1	70.7	0.16	15.8	0.9	0.5	0.03	0.36	1.47	4.2	4.51	0.0	0.1	0.05	0.0		0.017	0.003		
-	410.6	73.4	0.13	13.3	0.0	3.2	0.02	0.28	1.06	3.6	4.41	0.0	0.1	0.01	0.0		0.015	0.001		
-	460.5	72.7	0.17	14.1	0.5	0.8	0.03	0.36	1.14	3.3	4.79	0.1	0.0	0.03	0.0		0.016	0.002		
WN-2 -	24.65	74.4	0.13	14.3	0.9	0.4	0.02	0.29	1.08	3.2	4.55	0.0	0.1	0.04	0.0		0.015	0.002		
-	55.35	67.7	0.46	14.9	1.1	2.7	0.13	2.51	3.24	3.7	1.92	0.4	0.1	0.17	0.02		0.013	0.008		
-	85.2	68.4	0.49	15.5	1.2	2.8	0.17	2.58	3.44	3.4	1.84	0.3	0.1	0.19	0.0		0.012	0.008		
-	98.4	73.8	0.17	13.7	1.1	0.8	0.03	0.30	1.18	3.4	4.11	0.8	0.2	0.05	0.0		0.013	0.003		
-	124.6	74.6	0.14	13.8	1.0	0.2	0.02	0.28	1.02	3.3	4.59	0.0	0.1	0.03	0.0		0.015	0.002		
-	145.75	71.4	0.18	15.3	0.5	0.9	0.02	0.45	1.34	3.9	4.84	0.0	0.1	0.06	0.0		0.018	0.002		
WN-4 -	408.9	73.7	0.17	14.2	0.6	0.8	0.03	0.24	1.26	3.9	4.70	0.6	0.1	0.04	0.0	0.062	0.022	0.006	
-	468.95	72.6	0.17	14.3	0.5	0.8	0.03	0.33	1.30	3.8	5.10	0.6	0.1	0.06	0.01	0.070	0.022	0.007	
-	482.6	73.4	0.14	13.6	0.2	0.9	0.03	0.32	1.24	3.6	4.65	0.4	0.1	0.04	0.0	0.065	0.021	0.006	
-	505.77	71.5	0.13	14.4	0.3	0.7	0.03	0.36	1.23	3.9	5.04	0.5	0.1	0.02	0.00	0.066	0.021	0.004	
-	551.15	73.0	0.10	14.0	0.0	0.7	0.00	0.40	1.00	4.0	5.00	0.6	0.2	0.10	0.0	1.000	0.000	0.000	
-	564.3	70.3	0.22	14.9	0.4	1.4	0.04	0.45	1.54	4.1	4.62	0.6	0.1	0.07	0.0	0.064	0.022	0.006	
-	603.8	73.2	0.17	13.7	0.5	0.9	0.03	0.24	1.29	3.4	4.62	0.4	0.2	0.07	0.0	0.062	0.021	0.004	
-	631.4	72.2	0.14	14.1	0.2	0.9	0.02	0.17	1.35	3.7	4.98	0.5	0.1	0.06	0.0	0.068	0.021	0.005	
-	660.0	72.1	0.14	14.0	0.4	0.8	0.02	0.25	1.25	3.6	5.12	0.5	0.1	0.05	0.0	0.066	0.023	0.006	
-	692.6	74.0	0.16	14.0	0.4	0.7	0.03	0.35	1.34	3.6	4.66	0.4	0.0	0.03	0.0	0.062	0.023	0.006	
-	719.5	73.4	0.14	14.3	0.0	1.0	0.02	0.29	1.30	3.6	5.26	0.6	0.1	0.05	0.0	0.077	0.023	0.003	
-	746.9	70.5	0.23	14.4	0.6	1.2	0.04	0.44	1.56	3.7	4.95	0.3	0.0	0.08	0.01	0.103	0.025	0.006	
-	789.6	72.0	0.20	15.0	1.0	1.0	0.00	0.30	2.00	4.0	5.00	0.2	0.00	0.10	0.0	0.100	0.000	0.000	
-	809.4	71.0	0.30	15.0	1.0	1.2	0.00	0.60	2.00	4.0	5.00	0.1	0.0	0.10	0.0	0.100	0.000	0.000	
-	840.9	71.1	0.23	14.3	0.6	1.2	0.03	0.47	1.47	3.6	4.98	0.1	0.0	0.08	0.0	0.103	0.025	0.010	
-	863.1	70.0	0.20	15.0	0.0	0.6	0.00	0.40	0.50	3.0	9.00	0.2	0.00	0.10	0.0	0.200	0.000	0.000	
-	906.5	73.5	0.20	13.8	0.5	1.3	0.03	0.27	1.43	3.7	4.56	0.1	0.0	0.09	0.0	0.088	0.024	0.000	
-	928.6	73.2	0.19	13.7	0.4	1.2	0.03	0.32	1.34	4.0	4.75	0.3	0.00	0.07	0.0	0.88	0.027	0.007	

* Samples showing BA results by XRF before Nov. 1980
** Samples analyzed in April, 1983
▸ Estimate only due to unusual composition

Table 4. C.I.P.W. normative mineral composition for standard samples from Lac du Bonnet batholith

Sample No.	Q	C	OR	AB	AN	MGB	FEBI	MT	HM	TN	AP	PR	CC	WO	
URL-1	46.25	34.38	1.56	27.16	26.62	6.21	1.44	1.30	0.74	0.00	0.30	0.22	0.08	0.00	0.00
	68.35	32.94	1.55	25.99	28.49	6.49	1.62	1.52	0.74	0.00	0.37	0.22	0.08	0.00	0.00
	100.45	31.14	2.24	22.63	28.24	6.78	2.70	3.48	1.32	0.00	1.05	0.34	0.08	0.00	0.00
	131.15	31.48	1.19	25.15	31.26	6.71	1.38	1.61	0.58	0.00	0.36	0.19	0.07	0.00	0.00
	176.95	32.40	1.64	27.84	26.79	6.83	1.11	2.12	0.59	0.00	0.43	0.17	0.08	0.00	0.00
	230.35	30.74	1.46	19.23	33.55	8.89	1.75	2.52	1.03	0.00	0.49	0.26	0.08	0.00	0.00
	259.15	13.87	1.53	30.09	26.51	5.99	1.27	1.95	0.15	0.00	0.36	0.19	0.08	0.00	0.00
	302.25	25.78	0.72	21.76	39.13	7.86	1.36	2.09	0.58	0.00	0.40	0.24	0.08	0.00	0.00
	357.95	33.54	0.90	28.02	28.38	5.92	1.01	0.74	0.88	0.00	0.39	0.14	0.08	0.00	0.00
	397.65	31.12	1.60	13.17	34.90	9.38	3.89	4.42	0.29	0.00	0.75	0.41	0.08	0.00	0.00
	443.05	21.77	0.00	29.13	38.32	6.38	1.10	1.32	1.31	0.00	0.34	0.19	0.08	0.00	0.07
	496.55	29.89	0.63	25.03	31.91	6.96	1.48	3.03	0.30	0.00	0.47	0.22	0.08	0.00	0.00
	577.25	32.16	0.69	24.12	31.61	7.12	1.30	1.97	0.44	0.00	0.36	0.14	0.08	0.00	0.00
	592.45	41.54	1.33	41.81	12.04	1.15	0.30	1.00	0.44	0.00	0.22	0.10	0.08	0.00	0.00
	615.75	31.74	1.38	19.36	33.60	7.27	1.85	2.96	0.74	0.00	0.75	0.27	0.08	0.00	0.00
	662.25	31.85	1.27	24.99	29.95	7.40	1.20	2.20	0.44	0.00	0.43	0.19	0.08	0.00	0.00
URL-2	256.30	33.64	1.95	24.64	30.04	5.67	0.94	1.07	0.88	0.00	0.39	0.17	0.17	0.46	
	448.30	28.96	1.19	25.22	32.38	6.94	1.70	1.42	1.02	0.00	0.51	0.26	0.17	0.23	
	586.20	34.31	1.72	27.35	29.16	3.94	0.50	0.81	0.88	0.00	0.32	0.14	0.17	0.69	
	705.90	37.74	1.85	22.39	29.30	5.75	0.81	0.92	0.44	0.00	0.30	0.12	0.15	0.23	
	798.90	27.56	1.19	24.87	35.41	5.93	1.32	1.68	1.01	0.00	0.48	0.17	0.15	0.23	
	871.80	28.41	0.78	24.45	36.93	5.17	0.94	1.54	0.59	0.00	0.37	0.22	0.15	0.46	
	1001.40	33.27	1.77	24.05	30.72	5.67	0.93	1.76	0.58	0.00	0.45	0.19	0.15	0.46	
	1095.10	33.18	1.00	24.14	30.85	6.17	1.27	2.31	0.15	0.00	0.36	0.19	0.15	0.23	
URL-5	16.60	30.98	0.61	26.94	32.48	5.80	0.93	1.36	0.15	0.00	0.24	0.14	0.15	0.23	
	77.10	34.66	1.79	24.93	28.06	5.47	1.46	2.52	0.29	0.00	0.34	0.17	0.08	0.23	
	108.70	32.83	0.49	41.45	21.48	3.10	0.10	0.00	0.00	0.41	0.09	0.05	0.02	0.08	
	127.10	30.85	0.92	21.58	33.43	7.41	1.81	2.59	0.59	0.00	0.49	0.26	0.08	0.00	
	157.30	32.18	1.20	26.03	29.66	6.44	1.39	2.39	0.15	0.00	0.30	0.19	0.07	0.00	
	199.40	30.41	0.66	25.02	32.44	6.41	1.67	2.09	0.59	0.00	0.43	0.22	0.08	0.00	
	246.90	32.05	1.71	19.78	33.30	8.04	1.67	2.64	0.15	0.00	0.38	0.22	0.08	0.00	
	289.90	33.15	1.08	21.71	31.86	8.41	1.28	1.52	0.44	0.00	0.32	0.14	0.08	0.00	
	334.10	27.12	0.90	11.48	38.02	10.17	5.12	5.31	0.59	0.00	0.60	0.51	0.19	0.00	
	370.20	27.16	0.43	22.31	37.35	8.23	1.19	1.95	0.73	0.00	0.40	0.17	0.08	0.00	
	451.20	34.19	1.35	27.91	23.32	6.50	1.52	2.97	1.04	0.00	0.86	0.27	0.08	0.00	
	497.10	30.95	1.10	26.10	26.71	6.84	2.05	4.00	0.89	0.00	0.97	0.31	0.08	0.00	
WN-1	138.50	31.07	1.47	25.23	31.98	4.57	1.75	1.91	1.04	0.00	0.54	0.19	0.02	0.23	
	160.80	28.90	1.81	25.64	33.72	5.08	1.55	1.02	1.33	0.00	0.56	0.15	0.00	0.23	
	223.40	30.32	2.07	26.53	31.82	5.09	1.11	1.22	1.03	0.00	0.45	0.12	0.00	0.23	
	245.10	29.50	2.29	27.18	32.00	5.29	0.94	0.87	1.19	0.00	0.37	0.15	0.00	0.23	
	294.40	35.40	2.52	27.63	26.79	3.70	1.21	0.97	1.04	0.00	0.39	0.12	0.00	0.23	
	303.40	35.64	1.40	26.89	28.22	4.24	1.27	1.17	0.73	0.00	0.34	0.10	0.00	0.00	
	345.40	37.51	2.35	24.26	28.73	4.14	0.96	0.60	0.87	0.00	0.30	0.07	0.00	0.23	
	384.10	26.74	1.92	25.99	35.99	5.85	1.20	0.29	1.32	0.00	0.34	0.12	0.00	0.23	
	410.60	33.89	1.10	21.37	30.62	4.13	0.93	7.42	0.00	0.00	0.28	0.02	0.00	0.23	
	460.50	33.67	1.74	27.28	28.53	4.97	1.21	1.42	0.74	0.00	0.37	0.07	0.00	0.00	
WN	224.65	36.78	2.66	26.37	27.25	4.04	0.96	0.04	1.31	0.00	0.28	0.10	0.00	0.23	
	55.35	33.49	2.10	2.62	31.78	12.92	8.41	5.38	1.62	0.00	0.99	0.41	0.04	0.23	
	85.20	35.41	2.97	1.80	28.78	13.49	8.52	5.58	1.74	0.00	1.04	0.45	0.00	0.23	
	98.40	37.03	2.34	23.45	29.12	3.72	1.00	0.78	1.61	0.00	0.36	0.12	0.00	0.46	
	124.60	36.47	2.05	26.74	28.19	3.78	0.93	0.00	0.72	0.52	0.30	0.07	0.00	0.23	
	145.75	28.20	1.83	26.95	33.35	5.05	1.50	1.61	0.73	0.00	0.38	0.14	0.00	0.23	
WN-4	408.90	31.23	1.01	26.60	32.78	4.78	0.78	1.33	0.82	0.00	0.35	0.10	0.00	0.23	
	468.95	29.12	0.76	28.90	32.38	4.37	1.09	1.34	0.77	0.00	0.35	0.15	0.01	0.23	
	482.60	33.15	0.92	26.14	30.98	4.86	1.08	1.96	0.28	0.00	0.30	0.10	0.00	0.24	
	505.77	28.05	0.76	26.89	33.59	5.01	1.21	1.39	0.43	0.00	0.29	0.04	0.00	0.23	CM=.01
	551.15	29.82	1.04	28.15	34.37	2.74	1.34	1.63	0.00	0.00	0.21	0.24	0.00	0.46	
	564.30	25.39	0.95	25.13	35.76	5.86	1.52	2.95	0.57	0.00	0.47	0.18	0.00	0.23	
	603.80	34.43	1.67	26.31	29.22	4.22	0.79	1.61	0.77	0.00	0.36	0.16	0.00	0.46	
	631.40	29.86	0.72	28.56	32.01	5.33	0.59	1.91	0.35	0.00	0.30	0.14	0.00	0.23	
	660.00	29.94	0.72	29.48	31.40	4.87	0.85	1.55	0.52	0.00	0.31	0.12	0.00	0.23	
	692.60	32.73	0.84	26.21	30.84	5.95	1.15	1.21	0.64	0.00	0.34	0.07	0.00	0.00	
	719.50	30.28	0.90	29.29	30.55	5.01	0.95	2.30	0.07	0.00	0.29	0.13	0.00	0.23	
WN-4	746.90	27.95	0.62	27.67	31.85	6.59	1.49	2.27	0.84	0.00	0.49	0.19	0.02	0.00	
	789.60	25.69	0.00	27.99	33.66	8.16	0.99	1.5	1.44	0.00	0.42	0.24	0.00	0.00	
	809.40	24.80	0.00	27.17	33.81	8.20	1.98	1.72	1.45	0.00	0.63	0.24	0.00	0.00	
	840.90	28.76	0.79	27.66	31.31	6.05	1.58	2.23	0.92	0.00	0.50	0.20	0.00	0.00	
	863.10	17.75	0.00	52.15	25.71	0.89	1.34	1.39	0.00	0.00	0.43	0.24	0.00	0.00	
	906.50	32.22	0.68	25.09	31.39	5.81	0.88	2.50	0.71	0.00	0.43	0.22	0.00	0.00	
	928.60	29.37	0.00	26.17	34.42	5.21	1.07	2.39	0.64	0.00	0.41	0.17	0.00	0.00	

Q = Quartz
C = Corundum
OR = Orthoclase
AB = Albite
AN = Anorthite

MT = Magnetite
AP = Apatite
PY = Pyrite
CC = Calcite
MGBI = Phlogopite

FEBI = Annite
TN = Sphene
WO = Wolframite
HM = Hematite

Table 3. Modal analysis of standard samples from boreholes URL-1, -2, -5 and WN-1, -2, -4

Sample No.	PC	KF	QZ	Hb	Bi	MU	CH	EP	AP	ALLA	CB	OP	SP	RU	ZR	To
URL-1	40.3	35.25	34.76	26.02	-	2.30	0.49	0.25	tr	tr	0.08	tr	0.25	tr	tr	tr	
	66.4	35.69	25.84	29.79	-	4.36	0.74	0.49	tr	tr	tr	tr	0.08	tr	tr	tr	
	100.3	38.93	26.31	27.21	-	4.67	1.15	0.41	0.25	tr	0.33	0.08	0.37	0.08	tr	tr	
	131.2	37.35	31.20	25.59	-	2.57	0.41	0.16	0.16	tr	0.08	tr	0.08	0.08	tr	tr	
	177.0	34.16	31.36	33.43	-	2.87	0.66	0.33	tr	tr	0.16	tr	0.25	0.08	tr	tr	
	223.1	45.76	23.99	27.03	-	2.05	0.25	0.08	0.08	tr	0.25	tr	0.49	tr	tr	tr	
	270.4	38.42	26.19	29.97	-	3.53	0.57	0.66	0.08	tr	0.25	tr	0.16	0.16	tr	tr	
	294.2	46.84	19.31	28.51	-	4.19	0.16	0.33	0.25	tr	0.08	tr	0.25	0.08	tr	tr	
	329.6	33.99	36.37	26.77	-	1.97	0.41	0.25	0.08	tr	tr	tr	0.16	tr	tr	tr	
	382.3	41.88	26.38	26.62	-	2.22	0.41	0.08	0.16	tr	tr	tr	0.25	tr	tr	tr	
	357.1	38.47	25.70	32.67	-	2.07	0.08	0.33	tr	tr	tr	tr	0.66	tr	tr	tr	
	397.0	48.63	8.33	28.71	-	10.00	0.41	0.07	0.07	0.14	tr	0.07	0.07	0.27	tr	tr	
	443.1	31.20	43.19	22.99	-	1.55	0.16	0.25	0.16	tr	0.08	tr	0.41	tr	tr	tr	
	496.6	40.13	28.99	26.78	-	2.87	0.49	0.25	tr	tr	0.08	tr	0.41	tr	tr	tr	
	527.3	40.03	22.40	32.65	-	3.86	0.49	0.08	tr	tr	0.08	0.08	0.33	tr	tr	tr	
	592.3	38.35	23.31	30.69	-	0.16	0.33	0.33	0.08	tr	0.33	tr	0.90	tr	tr	tr	
	615.3	43.07	24.28	26.50	-	3.36	0.32	0.49	0.08	tr	0.25	tr	0.98	0.16	tr	tr	
	662.6	47.57	24.58	22.41	-	4.21	0.58	0.15	0.07	tr	tr	tr	0.36	0.07	tr	tr	
URL-2	256.2	33.67	31.29	30.53	-	2.60	0.37	0.55	0.08	tr	tr	tr	0.47	tr	tr	tr	
	443.2	32.40	36.46	25.47	-	4.15	0.34	0.51	tr	0.17	0.25	tr	0.25	tr	tr	tr	
	586.1	34.94	30.89	30.36	-	2.67	0.38	0.31	tr	tr	0.15	tr	0.31	-	tr	tr	
	703.8	41.79	18.20	36.85	-	2.54	0.31	0.08	-	tr	0.15	tr	0.08	-	tr	tr	
	795.8	43.55	22.19	28.68	-	4.44	0.16	0.41	0.08	tr	tr	tr	0.49	tr	tr	tr	
	871.1	41.71	22.72	30.72	-	4.04	0.24	0.24	-	tr	tr	tr	0.32	-	tr	tr	
	1091.3	38.90	31.30	23.49	-	4.68	0.16	0.32	0.08	0.16	tr	tr	0.80	tr	tr	tr	
	1095.0	41.04	24.64	30.00	-	3.20	0.32	0.40	tr	tr	tr	tr	0.24	tr	tr	tr	
URL-5	16.5	47.36	18.95	29.49	-	2.97	0.53	0.23	tr	tr	0.08	tr	0.33	tr	tr	tr	
	77.0	35.38	30.47	30.96	-	1.30	0.66	0.25	tr	tr	tr	tr	0.49	tr	tr	tr	
	103.2	18.93	54.89	25.72	-	-	0.08	0.16	-	-	-	0.16	tr	-	tr	-	
	126.8	41.18	24.77	29.45	-	3.77	0.16	0.25	0.08	tr	0.08	tr	0.25	tr	tr	tr	
	156.9	42.40	24.90	27.98	-	3.20	0.49	0.41	0.08	tr	tr	tr	0.58	tr	tr	tr	
	199.3	37.69	31.36	26.52	-	3.04	0.33	0.66	0.08	tr	0.08	tr	0.25	tr	tr	tr	
	246.8	48.93	16.61	29.85	-	2.47	0.66	0.58	0.25	tr	0.08	tr	0.33	tr	tr	tr	
	279.9	48.07	20.77	27.37	-	2.23	0.49	0.25	0.08	tr	tr	tr	0.74	tr	tr	tr	
	289.8	46.76	19.36	29.94	-	2.37	0.74	0.08	tr	tr	0.16	tr	0.08	tr	tr	tr	
	333.9	52.34	5.59	28.59	-	12.00	0.41	0.16	0.16	0.08	0.33	0.16	0.16	tr	tr	tr	
	370.1	38.72	26.74	28.96	-	3.94	0.74	0.41	tr	0.08	tr	tr	0.91	tr	tr	tr	
	451.1	35.49	29.19	33.92	-	4.74	0.50	0.33	tr	tr	tr	tr	0.58	0.25	tr	tr	
	497.0	35.22	29.38	32.43	-	6.73	0.08	0.16	tr	tr	0.25	tr	0.25	0.49	tr	tr	
WN-1	133.4P	43.6	24.6	26.0	-	3.4	1.2	0.5	tr	tr	tr	tr	0.5	tr	-	tr	
	160.7P	44.8	23.9	25.3	-	3.5	0.8	0.5	tr	tr	tr	tr	0.8	tr	-	tr	
	223.7P	47.7	19.2	28.7	-	2.6	0.9	tr	tr	tr	tr	tr	tr	tr	-	tr	
	245.8P	27.1	50.3	19.7	-	1.8	tr	0.5	tr	tr	-	tr	tr	tr	-	tr	
	298.3P	40.3	29.4	28.4	-	4.0	1.5	0.4	tr	0.4	tr	tr	0.5	tr	-	tr	
	303.3P	32.9	32.7	30.0	-	2.9	0.8	0.5	tr	tr	tr	tr	0.4	tr	-	tr	
	345.3P	33.6	33.6	28.3	-	2.6	1.0	0.3	tr	tr	-	tr	0.6	tr	-	tr	
	334.6P	43.4	24.6	25.6	-	3.4	1.4	0.6	tr	tr	-	tr	0.7	tr	-	tr	tr
	410.5P	33.2	31.6	31.3	-	2.2	1.0	0.5	tr	tr	-	tr	0.3	tr	-	tr	
	460.8P	30.4	31.2	34.9	-	2.3	tr	tr	tr	tr	-	tr	tr	tr	-	tr	
WN-2	24.55-P	39.5	21.5	35.5	-	1.7	0.5	0.8	tr	tr	-	tr	tr	tr	-	tr	-
	55.25-P	52.1	tr	28.7	-	25.6	tr	tr	1.4	0.4	tr	tr	0.3	tr	-	tr	tr
	85.1-P	50.5	tr	29.1	tr	17.6	tr	tr	2.0	tr	tr	tr	0.2	0.4	-	tr	tr
	98.3-P	37.0	26.8	31.6	-	1.5	0.8	0.8	tr	tr	-	tr	1.1	tr	-	tr	-
	124.5-P	33.3	28.5	34.4	-	2.1	0.8	0.5	tr	tr	-	tr	tr	tr	-	tr	-
	145.65P	33.7	30.4	29.1	-	4.6	1.1	0.5	tr	tr	-	tr	0.6	tr	-	tr	-
WN-4	408.8-Pg1	28.1	36.5	32.0	-	1.9	0.9	0.4	tr	tr	tr	tr	tr	tr	-	tr	
	408.8-Pg2	31.3	36.3	27.6	-	2.0	2.0	1.0	tr	tr	tr	tr	tr	tr	-	tr	
	468.85-Pg1		38.0	28.7	28.1	-	3.1	0.5	0.5	0.3	tr	tr	tr	0.5	tr	-	tr
	468.85-Pg2		39.1	26.5	34.7	-	2.9	1.1	0.5	tr	tr	tr	tr	tr	tr	-	tr
	482.2-Pg1	21.0	41.0	33.6	-	1.6	0.9	tr	tr	tr	tr	tr	tr	tr	-	tr	
	482.2-Pg2	34.3	33.4	27.7	-	1.8	0.7	tr	tr	tr	tr	tr	tr	tr	-	tr	
	505.37-Pg1		33.8	27.4	39.8	-	2.2	1.1	0.8	tr	tr	tr	tr	tr	tr	-	tr
	505.37-Pg2		35.0	30.7	31.8	-	1.3	1.0	0.3	0.3	tr	tr	tr	tr	tr	-	tr
	551.05-Pg1		33.6	34.5	28.0	-	2.2	1.1	0.4	tr	tr	tr	tr	0.2	tr	-	tr
	551.05-Pg2		35.2	31.1	28.8	-	2.9	1.1	0.5	tr	tr	tr	tr	0.3	tr	-	tr
	564.2-Pg1	41.1	26.8	24.9	-	3.7	1.3	1.5	tr	tr	tr	tr	0.5	tr	-	tr	
	564.2-Pg2	38.8	25.4	28.6	-	5.2	1.2	0.4	tr	tr	tr	tr	0.4	tr	-	tr	
	603.7-Pg1	37.2	28.8	31.5	-	1.6	0.3	0.2	tr	tr	tr	tr	0.4	tr	-	tr	
	603.7-Pg2	40.0	24.5	30.2	-	3.5	1.0	tr	tr	tr	tr	tr	0.3	tr	-	tr	
WN-4	631.3-Pg1	33.8	28.6	32.4	-	3.5	0.9	0.3	tr	tr	tr	tr	0.5	tr	-	tr	
	631.3-Pg2	32.6	27.4	37.3	-	1.6	0.3	0.5	tr	tr	tr	tr	0.3	tr	-	tr	
	659.9-Pg1	33.2	23.8	37.7	-	3.6	0.8	0.2	tr	tr	tr	tr	0.5	tr	-	tr	
	659.9-Pg2	36.4	27.3	32.0	-	2.8	0.7	tr	tr	tr	tr	tr	0.3	tr	-	tr	
	692.3-Pg1	36.4	29.0	29.4	-	3.6	0.6	tr	0.4	tr	tr	tr	0.4	tr	-	tr	
	692.3-Pg2	37.9	29.0	31.0	-	0.6	0.3	0.3	tr	tr	tr	tr	0.3	tr	-	tr	
	719.4-Pg1	25.2	42.3	27.7	-	2.3	0.7	0.5	tr	tr	tr	tr	0.9	tr	-	tr	
	719.4-Pg2	38.5	31.7	30.2	-	2.2	0.7	0.2	0.3	tr	tr	tr	0.3	tr	-	tr	
	746.8-Pg1	37.0	27.7	31.3	-	2.6	0.7	0.2	tr	tr	tr	tr	tr	tr	-	tr	
	746.8-Pg2	37.6	23.1	38.1	-	3.3	0.9	0.3	tr	tr	tr	tr	tr	tr	-	tr	
	789.3-Pg1	36.3	30.9	27.2	-	2.7	1.3	0.7	tr	tr	tr	tr	tr	tr	-	tr	
WN-4	809.3-Pg1	34.2	29.0	29.2	-	5.6	1.0	0.4	tr	tr	tr	tr	0.3	tr	-	tr	
	809.3-Pg2	34.2	27.1	29.7	-	5.2	1.9	1.1	tr	tr	tr	tr	0.9	tr	-	tr	
	840.8-Pg1	36.3	27.9	29.0	-	4.6	0.6	0.3	tr	tr	tr	tr	0.8	tr	-	tr	
	840.8-Pg2	28.5	32.0	31.9	-	5.6	1.2	0.4	tr	tr	tr	tr	0.4	tr	-	tr	
	863.3-Pg1	18.9	36.6	22.1	-	1.3	0.4	tr	tr	tr	tr	tr	tr	tr	-	tr	
	863.3-Pg2	17.3	32.3	27.7	-	0.8	0.4	0.8	tr	tr	tr	tr	0.6	tr	-	tr	
	906.4-Pg1	39.3	22.2	31.4	-	5.4	0.7	0.5	0.2	tr	tr	tr	0.2	tr	-	tr	
	906.4-Pg2	33.8	36.3	25.2	-	3.3	0.6	tr	0.3	tr	tr	tr	tr	tr	-	tr	
	928.2-Pg1	38.2	30.4	25.2	-	5.0	0.4	tr	tr	tr	tr	tr	0.4	tr	-	tr	
	928.2-Pg2	30.6	37.4	27.8	-	1.8	1.0	tr	tr	tr	tr	tr	1.0	tr	-	tr	

PC = Plagioclase Feldspar
KF = Potassium Feldspar
QZ = Quartz
Hb = Hornblende
Bi = Biotite
MU = Muscovite
CH = Chlorite
EP = Epidote
AP = Apatite
AL = Allanite
CB = Carbonate
OP = Opaques
SP = Sphene
RU = Rutile
ZR = Zircon
TO = Tourmaline
FL = Flourite
AN = Anorthite

CHAPTER III

PHYSICAL PROPERTIES

4. MECHANICAL PROPERTIES

MECHANICAL, THERMOMECHANICAL AND JOINT PROPERTIES OF ROCK SAMPLES FROM THE LAC DU BONNET BATHOLITH, MANITOBA

A. Annor* and R. Jackson**
Canada Centre for Mineral and Energy Technology,
555 Booth St., Ottawa, Ontario K1A 0G1

*: Canada Centre for Mineral and Energy Technology (CANMET), 555 Booth St., Ottawa, Ontario K1A 0G1.
**: Atomic Energy of Canada Limited on attachment to CANMET, Ottawa.

MECHANICAL, THERMOMECHANICAL AND JOINT PROPERTIES OF ROCK SAMPLES FROM THE LAC DU BONNET BATHOLITH, MANITOBA

A. Annor and R. Jackson
Canada Centre for Mineral and Energy Technology,
555 Booth St., Ottawa, Ontario K1A 0G1

INTRODUCTION

The method currently under consideration within the Canadian Nuclear Fuel Waste Management Program (NFWMP) for the safe, long term disposal of high-level nuclear wastes, involves the excavation of a vault deep in an igneous formation. For the safe design and construction of such an underground structure, an understanding of the stability and deformability of the rock mass is required in terms of not only the normal and in situ ambient conditions of stress and temperature, but also the anticipated stress and temperature changes that could result from the vault and waste emplacement. An important consideration in terms of engineering analysis and design is the ability to predict the combined behavior of the intact material and joint system in the rock as a unit. For this purpose, various mechanical tests such as bulk density, acoustic velocity, uniaxial and triaxial compressive strength, Brazilian tensile strength, slip and joint tests have been carried out at ambient and elevated temperatures. Samples from various research areas associated with the Canadian Nuclear Fuel Waste Management Program (NFWMP) were tested. Contributions to the uniaxial test data have also been made by Ontario Hydro (McKay, 1980). The principal objectives of the study have been to provide data and data interpretations for in situ test planning, vault design studies, and geosphere modelling activities. This paper discusses the mechanical and thermomechanical behaviour of rock samples from the URL and WN sites within the Lac du Bonnet batholith and how this data may be used to predict the combined behaviour of the intact rock and joint system as a unit.

As a general rule, an initial step in the geotechnical evaluation of a rock mass for purposes of underground construction is performing standardized

laboratory tests (CANMET[1], ISRM[2], and ASTM[3]-specifications) on drill core samples taken from the intended location of the structure. The test results provide input data for numerical models required to predict the deformation characteristics and failure envelope of the rock mass. The numerical model predictions can then be verified by carrying out in situ measurements at the proposed location of the structure. In addition to contributing to model predictions, the laboratory determined mechanical rock properties can be combined with geological field data and other geomechanical information to develop a characterization system for assessing rock mass performance.

Differences can exist between the numerical model predictions and the in situ geomechanical observations either because of the limitations of the numerical models used, or the gross uncertainties in the laboratory determined test results. It is important, therefore, that laboratory mechanical properties be determined under conditions that are as close as possible to in situ conditions of moisture content, stress and rock structure.

It is expected that the information in this paper will be used by AECL to plan in situ geotechnical experiments at the Underground Research Laboratory (URL) facility currently under construction in the Lac du Bonnet batholith. Additionally, the test results will permit the evaluation of the predictive capabilities of numerical models currently under development by AECL to estimate rock mass stability and deformability on the basis of in situ geotechnical testing at URL.

SAMPLES AND SAMPLE PREPARATION

The samples used for these tests and investigations consist of "standard engineering samples" (those representative of the borehole lithology), and "extended engineering samples" (those obtained from areas of specific geotechnical interest such as the proposed operating levels of URL). Geological descriptions of these samples are provided elsewhere by Chernis (1979), Chernis et al. (1978) and Wong (1984).

Sample preparation and testing procedures that were followed conformed as closely as possible with standards and specifications put forth by the American

[1] Canada Centre for Mineral and Energy Technology
[2] International Society for Rock Mechanics
[3] American Society for Testing and Materials

Society for Testing and Materials (ASTM, 1971a, 1971b), the CANMET Pit Slope Manual Specifications (Gyenge and Herget, 1977), the International Society for Rock Mechanics Suggested Methods (Brown, 1981) and the Procedures for Characterizing Rock Joints and Samples (Barton and Bakhtar, 1983).

Sample Preparation

Cylindrical test samples (44.5 mm diam.) with length to diameter (L/D) ratios ranging between 2.0 and 2.2 were used for the uniaxial compression and acoustic velocity measurements. With regards to the Brazilian tensile strength measurements, discs with thickness to diameter ratio of about 0.5 were tested. In the case of triaxial compression tests, the (L/D) ratio of the test samples was about 2.8.

Samples were cut slightly larger than their final dimensions using a water cooled diamond-saw. Sample ends were then ground until they were parallel to each other (within ±0.03 mm), and at right angles to the longitudinal axis. This was accomplished by using hardened steel jigs and a lapping wheel.

Samples used for measurements at ambient room temperature were generally tested in a dry state, after surface air drying in the laboratory. However, there were some special tests in which the effects of moisture content and specimen conditioning on the mechanical behaviour of rocks were examined. For these tests, samples were either oven dried or saturated with water prior to testing (Jackson, 1983; Jackson and Annor, 1985).

Strain gauges oriented to measure axial and circumferential strains were placed on opposite sides of the specimen for uniaxial elastic deformation measurements. The axial and circumferential gauges were connected in series to form single active gauges. The gauges were used in a half bridge configuration for strain measurements. The gauges used were from the BLH Electronics Co. SR-4, FAE series and Micro-Measurements Division, EA-500 BH series.

Triaxial Intact Test Samples

In the case of triaxial compression measurements, the prepared samples were encased in a thin wall (about 0.15 mm) annealed copper sleeve whose inner

dimensions were close to that of the sample. The jacket was then sealed mechanically by forcing steel rings over the tapered surfaces of a loading piston and a lower steel platen. This sealing arrangement prevented the pressurizing medium from entering the pores of the rock.

After initial sample preparation similar to that described above, the specimens to be used for triaxial slip tests were cut through the mid-height at a pre-determined angle of about 37° (Gyenge and Herget, 1977), with respect to the cylindrical core axis. The two halves of the sample were encased in an annealed copper sleeve ensuring that the surfaces of discontinuity matched perfectly. The sample and jacket assembly was attached to the piston and the bottom platen in the same manner as used for the intact samples. Sample preparation methods are described in further detail by Annor et al. (1981).

METHOD OF MEASUREMENT AND DATA ANALYSIS

Scope of Measurements

Three types of tests were carried out to obtain the strength and deformational properties (Young's Modulus and Poisson's ratio) of the rock samples. These are uniaxial compressive strength measurements, Brazilian tensile strength tests and triaxial compression measurements on intact and jointed (saw-cut) samples. The confining pressure and temperature ranges of the tests were 3.5 to 70 MPa and 21° to 200°C, respectively. Compressive wave velocity measurements were carried out to assist with the data interpretation and also to identify possible inter-relationships between static and dynamic elastic properties with stress. Such information could assist in seismic monitoring for possible changes in rock mass deformability with stress and temperature. Bulk densities of the test samples were also calculated to better compare the mechanical properties test results with data in the published literature, considering the wide range of values listed for granitic rock (Lama and Vutukuri, 1978; Touloukian and Ho, 1981). Additionally, in accordance with the Barton and Bakhtar (1983) procedure, rock joint parameters were determined on drilled core samples containing natural joints. The data would permit an eventual development of a rock mass characterization system for the Lac du Bonnet formation and also for estimating the strength and deformational behaviour of the joint systems in the rock under variable stress and temperature conditions.

Finally, tests were carried out to determine the effects of factors such as moisture content, specimen conditioning, stress relaxation and stress path on the mechanical properties data, as well as strength and deformational anisotropy characteristics of the test samples.

Bulk Density Measurements

Bulk density was estimated from direct measurements of the mass and volume of each sample. An electronic balance (resolution, 0.01 grams) and calipers (resolution 0.1 mm) were used for the measurements. Density was calculated by dividing the mass of the rock by its volume.

Acoustic Velocity (Compressive Wave) Determinations

The testing equipment for acoustic wave velocity measurements consisted of transmitting and receiving specimen platens containing piezoelectric transducers, a high voltage pulse generator, a Tektronix Type 555 dual beam oscilloscope with a delay sweep and a time base resolution of 0.1 μs/cm, and a Hoek triaxial cell. For a group of test samples, the velocity equipment was used with a 1.33 MN hydraulic press to measure specimen compressive wave transit time as a function of applied axial load. For a second group of samples, the equipment was used in conjunction with a Hoek cell and (a manually operated) hydraulic pump, and a loading frame, to measure sample compressive wave transit time as a function of applied hydrostatic pressure.

In the axial compressive wave velocity measurements, the test sample and transducer assembly was placed between the platens of the hydraulic press and was axially stressed in increments of about 2.7 MPa to a maximum stress level. Due to the structural limitations of the transducer platens, the maximum applied stress was about 43 MPa. At each incremental stress level, the transmitter piezoelectric transducer, excited by the pulse generator, was used to send compressive waves into the specimen which were detected by the receiver piezoelectric platen.

Compressive wave measurements as a function of variable hydrostatic pressure were similar to the axial dilational wave velocity tests described above. However, there were slight differnces in procedure used. Initially, the prepared

samples were encased in a rubber membrane, and then placed into the triaxial Hoek cell. Phenyl salicylate was used to attach the pulsing heads to the test sample. A hydraulic loading frame was used to apply a small axial load through the pulsing heads to a pre-established stress value. Confining pressure was then applied until a pressure equilibrium was reached. Measurements were carried out over the confining pressure range of 0.1 to 30 MPa. Delayed arrival time readings were taken at various pre-determined stress levels.

Prior to individual specimen time delay measurements, the transmitting and receiving transducers were placed in direct contact with each other and the zero delay time of the sonic system determined. The acoustic velocity measurements are described by Annor et al. (1979), Annor (1984), Jackson and Boudreau (1983) and Annor and Jackson (1985). Sample acoustic velocity (V_p) at each stress level was determined from the relationship:

$$V_p = \frac{L}{(t_p - t_o)} \qquad (1)$$

where:

L = sample length (m)

t_p = time of transit (s)

t_o = zero delay time of the sonic systems.

Uniaxial Compressive Strength Measurements

The equipment used by CANMET to measure axial and circumferential sample deformation under applied axial load consisted of Bruel and Kjaer Type 1526 strain indicators, Phillips PR9302 strain bridges, a Hewlett Packard 7046 B-X-Y recorder and a Mosley Autograph 2FRA X-Y recorder. The strain bridges were used in a half-bridge configuration for strain measurements. Axial and circumferential strain gauges were used to provide voltage analog outputs of strains produced in a test sample by axial loading. These analogs were then used to drive the two Y-axes of the recorders independently. The resulting stress-strain curves were used to determine Young's modulus and Poisson's ratio for each sample tested. The axial load was increased until failure occurred.

The standard samples for URL-1 and WN-4 boreholes were tested by Ontario Hydro (McKay, 1980, 1982). A method similar to that described above was used for carrying out the uniaxial compression measurements. Each sample was, however, subjected to three loading and unloading cycles to compensate for de-stressing effects on the sample due to drilling. Reported Young's modulus and Poisson's ratio were determined from the average value of the final two loading and unloading cycles (McKay, 1980, 1982).

In addition to the standard uniaxial compression measurements described above, two independent studies were undertaken to investigate the effects of sample moisture content on the laboratory determined uniaxial strength and deformational properties and de-stressing effects on the observed mechanical behaviour of test samples.

The methods of testing were identical to those already described under acoustic wave velocity and uniaxial compression measurements. The test samples were, however, conditioned differently prior to testing. A group of test specimens were heated slowly (0.35°C/min) to about 63°C and cooled down to room temperature before testing. For a second group of samples, the specimens were surface air dried in the laboratory before testing. A third group of specimens were immersed in water for at least seven days prior to testing. A detailed description of the test procedure is given in the following reports: Jackson (1983) and Jackson and Annor (1985). The calculated uniaxial compressive strengths, Poisson's ratios and Young's moduli of the three sample populations were then compared.

Young's modulus was calculated for each sample by determining the value of the tangent to the axial strain curve at 50% of failure load. The ratio of the tangent to the axial strain curve to the tangent to the transverse strain curve at 50% failure load was used to determine the sample's Poisson's ratio. The ultimate compressive strength of each sample was calculated by dividing the sample failure load by sample cross-sectional area.

Brazilian Tensile Strength Measurements

Brazilian tensile strength measurements were performed according to ASTM specification C496-71. The test specimens were loaded diametrically between two hardened steel platens in a hydraulic press. Load was applied until the

specimen failed. In the case of tests to determine strength anisotropy of the Lac du Bonnet granitic samples, the test specimens were selected such that two specimens were adjacent to each other along the core axis. One of the two samples was loaded along the core reference line, while the other was loaded perpendicular to this line.

The tensile strength of a specimen was derived from the relationship:

$$\sigma_t = \frac{2P}{\pi Dt} \qquad (2)$$

where:

σ_t = specimen tensile strength (MPa)
P = failure load (MN)
D = diameter of disc (m)
t = thickness of disc (m).

Triaxial Compression Measurements of Intact Samples

Equipment and procedures used for triaxial compression measurements at ambient room and elevated temperatures are described in the reports by Annor et al. (1981), Jackson (1984a,b) and Jackson and Boudreau (1983). In the measurements described by Jackson (1984a,b), two pairs of foil strain gauges (suitable for measurements at ambient room and elevated temperatures) were attached to the opposite sides of the sample-jacket assembly. The gauges were oriented to measure axial strains and were connected in two half-bridge configurations so that two independent axial deformation measurements could be obtained.

Samples were tested in an elevated temperature and pressure triaxial chamber described by Annor et al. (1981). A temperature range of 21° to 200°C and a confining pressure range of 0.1 and 70 MPa were used for the measurements. Sample heating rates were kept below 2°C/min to minimize thermal cracking (Richter and Simmons, 1974). Axial load was applied with a hydraulic press. The pressure vessel was externally heated with a cylindrical muffle furnace. Strain readings were simultaneously recorded on a Hewlett Packard 7046 B-X-Y recorder and by a Fluke data logger. A recording interval of 10 seconds was used for data logging on the Fluke data logger.

Prior to the actual measurements, a series of calibration tests were conducted using a hardened steel dummy sample. The objective of the calibration tests was to evaluate the strain gauge performance with increasing temperature and confining pressure. The combined effects of temperature and pressure on the performance of the strain gauges was found to be insignificant over the temperature and pressure ranges of the tests (Jackson and Boudreau, 1983).

In the measurements described by Annor et al. (1981), a linear variable differential transformer (LVDT) transducer was used to measure axial deformation of the samples under applied axial load. The recorded deformation measurements applied to the total deformation of the apparatus and sample. In order to obtain sample deformation, the apparatus was initially calibrated at room temperature and over the confining pressure range of 0 to 35 MPa. This was accomplished by testing a cylindrical steel dummy sample at the anticipated conditions of temperature and confining pressure and observing the differences in deformation between the assembly and the steel cylinder throughout the loading range. The apparatus deformation was deducted from the total deformation at each increment of load to obtain the specimen deformation. The axial strain of a sample was computed from the test sample deformation.

Tangent Young's modulus was estimated at 50% of failure strength. Triaxial compressive strength of a sample was calculated by dividing the deviatoral stress (stress difference) at failure by sample cross-sectional area.

All the triaxial compression tests at elevated temperatures described in this report are based on samples which were heated to the desired test temperature prior to the application of confining pressure. The effects of temperature or pressure cycling on the mechanical behaviour of test samples were not investigated in this study. Test results presented to date do not include investigations involving simultaneous heating of samples under confining pressure. The effects of pore pressure on rock properties have not yet been examined.

Triaxial Compression Measurements on Saw-Cut Samples (Slip Tests)

The procedures followed for sample-piston assembly and heating of samples are the same as for the intact samples. At the testing stage, however, the confining pressure was slowly applied to the lowest of four pre-determined test

levels, while a small axial load was applied simultaneously. The axial load was applied continuously at a slow rate until sliding occurred. At the point of failure corresponding to a stress level, the confining pressure was varied to the next stage. The axial load was re-applied until noticeable slippage had occurred. The slip tests were performed over the temperature range of 21° to 200°C and the confining pressure range of 0.75 MPa to 31.5 MPa. The test procedure is described by Gyenge and Herget (1977) and reported by Annor et al. (1981).

The parameters of interest were shear stress and normal stress acting across the surface of the sample failure plane. Normal stress was computed from the relationship:

$$\sigma_n = \frac{(\sigma_1 + \sigma_3)}{2} - \frac{(\sigma_1 - \sigma_3)}{2} \cos 2\beta \qquad (3)$$

where:

σ_n = normal stress (MPa)

Shear stress (τ) was computed from the equation:

$$\tau = \frac{(\sigma_1 - \sigma_3)}{2} \sin 2\beta \qquad (4)$$

Rock Joint Characterization Procedure

The procedure used to characterize the Lac du Bonnet drill core samples containing natural joints are described by Barton and Bakhtar (1983) and Jackson et al. (1985) and involved the following basic index tests:

(i) joint recognition;
(ii) joint wall compressive strength (JCS) determination;
(iii) joint roughness coefficient (JRC) determination by profiling and by tilt testing;
(iv) the estimation of the residual friction angle (ϕ_r).

Joint recognition involved the inspection, selection and identification of suitable jointed samples for characterization. A core sample was judged suitable for characterization if the joint angle of intersection with the core axis was less than 45°. The selected joint samples were identified for parameters such as joint orientation, the type of and thickness of joint infilling material and the degree of weathering.

Joint wall compressive strength was measured using a Schmidt (model-L) hammer. The core sample was bolted to a heavy metal base using a constant torque of about 35 Nm. Ten rebound values were taken with the Schmidt hammer on each sample. The strength was derived from the mean value of the highest 50% of the results. (Discounting of the low values resulted in automatic elimination of spurious "drummy" rebound values). Miller's (1965) technique for interpreting rock strength from the Schmidt hammer test results was used to derive joint wall compressive strength for each sample. This technique requires that the rock density is either estimated or somehow calculated. Joint roughness coefficient (JRC) was determined for each sample on the basis of tilt tests or by profiling, depending on the condition of the joint surfaces and joint orientation. These procedures are described in detail by Jackson et al. (1985).

RESULTS AND DISCUSSION

Results

The data for the density and uniaxial mechanical tests are listed in Table 7. The data for the Brazilian tensile tests and triaxial mechanical tests (intact and saw-cut) are listed in Tables 8, 9 and 10, respectively. The results for the joint tests are compiled in Tables 11 and 12. Tables 7-12 are found in the Appendix.

Density

Density is an index property of a rock and it can be used to infer the mechanical behaviour of a rock mass. Low density values often indicate a rock with high deformability, low strength, high permeability and porosity. The mean and standard deviation for the bulk density values for Lac du Bonnet rock samples are summarized in Table 1, in terms of the combined, as well as separate data for URL and WN sites.

These values compare favourably with published literature density values for rock types with similar mineralogical compositions as found in the Lac du Bonnet batholith (Touloukian and Ho, 1981). A profile of density variation with depth is provided in Figure 1 and indicates a slight variation of rock density with increasing depth. A scatter of density values appears in the upper zones of the Lac du Bonnet batholith and can be attributed to the effects of rock alteration and compositional changes. A histogram of density values for the Lac du Bonnet rock samples is provided in Figure 2.

General Trends of Uniaxial Mechanical Property Data

The uniaxial strength and deformational properties of the Lac du Bonnet batholith can generally be classified into three principal zones on the basis of mechanical properties test data available to date. These are upper, transitional and lower zones. These subdivisions also conform approximately to the three principal zones of rock alteration found in the Lac du Bonnet batholith (Kamineni et al. 1984). In terms of variation of rock alteration with depth at the WN and URL sites, a pink granite occurs in the upper regions followed by a zone of greenish-grey granite which changes to grey granite at depth. Differences noted in

Table 1. Bulk density values for Lac du Bonnet rock samples (after Drury, 1986)

		Density	
Location	Number of samples	Mean (Mg/m^3)	Std. deviation (Mg/m^3)
WN	227	2.64	0.06
URL	352	2.63	0.04
Combined	579	2.63	0.05

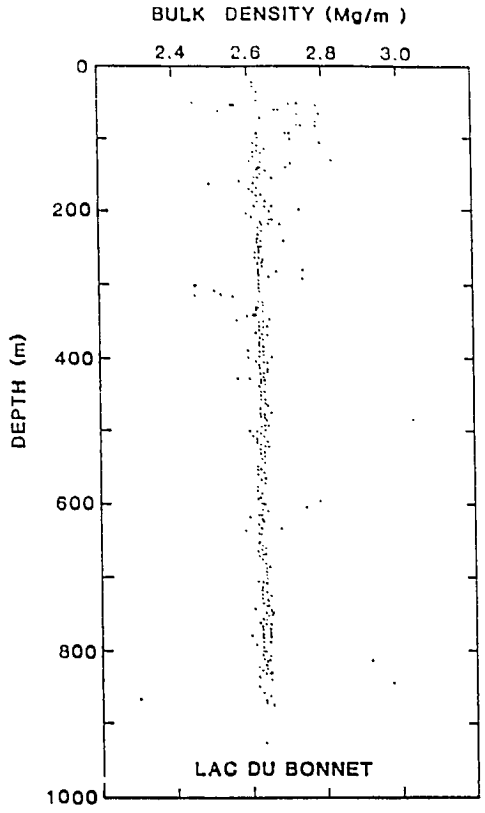

Figure 1. Depth profile of bulk density for Lac du Bonnet rock samples (after Drury, 1986).

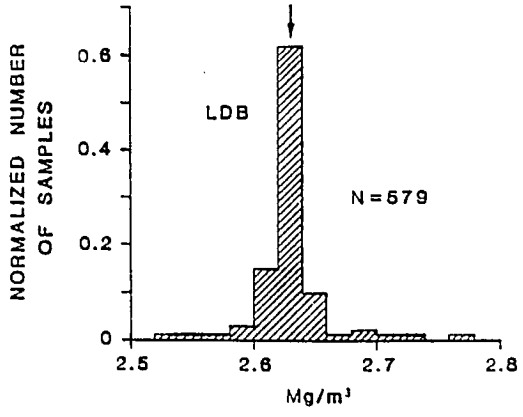

Figure 2. Histogram of bulk density for Lac du Bonnet rock samples.

strength, deformation (Young's modulus and Poisson's ratio) and acoustic velocity properties conform to these variations. The uniaxial mechanical properties are summarized in Figure 3. The results show trends of decreasing compressive strength, compressive wave velocity and Young's modulus and increasing Poisson's ratio with increasing depth. The range, mean and standard deviation values for the uniaxial mechanical properties are summarized in Table 2. Distributions of the properties in terms of sample populations are also provided in Figure 4-8. These values compare favourably with published data in the referenced literature for granitic rocks with similar mineralogical compositions as the Lac du Bonnet formation. Considering the wide range of data on granitic rocks, the test results were compared only with those published for granitic rock with densities in the range of 2.61 to 2.68 Mg/m^3. A summary of the published reference data is provided in Table 3.

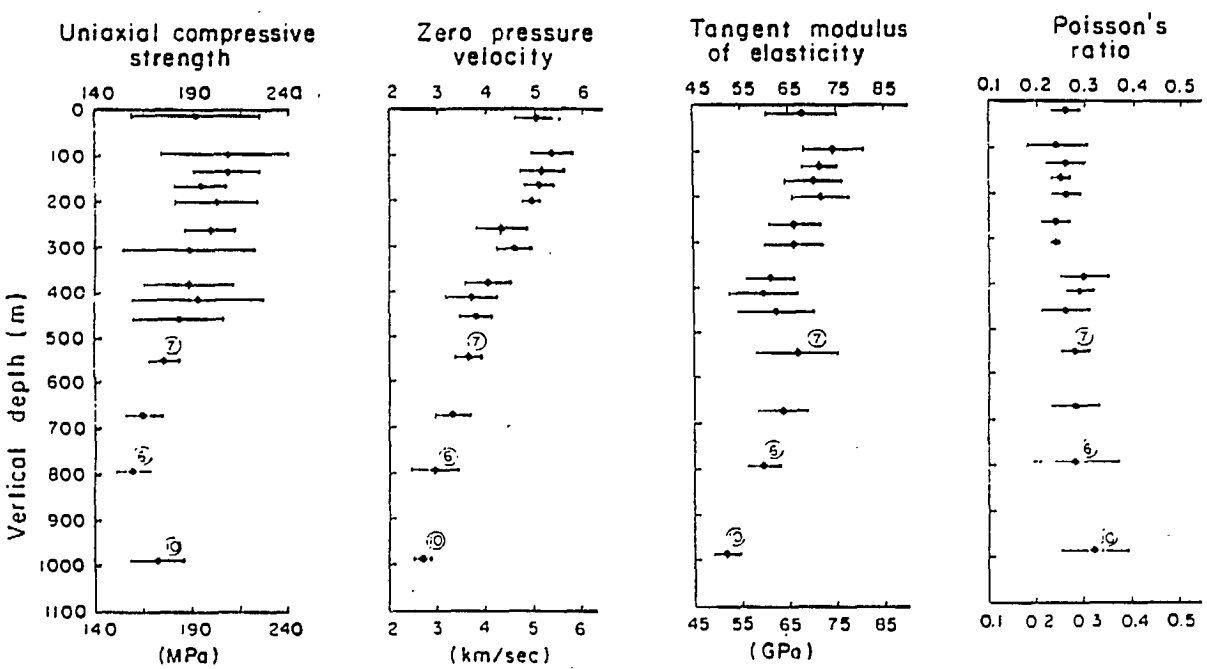

Figure 3. Variation of unconfined mechanical properties of Lac du Bonnet granite with depth.

Table 2. Statistical summary of uniaxial mechanical rock properties data for Lac du Bonnet samples

Borehole and rock type identification		Uniaxial comp. strength (MPa)	Young's modulus (GPa)	Poisson's ratio	P-wave velocity at zero pressure (km/s)	Brazilian tensile strength (MPa)
WN-1,2						
URL-B9, B10, 1,	N	81	81	81		39
2, 5, 7	Mean	200	69.1	0.26		9.32
(Pink) granite	Std. dev.	22	5.8	0.04		1.26
Upper zone	Range	134-248	53.6-86.0	0.18-0.44		6.17-12.07
WN-1, 4	N	34	34	34		26
URL-1, 2, 5, 6	Mean	179	61.8	0.28		10.38
	Std. dev.	27	9.4	0.04		1.67
Transitional zone	Range	95-231	27.4-78.7	0.20-0.39		5.96-12.99
	N	20	20	20		14
WN-4	Mean	167	55.7	0.30		8.72
URL-2	Std. dev.	13	4.9	0.07		1.98
(Grey) granite	Range	147-198	46.6-64.4	0.13-0.43		6.22-11.52
Lower zone						
Combined data	N	137	137	137	156	47
including	Mean	190	65.3	0.27	4.43	9.56
Special Test	Std. dev.	25	8.4	0.05	0.92	1.88
Results						

N = number of samples or specimens

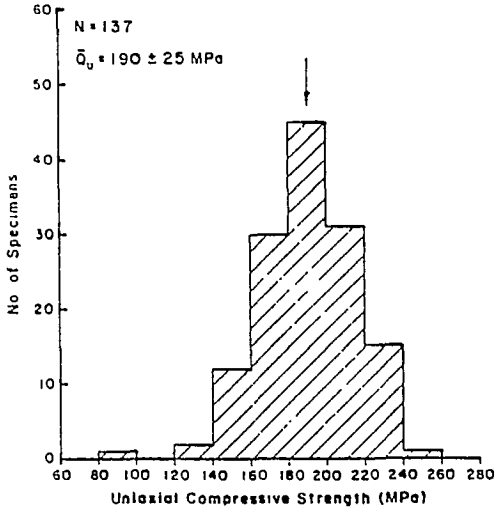

Figure 4. Histogram of uniaxial compressive strength for Lac du Bonnet rock samples.

In terms of engineering classification, the Lac du Bonnet granitic formation falls into the range of high strength to very high strength rock, with medium modulus ratio (Figure 9). This is based on the Deere and Miller (1966) classification for intact rocks. Modulus ratio for this classification is defined as follows:

$$\text{Modulus ratio} = \frac{\text{Tangential Young's modulus at 50\% ultimate strength}}{\text{Uniaxial compressive strength}}$$

and is interpreted as follows:

High modulus ratio: >500
Medium modulus ratio: 200 < modulus < 500
Low modulus ratio: <200

The uniaxial test data are also reported by Annor and Geller (1979); Annor et al. (1979); Jackson (1982a,b, 1983, 1984b); Jackson and Boudreau (1983); Jackson and Annor (1985a); Annor and Jackson (1982); Annor and Jackson (1985).

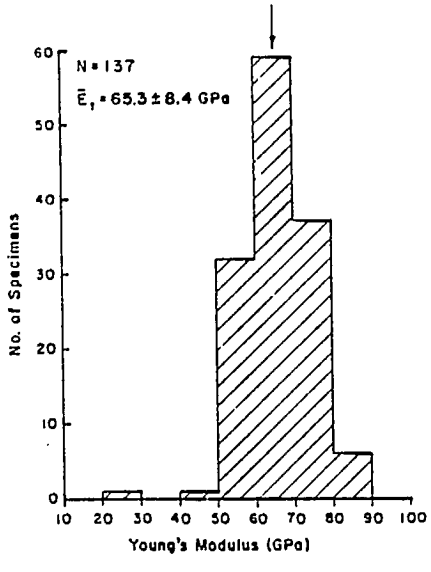

Figure 5. Histogram of Young's modulus for Lac du Bonnet rock samples.

Triaxial Mechanical Properties and the Effect of Temperature

A comprehensive study of the triaxial mechanical behaviour of the Lac du Bonnet formation with temperature was limited to the pink granite. The samples originated from the proposed operating levels at URL (50 m to 260 m depths), and at the WN drill site, where two horizons from drill hole WN-1 (150 m to 175 m and 320 m to 350 m depth) were, at one time, being considered for a shallow underground facility (Larocque and Annor, 1982). The effects of pressure and temperature on the mechanical behaviour of the samples are also described in detail elsewhere by the following investigators: Annor et al. (1981); Annor and Jackson (1982); Jackson (1984a,b); Annor and Jackson (1985) and Jackson and Annor (1985). Generalized observations are as follows:

In general, triaxial compressive strengths of the tested samples increased with increasing confining pressure (Figure 10) and decreased with increasing temperature (Figure 11). There was about a 55 percent increase in triaxial compressive strength over the confining pressure range of 3.5 to 17.0 MPa, and a further increase of 31% from 17 to 35 MPa confining pressure.

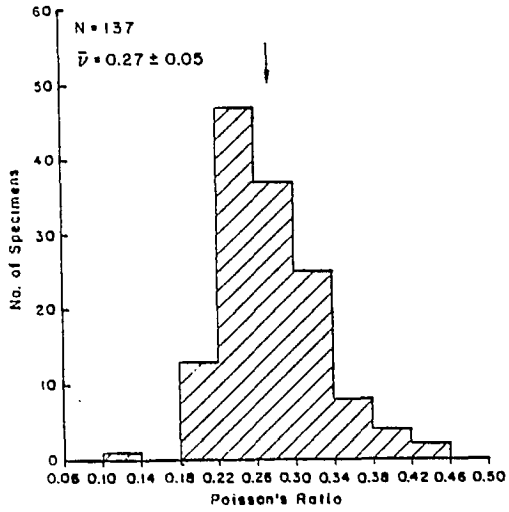

Figure 6. Histogram of Poisson's ratio for Lac du Bonnet samples.

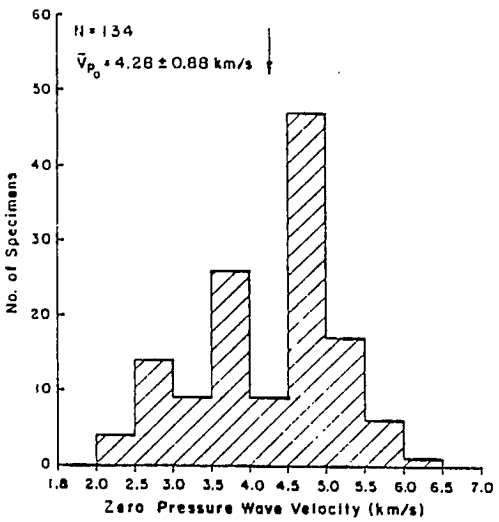

Figure 7. Histogram of zero pressure compressive wave velocity.

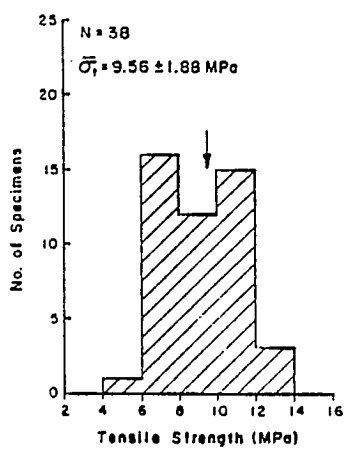

Figure 8. Histogram of tensile strength for Lac du Bonnet rock samples.

The greatest decrease in triaxial compressive strength with increasing temperature (15%) occurred at the lowest confining pressure (3.5 MPa). It should be noted that 3.5 MPa represents a confining pressure level well below the value of the overburden pressure equivalent to sample depth, or the mean tensile strength of the rock. At higher confining pressure levels reductions in strength with increasing temperature were minimal. This suggests that under in situ confining pressure levels temperature levels of up to 200°C may not have significant effect on rock strength.

Generally, the eleastic moduli of hard crystalline, or homogeneous rocks with low porosities are not affected by confining pressure (Lama and Vutukuri, 1978). This is supported by the present study where at 21°C, Young's modulus remained relatively unchanged with increasing confining pressure for the pink granitic samples (Figure 12). The Young's moduli determined for gray granite specimens, however, do show some stress dependency, exhibiting lower values at the lower confining pressures. The mean Young's modulus value at 21°C for the pink Lac du Bonnet granitic samples was 67 GPa.

Table 3. Summary of literature-referenced uniaxial mechanical properties data for granitic rocks

Location and granitic rock description	Bulk density (ρ) (Mg/m^3)	Uniaxial compressive strength (Qu)	Young's modulus (E) (GPa)	Poisson's ratio (ν)	Tensile strength (σ_t) (MPa)	Reference
1. U.S.A. Md., contains quartz and syenite	2.65	251.0	52.54	-	20.68 (R)	(Wueker, 1956)
2. U.S.A. Pikes Peak, dense mg	2.65	226.0	70.6	0.18	11.90	(Miller, 1965)
3. U.S.A. Barre, Vt., contains quartz	2.64	194.4	61.4	0.39	10.70	(Miller, 1965)
4. U.S.A. Rose Granite Pedernal Hills, N.M.	2.64	308.0	69.64	0.28	-	(Michalopoulos and Triandafilidis, 1976)
5. U.S.A. Raymond, Calif. Raymond granite	2.64	178.0	58.6	0.26	-	(Michalopoulos and Triandafilidis, 1976)
6. Canada, Grenville Que, Cg, 80% orthoclase	2.61	172.0	65.8	-	-	(Coates & Parsons, 1966)
7. U.S.A. Barre, Vt., Perpendicular to bedding	2.64	200.0	58.6	-	13.50	(Hawkes et al. 1973)
8. U.S.A., Mg-Cg (a)	2.66	228.9	30.4*	0.04*	19.99	(Obert et al. 1946)
(b)	2.66	225.2	27.4*	0.10	25.37 (R)	
(c)	2.66	244.1	44.2*	0.31*	18.41 (R)	
9. Atikokan granite Mean	2.65	212.0	73.9	0.26	-	(Annor and Jackson, 1982)
(N=50 samples) Std. dev.	0.02	26.0	15.2	0.05		

Numbers 1-8 were compiled and condensed from: Lama and Vutukuri (1978).
*Dynamic test values.
(R) refers to test in bending.

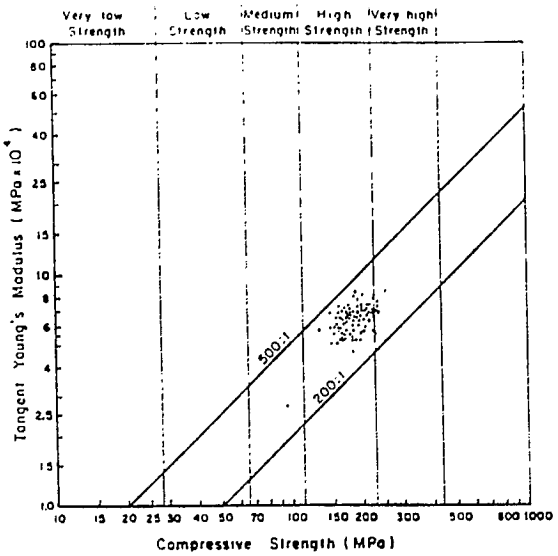

Figure 9. Engineering classification of intact rock for Lac du Bonnet samples.

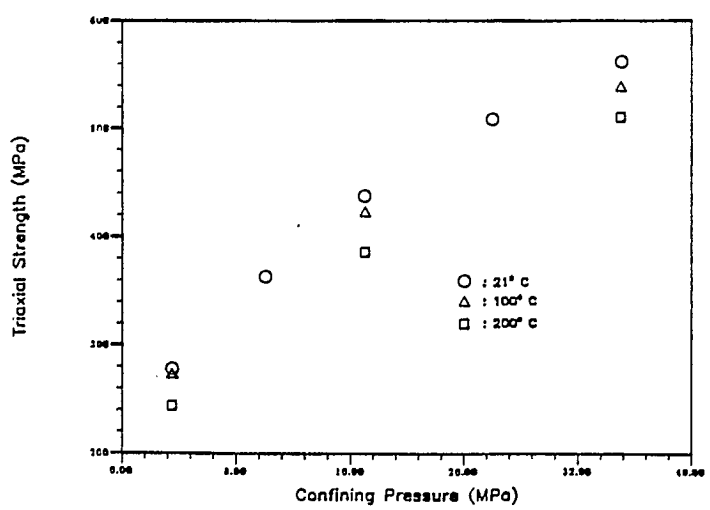

Figure 10. Variation of mean triaxial compressive strength with confining pressure for Lac du Bonnet granitic samples.

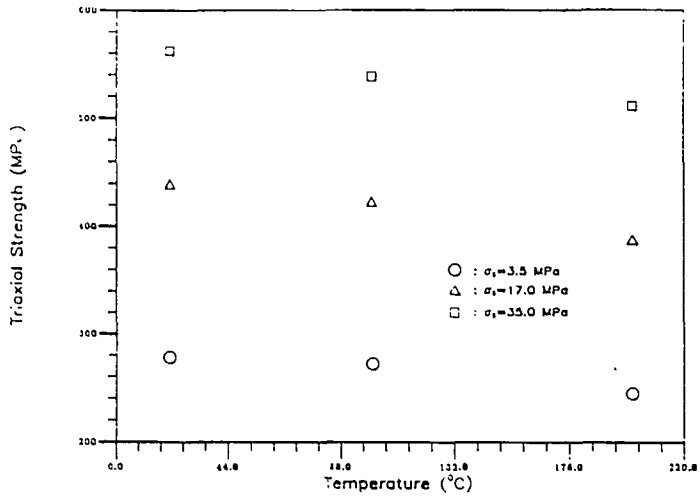

Figure 11. Variation of mean triaxial compressive strength vs temperature for Lac du Bonnet granitic samples.

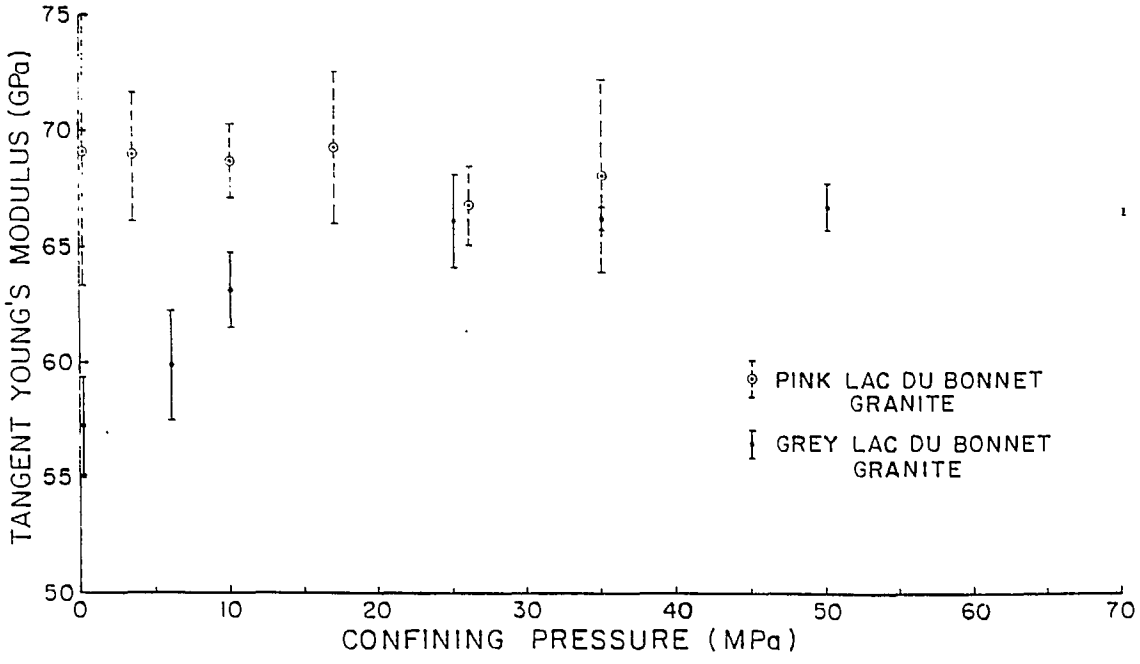

Figure 12. Variation of Young's modulus of elasticity with confining pressure for Lac du Bonnet samples.

The Young's modulus values for the Lac du Bonnet pink granitic specimens appear relatively independent of stress at 21° and 100°C. At 200°C, however, this stress dependency became more pronounced, especially at a confining pressure of 3.5 MPa (Figure 13). This can be attributed to the increase in rock crack porosity as a result of thermal crack development.

The variation of Young's modulus with temperature suggests that temperature levels of up to 200°C may not affect the elastic properties of the Lac du Bonnet rock mass under in situ stress conditions. However, at confining pressures below equivalent in situ overburden pressure the rock could exhibit some decrease in modulus of elasticity with increasing temperature. A statistical summary of the triaxial compressive strength and deformational properties data is provided in Table 4.

Effects of Stress Relaxation

To examine the effects of stress relaxation on the strength, elastic deformation and acoustic wave test data, core samples were selected from the

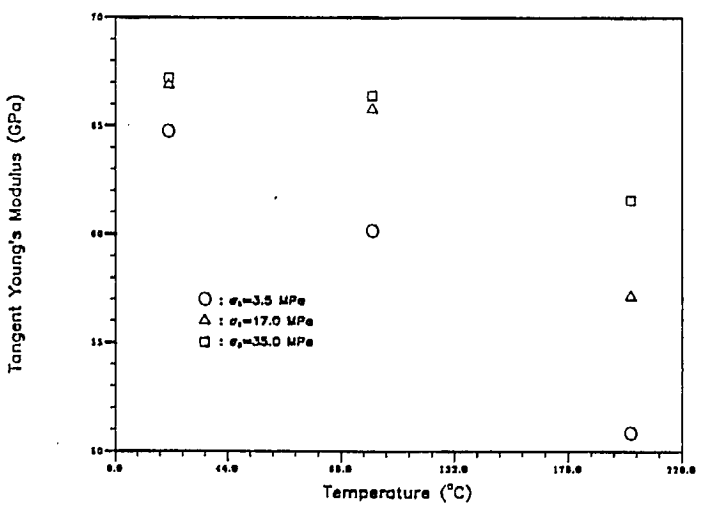

Figure 13. Variation of mean Young's modulus of elasticity with temperature for Lac du Bonnet granitic samples.

lower reaches of the deepest boreholes at the URL site for various mechanical properties tests (Jackson and Boudreau, 1983). Data from triaxial compression tests and compressive wave velocity measurements carried out over the confining pressure range of 5 to 70 MPa were obtained. These values corresponded to the estimated principal stresses prevailing at the sample depths of interest at the URL site (Herget, 1980). The core samples used for the investigations originated from boreholes URL-2, URL-5 and URL-6.

Unlike porous rocks, the elastic modulus of homogeneous crystalline rock such as granite does not generally indicate a large stress dependency (Lama and Vutukuri, 1978). The variation of Young's modulus with confining pressure can therefore provide some indication of the degree of microcracking to which a test sample has been subjected. The Lac du Bonnet grey granitic samples have shown considerable stress dependency effects at low confining pressure levels in comparison with the pink granitic samples (Jackson and Boudreau, 1983; Annor and Jackson, 1985). The stress dependency effects were eliminated at confining pressure levels equivalent to the depth of the test sample (Figure 12).

Table 4. Statistical Summary of triaxial strength and deformational properties data for Lac du Bonnet granitic samples

	Temperature (°C)								
	(21°C)			(100°C)			(200°C)		
Confining Pressure (MPa)	N	Mean	Std. dev.	N	Mean	Std. dev.	N	Mean	Std. dev.
				Triaxial Strength (MPa)					
3.5	13	278	19	8	272	8	10	244	22
10.0	12	363	14						
17.0	11	438	22	8	422	14	8	286	23
26.0	8	509	18						
35.0	18	562	27	8	538	18	8	511	18
				Young's Modulus (GPa)					
3.5	13	64.73	8.53	8	60.14	10.29	10	50.84	8.79
5.0	2	59.93							
10.0	12	59.93							
15.0	2	58.0	0.34						
17.0	11	66.88	5.23	8	65.77	8.26	8	57.15	12.10
25.0	2	66.11	2.75						
26.0	8	66.81	1.71						
30.0	2	61.12	0.30						
35.0	18	67.20	3.59	8	66.39	11.69	9	61.57	11.05
50.0	6	66.70	2.07						
55.0	2	66.37							
70.0	2	66.71							

Std. dev. = standard deviation
*Estimated values
N = number of samples or specimens

These observations suggest that the grey granitic samples from the deeper levels of the boreholes were subjected to significant stress relaxation after drilling. This resulted in increased sample porosity and consequently low Young's modulus values. In terms of the possible in situ rock mass behaviour, the stress relaxation could result in slabbing along the walls of an underground excavation located at deeper levels of the formation.

Compressive wave velocity measurements can also provide a means of identifying structural changes that can occur in a core sample due to drilling induced damage or stress relaxation. The compressive wave velocity investigations of the Lac du Bonnet core samples have indicated that pressures exceeding the overburden stress equivalent to sampling depth are required to restore the laboratory compressive wave velocity values to within the projected range of the in situ values measured by Huang and Hunter (1980). The differences between the laboratory and in situ compressive wave velocities can be attributed to stress relaxation effects and to differences in moisture content between the laboratory samples and the rock mass in situ (Annor, 1984). Studies have shown that increasing the moisture content of Lac du Bonnet granitic samples resulted in at least a 25% increase in their compressive wave velocities. Increased moisture content however, seems to have no pronounced effect on unconfined strength and deformation properties of these samples (Jackson and Annor, 1985).

The lack of agreement between in situ observations and predictions based on laboratory mechanical properties can be attributed not only to relaxation effects, but also to scale effects. The predictions can, however, be improved if larger size samples are tested in the laboratory. In the absence of such tests, appropriate scale reduction factors may be applied to laboratory small scale test data to provide an estimate of in situ values.

Some empirical relationships have been developed by various investigators for relating laboratory rock strength and deformation property values to in situ conditions. For example, Hoek and Brown (1980) have suggested the following relationship for relating laboratory small scale data to in situ rock mass unconfined strength:

$$Qu = Qu_{50} \left(\frac{50}{d}\right)^{0.18} \qquad (5)$$

where:

Qu_{50} = uniaxial compressive strength of a 50 mm diam. sample
d = diameter of laboratory rock sample in (mm).

This relationship is applicable to unjointed intact rock diameters between 10 and 200 mm. In the case of a jointed rock mass, it is suggested that strength variation be linked to discontinuity spacing.

In terms of in situ rock mass deformation, Hauze (1980) has proposed the following generalized relationship between field and laboratory determined Young's modulus values:

$$0.20 < E_f/E_l < 0.60 \qquad (6)$$

where E_f and E_l refer to Young's modulus determined in the field and laboratory, respectively.

With regard to the mechanical properties measurements involving the Lac du Bonnet samples, core sample sizes greater than 45 mm diameter have been unavailable. Extrapolation of in situ rock mass properties from laboratory tests on samples of one diameter alone is not recommended. However, according to equation 6, the Young's modulus of the Lac du Bonnet rock mass may range between 12 and 60 GPa depending on depth. Laboratory testing of larger size samples is recommended.

The stress distribution in a rock mass surrounding an underground excavation can be influenced significantly by the directional variations of the strength and deformational properties of the rock (Hoek and Brown, 1980). Anisotropic characteristics of these properties in a rock mass can be studied in the laboratory on core samples taken from three orthogonal directions of the rock.

The determination of the directional variations of strength and deformation properties of the Lac du Bonnet samples has not been possible because of inappropriate drillhole orientations and small core sample sizes. Strength anisotropy has, however, been estimated from Brazilian tensile strength measurements (Jackson and Boudreau, 1983; and Annor and Jackson, 1985). There is some indication of directional differences in tensile strength of up to 10%. However, it has so far not been possible to transfer the core sample orientations to

the co-ordinates of the rock mass. Also, a comprehensive study is currently being carried out by CANMET and AECL to evaluate the strength and deformational anisotropy behaviour of the Lac du Bonnet formation using URL shaft core samples.

Laboratory determined mechanical rock properties can be influenced by, among other factors, the stress and temperature paths followed during testing. These effects can also account for the noted differences between laboratory and in situ measured properties. In triaxial compression test results reported to date, the samples were heated to the desired test temperature while unconfined, before applying confining pressure. A program is currently underway by CANMET and AECL to evaluate the effects of various combinations of pressure and temperature paths on the mechanical properties of Lac du Bonnet rock samples (Simmons et al. 1984).

Rock Strength Failure Characteristics

are carried out at variable stresses to duplicate the in situ stress conditions existing in the rock mass. The test data are then used to develop relationships between the in situ compressive and shear stresses that could exist under failure conditions (Hoek and Brown, 1980).

Two strength envelopes are generally required for this purpose depending on the condition of the rock mass and the purpose of the excavation. These are the peak shear strength envelope of relatively intact rock material and the residual strength envelope of the jointed rock mass. The strength characteristics of the intact rock material can be expressed in terms of established empirical criteria or on the basis of theoretical assumptions. In terms of practical considerations, the two most commonly employed criteria are:

1. the Mohr-Coulomb (Goodman, 1980); and
2. the Hoek and Brown (1980) failure criteria for rocks.

The Mohr-Coulomb criterion can be expressed in terms of the principal stresses at peak load conditions as follows:

$$\sigma_1 = \sigma_c + \sigma_3 \tan^2 (45° + \phi/2) \quad (7)$$

where:

σ_1 = principal stress at failure
σ_c = uniaxial compressive strength
σ_3 = confining pressure
ϕ = angle of internal friction.

In terms of the Hoek and Brown (1980) analysis, the principal stress associated with the failure of the rock is expressed as follows:

$$\sigma_1 = \sigma_3 + \sqrt{m\sigma_c\sigma_3 + s\sigma_c^2} \quad (8)$$

where:

σ_1 = the major principal stress at failure
σ_3 = the minor principal stress applied to the rock sample
σ_c = the uniaxial compressive strength of the intact rock material in the rock sample
m,s = constants which depend on the properties of the rock and its structure.

The uniaxial compressive strength of an intact sample (σ_{cs}) is calculated from the relationship:

$$\sigma_{cs} = \sqrt{s\sigma_c^2} \quad (9)$$

This relationship is obtained by substituting $\sigma_3 = 0$ in equation 7. For intact rock, $\sigma_{cs} = \sigma_c$ and "s" is taken to be 1. In the case of previously broken rock, "s" is taken to be less than 1 and the unconfined strength of the rock is given by equation 9. Also, the uniaxial-tensile strength (σ_t) of the rock sample can be estimated from the following equation (Hoek and Brown, 1980):

$$\sigma_t = 1/2\,\sigma_c\,(m - \sqrt{m^2 + 4s}) \quad (10)$$

The Hoek and Brown (1980) criterion for rocks has been used to develop the strength envelope for the Lac du Bonnet samples. The values in Tables 7, 8 and 9 were used for σ_c, σ_t, and σ_3, in equations 7 to 10 for these analyses. The results of the analysis are summarized in Table 5 and represented graphically in Figures 14-18 in terms of rock sample colouration and test temperature. The accuracy of the analysis depends on the availability of both uniaxial compressive and tensile strength data as well as triaxial compressive strength results. It should be noted that the complete range of data (i.e., uniaxial, triaxial and tensile strength values) were only available for measurements at ambient room temperature.

The estimated mean material constant value "m" for the unheated Lac du Bonnet granitic samples is 29.9. This value is based on a population of 250 samples. The "m" values reported in the published literature for unheated granitic rock samples by Hoek and Brown (1980) range between 20.8 and 32.8, with an average reported value (for these rocks) of 29.2. In terms of rock sample colouration,

Table 5. Analysis of rock fracture data (based on Hoek and Brown, 1980) analysis

Rock type	No. of samples (N)	Mean uniaxial compressive strength (σ_c) (MPa)	m	s	r	Comments
Lac du Bonnet granite (combined URL and WNRE samples)	250	232	29.85	1.00	0.933	Includes pink and grey samples (unheated)
Lac du Bonnet granite (combined URL and WNRE pink coloured samples)	91	241	31.17	1.00	0.965	Pink samples (unheated)
Lac du Bonnet granite (combined URL and WNRE grey coloured samples)	174	222	30.54	1.00	0.924	Grey samples (unheated)
Lac du Bonnet (URL & WNRE) – granitic samples	20		30.06	1.00	0.988	Pink coloured samples (σ_3 = 3.5, 17.0 and 35.0 MPa) Test temperature = 100°C
Lac du Bonnet (URL & WNRE) – granitic samples	24		37.56	1.00	0.973	Pink coloured samples Test temperature = 200°C

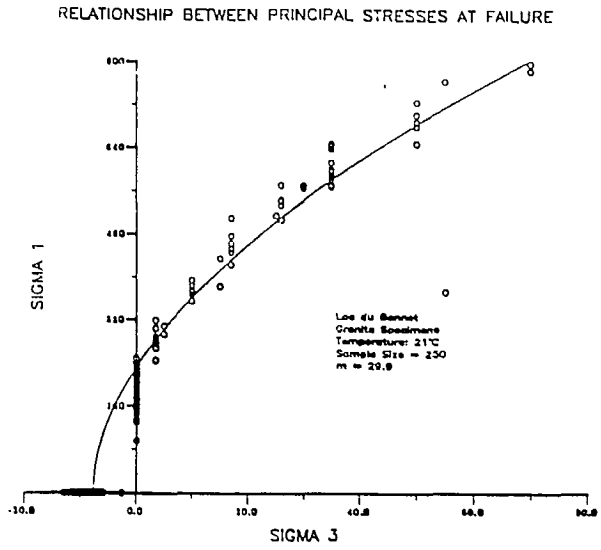

Figure 14. Strength envelope for Lac du Bonnet granitic samples (combined data at 21°C using Hoek and Brown, 1980 method of analysis).

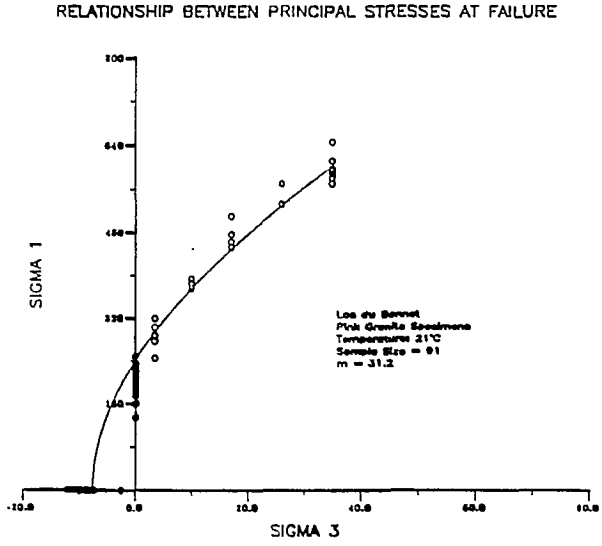

Figure 15. Strength envelope for Lac du Bonnet pink granite samples (21°C).

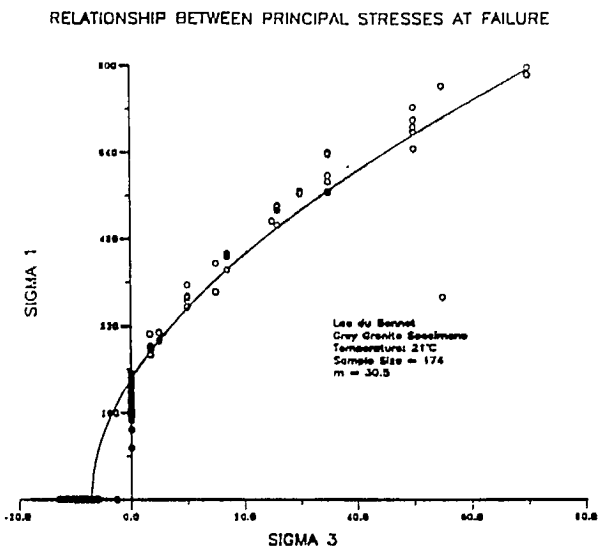

Figure 16. Strength envelope for Lac du Bonnet grey granite samples (21°C).

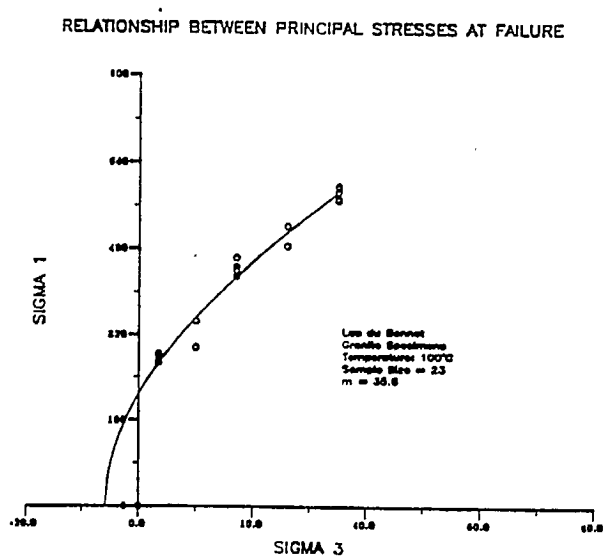

Figure 17. Strength envelope for Lac du Bonnet granite samples (100°C).

the mean "m" values for the unheated pink and grey Lac du Bonnet granitic samples were 31.2 and 30.5, respectively. There is a very good agreement between the calculated material constant values for the unheated Lac du Bonnet granitic samples and values reported in the referenced literature for granitic rocks. Additionally, the uniaxial compressive and tensile strength data, triaxial compressive strength values and the calculated material constants for the Lac du Bonnet granitic samples at 21°C suggest a very competent rock.

The estimated material constants for the heated Lac du Bonnet granitic samples are also summarized in Table 5. The values cannot be directly compared with the material constants determined at ambient room temperature due to the absence of elevated temperature uniaxial compressive and tensile strength test data. Data at elevated temperature do not exist in the published literature with which our results can be compared.

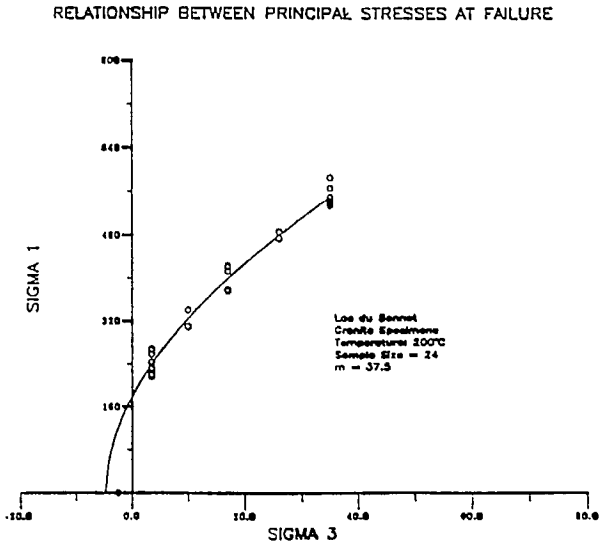

Figure 18. Strength envelope for Lac du Bonnet granite samples (200°C).

The strength envelope parameters for the Lac du Bonnet sample based on Mohr's circle analysis are presented in Figures 19-21. The angle of internal friction for the unheated samples ranged between 48° and 60° depending on confining pressure (Annor et al., 1981; Jackson, 1984a,b). There was, however, no significant change in the angle of internal friction with increasing temperature at a constant confining pressure.

Fractured Rock Material Properties

Fractured rock material properties data are required for the prediction of in situ mechanical behaviour of a rock mass. The strength envelope of the fractured rock can be determined from the results of stiff tests conducted on failed rock samples. Essential parameters of the strength envelope for the fractured rock are the basic friction angle (ϕ_b) and the friction angle (ϕ).

The basic friction angle, determined for saw-cut samples (Annor et al. 1981) and on core samples containing predominantly clean joints (Jackson et al. 1985),

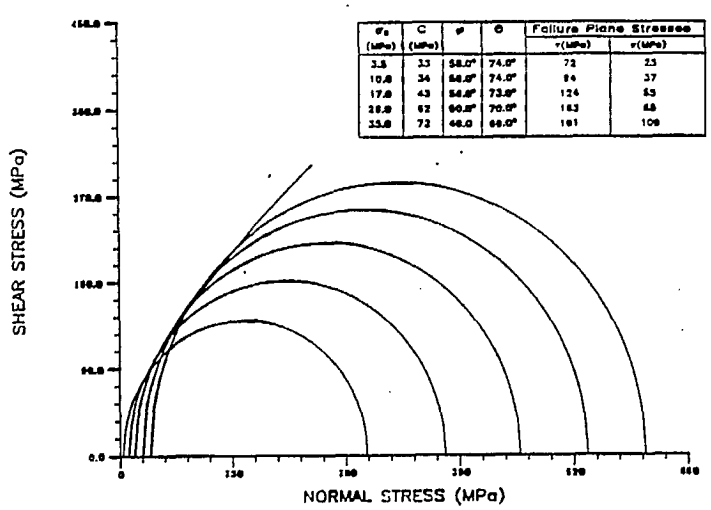

Figure 19. Mohr's circle and strength envelope for Lac du Bonnet granitic samples (21°C).

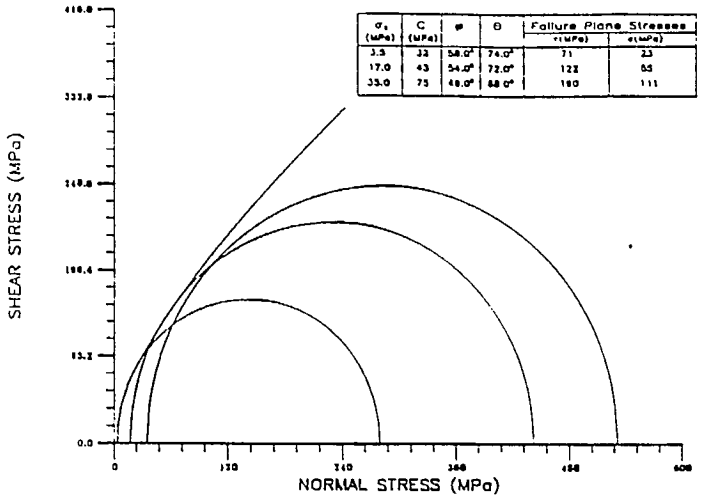

Figure 20. Mohr's circle and strength envelope for Lac du Bonnet granitic samples (100°C).

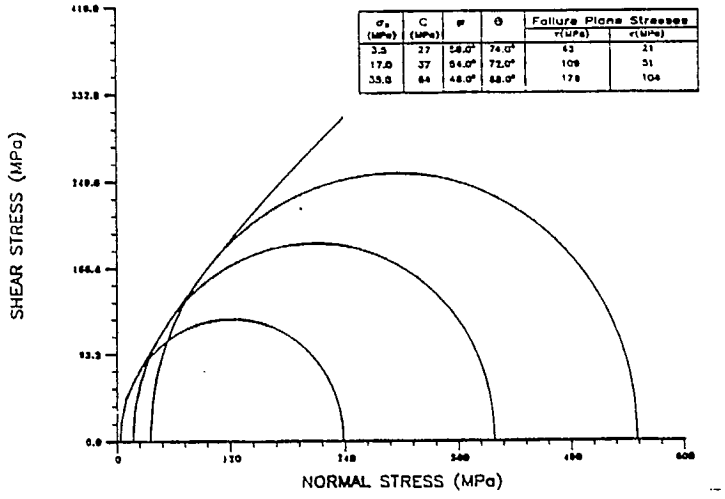

Figure 21. Mohr's circle and strength envelope for Lac du Bonnet granitic samples (200°C).

was estimated to be 30° by Annor et al. (1981) and 31° by Jackson et al. (1985). These values agree very well with basic friction angle values published by Barton and Bakhtar (1983). Annor et al. (1981) concluded that the basic friction angle for Lac du Bonnet granite samples was not affected by temperature over the temperature range of 21°C and 200°C (Figure 22). Individual sample data are appended to this paper.

The failure envelope of the joint systems present in a rock mass can also be described in terms of the Barton-Bandis rock joint characterization model (Barton and Bakhtar, 1983). This model is expressed as follows:

$$\tau = \sigma_n \tan (JRC \log_{10} \frac{JCS}{\sigma_n} + \phi_r) \quad (11)$$

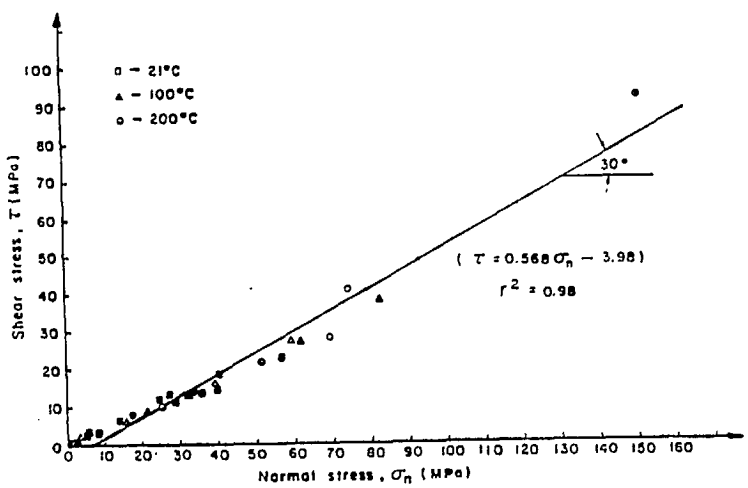

Figure 22. Frictional strength of saw-cuts in Lac du Bonnet granitic samples as a function of temperature.

where:

τ = shear strength of the joint (MPa)
σ_n = normal stress acting across the joint surface (MPa)
JRC = joint roughness coefficient
JCS = joint wall compressive strength (MPa)
ϕ_r = residual friction angle.

A major advantage of the above model is that values of ϕ_r, JCS and JRC can be easily determined from simple index tests. The procedure is described by Jackson et al. (1985) and also by Barton and Bakhtar (1983). The residual friction angle defined in equation 11 can also be estimated from the following relationship:

$$\phi_r = (\phi_b - 20) + \frac{r}{R} \times 20 \qquad (12)$$

where:

ϕ_b = the basic friction angle
r = Schmidt hammer rebound value on weathered joint surface
R = Schmidt hammer rebound value on unweathered surface.

Rock joint parameters for Lac du Bonnet samples are summarized in Tables 11 and 12.

A total of 139 Lac du Bonnet research area rock joint samples were investigated in accordance with the Barton-Bandis joint model (Barton and Bakhtar, 1983). The characterized samples fell into two categories. The first category was composed of joint samples that were suitable for all the index tests required for characterization according to the Barton-Bandis joint model. For this group, JRC was back-calculated from the other index properties of the joint sample. The index parameters for this category and the estimated peak shear strength and JRC values are summarized in Table 11. The range of calculated JRC values was 2.99 to 8.86. The mean and standard deviation of the JRC values were 6.45 and 1.40, respectively. These were based on a sample population of 62. Other relevant joint sample information such as sample depth, strike and dip angles, uniaxial compressive strength, joint wall compressive strength and the types of infilling materials contained in a joint are appended to this report.

The second category of samples was comprised of joint core specimens which were unsuitable for some of the index characterization tests required by the Barton-Bandis model. For example, most of the samples in this category could not be subjected to tilt tests because of either insufficient joint length or poor orientations of the fracture planes. For these samples (Table 12), the joint roughness coefficients (JRC) were visually estimated for the shear strength approximations. Seventy-seven samples of this type were examined. The estimated JRC and peak shear strength values are also summarized in Table 6. The range of calculated JRC values were 3.5 to 13.0; and the mean and standard deviation values were 6.0 and 1.9, respectively.

The mean and standard deviation of JRC values for the Lac du Bonnet samples (Table 6) are within the range of values (6.7 to 9.7) back-calculated by Barton and Choubey (1978) for slightly weathered tectonic joints in granite. There was no correlation between the calculated JRC values and strike and dip orientations, or sample depth for the Lac du Bonnet jointed samples.

Table 6. Summary of rock joint characterization data for Lac du Bonnet drill core samples

	Unconfined* compressive strength intact rock material (σ_c) (MPa)	Joint wall* compressive strength (JCS) (MPa)	Joint roughness coefficient (JRC)		
			Calculated	Visually estimated	Combined
No. of samples	139	139	62	77	139
Range	82-241	45-196	2.99-8.86	3.50-13.00	2.99-13.00
Mean	179.8	114.3	6.45	6.00	6.28
Std. dev.	34.9	33.3	1.40	1.90	1.55

*Based on Schmidt hammer (Model-L) results.

The predominant infilling material for the characterized joint samples was hematite (HE). The following materials were also present in the joints: calcite (CA), chlorite (CL), clay (CY), biotite (BI), pyrite (PY), sericite (SR), goethite-limonite (GO) and quartz (QZ). These are indicated in the appendix. Various researchers have indicated that the shear strength of a rock joint is influenced significantly by the thickness, strength, and fabric of the infilling materials (Barton and Bakhtar, 1983; Lama and Vutukuri, 1978; Lama, 1978 and Tulinov and Molokov, 1971). The strength and thickness of the joint infilling materials were not determined for the Lac du Bonnet samples.

Rock Mass Characterization

A rock mass classification system provides a basis for assessing the suitability of a rock body for major geotechnical projects. Two generally accepted geotechnical engineering classification systems (Hoek and Brown, 1980; Lama and Vutukuri, 1978) are the:

1. Norwegian Geotechnical Institute (NGI) Q-Index System; and
2. The CSIR classification system.

Both classification systems are based on geological information recorded under field conditions, as well as mechanical rock property data from drill core samples. The following parameters are required for the NGI system:

1. Rock Quality Designation (RQD) from core log.
2. Number of joint sets.
3. Joint Roughness Coefficient (JRC).
4. Joint alteration.
5. Joint water and stress reduction factors.

In the case of the CSIR system, the following rock parameters are of interest:

1. Unconfined compressive strength (σ_c).
2. Rock Quality Designation (RQD).
3. Joint spacing.
4. Joint condition, water condition.
5. Joint orientation.

Ratings are assigned to these parameters as defined for each system. Visual assessments of joint roughness and joint alteration are required and ratings are then applied according to descriptions applicable to each classification system. The data collected on Lac du Bonnet drill core samples containing natural joints can provide some of the parameters required to develop a rock mass characterization system for the Lac du Bonnet batholith. The uniaxial compressive strength and JRC values are summarized in Table 6.

CONCLUSIONS AND RECOMMENDATIONS

The results of the mechanical rock properties investigations on small scale intact and jointed Lac du Bonnet core samples have provided strength and deformation data and interpretations that permit vault design studies, in situ test planning and geosphere modelling activities to be carried out. Possible applications, as well as limitations of the test data, have also been indicated. In terms of the generalized behaviour of the Lac du Bonnet formation with temperature and pressure, as well as environmental factors which might influence the laboratory test results, the following conclusions can be made:

1. The unconfined mechanical behaviour of the Lac du Bonnet granitic samples show trends of decreasing compressive strength, compressive wave velocity and Young's modulus and increasing Poisson's ratio with increasing depth. While these trends can be attributed to changes in rock alteration with increasing depth, they also suggest significant effects of stress relaxation of the core samples due to drilling. The stress relaxation effects seem to be more pronounced for the grey granite than the pink and could result in slabbing of the walls of an excavation founded at depth in the grey granitic rock.

2. The Lac du Bonnet granitic samples can be classified with the system of Deere and Miller (1966) as a high strength to very high strength rock, with a medium modulus ratio. The strength, deformation and acoustic velocity values of the Lac du Bonnet rock compare favourably with literature published data on granitic rock with similar mineralogical compositions.

3. The unconfined strength and deformational properties of the rock samples investigated were unaffected by variation in moisture content. However, compressive wave velocity increased with increased sample moisture content suggesting that differences between in situ static and dynamic properties of the Lac du Bonnet formation could be due to differences in moisture content.

4. There is some evidence of strength anisotropy in Lac du Bonnet samples on the basis of limited data. A comprehensive program is currently under way to establish conclusive evidence.

5. Temperature levels of up to 100°C do not have any pronounced effects on the strength and deformational properties of Lac du Bonnet granitic samples. However, a significant reduction in these properties occurs at 200°C in tests performed with applied confining pressures less than the maximum estimated overburden stress equivalent at sample depth, or the tensile strength of the rock.

6. It is recommended that:

   (a) Studies should be carried out to establish the effects of scale on the mechanical behaviour of both intact and fractured Lac du Bonnet rock samples. The information is required to relate the laboratory determined properties to in situ conditions.

   (b) The mechanical behaviour of jointed samples should be investigated as a function of temperature to understand possible rock mass behaviour at elevated temperatures.

   (c) Laboratory studies on the effects of stress and temperature paths on the mechanical properties of Lac du Bonnet rock samples be continued.

REFERENCES

Annor, A., Larocque, G.E., and Chernis, P. 1979. Uniaxial compression tests, Brazilian tensile strength and dilatational velocity measurements on rock specimens from Pinawa and Chalk River, Division Report MRP/MRL 79-60 (TR); CANMET, Energy, Mines and Resources Canada.

Annor, A. 1984. Mechanical properties of rock samples from Pinawa, Manitoba. CANMET Division Report ERP/MRL 84-48 (TR) Energy, Mines and Resources Canada, Ottawa.

Annor, A. and Geller, L. 1979. Dilatational velocity, Young's modulus, Poisson's ratio, uniaxial compressive strength and Brazilian tensile strength for WN1 and WN2 samples; CANMET-Mining Research Laboratories Technical Data 303410-M01/78.

Annor, A., Miles, P., Kapeller, F., and Larocque, G. 1981. High temperature and pressure triaxial compression tests on rock samples from Pinawa and Creighton mine; Atomic Energy of Canada Ltd.; Techn Record TR-158, WNRE; Pinawa, Manitoba.

Annor, A. and Jackson, R. 1982. Summary of uniaxial elastic properties and thermal expansion data for Pinawa granite samples (URL-1, 2, 5 and WN-1, 2 and 4); Division Report MRP/MRL 82-82 (OP); CANMET, Energy, Mines and Resources Canada; Ottawa.

Annor, A. 1984. Mechanical properties of rock samples from Pinawa, Manitoba; Division Report ERP/MRL 84-48 (TR); CANMET, Energy, Mines and Resources Canada; Ottawa.

Annor, A. and Jackson, R. 1985. Mechanical properties of rock samples from the Lac du Bonnet batholith, Manitoba; Division Report ERP/MRL 81-41 (TR); CANMET, Energy, Mines and Resources Canada; Ottawa.

Annor, A. and Jackson, R. 1984. Mechanical properties of rock samples from Atikokan, Ontario; Division Report ERP/MRL 84-63 (TR); CANMET, Energy, Mines and Resources Canada; Ottawa.

ASTM. 1971a. Standard test for unconfined compressive strength of intact rock specimens; ASTM Test D2937-71A.

ASTM. 1971b. Standard test for splitting tensile strength of cylindrical concrete specimens; ASTM Test C496-71.

Barton, N. and Bakhtar, K. 1983. Rock joint description and modelling for the hydrothermomechanical design of nuclear waste repositories; Tera Tek Engineering; Report TRE-83-10; University Research Park, Salt Lake City, Utah.

Barton, N. and Choubey, V. 1978. The shear strength of rock joints in theory and practice; Norwegian Geotechnical Institute Publication No. 119; Oslo. Norway.

Chernis, P.J. 1979. Petrographical analysis of borehole samples (Label-P specimens) from WN-1, WN-2, CR-6 and CR-7; Technical Data 7878/T5; Electrical Seismic Rock Property Laboratory, Geological Survey of Canada, Ottawa.

Chernis, P.J., Overton, A., and Katsube, T.J. 1978. Preliminary investigation of WN-1 standard samples; Technical Data 7879-D3; Electrical Seismic Rock Property Laboratory, Geological Survey of Canada; Ottawa.

Chernis, P.J., Wadden, M.M., Anderson, J., and Katsube, T.J. 1974. Preliminary investigation of WN-4 standard samples; TM.303405 M11/80; Electrical Seismic Rock Property Laboratory, Geological Survey of Canada; Ottawa.

Coates, D.J. and Parsons, R.C. 1966. Experimental criteria for classification of rock substances; Int. J. Rock. Mech. & Min. Sci., v. 3, p. 181-189.

Deere, J.J. and Miller, R.P. 1966. Engineering classification of index properties for intact rock; Air Force Weapon's Laboratory; Technical Report No. AFWL-TR-65-116.

Drury, M. in press. "Thermophysical Properties of Rock Samples from WNRE and URL Boreholes" – Second Level Document for concept Assessment in the Geoscience Program, Atomic Energy of Canada Limited, Technical Report, AECL No. 84-10X.

Goodman, R.E. 1980. "Introduction to Rock Mechanics"; John Wiley and Sons, Inc.; New York, p. 75-92.

Gyenge, M. and Herget, G. 1977. Pit Slope Manual Supplement 3-2; Laboratory tests for design parameters; CANMET Report 77-26; CANMET, Energy, Mines and Resources Canada; Ottawa.

Hauze, F.E. 1980. Scale effects in the determination of rock mass strength and deformability; Rock Mech. v. 12, p. 167-192.

Hawkes, I., Mellor, M., and Gariepy, S. 1973. Deformation of rocks under uniaxial tension; Int. J. Rock Mech. & Min. Sci. and Geomech. Abstr., v. 10, p. 493-507.

Herget, G. 1980. Regional stresses in the Canadian Shield; Division Report MRP/MRL 80-8 (OP); CANMET, Energy, Mines and Resources Canada.

Hoek, E. and Brown, E.T. 1980. Underground excavation in rock; The Institution of Mining and Metallurgy 131-159; London.

Huang, C. and Hunter, J.S. 1980. The 1978 progress report on the seismic and downhole surveys at the Chalk River and Whiteshell research areas; Atomic Energy of Canada Limited; Report TR-31.

Jackson, R.D. 1982a. Dilatational velocity, Young's modulus, Poisson's ratio and uniaxial compressive strength for URL-2 and URL-5 samples; Division Report ERP/MRL 82-60 (TR).

Jackson, R.D. 1982b. Dilatational velocity, Young's modulus, Poisson's ratio, uniaxial compressive strength and Brazilian tensile strength for URL-1 and URL-5 extended engineering samples. Division Report ERP/MRL 82-61 (TR), CANMET, Energy, Mines and Resources Canada; Ottawa.

Jackson, R. 1983. The effect of oven drying specimens on uniaxial elastic properties; Division Report ERP/MRL 83-16 (TR); CANMET, Energy, Mines and Resources Canada; Ottawa.

Jackson, R. 1984a. High temperature and pressure triaxial compression tests on samples from borehole URL-6; Division Report ERP/MRL 84-22 (TR); CANMET, Energy, Mines and Resources Canada; Ottawa.

Jackson, R. 1984b. Summary of mechanical properties of Lac du Bonnet and Eye Eashwa specimens; Division Report MRP/MRL 84-85 (TR); CANMET, Energy, Mines and Resources Canada; Ottawa.

Jackson, R. and Annor, A. 1985. Thermomechanical properties of rock samples from the Lac du Bonnet and the eye Dashwa lakes plutons; Division Report ERP/MRL 85-42 (TR); CANMET, Energy, Mines and Resources Canada; Ottawa.

Jackson, R. and Annor, A. 1985. The effects of water content on the uniaxial

Jackson, R. and Boudreau, C. 1983. Special ambient temperature mechanical properties studies to determine the effects of stress release on URL core samples; Division Report ERP/MRL 84-17 (TR); CANMET, Energy, Mines and Resources Canada; Ottawa.

Jackson, R. and Paquette, D. 1984. "A summary of mechanical property test data on samples from borehole URL-7, URL-B9-1, 2 and 3, URL-B10-1, and URL-B26-1 at Lac du Bonnet, Manitoba"; Division Report ERP/MRL 84-31 (INT); CANMET, Energy, Mines and Resources Canada; Ottawa.

Kamineni, D.C., Dugal, J.J.B., and Ejeckam, R.B. 1984. "Geochemical investigation of granitic core samples from boreholes at the Underground Research Laboratory site, near Lac du Bonnet, Manitoba"; Atomic Energy of Canada Limited; Whiteshell Nuclear Research Establishment, Pinawa, Manitoba; Report No. (TR-221); May.

Lama, R.D. 1978. "Influence of thickness to fill on shear strength of rough rock joints at low normal stresses"; Grundlagen und Anwendung der Felsmechanik, Felsmechanik Kolloquium Karlsruhe 1978; Trans Tech Publications; Clausthal, Germany.

Lama, R.D. and Vutukuri, V.S. 1978. "Handbook on mechanical properties of rocks"; Trans. Tech. Publications; Clausthal, Germany.

Larocque, G.E. and Annor, A. 1984. "Overview rock mechanics/rock properties"; In 17th Nuclear Fuel Waste Management Information Meeting Proceedings, Ottawa, Feb. Atomic Energy of Canada Limited Technical Record TR-299, Whiteshell Nuclear Research Establishment, Pinawa, Manitoba.

McKay, D.A. 1982. "AECL core testing program, CR-5, CR-8, CR-9, WN-4, ATK-1 series cores"; Ontario Hydro Research Division Report 80-431-K; Toronto.

Michalopoulos, A.P. and Triandafilidis, G.E. 1976. "Influence of water on hardness, strength and compressibility of rock"; Bull. Association of Eng. Geol. v. XIII, No. 1, p. 1-22.

Miller, R.P. 1965. "Engineering classification and index properties for intact rock"; Ph.D. Thesis, Univ. Ill. Urbana, Ill.

Obert, L., Windes, S.L., and Duval, W.I. 1946. "Standardized test for determining the physical properties of mine rock"; US Bureau of Mines Report of Investigation 3891.

Price, N.J. 1960. "The compressive strength of coal measured rocks"; Coll. Engineering, v. 37, p. 283-292.

Richter, D. and Simmons, R. 1974. "Thermal expansion behaviour of igneous rocks"; Int. J. Rock Mech. and Min. Sci. and Geomech. Abstr., v. 11, p. 403-411; Pergamon Press.

Simmons, G.R., Annor, A., Baumgartner, P., Lang, P.W., Larocque, G.E., and Wilkins, B.J. 1984. "The geomechanics program – A review"; Proceedings of the Eighteenth Information Meeting on the Nuclear Waste Management Program (1984 General Meeting); Atomic Energy of Canada Limited, Whiteshell Nuclear Research Establishment, Pinawa, Manitoba; Report No. (TR-320); p. 23-44.

Touloukian, Y.S. and Ho, C.Y. 1981. "Physical properties of rocks and minerals"; McGraw-Hill/CINDAS Data Series on Material Properties; McGraw-Hill Book Company II-2:29-176.

Tulinov, R. and Molokov, L. 1971. "Role of joint filling material in shear strength of rocks"; Symposium Soc. Internat. Mecanique des Roches; Nancy.

Wild, V.W. and McKittrick, D.P. 1971. "Northfield mountain underground power station"; Symposium on Underground Rock Chambers, Arizona; Amer. Soc. Civil Engineers, p. 287-331.

Wong, A.S. 1984. Modal analyses of URL-01, URL-02, URL-05 and URL-06 Extended Engineering core samples from the Underground Research Laboratory site near Lac du Bonnet, Manitoba. CANMET Division Report ERP/MRL 84-27 (TR), Energy, Mines and Resources Canada; Ottawa.

Wylie, M.R.J., Gregory, A.R., and Gardner, G.H.E. 1958. "An experimental investigation of factors affecting elastic wave velocities in porous media"; Geophysics, v. 23, p. 459-493.

APPENDIX

Table 7. Individual sample data showing sample identification, vertical depth of sample, Young's modulus, Poisson's ratio, uniaxial compressive strength, compressive wave velocity at σ3=0.1 MPa, and bulk density. The data have been divided into three zones for purposes of engineering analysis.

(a) Summary of uniaxial compression data for surface air dried URL samples

Sample Identification	Vertical Depth (m)	Young's Modulus (E) (GPa)	Poisson's Ratio (ν)	Uniaxial Compressive Strength (Qu) (MPa)	Compressive Wave Velocity at σ3=0.1 MPa (vp) (km/s)	Bulk Density (ρ) (Mg/m³)
assumed pink zone:						
URLB9-0.00	0.0	64.4	0.28	183	4.34	2.61
URLB10-0.15	0.2	93.6	0.29	177	4.42	2.62
URLB9-3.90	3.9	65.2	0.26	134	5.32	2.63
URLB9-14.46	14.5	64.9	0.29	191	5.48	2.62
URL5-16.4	16.2	73.0	0.27	219	5.07	2.62
URL1-46.4	45.8	77.1	0.24	229	5.67	2.65
URL1-68.5	66.4	82.2	0.25	186	6.06	2.65
URL5-76.9	74.7	73.0	0.22	230	5.67	2.65
URL1-107.40	100.6	86.0	0.29	248	5.60	2.69
URL5-108.30	104.6	72.5	0.38	199	5.14	2.59
URL5-126.60	122.7	70.4	0.18	175	5.04	2.64
URL5-128.00	124.1	71.4	0.29	196	4.87	2.63
URL5-129.30	125.3	66.2	0.30	200	5.10	2.63
URL5-133.00	128.8	80.0	0.30	221	5.44	2.64
URL7-135.47	130.9	71.6	0.23	227	5.42	2.63
URL5-131.03	131.0	67.1	0.23	190	5.40	2.63
URL7-138.46	133.7	70.2	0.27	209	5.68	2.64
URL7-143.27	138.4	68.7	0.24	181	5.68	2.64
URL7-155.86	150.6	70.4	0.22	219	5.68	2.64
URL5-157.20	152.8	71.4	0.26	180	4.97	2.59
URL7-170.70	164.9	65.4	0.22	201	5.27	2.63
URL1-177.10	170.4	83.4	0.27	200	5.18	2.61
URL1-177.40	170.7	69.7	0.25	184	4.90	2.63
URL7-181.80	175.6	65.4	0.25	183	4.81	2.64
URL1-184.68	178.0	70.9	0.27	192	5.06	2.62
URL7-184.70	178.4	65.4	0.24	180	4.83	2.63
URL1-191.38	184.7	71.4	0.25	176	5.17	2.62
URL7-192.90	186.3	67.3	0.26	234	4.91	2.63
URL7-197.36	191.1	67.2	0.27	221	4.74	2.64
URL5-199.10	192.9	73.5	0.30	191	5.09	2.63
URL1-230.50	221.1	84.9	0.23	189	5.26	2.61
URL5-246.50	238.5	69.0	0.25	226	5.45	2.63
URL1-254.30	244.9	75.0	0.26	197	4.51	2.62
URL2-256.00	247.1	64.9	0.25	203	3.84	2.63
URL5-274.51	265.9	58.1	0.22	179	4.03	2.64
URL5-277.59	269.0	64.9	0.26	193	3.95	2.62
URL5-281.63	271.1	61.4	0.28	191	4.08	2.62
URL1-282.68	272.4	70.9	0.19	203	4.57	2.63
URL1-283.80	273.4	60.2	0.19	192	4.10	2.63
URL5-289.70	279.8	66.2	0.24	197	4.07	2.63
URL1-292.90	280.5	65.8	0.22	160	4.85	2.65
URL1-299.90	287.5	65.8	0.24	177	4.51	2.62
URL1-302.40	290.0	74.5	0.25	208	4.74	2.63
end of assumed pink zone						
assumed transition zone:						
URL5-334.00	322.2	58.8	0.25	199	4.40	2.65
URL5-370.00	357.5	56.2	0.25	176	3.77	2.63
URL6-373.80	373.8	59.2	0.39	181	3.73	2.63
URL6-374.70	374.7	61.7	0.31	170	3.84	2.63
URL6-374.98	375.0	58.5	0.33	204	3.74	2.63
URL1-397.80	397.8	61.4	0.26	155	4.32	2.66
URL6-391.38	391.4	55.5	0.32	197	3.71	2.63
URL6-391.61	391.6	56.6	0.29	170	3.55	2.65
URL6-391.89	391.9	56.4	0.31	183	3.73	2.63
URL6-392.17	392.2	58.2	0.30	145	3.47	2.60
URL1-443.20	422.7	68.6	0.30	146	2.87	2.61
URL5-441.75	426.0	56.1	0.31	227	3.70	2.66
URL5-441.98	426.3	52.9	0.30	186	3.57	2.66
URL5-442.26	426.5	56.7	0.27	224	3.64	2.65
URL5-442.54	426.8	56.6	0.29	200	3.83	2.65
URL2-448.10	430.3	53.5	0.22	179	3.70	2.64
URL5-450.90	434.9	54.0	0.36	163	3.48	2.65
URL1-496.70	472.7	64.6	0.31	154	3.47	2.64
URL5-496.80	479.0	53.1	0.27	186	3.52	2.63
URL1-527.40	501.1	66.4	0.32	180	3.57	2.64
URL2-586.00	559.8	52.6	0.26	181	3.16	2.62
URL1-592.60	561.5	64.4	0.30	167	3.38	2.64
URL1-662.40	635.7	63.6	0.36	166	3.61	2.66
end of assumed transition zone						
assumed grey zone:						
URL2-705.70	668.9	56.2	0.22	152	3.49	2.63
URL2-798.60	752.7	58.5	0.13	158	3.66	2.64
URL2-871.50	815.6	53.8	0.28	163	3.43	2.63
URL2-1001.20	929.8	51.0	0.24	156	2.81	2.63
URL2-1080.32	991.0	51.6	0.30	198	2.53	2.62
URL2-1080.55	991.2	51.8	0.22	190	2.45	2.63
URL2-1080.83	991.5	51.9	0.40	163	2.52	2.63
URL2-1081.06	991.7	52.5	0.30	166	2.48	2.63
URL2-1081.67	992.2	54.3	0.34	178	2.62	2.63
URL2-1081.90	992.4	51.8	0.36	162	2.86	2.63
URL2-1082.21	992.7	52.0	0.43	160	2.88	2.63
URL2-1082.44	992.9	46.6	0.35	180	2.71	2.62
URL2-1094.80	1004.3	55.9	0.30	172	2.91	2.63
end of assumed grey zone						

Sample Identification	Vertical Depth (m)	Young's Modulus (E) (GPa)	Poisson's Ratio (v)	Uniaxial Compressive Strength (Qu) (MPa)	Compressive Wave Velocity at σ3=0.1 MPa (vp) (km/s)	Bulk Density (ρ) (Mg/m³)

(b) Summary of mean and standard deviation of mechanical properties

Mean mechanical properties		Pink zone	Transitional zone	Grey zone
Young's Modulus (GPa)	Mean	69.8	58.5	52.9
	Std. dev.	6.8	±.6	2.9
Poisson's Ratio	Mean	0.25	0.30	0.30
	Std. dev.	0.04	0.04	0.08
Uniaxial Compressive Strength (MPa)	Mean	197	180	169
	Std. dev.	22	22	14

(c) Summary of uniaxial compression data for surface air dried WN samples

Sample Identification	Vertical Depth (m)	Young's Modulus (E) (GPa)	Poisson's Ratio (v)	Uniaxial Compressive Strength (Qu) (MPa)	Compressive Wave Velocity (v_o)* (km/s)	Compressive Wave Velocity (v)** pressure (MPa)	Compressive Wave Velocity (v)** vp (km/s)	Bulk Density (ρ) (Mg/m³)
assumed pink zone:								
WN2-24.75	23.9	70.0	0.23	233	4.90	0.62	4.98	2.63
WN2-55.45	53.5	74.0	0.23	173	5.10	1.43	5.23	2.73
WN1-74.03		67.5	0.28	209	4.77			2.63
WN1-74.25		62.7	0.30	180	4.60			2.54
WN1-74.76	72.8	62.6	0.44	176	4.70			2.63
WN1-75.05		64.6	0.20	199	4.71			2.62
WN1-75.27		68.6	0.25	190	4.95			2.63
WN1-76.03	73.5	70.4	0.24	197	4.74			2.63
WN1-76.25		68.3	0.24	208	4.63			2.62
WN1-76.63		71.0	0.26	218	4.91			2.62
WN1-76.74		81.2	0.37	208	4.90			2.62
WN1-78.00	74.8	71.4	0.23	205	4.90			2.63
WN1-78.11		71.4	0.23	206	4.81			2.64
WN1-79.41		71.8	0.30	199	4.60			2.62
WN2-85.40	82.2	73.0	0.21	159	5.40	2.22	5.46	2.75
WN2-98.50	94.7	69.0	0.21	232	5.10	2.46	5.26	2.65
WN2-124.70	119.8	69.0	0.21	235	4.70	3.09	4.98	2.63
WN1-138.60	133.9	69.0	0.26	213	4.80	3.46	4.96	2.64
WN2-145.35	140.0	71.0	0.21	224	4.50	3.68	4.78	2.64
WN1-153.90		62.7	0.23	199	4.95			2.63
WN1-154.14		63.6	0.24	199	4.92			2.63
WN1-154.30		64.8	0.24	197	4.87			2.62
WN1-154.50		72.3	0.27	213	4.88			2.63
WN1-154.96	147.3	68.9	0.23	226	4.98			2.63
WN1-155.12		63.3	0.26	198	4.90			2.63
WN1-155.29		71.0	0.31	201	4.90			2.63
WN1-155.44		70.9	0.30	209	4.79			2.64
WN1-155.60		67.2	0.27	211	4.73			2.63
WN1-155.76		66.8	0.28	196	4.80			2.64
WN1-160.90	155.3	66.0	0.29	191	4.70	4.02	4.94	2.64
WN1-224.00	215.7	72.0	0.30	210	4.80	5.58	5.00	2.64
WN1-246.00	236.7	71.0	0.20	219	4.70	6.10	5.01	2.63
WN1-294.50	282.3	71.0	0.27	205	4.80	7.32	5.14	2.64
WN1-303.50	291.3	67.0	0.24	224	4.70	7.51	5.14	2.63
WN1-345.50	330.9	70.0	0.24	227	4.80	8.53	5.10	2.63
WN1-384.80	367.7	69.0	0.29	219	4.90	9.59	5.35	2.66
end of assumed pink zone								
assumed transition zone:								
WN4-409.00	387.7	67.8	0.21	211	4.11	10.12	5.11	2.65
WN1-410.70	391.5	73.0	0.22	231	4.80	10.10	5.18	2.63
WN1-460.60	438.2	64.0	0.24	214	4.30	11.29	4.84	2.63
WN4-469.25	445.3	66.1	0.23	169	4.12	11.56	5.23	2.65
WN4-482.30	457.1	68.5	0.23	182	3.62	11.88	4.63	2.65
WN4-505.57	478.2	74.9	0.20	217	3.96	12.38	4.94	2.64
WN4-551.45	519.5	71.4	0.25	166	3.91	13.49	4.76	2.65
WN4-564.40	531.0	78.7	0.25	192	3.78	13.84	4.80	2.66
WN4-603.60	565.6	72.1	0.28	168	3.90	14.70	4.78	2.65
WN4-660.30	614.8	69.7	0.25	165	3.56	15.96	4.50	2.65
WN4-692.70	642.4	68.9	0.27	168	3.69	16.62	4.75	2.64
WN4-719.10	664.4	68.6	0.23	158	3.36	17.20	4.59	2.64
end of assumed transition zone								
assumed grey zone:								
WN4-747.20	687.8	64.4	0.34	131	2.96	17.93	4.54	2.66
WN4-789.90	722.8	60.7	0.32	155	3.20	18.77	4.29	2.65
WN4-809.70	738.7	56.5	0.26	166	2.60	19.23	4.23	2.66
WN4-841.10	763.5	62.9	0.25	171	2.63	19.83	4.16	2.65
WN4-863.60	781.1	59.1	0.39	147	2.89	20.08	4.50	2.62
WN4-906.80	813.9	63.8	0.34	165	2.47	21.15	4.37	2.65
WN4-928.30	829.7	59.4	0.27	151	2.50	21.56	4.11	2.65
end of assumed grey zone								

* at σ3 = 0.1 MPa
** at overburden pressure equivalent to sample depth

(d) Summary of mean and standard deviation of mechanical properties data for Lac du Bonnet granitic samples

Mean mechanical properties		Pink zone	Transitional zone	Grey zone
Young's Modulus (GPa)	Mean	69.0	70.3	61.0
	Std. dev.	3.3	4.0	2.9
Poisson's Ratio	Mean	0.26	0.24	0.31
	Std. dev.	0.05	0.02	0.05
Uniaxial Compressive Strength (MPa)	Mean	206	187	162
	Std. dev.	17	25	12

(e) Summary of uniaxial compression data for water saturated WN samples

Sample Identification	Vertical Depth (m)	Young's Modulus (E) (GPa)	Poisson's Ratio (ν)	Uniaxial Compressive Strength (Qu) (MPa)	Compressive Wave Velocity at σ3=0.1 MPa (vp) (km/s)	Bulk Density (ρ) (Mg/m^3)
assumed pink zone:						
WN1-74.14	72.3	62.0	0.26	188	5.91	2.62
WN174.54		74.5	0.27	190	6.06	2.63
WN1-74.65		73.4	0.36	178	6.16	2.63
WN1-75.16		72.0	0.27	172	5.86	2.63
WN1-76.85		72.7	0.29	218	5.92	2.62
WN1-78.22	74.3	75.3	0.28	213	6.11	2.63
WN1-78.36		67.4	0.25	216	5.93	2.62
WN1-78.47		71.3	0.28	210	5.97	2.62
WN1-79.30		73.7	0.28	184	5.79	2.62
WN1-79.52	76.3	70.4	0.26	215	5.88	2.62

(f) Summary of mean and standard deviation for mechanical properties

	Young's Modulus (GPa)	Poisson's Ratio	Uniaxial Compressive Strength (MPa)	Compressive Wave Velocity (km/s)	Bulk Density (Mg/m^3)
Mean	71.2	0.28	198		
Standard deviation	4.0	0.03	17.7		

(g) Summary of uniaxial compression data for oven dried WN and URL samples

Sample Identification	Vertical Depth (m)	Young's Modulus (E) (GPa)	Poisson's Ratio (ν)	Uniaxial Compressive Strength (Qu) (MPa)	Compressive Wave Velocity at σ3=0.1 MPa (vp) (km/s)	Bulk Density (ρ) (Mg/m^3)
assumed pink zone:						
WN1-74.36	72.41	67.2	0.28	175	4.47	2.61
WN1-76.36		67.7	0.18	216	4.89	2.61
WN1-77.30		75.6	0.28	201	4.97	2.63
WN1-78.69	75.49	68.2	0.28	190	4.75	2.62
URL5-129.40 @	125.40	66.7	0.24	198	4.64	2.63
URL5-134.90 @	131.13	63.7	0.25	203	4.49	2.63
URL1-283.90 @	273.46	60.2	0.23	187	4.44	2.63
WN1-335.54	323.34	62.8	0.29	212	4.60	2.62
WN1-335.76		66.8	0.28	201	4.66	2.62
WN1-335.87		65.6	0.24	211	4.59	2.62
WN1-335.98		63.0	0.18	181	4.65	2.62
WN1-336.09	324.09	64.3	0.24	199	4.62	2.62

@ estimated values for compressive wave velocity

(h) Summary of mean and standard deviation for mechanical properties

	Young's Modulus (GPa)	Poisson's Ratio	Uniaxial Compressive Strength (MPa)	Compressive Wave Velocity (km/s)	Bulk Density (Mg/m^3)
Mean	66.0	0.25	198		
Standard deviation	3.9	0.04	12.6		

Table 8. Individual sample data showing sample identification, vertical depth and tensile strength

(a) Summary of tensile strength data for WN samples

Sample Identification	Vertical depth (m)	Tensile strength (MPa)
assumed pink zone:		
WN1-324.50	312.3	8.20
WN1-324.52		9.90
WN1-324.54		7.50
WN1-324.56		10.0
WN1-324.58		8.80
WN1-324.59		8.50
WN1-324.60	312.4	9.50
end of assumed pink zone		
assumed grey zone:		
WN4-409.00	387.7	10.64
WN4-469.25	445.3	12.99
WN4-482.35	457.1	10.47
WN4-505.57	478.2	12.44
WN4-551.45	519.5	11.21
WN4-564.40	531.0	11.52
WN4-603.60	656.6	12.06
WN4-631.70	590.2	11.87
WN4-660.30	614.8	11.06
WN4-692.70	642.4	11.37
WN4-719.10	664.4	11.65
WN4-747.20	687.8	8.64
WN4-789.90	722.8	11.36
WN4-809.70	738.7	8.66
WN4-841.10	763.5	11.45
WN4-836.60	781.1	10.66
WN4-906.80	813.9	11.52
WN4-928.30	829.7	10.53

(b) Summary of tensile strength data for URL samples

assumed pink zone:		
URL7-61.36	56.1	11.44
URL7-61.39		10.73
URL5-127.87	123.9	8.81
URL5-133.12		9.81
URL5-133.25		8.16
URL7-138.46		10.69
URL5-138.98		9.93
URL7-139.77		12.07
URL7-139.80		10.79
URL7-143.27		10.30
URL7-159.20		10.11
URL7-159.23	153.9	11.36
URL7-159.26		9.86
URL7-163.74		10.13
URL7-163.77		9.49
URL7-163.80		8.93
URL7-170.71		10.12
URL1-170.50	164.3	9.27
URL7-181.81		8.20
URL1-184.34		9.58
URL1-184.37		9.58
URL7-184.71		7.41
URL1-191.67	185.0	9.53
URL7-197.87	191.1	10.41
URL5-274.61	266.0	7.99
URL5-274.64		9.02
URL5-277.73		7.16
URL5-281.73	271.8	6.17
URL1-283.07		8.96
URL1-292.87		8.62
URL1-293.00		8.08
URL1-300.00	287.6	8.18
end of assumed pink zone		
assumed grey zone:		
URL6-374.46	374.5	8.71
URL6-374.48		8.66
URL6-374.80		8.46
URL6-374.82		8.39
URL6-391.60		5.96
URL6-391.84		7.82
URL6-391.87	391.9	7.80
URL5-441.70	426.0	9.31
URL5-441.73		9.87
URL5-442.08		9.97
URL5-442.10	426.4	8.75
URL5-442.49		10.51
URL5-442.51		9.95
URL5-442.77		10.10
URL5-442.80	427.1	9.46
URL2-1080.27	991.0	6.97
URL2-1080.29		6.94
URL2-1080.78		7.12
URL2-1080.80	991.4	6.63
URL2-1081.64		7.46
URL2-1082.17		7.96
URL2-1082.19	992.7	6.22

Table 9. Individual sample data for triaxial compression measurements showing sample identification, bulk density, confining pressure, temperature, triaxial strength, Young's modulus (tangent modulus of elasticity)

Sample Identification	Bulk Density (Mg/m^3)	Confining Pressure (MPa)	Temperature (°C)	Triaxial Strength (MPa)	Young's Modulus (GPa)
URL1-179.82	2.64	3.5	21	272	65.79
URL1-189.62	2.64	3.5	21	276	70.00
URL5-127.62	2.64	3.5	21	285	67.94
URL5-136.90	N/A	3.5	21	299	71.30
URL6-224.50	2.65	3.5	21	280	68.87
URL6-256.67	2.62	3.5	21	302	68.08
URL7-132.00	2.68	3.5	21	315	70.66
URL7-188.20	2.65	3.5	21	264	68.33
URL6-374.22	2.63	5.0	21	303	56.59
URL6-392.04	2.63	5.0	21	288	63.28
URL1-179.70	2.64	10.0	21	344	67.03
URL1-189.23	2.64	10.0	21	363	67.61
URL2-1080.14	2.63	10.0	21	345	60.16
URL2-1081.77	2.63	10.0	21	356	60.55
URL5-128.46	2.65	10.0	21	371	70.99
URL5-137.15	2.63	10.0	21	365	67.06
URL6-224.62	2.65	10.0	21	384	68.26
URL6-257.60	2.62	10.0	21	364	70.86
URL6-373.69	2.63	10.0	21	344	66.32
URL6-391.25	2.63	10.0	21	361	65.42
URL7-144.00	2.63	10.0	21	383	69.75
URL7-174.42	2.63	10.0	21	376	68.33
URL5-442.13	2.66	15.0	21	419	58.67
URL5-442.94	2.66	15.0	21	367	59.34
URL1-179.45	2.64	17.0	21	429	69.42
URL1-189.49	2.64	17.0	21	405	64.93
URL5-127.74	2.62	17.0	21	436	71.11
URL5-136.69	2.64	17.0	21	435	72.00
URL6-224.74	2.65	17.0	21	435	66.63
URL6-257.72	2.63	17.0	21	434	68.69
URL6-391.48	2.63	25.0	21	488	68.87
URL6-391.71	2.63	25.0	21	488	63.36

Sample Identification	Bulk Density (Mg/m^3)	Confining Pressure (MPa)	Temperature (°C)	Triaxial Strength (MPa)	Young's Modulus (GPa)
URL1-179.58	2.67	26.0	21	516	67.33
URL1-179.95	2.64	26.0	21	479	69.33
URL5-128.33	2.65	26.0	21	506	66.41
URL5-137.28	2.63	26.0	21	505	64.88
URL6-225.50	2.64	26.0	21	507	64.86
URL6-257.84	2.64	26.0	21	513	66.21
URL7-150.26	2.59	26.0	21	506	66.31
URL7-166.55	2.63	26.0	21	543	69.16
URL5-441.85	2.66	30.0	21	534	60.99
URL5-442.64	2.66	30.0	21	539	61.25
URL1-180.20	2.63	35.0	21	534	71.03
URL1-189.20	2.63	35.0	21	563	69.26
URL2-1080.41	2.63	35.0	21	601	65.44
URL2-1081.49	2.63	35.0	21	532	67.04
URL5-128.20	2.63	35.0	21	562	69.41
URL5-137.02	2.64	35.0	21	534	65.54
URL6-224.90	2.65	35.0	21	552	69.46
URL6-258.08	2.63	35.0	21	551	70.10
URL7-134.16	2.63	35.0	21	611	69.02
URL7-181.00	2.64	35.0	21	558	69.18
URL-B4-9.75	2.64	35.0	21	606	70.01
URL-B26-5.00	2.63	35.0	21	576	76.20
URL2-1080.92	2.62	50.0	21	674	67.46
URL2-1082.31	2.64	50.0	21	636	64.57
URL2-1080.63*	2.63	50.0	21	651	66.74
URL2-1082.03*	2.63	50.0	21	638	64.11
URL6-374.85	2.65	50.0	21	597	69.21
URL6-392.27	2.63	50.0	21	629	68.52
URL5-441.57	2.63	55.0	21	317**	62.94
URL5-442.36	2.66	55.0	21	708	63.80
URL2-1080.63	2.63	70.0	21	727†	66.71
URL2-1082.03	2.63	70.0	21	713†	66.27
URL6-226.25	2.65	3.5	100	275	74.67
URL6-256.51	2.62	3.5	100	278	71.42

Sample Identification	Bulk Density (Mg/m^3)	Confining Pressure (MPa)	Temperature (°C)	Triaxial Strength (MPa)	Young's Modulus (GPa)
URL6-225.74	2.68	10.0	100	286*	73.40
URL6-258.20	2.62	10.0	100	335	70.76
URL6-225.62	2.66	17.0	100	421	72.73
URL6-258.46	2.63	17.0	100	413	76.73
URL6-225.90	2.66	26.0	100	459	61.91
URL6-258.82	2.62	26.0	100	496	65.66
URL6-226.02	2.64	35.0	100	534	74.44
URL6-258.70	2.63	35.0	100	536	73.54
URL6-226.37	2.64	3.5	200	239	63.99
URL6-227.42	2.64	3.5	200	217	61.22
URL6-226.60	2.63	10.0	200	299	82.87††
URL6-228.33	2.63	10.0	200	330	72.68
URL6-226.72	2.64	17.0	200	359	68.74
URL6-259.26	2.63	17.0	200	359	62.84
URL6-227.30	2.64	26.0	200	448	70.11
URL6-228.18	2.65	26.0	200	460	81.93††
URL6-225.10	2.63	35.0	200	550	75.85
URL6-226.94	2.65	35.0	200	501	67.31

* Samples were previously cycled to $\sigma 3$ = 70.0 MPa
** Failure occurred along a pre-existing fracture plane
† Triaxial strengths were estimated using failure strength determined at 3=50 MPa
†† Value was treated as an outlier

Table 10. Individual sample data for triaxial compression measurements showing sample identification, test temperature, angle of cut, major principal stress, confining pressure, normal stress and shear stress

Results of triaxial compression tests on saw-cut Pinawa granite specimens

Specimen Identification test# Depth ID	Test Temperature (°C)	Angle of cut	Major Principal Stress (σ1) (MPa)	Confining Pressure (σ3) (MPa)	Normal Stress (σn) (MPa)	Shear Stress (τ) (-)(MPa)
			8.58	0.75	5.74	3.76
			33.18	9.10	24.46	11.57
WN1-171.30	21	37	45.62	17.50	35.44	13.51
			73.50	25.90	56.27	22.88
			1.81	0.75	1.14	0.507
			22.5	9.1	14.1	6.5
WN-170.31	21	37.5	44.6	17.5	27.5	13.1
			64.3	25.9	40.1	18.5
			12.6	6.3	8.6	3.0
			30.9	14.7	20.7	7.8
WN1-170.32	21	37.5	51.4	23.1	33.6	13.7
			70.7	31.5	46.0	18.9
			9.0	3.5	5.54	2.67
			23.1	11.9	16.1	5.4
WN1-170.33	21	37.5	43.8	20.3	29.0	11.3
			59.3	28.7	40.0	14.8
			20.31	6.3	15.23	6.73
			42.33	14.7	32.32	13.28
WN1-170.34	101	37	79.51	23.1	59.08	27.11
			112.11	31.5	82.92	38.74
			5.29	0.75	3.65	2.18
			28.31	9.10	21.36	9.23
WN1-170.95	132	37	52.19	17.50	39.63	16.67
			81.08	25.90	61.10	26.52
			1.57	3.5	2.27	0.93
			33.89	11.9	25.93	10.57
WN1-170.55	200	37	104.67	20.3	74.12	40.55
			219.36	28.7	150.33	91.63
			23.74	6.3	17.42	8.38
			44.04	14.7	33.42	14.10
WN1-170.84	202	37	67.92	23.1	51.69	21.54
			90.23	31.5	68.97	28.23

Table 11. Individual sample data on rock joint sample properties, and estimated peak shear strength based on calculated joint roughness coefficient (JRC) values

Joint sample properties: Calculated joint roughness coefficient (JRC) and peak shear strength estimation for Lac du Bonnet drilled core samples

Sample Number	Strike	Dip	Material Comp. Strength (MPa)	Joint Wall Comp. Strength (MPa)	JRC	Normal Stress (MPa)	Shear Strength (MPa)	Filling Material
[illegible]-SM-E75 6.83	292.	70.	[illegible]	[illegible]	6.99	[illegible]	[illegible]	SE,CA,CO
						0.001	0.002	
						0.010	0.013	
						0.100	0.102	
						1.000	0.812	
						10.000	6.383	
						100.000	48.917	
[illegible]-SM-E83 2.35	200.	31.	183.	97.	5.86			HE,CL,CA,PY
						0.001	0.003	
						0.010	0.018	
						0.100	0.131	
						1.000	0.955	
						10.000	6.938	
						100.000	48.703	
225-SM-E75 2.318	106.	59.	181.	129.	7.13			CA,HE,CY
						0.001	0.002	
						0.010	0.015	
						0.100	0.119	
						1.000	0.923	
						10.000	7.132	
						100.000	54.129	
225-SM-E75 3.937	213.	57.	223.	153.	7.45			CA,CY,HE
						0.001	0.002	
						0.010	0.016	
						0.100	0.125	
						1.000	0.961	
						10.000	7.372	
						100.000	55.319	
225-SM-E75 4.552	212.	57.	201.	126.	5.83			CY,CA,HE,CL
						0.001	0.002	
						0.010	0.012	
						0.100	0.099	
						1.000	0.808	
						10.000	6.318	
						100.000	31.537	
225-SM-E75 5.422	217.	33.	182.	106.	5.44			CA,HE,CY,CL
						0.001	0.001	
						0.010	0.011	
						0.100	0.092	
						1.000	0.760	
						10.000	6.201	
						100.000	49.362	
228-SM-E75 5.699	175.	51.	182.	93.	7.73			CA,HE,CY
						0.001	0.002	
						0.010	0.015	
						0.100	0.112	
						1.000	0.835	
						10.000	6.640	
						100.000	46.730	
225-SM-E83 3.185	146.	83.	160.	125.	8.75			CA,CO
						0.001	0.003	
						0.010	0.021	
						0.100	0.144	
						1.000	1.054	
						10.000	7.748	
						100.000	55.471	
225-SM-S75 4.305	195.	54.	219.	176.	6.32			NONE
						0.001	0.002	
						0.010	0.013	
						0.100	0.113	
						1.000	0.923	
						10.000	7.353	
						100.000	53.000	
225-SM-S83 8.315	160.	83.	219.	129.	7.09			NONE
						0.001	0.002	
						0.010	0.013	
						0.100	0.113	
						1.000	0.881	
						10.000	6.829	
						100.000	51.399	
103-SM-N75 6.35	30.	82.	211.	135.	6.36			CA,HE,CY
						0.001	0.002	
						0.010	0.014	
						0.100	0.110	
						1.000	0.871	
						10.000	6.875	
						100.000	53.038	
103-SM-N75 6.73	40.	83.	198.	145.	6.00			CA,HE,CY
						0.001	0.002	
						0.010	0.013	
						0.100	0.107	
						1.000	0.865	
						10.000	6.968	
						100.000	53.099	
103-SM-N75 6.50	204.	89.	198.	128.	6.67			CA,HE,CY
						0.001	0.002	
						0.010	0.014	
						0.100	0.110	
						1.000	0.873	
						10.000	6.860	
						100.000	52.670	
103-SM-N75 7.42	25.	86.	213.	96.	5.91			CA,HE,CY
						0.001	0.001	
						0.010	0.011	
						0.100	0.091	
						1.000	0.738	
						10.000	5.896	
						100.000	45.815	
103-SM-N83 6.70	9.	84.	224.	148.	6.07			CA,HE,CL
						0.001	0.002	
						0.010	0.013	
						0.100	0.106	
						1.000	0.859	
						10.000	6.850	
						100.000	53.933	
103-SM-N83 7.10	8.	89.	239.	180.	6.97			CA,HE,CL
						0.001	0.002	
						0.010	0.016	
						0.100	0.123	
						1.000	0.962	
						10.000	7.514	
						100.000	57.622	
103-SM-N83 7.90	183.	89.	239.	126.	7.18			CA,HE,CL
						0.001	0.002	
						0.010	0.014	
						0.100	0.112	
						1.000	0.870	
						10.000	6.705	
						100.000	50.203	

Sample Number	Trace	Dip	Material Comp. Strength (MPa)	Joint Wall Comp. Strength (MPa)	JRC	Normal Stress (MPa)	Shear Strength (MPa)	Infilling Material
[illegible]	[illegible]	[illegible]	134.	73.	[illegible]	[illegible]	[illegible]	CA,HE
						0.001	0.001	
						0.010	0.012	
						0.100	0.099	
						1.000	0.842	
						10.000	[illegible].106	
						100.000	59.369	
[illegible]-SM-L81 5.99	[illegible]	90.	[illegible]	177.	5.99			CL,HE,CY
						0.001	0.002	
						0.010	0.013	
						0.100	0.108	
						1.000	0.879	
						10.000	[illegible].211	
						100.000	56.610	
[illegible]-SM-S73 2.50	136.	32.	139.	129.	4.38			CA
						0.001	0.001	
						0.010	0.010	
						0.100	0.087	
						1.000	0.738	
						10.000	6.214	
						100.000	51.362	
[illegible]-SM-S83 1.30	194.	59.	200.	107.	2.99			CL,PY,CA,CO
						0.001	0.001	
						0.010	0.008	
						0.100	0.070	
						1.000	0.622	
						10.000	5.314	
						100.000	48.317	
URL1 29.46	134.	60.	208.	173.	6.46			NONE
						0.001	0.002	
						0.010	0.015	
						0.100	0.118	
						1.000	0.940	
						10.000	7.473	
						100.000	58.477	
URL1 39.05	36.	74.	136.	133.	7.96			CA,HE,CL
						0.001	0.003	
						0.010	0.018	
						0.100	0.130	
						1.000	0.986	
						10.000	7.840	
						100.000	54.765	
URL1 54.87	37.	77.	214.	117.	5.70			HE
						0.001	0.001	
						0.010	0.012	
						0.100	0.095	
						1.000	0.777	
						10.000	6.285	
						100.000	49.751	
URL1 65.73	38.	74.	222.	69.	8.03			CA,HE
						0.001	0.002	
						0.010	0.012	
						0.100	0.090	
						1.000	0.670	
						10.000	4.834	
						100.000	32.034	
URL1 69.28	58.	32.	224.	97.	5.58			CA,HE
						0.001	0.001	
						0.010	0.011	
						0.100	0.087	
						1.000	0.713	
						10.000	5.776	
						100.000	45.306	
URL1 86.28	59.	36.	192.	73.	5.23			CA,HE,CY
						0.001	0.001	
						0.010	0.010	
						0.100	0.079	
						1.000	0.636	
						10.000	5.307	
						100.000	41.869	
URL1 87.87	45.	33.	222.	135.	7.46			NONE
						0.001	0.002	
						0.010	0.016	
						0.100	0.120	
						1.000	0.923	
						10.000	7.065	
						100.000	52.687	
URL1 93.67	37.	77.	167.	147.	6.31			NONE
						0.001	0.002	
						0.010	0.015	
						0.100	0.119	
						1.000	0.955	
						10.000	7.635	
						100.000	60.220	
URL1 121.72	37.	69.	136.	136.	5.35			CA,HE
						0.001	0.002	
						0.010	0.013	
						0.100	0.108	
						1.000	0.892	
						10.000	7.370	
						100.000	60.180	
URL1 326.14	91.	20.	127.	110.	4.83			HE,CL
						0.001	0.001	
						0.010	0.011	
						0.100	0.095	
						1.000	0.802	
						10.000	6.718	
						100.000	55.388	
URL1 326.59	121.	60.	127.	45.	5.45			HE,CL
						0.001	0.001	
						0.010	0.009	
						0.100	0.073	
						1.000	0.597	
						10.000	4.741	
						100.000	36.219	
URL1 465.36	30.	58.	146.	126.	4.31			BI
						0.001	0.001	
						0.010	0.011	
						0.100	0.093	
						1.000	0.791	
						10.000	6.707	
						100.000	56.202	
URL2 6.95	38.	60.	110.	39.	8.03			CA,HE
						0.001	0.003	
						0.010	0.018	
						0.100	0.133	
						1.000	0.987	
						10.000	7.318	
						100.000	52.641	
URL2 81.86	69.	60.	206.	65.	8.03			CL,BI
						0.001	0.002	
						0.010	0.014	
						0.100	0.104	
						1.000	0.772	
						10.000	5.596	
						100.000	37.992	

Sample Number	Ke	UCS	Uniaxial Comp. Strength (MPa)	Point Load Comp. Strength (MPa)	BRC	Normal Stress (MPa)	Shear Strength (MPa)	Critical Material
[illegible]	[illegible]	[illegible]	[illegible]	[illegible]	[illegible]	0.001	0.001	HE
						0.010	0.011	
						0.100	0.090	
						1.000	0.777	
						10.000	6.632	
						100.000	56.012	
[illegible]	[illegible]	[illegible]	[illegible]	[illegible]	5.62			CA,HE
						0.001	0.001	
						0.010	0.010	
						0.100	0.090	
						1.000	0.790	
						10.000	6.911	
						100.000	52.028	
URL3 6.33	1.4.	72.	190.	121.	5.28			HE,CL.
						0.001	0.001	
						0.010	0.011	
						0.100	0.096	
						1.000	0.759	
						10.000	6.402	
						100.000	51.724	
[illegible]	2.7.	73.	203.	127.	7.30			CA,HE
						0.001	0.002	
						0.010	0.016	
						0.100	0.119	
						1.000	0.917	
						10.000	7.005	
						100.000	52.109	
URL3 35.66	1.1.	61.	173.	120.	6.17			HE
						0.001	0.002	
						0.010	0.013	
						0.100	0.105	
						1.000	0.846	
						10.000	6.741	
						100.000	52.752	
URL3 65.39	1.1.	24.	149.	94.	6.40			HE,CY
						0.001	0.002	
						0.010	0.013	
						0.100	0.102	
						1.000	0.815	
						10.000	6.438	
						100.000	49.375	
URL3 65.76	291.	52.	198.	137.	6.61			NONE
						0.001	0.002	
						0.010	0.014	
						0.100	0.112	
						1.000	0.859	
						10.000	7.006	
						100.000	54.091	
URL3 91.65	127.	35.	222.	196.	5.32			HE,CL
						0.001	0.002	
						0.010	0.013	
						0.100	0.106	
						1.000	0.882	
						10.000	7.286	
						100.000	59.306	
URL3 106.24	352.	55.	175.	137.	8.31			BI,PY
						0.001	0.003	
						0.010	0.019	
						0.100	0.139	
						1.000	1.036	
						10.000	7.731	
						100.000	56.367	
URL3 211.10	42.	24.	135.	135.	5.71			NONE
						0.001	0.002	
						0.010	0.014	
						0.100	0.111	
						1.000	0.905	
						10.000	7.386	
						100.000	59.471	
URL3 216.40	367.	23.	176.	152.	6.18			NONE
						0.001	0.002	
						0.010	0.014	
						0.100	0.114	
						1.000	0.916	
						10.000	7.346	
						100.000	58.021	
URL3 223.01	11.	53.	184.	131.	5.31			HE
						0.001	0.001	
						0.010	0.012	
						0.100	0.097	
						1.000	0.807	
						10.000	6.642	
						100.000	53.819	
URL3 232.03	37.	52.	196.	136.	5.61			HE,CL
						0.001	0.003	
						0.010	0.019	
						0.100	0.136	
						1.000	1.012	
						10.000	7.513	
						100.000	59.302	
URL3 257.89	2.	78.	214.	62.	8.11			CA,HE,SR
						0.001	0.002	
						0.010	0.013	
						0.100	0.098	
						1.000	0.736	
						10.000	5.375	
						100.000	36.683	
URL3 258.63	61.	23.	176.	89.	3.30			HE,CL,CY,QTZ
						0.001	0.001	
						0.010	0.008	
						0.100	0.071	
						1.000	0.623	
						10.000	5.435	
						100.000	46.695	
URL3 261.60	332.	68.	129.	123.	8.80			NONE
						0.001	0.004	
						0.010	0.022	
						0.100	0.153	
						1.000	1.112	
						10.000	8.163	
						100.000	58.727	
URL6 16.52	323.	82.	248.	119.	7.33			HE,CL
						0.001	0.002	
						0.010	0.013	
						0.100	0.113	
						1.000	0.871	
						10.000	6.622	
						100.000	48.722	
URL6 83.70	N/A	N/A	237.	127.	8.35			NONE
						0.001	0.003	
						0.010	0.018	
						0.100	0.128	
						1.000	0.933	
						10.000	7.073	
						100.000	50.800	

Sample Number	Ke	UCS	Uniaxial Comp. Strength (MPa)	Point Load Comp. Strength (MPa)	BRC	Normal Stress (MPa)	Shear Strength (MPa)	Critical Material
[illegible]	[illegible]	[illegible]	[illegible]	[illegible]	4.33			HE
						0.001	0.001	
						0.010	0.011	
						0.100	0.090	
						1.000	0.777	
						10.000	6.632	
						100.000	56.012	
URL6 93.71	1.2.	41.	134.	104.	3.67			CA,HE
						0.001	0.001	
						0.010	0.010	
						0.100	0.090	
						1.000	0.790	
						10.000	6.911	
						100.000	52.028	
URL6 99.00	1.5.	85.	241.	179.	6.67			HE,CL.
						0.001	0.002	
						0.010	0.015	
						0.100	0.118	
						1.000	0.937	
						10.000	7.391	
						100.000	57.267	
URL6 113.00	333.	78.	222.	172.	6.66			CA,HE
						0.001	0.002	
						0.010	0.015	
						0.100	0.118	
						1.000	0.938	
						10.000	7.408	
						100.000	57.478	
URL6 207.29	200.	32.	197.	147.	5.67			HE
						0.001	0.002	
						0.010	0.013	
						0.100	0.104	
						1.000	0.849	
						10.000	6.911	
						100.000	55.373	
URL6 216.09	125.	59.	218.	165.	7.67			HE,CL
						0.001	0.003	
						0.010	0.018	
						0.100	0.132	
						1.000	1.007	
						10.000	7.686	
						100.000	57.430	
URL7 142.36	344.	79.	135.	94.	5.22			CA,HE
						0.001	0.001	
						0.010	0.011	
						0.100	0.095	
						1.000	0.778	
						10.000	6.340	
						100.000	50.626	
URL7 144.60	123.	60.	163.	112.	7.44			CA,HE
						0.001	0.002	
						0.010	0.016	
						0.100	0.119	
						1.000	0.916	
						10.000	6.999	
						100.000	52.162	
URL7 153.26	343.	69.	149.	70.	8.78			HE,CY
						0.001	0.002	
						0.010	0.016	
						0.100	0.116	
						1.000	0.836	
						10.000	6.183	
						100.000	42.337	

Table 12. Individual sample data on rock joint sample properties and estimated peak shear strength based on estimated joint roughness coefficient (JRC) values

Joint sample properties: Visually estimated joint roughness coefficient (JRC) and peak shear strength estimation for Lac du Bonnet drilled core samples

Sample Number	Strike	Dip	Material Comp. Strength (MPa)	Joint Wall Comp. Strength (MPa)	JRC Estimate	Normal Stress (MPa)	Shear Strength (MPa)	Infillin. Materia.
[illegible]	[illegible]	[illegible]	222.	117.	5.5			CL
						0.001	0.001	
						0.010	0.011	
						0.100	0.092	
						1.000	0.759	
						10.000	6.177	
						100.000	49.214	
URL1 69.03	76.	46.	222.	99.	7.0			CA,HE
						0.001	0.002	
						0.010	0.013	
						0.100	0.102	
						1.000	0.801	
						10.000	6.174	
						100.000	45.975	
URL1 77.05	151.	31.	190.	155.	7.0			CY,HE
						0.001	0.002	
						0.010	0.016	
						0.100	0.123	
						1.000	0.963	
						10.000	7.515	
						100.000	57.561	
URL1 103.51	146.	41.	168.	115.	5.0			CA,CH
						0.001	0.001	
						0.010	0.011	
						0.100	0.092	
						1.000	0.770	
						10.000	6.393	
						100.000	52.263	
URL1 109.30	56.	65.	158.	73.	8.5			CA,HE
						0.001	0.002	
						0.010	0.016	
						0.100	0.114	
						1.000	0.896	
						10.000	6.184	
						100.000	42.928	
URL1 123.47	25.	87.	133.	120.	8.5			CA,HE
						0.001	0.003	
						0.010	0.020	
						0.100	0.145	
						1.000	1.067	
						10.000	7.917	
						100.000	57.426	
URL1 142.93	37.	87.	173.	150.	5.0			CL,HE
						0.001	0.001	
						0.010	0.012	
						0.100	0.100	
						1.000	0.835	
						10.000	6.968	
						100.000	57.627	
URL1 151.27	18.	78.	158.	98.	5.0			SI
						0.001	0.001	
						0.010	0.011	
						0.100	0.088	
						1.000	0.738	
						10.000	6.110	
						100.000	49.698	
URL1 151.40	53.	65.	158.	129.	4.5			NONE
						0.001	0.001	
						0.010	0.011	
						0.100	0.092	
						1.000	0.781	
						10.000	6.618	
						100.000	55.420	
URL1 325.40	140.	46.	173.	127.	4.0			NONE
						0.001	0.001	
						0.010	0.010	
						0.100	0.085	
						1.000	0.733	
						10.000	6.309	
						100.000	53.725	
URL1 325.56	57.	58.	127.	85.	6.0			CL,SI
						0.001	0.002	
						0.010	0.012	
						0.100	0.098	
						1.000	0.790	
						10.000	6.328	
						100.000	49.646	

Sample Number	Strike	Dip	Material Comp. Strength (MPa)	Joint Wall Comp. Strength (MPa)	JRC Estimate	Normal Stress (MPa)	Shear Strength (MPa)	Infillin. Materia.
URL2 125.76	[illegible]	46.	167.	147.	8.5			NONE
						0.001	0.003	
						0.010	0.022	
						0.100	0.136	
						1.000	0.127	
						10.000	5.368	
						100.000	51.098	
URL2 310.63	127.	31.	59.	45.	4.5			CL,SI
						0.001	0.001	
						0.010	0.008	
						0.100	0.072	
						1.000	0.603	
						10.000	5.203	
						100.000	45.363	
URL2 330.92	110.	39.	166.	166.	5.0			HE
						0.001	0.001	
						0.010	0.012	
						0.100	0.104	
						1.000	0.873	
						10.000	7.293	
						100.000	60.333	
URL2 13.75	153.	31.	175.	66.	7.0			HE
						0.001	0.002	
						0.010	0.013	
						0.100	0.102	
						1.000	0.797	
						10.000	6.145	
						100.000	45.721	
URL2 43.30	37.	44.	163.	68.	6.0			CY,PEGA
						0.001	0.001	
						0.010	0.010	
						0.100	0.084	
						1.000	0.677	
						10.000	5.340	
						100.000	40.607	
URL2 68.52	159.	43.	122.	77.	4.5			CA,SI
						0.001	0.001	
						0.010	0.010	
						0.100	0.082	
						1.000	0.696	
						10.000	5.837	
						100.000	48.283	
URL2 79.79	18.	66.	211.	80.	6.5			CA,HE
						0.001	0.001	
						0.010	0.011	
						0.100	0.091	
						1.000	0.726	
						10.000	5.637	
						100.000	42.266	
URL2 93.97	245.	15.	188.	96.	5.0			HE
						0.001	0.001	
						0.010	0.010	
						0.100	0.083	
						1.000	0.707	
						10.000	5.833	
						100.000	47.173	
URL2 99.80	53.	33.	219.	110.	7.0			CA,SI
						0.001	0.002	
						0.010	0.014	
						0.100	0.108	
						1.000	0.842	
						10.000	6.322	
						100.000	49.017	
URL2 101.72	125.	75.	217.	103.	6.5			CA,HE
						0.001	0.002	
						0.010	0.013	
						0.100	0.100	
						1.000	0.792	
						10.000	6.217	
						100.000	47.417	
URL2 111.49	39.	56.	87.	58.	5.0			CL,CA,SI
						0.001	0.001	
						0.010	0.010	
						0.100	0.086	
						1.000	0.703	
						10.000	5.797	
						100.000	46.848	
URL2 114.27	69.	64.	186.	116.	9.0			CA,HE
						0.001	0.003	
						0.010	0.020	
						0.100	0.140	
						1.000	1.014	
						10.000	7.371	
						100.000	51.823	

				66.								66.		5.0				HE
						0.001	0.001								0.001	0.001		
						0.010	0.009								0.010	0.011		
						0.100	0.079								0.100	0.092		
						1.000	0.648								1.000	0.769		
						10.000	5.415								10.000	6.936		
						100.000	49.390								100.000	50.191		
		27.	32.	181.	89.	7.0			CY,DI		53.	54.	204.	125.	6.0			HE
						0.001	0.002								0.001	0.002		
						0.010	0.013								0.010	0.012		
						0.100	0.103								0.100	0.101		
						1.000	0.302								1.000	0.318		
						10.000	5.140								10.000	6.366		
						100.000	46.031								100.000	51.392		
		207.	66.	220.	120.	5.5			HE			59.	232.	140.	5.5			HE
						0.001	0.001								0.001	0.003		
						0.010	0.011								0.010	0.020		
						0.100	0.095								0.100	0.142		
						1.000	0.781								1.000	1.030		
						10.000	6.367								10.000	7.783		
						100.000	50.916								100.000	56.311		
		123.	77.	143.	122.	8.0			HE			64.	173.	107.	6.0			NONE
						0.001	0.003								0.001	0.002		
						0.010	0.018								0.010	0.012		
						0.100	0.135								0.100	0.109		
						1.000	1.019								1.000	1.803		
						10.000	7.682								10.000	8.437		
						100.000	46.630								100.000	50.451		
		196.	66.	194.	103.	5.0			NONE			33.	135.	119.	6.5			NONE
						0.001	0.002								0.001	0.002		
						0.010	0.016								0.010	0.014		
						0.100	0.118								0.100	0.114		
						1.000	1.893								1.000	1.911		
						10.000	6.688								10.000	7.222		
						100.000	43.234								100.000	36.263		
		242.	59.	198.	70.	6.0			DI			29.	131.	103.	6.0			CL,DI
						0.001	0.001								0.001	0.001		
						0.010	0.010								0.010	0.009		
						0.100	0.084								0.100	0.079		
						1.000	0.674								1.000	0.683		
						10.000	5.316								10.000	5.833		
						100.000	40.393								100.000	49.313		
		261.	51.	175.	110.	5.5			DI			58.	136.	110.	8.0			NONE
						0.001	0.001								0.001	0.002		
						0.010	0.011								0.010	0.017		
						0.100	0.095								0.100	0.127		
						1.000	0.781								1.000	0.939		
						10.000	6.367								10.000	7.209		
						100.000	50.923								100.000	52.696		
		313.	31.	197.	109.	6.0			CY,HE			49.	166.	146.	7.0			CL,HE
						0.001	0.001								0.001	0.022		
						0.010	0.009								0.010	0.016		
						0.100	0.079								0.100	0.124		
						1.000	0.679								1.000	0.972		
						10.000	5.813								10.000	7.386		
						100.000	49.136								100.000	58.168		
		337.	21.	136.	98.	7.5			CY,HE		N/A	N/A	100.	70.	5.0			HE
						0.001	0.002								0.001	0.001		
						0.010	0.016								0.010	0.010		
						0.100	0.119								0.100	0.087		
						1.000	0.913								1.000	0.731		
						10.000	6.989								1.000	0.731		
						100.000	51.947								10.000	6.049		
															100.000	49.165		
		41.	38.	181.	99.	6.0			CA,HE									
						0.001	0.001											CA
						0.010	0.012								0.001	0.002		
						0.100	0.096								0.010	0.014		
						1.000	0.774								0.100	0.108		
						10.000	6.188								1.000	0.849		
						100.000	48.232								10.000	6.376		
															100.000	49.484		
		333.	24.	196.	107.	6.5			HE									
						0.001	0.001											CA
						0.010	0.010								0.001	0.001		
						0.100	0.083								0.010	0.008		
						1.000	0.701								0.100	0.070		
						10.000	5.299								1.000	0.588		
						100.000	43.850								10.000	4.866		
															100.000	39.283		
		15.	19.	173.	98.	6.5			QZ,HE									
						0.001	0.001											CA
						0.010	0.010								0.001	0.003		
						0.100	0.082								0.010	0.021		
						1.000	0.697								0.100	0.146		
						10.000	5.866								1.000	1.059		
						100.000	48.346								10.000	7.713		
															100.000	39.623		

Fracture Number	Strike	Dip	Intact Comp. Strength (MPa)	Joint Wall Comp. Strength (MPa)	JRC Estimate	Normal Stress (MPa)	Shear Strength (MPa)	Fill Material	Fracture Number	Strike	Dip	Intact Comp. Strength (MPa)	Joint Wall Comp. Strength (MPa)	JRC Estimate	Normal Stress (MPa)	Shear Strength (MPa)	Fill Material
[illegible]	[illegible]	[illegible]	[illegible]	[illegible]	[illegible]	[illegible]	[illegible]	[illegible]	[illegible]	[illegible]	[illegible]	[illegible]	[illegible]	[illegible]	[illegible]	[illegible]	CL,PY
						0.001	0.002								[illegible]	[illegible]	
						0.010	0.017								[illegible]	[illegible]	
						0.100	0.124								[illegible]	[illegible]	
						1.000	0.938								1.000	0.693	
						10.000	7.045								10.000	5.368	
						100.000	51.313								100.000	39.850	
[illegible] 79.91	[illegible]	[illegible]	[illegible]	[illegible]	[illegible]			SR,HE	[illegible]	[illegible]	[illegible]	[illegible]	[illegible]	[illegible]			CL,BI
						0.001	0.001								[illegible]	0.001	
						0.010	0.007								[illegible]	[illegible]	
						0.100	0.060								[illegible]	0.081	
						1.000	0.520								[illegible]	[illegible]	
						10.000	4.463								10.000	[illegible]	
						100.000	37.360								100.000	47.475	
URL6 76.63	[illegible]	[illegible]	[illegible]	[illegible]	[illegible]			CY,HE	URL6 134.62	[illegible]	[illegible]	[illegible]	[illegible]	[illegible]			CL,HE
						0.001	0.001								0.001	0.002	
						0.010	0.009								0.010	0.015	
						0.100	0.077								0.100	0.114	
						1.000	0.648								1.000	0.890	
						10.000	5.413								10.000	6.912	
						100.000	48.368								100.000	52.398	
URL6 74.97	356.	90.	146.	83.	6.5			CA,HE	URL6 143.63	75.	64.	222.	192.	5.0			NONE
						0.001	0.002								0.001	0.001	
						0.010	0.013								0.010	0.012	
						0.100	0.100								0.100	0.102	
						1.000	0.797								1.000	0.834	
						10.000	6.255								10.000	7.128	
						100.000	47.783								100.000	58.865	
URL6 36.27	[illegible]	[illegible]	[illegible]	77.	7.5			HE	URL6 158.90	363.	56.	158.	102.	4.0			CL,CA
						0.001	0.002								0.001	0.001	
						0.010	0.014								0.010	0.009	
						0.100	0.107								0.100	0.080	
						1.000	0.826								1.000	0.693	
						10.000	6.239								10.000	5.963	
						100.000	45.669								100.000	50.531	
[illegible]	67.	8.	126.	81.	4.5			CY,HE	URL6 161.00	360.	84.	213.	179.	5.0			CA,HE
						0.001	0.001								0.001	0.001	
						0.010	0.010								0.010	0.012	
						0.100	0.083								0.100	0.100	
						1.000	0.702								1.000	0.842	
						10.000	5.910								10.000	7.031	
						100.000	48.950								100.000	57.996	
URL6 36.87	348.	42.	126.	83.	6.0			NONE	URL6 263.36	37.	31.	181.	143.	4.5			NONE
						0.001	0.002								0.001	0.001	
						0.010	0.012								0.010	0.011	
						0.100	0.098								0.100	0.092	
						1.000	0.795								1.000	0.784	
						10.000	6.368								10.000	6.643	
						100.000	49.831								100.000	55.632	
URL6 87.58	65.	11.	138.	80.	4.5			CY,HE	URL6 266.13	12.	29.	132.	116.	5.0			HE
						0.001	0.001								0.001	0.001	
						0.010	0.009								0.010	0.012	
						0.100	0.078								0.100	0.097	
						1.000	0.665								1.000	0.813	
						10.000	5.372								10.000	6.773	
						100.000	45.843								100.000	55.702	
URL3 99.52	240.	82.	211.	112.	8.0			SR,HE	URL7 22.16	270.	78.	186.	102.	7.5			CA,HE
						0.001	0.002								0.001	0.002	
						0.010	0.016								0.010	0.015	
						0.100	0.120								0.100	0.113	
						1.000	0.906								1.000	0.866	
						10.000	6.790								10.000	6.390	
						100.000	49.152								100.000	48.325	
URL3 102.12	202.	20.	172.	108.	6.0			CL,HE	URL7 63.27	234.	55.	219.	87.	13.0			NONE
						0.001	0.002								0.001	0.032	
						0.010	0.012								0.010	0.038	
						0.100	0.100								0.100	0.190	
						1.000	0.808								1.000	1.159	
						10.000	6.477								10.000	7.321	
						100.000	50.801								100.000	42.872	
URL3 103.85	91.	16.	169.	79.	5.5			CL,BI	URL7 68.72	163.	82.	170.	103.	6.0			CA,HE
						0.001	0.001								0.001	0.002	
						0.010	0.010								0.010	0.012	
						0.100	0.085								0.100	0.099	
						1.000	0.700								1.000	0.801	
						10.000	5.633								10.000	6.418	
						100.000	48.481								100.000	50.279	
URL3 259.00	216.	35.	216.	133.	6.5			CA,HE	URL7 34.88	31.	90.	150.	121.	6.0			CA,HE
						0.001	0.002								0.001	0.002	
						0.010	0.010								0.010	0.013	
						0.100	0.108								0.100	0.107	
						1.000	0.859								1.000	0.866	
						10.000	6.787								10.000	6.973	
						100.000	52.419								100.000	55.191	
URL6 18.39	35.	76.	236.	150.	7.0			CA,HE	URL7 135.42	67.	70.	173.	115.	9.0			CA,HE
						0.001	0.002								0.001	0.003	
						0.010	0.015								0.010	0.020	
						0.100	0.116								0.100	0.141	
						1.000	0.905								1.000	1.023	
						10.000	7.038								10.000	7.440	
						100.000	53.481								100.000	52.384	
URL6 21.63	145.	47.	189.	95.	3.5			CL,BI	URL7 164.60	122.	32.	198.	107.	7.5			CL,HE
						0.001	0.001								0.001	0.002	
						0.010	0.008								0.010	0.015	
						0.100	0.072								0.100	0.116	
						1.000	0.629								1.000	0.875	
						10.000	5.468								10.000	6.668	
						100.000	46.995								100.000	49.162	
URL6 93.06	N/A	N/A	216.	126.	7.5			HE	URL7 173.17	119.	18.	165.	80.	5.0			NONE
						0.001	0.002								0.001	0.001	
						0.010	0.016								0.010	0.010	
						0.100	0.118								0.100	0.082	
						1.000	0.909								1.000	0.684	
						10.000	6.965								10.000	5.625	
						100.000	51.373								100.000	45.276	

5. PETROPHYSICS

PORE STRUCTURE CHARACTERISTICS OF GRANITIC ROCK SAMPLES FROM THE WHITESHELL RESEARCH AREA

T.J. Katsube* and J.P. Hume**
Geological Survey of Canada,
601 Booth St., Ottawa
Ontario K1A 0E8

*: Geological Survey of Canada (GSC), 601 Booth St., Ottawa, Ontario K1A 0E8
**: Atomic Energy of Canada Ltd. (on attachment to GSC, Ottawa)

PORE STRUCTURE CHARACTERISTICS OF GRANITIC ROCK SAMPLES FROM THE WHITESHELL RESEARCH AREA

T.J. Katsube and J.P. Hume
Geological Survey of Canada, 601 Booth St.,
Ottawa, Ontario K1A 0E8

INTRODUCTION

It is essential that the pore structure and pore distribution of the rocks around a nuclear fuel waste disposal vault be known since these pores form a potential radionuclide release path between the vault and the surface. Porosity, permeability, formation factor (determined from electrical measurements) and other parameters have been measured on separate specimens from identical samples in order to achieve this objective. These measurements have been carried out on over 100 core samples (Standard Core Samples) which were systematically collected from various boreholes in the URL and WN sites of the WNRE research area. This paper contains data and results of data analysis of these measurements, and discusses the pore structure characteristics of the Lac du Bonnet batholith.

THEORY

Radionuclide Transport Theory

The forces and mechanisms that are likely to transport the radionuclides from the vault to the surface are the hydraulic gradient and advection and the concentration gradient and diffusion. The transport equations selected for advection and diffusion will determine the pore structure parameters that must be considered. The following equations (Freeze and Cherry, 1979; deWeist, 1965) related to advection are selected to estimate the time it would take the radionuclides to reach the surface from the vault and the rate of release:

$$k_s = d^2/(12\tau) \quad (1)$$

$$v_s = ck_s I \quad (2)$$

$$t = x/v_s \quad (3)$$

$$Q = V_E A \tag{4}$$

$$V_E = ck_E I \tag{5}$$

where

A = area of the rectangular column
I = hydraulic gradient
Q = flow rate
k_s = specific permeability
k_E = equivalent rock mass permeability
t = time
x = distance in the direction of flow (radionuclide travel distance)
d = pore or fracture aperture width
c = coefficient related to viscosity and density of the fluid in the fractures and pores
v_s = flow velocity
v_E = equivalent rock mass flow velocity
τ = tortuosity.

The following solution (Wadden and Katsube, 1982) of the diffusion equation (Fick's second law) is one of the equations used to estimate the time (transit time) it takes for radionuclides to travel a certain distance from the source:

$$\frac{C}{C_o} = \text{erfc}\left(\frac{x\tau_A}{2\sqrt{Dt}}\right) \tag{6}$$

where

D = diffusion coefficient of the radionuclides ($m^2\ S^{-1}$)
C_o = initial concentration (mol L^{-1})
C = concentration of diffusing species in solution (mol L^{-1})
x = distance in the direction of diffusion (m)
τ_A = apparent tortuosity.

Tortuosity (τ) implies the true tortuosity (Katsube et al., 1985) and the apparent tortuosity (τ_A) includes the effect of pocket and blind pores (Katsube et al., 1986). The following equations (Katsube et al. 1986) can also be used to estimate the time (steady state time) it takes the radionuclides to reach a certain point from the source and the radionuclide release rate at that point:

$$\frac{C}{C_o} = \frac{A\phi_E}{V}\left(\frac{D}{x\tau_A^2}t - \frac{x}{6}\right) \tag{7}$$

$$t_B = \frac{\tau_D^2 x^2}{6D} \tag{8}$$

$$M = \left(\frac{AD}{Vx}\right) \frac{\phi_E}{\tau_A^2} \tag{9}$$

where

t_B = radionuclide break-through time

M = radionuclide concentration gradient

V = volume of the body of water (Katsube et al. 1986) into which the release takes place

ϕ_E = effective porosity.

Equations (7)-(9) are usually used for the analysis of the results from laboratory diffusion experiments.

From the equations it is evident that the basic pore structure parameters required to estimate the radionuclide transport times are as follows: aperture (d), tortuosity (τ), equivalent rock mass permeability (k_E), apparent tortuosity (τ_A) and effective porosity (ϕ_E).

Definition of Pore Structure Parameters

The pore structure models used in this study have been discussed in a number of papers (e.g., Katsube et al. 1985; Katsube and Kamineni, 1983; Wadden and Katsube, 1982). Here the discussion will be limited to the five pore structure parameters required to estimate radionuclide transport rates.

Crystalline rocks contain a complex network of microfractures with different apertures and lengths (e.g. Chernis and Robertson, this volume). However, it is possible to represent this network by a number of basic bulk parameters (Katsube et al. 1985). These are aperture (d), tortuosity (τ), path frequency (n) and pocket porosity (ϕ_p). Path frequency is the number of paths per unit area of the rock. These parameters are the effective, average, or equivalent, parameters that represent the characteristics of all microfracture segments that constitute the fluid and ionic transport paths of the complex microfracture network in a crystalline rock. Pocket porosity (ϕ_p) is the porosity of the blind and dead end pores connected to the complex microfracture network.

The effective porosity (ϕ_E) is the total porosity of all interconnected pores and, from Katsube et al. (1985), it can be defined as follows:

$$\phi_E = \phi_p + \pi n d. \tag{10}$$

Equivalent rock mass permeability (k_E) is the parameter determined by actual permeability measurements of rock samples and, from Brace (1977), it can be defined by,

$$k_E = \frac{nd^3}{12\tau}. \tag{11}$$

Many parameters such as aperture (d), tortuosity (τ), path frequency (n), pocket porosity (ϕ_p) and apparent tortuosity (τ_A) can not be measured directly. Therefore, these parameters must be derived from other parameters such as equivalent rock mass permeability (k_E), effective porosity (ϕ_E) and formation factor (F) that can be measured directly.

From Ward and Frazer (1967), formation factor (F) can be defined by,

$$F = \frac{\tau}{nd}. \tag{12}$$

It is now obvious that aperture can be derived from equations (11) and (12):

$$d = \sqrt{12\, k_E F}. \tag{13}$$

The path frequency (n) and tortuosity (τ) can be derived from equations (10)-(12), if it is assumed that $\phi_p = 0$:

$$\tau = \sqrt{\phi_E F} \qquad (\phi_p = 0) \tag{14}$$

$$n = \sqrt{\frac{\phi_E}{12\, k_E F^2}} \qquad (\phi_p = 0)\ . \tag{15}$$

However, it is often unrealistic to assume that $\phi_p = 0$. The tortuosity derived from equations (10) and (12), with the assumption that $\phi_p \neq 0$, is expressed by the apparent tortuosity (τ_A):

$$\tau_A = \sqrt{\phi_E F} \qquad (\phi_p \neq 0)\ . \tag{16}$$

Since it is unrealistic to assume $\phi_p = 0$, it is sometimes practical to derive the ratio of n and τ from equations (11) and (12):

$$\frac{n}{\tau} = \sqrt{\frac{1}{12\, k_E F^3}} \,. \tag{17}$$

Katsube et al. (1985) developed a new method for the direct determination of tortuosity values. Unfortunately, the tortuosity values can not be determined for individual samples, but can be determined for a group of samples that show evidence of having similar tortuosities. The existence of such groups is justified by the multiple regression analysis studies carried out by Agterberg et al. (1985).

The Approach

Although methods have been developed to determine or derive the parameters required for estimating the radionuclide transport times between the source and a specific point, the question remains as to how representative they are of the actual in situ transport conditions. For this reason, studies of stress release effects, mercury porosimetry and diffusion have been carried out.

As rock samples located at great depths are brought to the surface they expand due to stress release. This release results in an increase in porosity and permeability and a decrease in formation factor values. The degree of stress release can be determined from non-linear stress-strain measurements described by Annor and Katsube (1983). The parameter that indicates the degree of stress release is the crack porosity (ε). This concept was established by Walsh (1965). The values of this parameter can be analysed in relation to other parameters, such as porosity and permeability, in order to determine the in situ values of these parameters.

Rocks consist of a very complex network of pores of various sizes and configurations, as stated previously. The characteristics of the network are represented by a few bulk pore structure parameters. This representation is theoretically justified by the random network and mixing laws (Madden, 1976) as discussed in Wadden and Katsube (1982). This representation is also experimentally justified by the work on mercury porosimetry reported in Katsube and Walsh (in press). The distribution of porosity for various pore sizes is obtained by this

method (Katsube, 1981). In the work by Katsube and Walsh (in press) it has been shown that there is a good relationship between the aperture values derived from formation factor and permeability measurements using equation 13 and the geometric mean of aperture values obtained from the mercury porosimetry data. These measurements were carried out on standard samples from the WN boreholes at WNRE and borehole samples from Atikokan, Otnario. These studies indicate that the validity of using bulk parameters to represent the complex network characteristics can be verified by the use of mercury porosimetry.

Since the purpose of determining the pore structure parameters is to estimate radionuclide transport rates, it is necessary to verify the theories that suggest such estimates are possible using bulk parameter measurements. Diffusion measurements have been carried out for this purpose. It has been shown in equations 7-9 that diffusion rates can be estimated by the bulk parameters τ_A and ϕ_E. It has also been shown by Katsube et al. (1986) that tortuosity and effective porosity can be determined from diffusion measurements. The tortuosity and porosity determined from these measurements are diffusion tortuosity (τ_D) and diffusion porosity (ϕ_D). The validity of using apparent tortuosity (τ_A) and effective porosity (ϕ_E) for estimating the radionuclide transport rates can be verified by comparing these parameters with τ_D and ϕ_D.

METHODS OF MEASUREMENT

Effective Porosity Measurements

The effective porosity of rock samples from the WN and URL sites was determined using the immersion (Katsube, 1981) technique. The volume of pore space is determined from the difference in weight between an oven-dried rock and the same specimen saturated with distilled water. In this case the rock was placed under vacuum for 15 minutes in order to remove air and other gases that may be trapped within the pores. The sample was then immersed in distilled water (still under vacuum) for another 15 minutes. The saturated sample was then removed from the vacuum chamber and its mass was measured using a Mettler H10T analytical balance. Subsequently the sample was heated to 105°C for 4 hours and then placed in a dessicator and allowed to cool to room temperature (approximately 20 minutes were required for the sample to cool). Finally, its mass

was again measured using the analytical balance. The difference in mass between the sample in the water-saturated condition and the oven dry condition permits the volume of pores to be calculated. The bulk volume of the rock is calculated from caliper measurements of the sample dimensions. The effective porosity is the ratio of pore volume to the bulk volume of the sample.

Permeability Measurements

There are a number of techniques available for measuring the intrinsic permeability of rock samples under both laboratory and in-situ conditions. The laboratory measurements of permeability were performed by Terratek (Salt Lake City, Utah) using the steady state transient pulse technique developed by (Brace et al. 1968). The samples were right circular cylinders 4.5 cm in diameter and 2 cm in length. The apparatus used to perform the permeability measurements is comparable to the one used by Heard et al. (1979).

Formation Factor Measurements

Archie (1942) found that the following relationship existed between the resistivity (ρ_R) of a sample saturated with an electrolyte and the resistivity (ρ_o) of that electrolyte:

$$F = \frac{\rho_R}{\rho_o} \tag{18}$$

where
F is the formation factor.

The definition of the formation factor in equation 12 is based upon the assumptions (Patnode and Wyllie, 1950) that (1) the sample is 100% saturated with an electrolyte solution and (2) current is conducted through the sample only via the electrolyte solution saturating the pore space. The second assumption indicates that the formation factors in equations 12 and 18 are equal only if there is no possibility of current conduction by the rock matrix surrounding the pore spaces. If the rock matrix of the sample is not a perfect insulator, F determined by equation (18) is only an apparent formation factor.

A number of authors (e.g., Patnode and Wyllie, 1950; De Witte, 1950; Howell, 1953) have pointed out that the assumption of a perfectly insulating matrix is frequently invalid. There are a number of possible reasons for this: (1) the presence of highly conductive minerals in the rock matrix, (2) electric double layer effects and (3) ion-exchange effects associated with a layer of clay lining the pore walls. This suggests that a correction must be made for these surface conduction effects when measuring formation factors. In order to account for this correction the following equation was suggested by Patnode and Wyllie (1950) who first recognized the need to consider surface resistivity:

$$\frac{1}{F_a} = \frac{1}{F} + \frac{\rho_w}{\rho_c} \tag{19}$$

where

F_a = apparent formation factor
F = true formation factor
ρ_w = pore water resistivity
ρ_c = surface resistivity.

The samples used in these measurements are cylinders 1 cm in length and 4.5 cm in diameter. They are prepared for measurements by placing them under vacuum for 15 minutes in order to remove gases trapped in pore spaces. They are then immersed in saline solution (still under vacuum) and allowed to stand for 30 minutes.

The saturated rock samples are placed in a capacitive type sample holder (Katsube and Collet, 1973) with a graphite electrode covering each face. The cylindrical surface of the sample is dried with a tissue before beginning the resistivity measurement. The sample holder is placed in an enclosed area in order to reduce air movement around it. This is a precautionary measure designed to minimize the evaporation of fluid from the rock pores. Finally, the sample holder is connected to an automatic impedance measuring system. The resistivities are measured over a frequency range of 10-1000 Hz (Katsube, 1981). The practical details concerning the operation of this system are described in the paper by Gauvreau and Katsube (1975).

After the measurement is complete the samples are soaked in distilled water for approximately one hour to rinse the saline solution from the rock pores. The samples are then air-dried. The procedure described above is repeated using 0.05, 0.10, 0.20 and 0.50 M NaCl solutions. This determines an apparent formation factor (F_a) at each concentration of solution (Worthington, 1975). Equation (19) is actually used to calculate the true formation factor (F) of a sample. Measuring F_a at several different values of ρ_w and then plotting $1/F_a$ versus ρ_w should give a straight line with a slope of $1/\rho_c$ and y intercept equal to 1/F.

Crack Porosity Measurements

When stress is applied to a rock specimen it contracts and the strain that develops is linearly related to the applied stress. However, at very low levels of stress the relationship between stress and strain is non-linear (Annor and Katsube, 1983). This non-linearity is considered to be due to the closure of microcracks that developed as a result of stress release in a rock sample. Crack porosity (ε) is obtained by extrapolating the linear portion of the stress-strain curve to the zero pressure intercept on the strain axis.

The crack porosity (ε) is equivalent to the extensional strain which is defined as the change in the length or thickness of the specimen divided by its mean length:

$$\varepsilon = \frac{\Delta l}{l} \times 100 \qquad (20)$$

where

l = length of specimen,

Δl = change in length as a result of loading the specimen.

Figure 12 in Katsube et al. (1982) shows a simplified model of crack porosity. Crack porosity (ε) is shown as the reduction in aperture of a single tortuous fracture.

The non-linear stress-strain measurements are carried out at the same time as the mechanical tests described by Annor and Jackson (this volume). Standard core samples 4.5 cm in diameter and 10 cm in length are used for these measurements. Strain gauges oriented to measure both axial and transverse

strain were attached to two opposite sides of the specimens. The load was applied in the axial direction and a strain bridge (Phillip PR9302) and recorder were used to record the voltage analog outputs of the axial and transverse strains produced in the sample. These records were translated into stress-strain curves, and only the axial records were used to determine the crack porosity. These measurements were carried out at the CANMET Rock Mechanical Laboratory and further details of the experimental method are described in Annor and Katsube (1983).

Pore Size Distribution

The pore-size distribution of porous materials is determined using mercury intrusion porosimetry. The results have been reported for a number of different materials such as paper (McKnight et al., 1958), textiles (Burleigh et al., 1949), coal (Zurietering and van Krevelen, 1954) and petroleum reservoir rocks (Meyer, 1953; Bucker et al., 1956). This technique, which was first suggested by E.M. Washburn (1921), uses a device called a mercury porosimeter. This is an apparatus capable of generating sufficiently high pressures (up to 60,000 psi or 420 MPa) to force mercury into all accessible pores and then measure the volume of mercury taken up by the pores (Rootare, 1970). Theoretically, mercury intrusion porosimetry should be able to measure the diameter of all pores down to the diameter of the mercury atom (approximately 3.14×10^{-10} m). In practice, this lower limit has not yet been attained. Drake (1949) has managed to force mercury into pores down to 1.8×10^{-9} m in radius.

In mercury porosimetry it is assumed that the pores in a substance are cylindrical. If this is the case, the Washburn equation is used to relate the pressure required to force mercury into the cores to the pore radius:

$$d = \frac{-2\gamma \cos\theta}{p} \qquad (21)$$

where

d = pore radius

γ = surface tension of mercury = 0.480 N/m

θ = contact angle

p = pressure.

There is no general consensus as to the correct value to be used for the contact angle, θ. In most practical applications of mercury porosimetry, θ is assigned a value between 130 and 140° (Rootare, 1970). The porosity vs pore-size distribution of a rock can be determined by evacuating moisture and gases by vacuum and then forcing mercury into it under pressure. Since the relationship expressed by equation (21) exists between pore-size (d) and pressure (p), the larger the applied pressure (p), the smaller the pore-size (d) intruded by mercury. A good review of the technique can be found in the paper by Rootare (1970). The pore-size distribution of WN and URL rock samples have been determined by the Micromeretics Instrument Corporation, Atlanta, Georgia, U.S.A., and the Ontario Research Foundation, Mississauga, Ontario. A micromeritics mercury porosimeter, Auto Pore 9200, was used for the measurement. The pressure range used is 0.14-410 MPa. The equivalent pore-size range is about 10-0.003 micrometres. The specimens used are segments cut out of discs and their dimensions are in the order of 1 x 1 x 2 centimeters.

Diffusion Measurements

The diffusion coefficients of ionic species in crystalline rocks are determined using the diaphragm cell technique proposed by Garrels et al. (1949). A diffusion cell apparatus is divided into 2 equal compartments. A 1 cm thick granite specimen is placed in a sample holder which is then inserted into the wall that partitions the diffusion cell. A 1 M sodium iodide solution is placed in one compartment and distilled water is placed in the other compartment. The diffusion of iodide through the rock sample from the high concentration reservoir to the low concentration reservoir is monitored by means of a specific ion electrode. The experimental technique used to measure diffusion coefficients is described in greater detail in papers by Wadden and Katsube (1982) and Katsube et al. (1986).

EXPERIMENTAL RESULTS

The experimental results for all measurements except the diffusion and mercury porosimetry measurements are listed in Table 11 in the Appendix.

Effective Porosity

The values of effective porosity (ϕ_E) for all of the WN and URL samples are summarized in Table 1. For comparison purposes the values obtained by other investigators have also been included in this table. The ranges of porosity values from the WN and URL research sites are 0.16-0.54 percent and 0.14-0.67 percent, respectively. The average value of ϕ_E for both WN and URL samples is 0.36 percent. The results for samples from the WN and URL sites vary considerably from the porosity values that other investigators have obtained for granites (Table 1). For example, Alexander et al. (1981) recorded a mean value of 0.56 percent for the effective porosity of granites from an Altnabreac borehole. The table presented in the Results section provides other examples of similar discrepancies. These discrepancies may be simply coincidental (i.e., rocks from different locations with different geological histories may differ with respect to porosity). However, the observed differences may also be due to variations in the

Table 1. Porosity of Granites (Percent)

Rock	# of	Min.	Max.	Mean	Reference
WN1	10	0.29	0.43	0.353	Katsube et al., 1985
WN2	6	0.16	0.28	0.237	Katsube et al., 1985
WN4	18	0.28	0.54	0.404	Katsube et al., 1985
All WN samples	34	0.16	0.54	0.359	
URL-1	16	0.22	0.61	0.365	Katsube et al., 1985
URL-2	8	0.32	0.67	0.498	Katsube et al., 1985
URL-5	12	0.33	0.67	0.446	Katsube et al., 1985
All URL samples	67			0.359	
Granite, Sherman (Effective Flow Porosity)				0.002	Pratt et al. (1974)
Granite, Barre, VT.	1			0.079	Hanley et al. (1978)
Granite, Westerly, RI.	1			0.106	Hanley et al. (1978)
Granite, Stone Mt., GA.				0.30	Brace (1965)
Granite	45			0.40	Franklin et al. (1970)
Granite, Tucson, AZ.	1			0.611	Norton et al. (1977a)
Granite	6			0.7	Mellor (1971)
Granite	26	0.4	4.8	0.9	Izett (1960)
Granite, Laramie, WY.	1			1.08	Norton et al. (1977a)
Granite, Westerly, RI.				1.1	Brace (1965)
Granite, Carroll and Frederick Counties, MD.	17	0.44	3.98	1.11	Houser (1962)
Granite, Troy, AZ.	1			1.36	Norton et al. (1977)
Granite	322	0.1	11.2	1.40	Kessler et al. (1940)
Granite, Equigranular Globe-Miami, AZ.	1			1.77	Norton et al. (1977)
Granite, Texas Canyon, AZ.	1			2.96	Norton et al. (1977)
Granite	9	0.7	5.5	3.0	Norton et al. (1977)
Granite, Altnabieac, ALA	32	0.39	2.67	0.56	Alexander et al. (1981)
Granite, DRAMMEN				1.21 1.88	Heimli (1974)
Granite, HALDEN				0.50	Heimli (1974)
Granite, FINNSJON	30	0.18	0.54	0.29	Skagius and Neretnieks (1985)

techniques used to determine the effective porosities. The majority of investigators use a modification of the previously-described saturation technique for determining effective porosity. For example, Skagius and Neretnieks (1985) saturate granite samples for a period of one week instead of simply a matter of minutes. In addition, a number of investigators (e.g., Izett, 1960) determine the oven-dry mass of a sample prior to determining its saturated mass. It has not yet been concluded whether such variations in the measuring technique influence the values obtained for effective porosities.

Permeability

The results of the permeability measurements for WN and URL samples are presented in Table 2. Values obtained by other investigators are also included for comparison purposes. The mean values of intrinsic permeability for the WN and URL sites are 6.2 and 14.8 darcies, respectively. In general, these values are in agreement with permeability values reported by other investigators.

Table 2. Permeability of Granites (microdarcies)

Rock	# of	Min.	Max.	Mean	Reference
Granite - WN1	10	0.69	3.37	1.63	Katsube et al. (1985)
- WN2	6	0.06	0.82	0.43	Katsube et al. (1985)
- WN4	18	1.7	24.5	10.68	Katsube et al. (1985)
WN samples	34	0.06	24.5	6.21	Katsube et al. (1985)
Granite - URL-1	16	0.10	72.8	11.54	Katsube et al. (1985)
- URL-2	7	1.7	44.4	24.51	Katsube et al. (1985)
- URL-5	2	0.32	0.71	0.52	Katsube et al. (1985)
- URL-7	31	0.01	440.0	15.21	Katsube et al. (1985)
All URL samples	56	0.01	440.0	14.79	Katsube et al. (1985)
Granite, Barriefield, Ont. Lab Test				0.051	Ohle (1951)
Granite, Sherman				1.035	Pratt et al. (1974)
Granite Laramie, (Lab Test)					
Granite (Field Pumping Test)	1			4.14	Delisle (1975)
Granite, Quincy GA. (Lab Test)				4.55	Ohle (1951)
Granite, Hardhat Field Test-Horizontal				41.41	Morris et al. (1967)
Granite, Hardhat Field Test - Vertical				72.46	Boardman et al. (1966)
Granite, Diorite Gabbro Coarse grained fractured field pumping tests)	106				Rasmussen (1964)
Granite, Weathered	7	341, 614.91	5,383, 022.77	1,656 314.7	Morris et al. (1967)

Formation Factor

The results of the formation factor measurements are summarized in Table 3. The mean values of formation factor for the WN and URL sites are 3.23×10^3 and 3.07×10^3, respectively. These values are substantially lower than the formation factor values obtained by Skagius and Neretnieks (1986) and less than half the values reported by Walsh and Brace (1984). The possible cause of the variation is a topic for future investigation.

Crack Porosity

The crack porosity was determined for 16 standard samples from WN series boreholes (WN-1, -2 and -4), 6 special samples from boreholes URL-1 and 26 from boreholes URL-2 and URL-5. These results are listed in Table 4. Some results have been reported by Katsube (1981) and Annor and Katsube (1983). The ranges of these results are also listed in Table 5 for the purpose of comparison with values obtained by other investigators. These results are about one order of

Table 3. Formation factors of granites

Rock	# of Samples	Min.	Max.	Mean	Reference
Granite - WN1	10	1.67×10^3	3.31×10^3	2.27×10^3	Katsube et al. (1983)
- WN2	6	4.00×10^3	16.4×10^3	7.55×10^3	Katsube et al. (1983)
- WN3	18	1.2×10^3	3.6×10^3	2.61×10^3	Katsube et al. (1983)
All WN samples	34	1.2×10^3	16.4×10^3	3.23×10^3	Katsube et al. (1983)
Granite - URL1	16	0.61×10^3	8.79×10^3	2.50×10^3	Katsube et al. (1983)
- URL2	7	0.38×10^3	0.82×10^3	0.54×10^3	Katsube et al. (1983)
- URL5	12	0.54×10^3	4.02×10^3	1.72×10^3	Katsube et al. (1983)
- URL7	31	0.96×10^3	11.5×10^3	4.54×10^3	Katsube et al. (1983)
All URL Samples	66	0.38×10^3	11.5×10^3	3.07×10^3	Katsube et al. (1983)
Westerly Granite	3	1.5×10^3	20.0×10^3	10.75×10^3	Walsh & Brace (1984)
Chelmsford Granite	1	$.40 \times 10^3$	1.5×10^3	7.70×10^3	Walsh & Brace (1984)
Finnsjon, Granite	4	6.5×10^5	10.1×10^5	7.73×10^5	Skagius and Neretnieks (1985)
Gidea, Granite	2	23.8×10^5	25.1×10^5	24.4×10^5	Skagius and Neretnieks (1985)
Svartboberget, Granite	2	38.2×10^5	63.5×10^5	50.9×10^5	Skagius and Neretnieks (1985)

Table 4. Crack porosity, ε (%) of WN and URL standard samples

Sample		ε
WN-1	- 138	0.021
	- 160	0.017
	- 223	0.016
	- 245	0.019
	- 294	0.020
	- 303	0.012
	- 345	0.024
	- 384	0.020
	- 410	0.028
	- 460	0.036
WN-2	- 24	0.016
	- 55	0.008
	- 85	0.004
	- 98	0.008
	- 124	0.012
	- 145	0.028
URL-2	- 256	0.036
	- 448	0.074
	- 586	0.083
	- 705	0.072
	- 798	0.052
	- 871	0.084
	- 1001	0.124
	- 1095	0.118
URL-5	- 16.5	0.006
	- 77.0	0.004
	- 108	0.006
	- 126	0.016
	- 156	0.010
	- 199	0.010
	- 246	0.010
	- 279	
	- 289	0.040
	- 333	0.016
	- 370	0.060
	- 451	0.068
	- 497	0.076

Table 5. Crack porosities (%) of rock samples

Rock	# of Samples	Min.	Max.	Mean	Reference
CR6	10	0.002	0.026	0.011	Katsube and Annor, 1984
CR7	67	0.004	0.025	0.014	Katsube and Annor, 1984
Overall CR	16	0.002	0.026	0.012	Katsube and Annor, 1984
WN1	9	0.012	0.036	0.024	Annor and Katsube, 1983
WN2	6	0.004	0.028	0.013	Annor and Katsube, 1983
Overall WN	15	0.004	0.036	0.019	Annor and Katsube, 1983
Oak Hall Limestone	-	-	-	0.00	Brace, 1965
Frederick Diabase	-	-	-	0.00	Brace, 1965
Rutland, Quartzite	-	-	-	0.100	Brace, 1965
Westerly Granite	-	-	-	0.200	Brace, 1965
Stone Mountain Granite	-	-	-	0.35	Brace, 1965
Casco Granite	-	-	-	0.45	Nur and Simmons, 1969
Troy Granite	-	-	-	0.10	Nur and Simmons, 1969
Bedford Limestone	-	-	-	0.20	Nur and Simmons, 1969
Solenhofen Limestone	-	-	-	0.00	Nur and Simmons, 1969
Wetabuck, Dolomite	-	-	-	0.22	Nur and Simmons, 1969
Barre. Granite	-	-	-	0.30	Nur and Simmons. 1969

magnitude smaller than the results previously reported for granites and other types of rocks (excluding those reported as 0.00%). The reason for our values of crack porosity (ε) to be considered smaller than the results reported by others is not well understood. However, one point of importance is that our method of measurement has a maximum sensitivity of about 0.004% whereas, judging from the values reported by others, their maximum sensitivity is about 0.1%. There is a possibility that the values reported as a ratio of 0.00 could fall within the same ranges as the WN and URL.

Pore Size Distribution

The pore size distribution was determined for 32 standard samples from three boreholes (WN-1, WN-2 and WN-4). The results for all of the 32 samples are listed in Table 6. These results are compiled from Katsube (1981) and Katsube and Walsh (in press). The pore sizes cover a range of 0.0025 micrometres to 4 micrometres. This falls within the same range as the mean values reported by other researchers.

Table 6. Pore size distribution for WNRE samples (porosity in percent in micro-meters)

Sample / Pore Size (micro meters)	.0025 -.0040	-.0063	-0.0100	-.016	-.025	-.040	-.063	-.100	-.160	-.250	-.400	-.630	-.100	-1.60	-2.504
WN2 - 24	0.0260	0.0260	0.0780	0.0780	0.0780	0.0260	0.0260	0.0260	0.0260	0.0520	0.0520	0.0260	0	0	00
- 55	0	0	0	0.0269	0.0269	0	0.0538	0.0269	0.0269	0	0	0.0269	0	0	00
- 85	0.1370	0.1370	0.0820	0.1100	0.0820	0.0550	0.0550	0.0550	0.0550	0	0	0	0	0	00
- 93	0.0240	0.0726	0.0240	0.0240	0	0.0240	0.0240	0.0240	0.0240	0.0474	0.0240	0	0	0	00
- 124	0	0	0	0	0	0.0271	0.0542	0.0271	0.0271	0.0542	0.0271	0.0542	0	0	00
WN1 - 138	0	0	0	0	0.0274	0.0274	0.0274	0.0274	0.0274	0.0547	0.0547	0.0547	0	0	00
WN2 - 145	0	0	0	0	0.0274	0.0274	0.0274	0.0274	0.0274	0.0547	0.0547	0.0547	0	0	00
WN1 - 160	0.0260	0.0790	0.1050	0.0790	0.0570	0.0570	0.0260	0.0260	0	0.0790	0.0530	0.0260	0	0	00
- 223	0	0.0260	0.0790	0.0530	0.0260	0	0.0260	0.0530	0.0260	0.0530	0.0260	0.0530	0	0	00
- 245	0	0.0530	0.0790	0.0530	0	0	0.0260	0.0530	0	0.0530	0.0530	0.0530	0	0	00
- 294	0	0.0833	0.0555	0.0277	0.1075	0.1075	0.1075	0.1075	0.0277	0.1075	0.0277	0.1075	0.0555	0.0555	0.0270
- 303	0	0	0	0	0.0260	0.0260	0	0.0260	0.0260	0.0530	0.1050	0.0260	0	0	00
- 345	0	0	0.0260	0.0520	0.0260	0	0.0260	0	0	0	0.0790	0.0790	0	0	00
- 384	0.0530	0.0530	0.0790	0.0790	0.0260	0.0790	0.0530	0.0530	0	0	0	0.0260	0	0.0260	00
- 410	0.0520	0.0520	0.0520	0.0520	0	0.0520	0.0260	0.0520	0.0790	0.0520	0.0520	0.0520	0	0	00
- 460	0	0	0.0855	0	0	0	0	0.0570	0.0285	0.0855	0.0285	0.0285	0	0	00
WN4 - 468	0.1048	0.0524	0.1310	0.0262	0.0786	0	0	0	0	0	0.0262	0	0.0524	0	00
- 482	0	0.0786	0.0262	0.0262	0	0	0.0524	0	0	0	0	0	0.1572	0.0524	00
- 505	0	0	0	0	0	0.0262	0	0	0.0262	0	0	0	0.2096	0.0262	00
- 551	0	0	0	0.0262	0	0	0	0	0	0	0	0.	0.1834	0	00
- 564	0	0	0	0.0262	0	0	0.0262	0	0	0	0	0.0262	0.0524	0	00
- 603	0	0	0	0.0263	0	0	0.0263	0	0	0	0.0263	0.0263	0.0263	0.0263	00
- 631	0	0	0	0	0	0	0	0.0262	0.0262	0	0	0.0262	0.1834	0.0524	00
- 659	0	0.0261	0	0.0261	0	0.0261	0.0261	0.0261	0	0	0	0	0.2088	0.0783	00
- 692	0	0	0	0	0.0262	0	0	0	0.0262	0	0	0.0262	0.0262	0.0786	0.0262
- 719	0	0	0	0.0260	0	0.0520	0.0260	0	0	0	0.0260	0.0260	0.2080	0.0260	00
- 746	0	0	0	0	0	0	0.0263	0	0	0	0.0263	0	0.1578	0.0789	00
- 789	0	0	0	0	0.0262	0	0	0	0	0	0.0262	0	0.2096	0.0524	00
- 840	0	0.0426	0.0263	0.0263	0	0.0263	0	0.0263	0.0263	0.0263	0	0.2367	0.1315	0.0263	0.0260
- 863	0	0	0	0.0258	0	0.0258	0	0	0.0258	0	0	0.0258	0.2322	0.1290	0.0250
- 905	0	0	0	0.0261	0	0	0	0	0	0	0.0261	0.0522	0.2088	0.0522	0
- 928	0	0	0	0.0261	0.0261	0.0261	0.0261	0	0	0.0261	0.0261	0.0261	0.2610	0.1566	0.0520

There appears to be only 1 previous study of pore-size distributions (obtained from mercury intrusion porosimetry) for granites reported in the scientific literature. Sherwood and Huang (1969) obtained pore-size distribution data for 16 samples of igneous and metamorphic rocks from the Piedmont region of Virginia. These crystalline rocks contained significant concentrations of pores of two to four different sizes (i.e., the pore-size distribution for igneous rocks ranged from bimodal to quadrimodal). The mean pore diameter of the crystalline rock samples ranged from 0.0104 to 0.866 micrometres. The same authors also tested 12 carbonate rocks in the same area of Virginia. The carbonate samples had a pore distribution with mean pore diameters ranging from 0.0113 to 0.088 micrometres. Wardlaw (1976) also obtained pore size distributions of carbonate rocks using mercury porosimetry. The measured pores ranged in size from 0.1 to 2 micrometres. Drake and Ritter (1945) measured pore-size distributions of activated clay pellets. The average pore diameters ranged from 9.3×10^{-3} to 1.10×10^{-2} micrometres.

The pore size distribution for a set of 10 samples from a depth of 0 to 410 metres from the WN site shows a tri-modal distribution (Agterberg et al. 1984), with the following means (d_1, d_2, d_3) of the three pore size components:

Component 1: $d_1 = 0.00927$ micrometres
Component 2: $d_2 = 0.0628$ micrometres
Component 3: $d_3 = 0.290$ micrometres

The term "depth" in this paper actually represents the "downhole length", because there is little difference between the two. The porosities of the three components for this set are listed in Table 7. These three components have also been represented by the following three types of pores (Katsube, 1981): nano-pores, intermediate pores and micro-pores. Component 1 has also been sub-divided into sub-nanopores and nano-pores (Katsube, 1981). This sub-division has been meaningful in certain cases (Katsube and Walsh, in press). Katsube and Walsh (in press) compared the geometrical mean of the entire pore size distribution (excluding the sub-nanopores) with the aperture (d) values (equation 13), which are bulk pore parameters, and found a relatively good correlation between the two parameters. The existence of this relatively good correlation indicates that the pore size distribution is significant in relation to fluid flow and that the bulk pore size represents certain characteristics of the complex network of pores. The pore size distribution represents the porosity distribution of the various sizes of pores which constitute the complex network of pores within the rock.

Diffusion Measurements

Diffusion measurements have been carried out on 15 specimens from 14 samples from the WN and URL sites. The results have been reported by Wadden and Katsube (1983) and Katsube et al. (1986). The pore structure parameters, such as formation factor, effective porosity and tortuosity, have been determined by these measurements and the results have been compared with the same parameters obtained by other methods. The correlation for the formation factor was good, but rather poor for the other parameters. These results are based on a very small number of samples and further work is required in order to complete this study.

The results of diffusion experiments are often expressed in terms of diffusivity, ψ. This parameter is defined by the following equation:

$$\psi = \frac{D_i}{D_o} \qquad (22)$$

$$D_i = \frac{D_o \phi}{\tau^2}$$

Table 7. Porosities of the three components (Agterberg et al. 1984)

Sample	T	Porosities 1	2	3
WN2 - 24	0.496	0.257	0.129	0.110
WN2 - 85	0.764	0.572	0.164	0.028
WN1 - 138	0.421	0.162	0.058	0.201
WN1 - 223	0.421	0.195	0.081	0.145
WN1 - 245	0.421	0.227	0.043	0.151
WN1 - 303	0.289	0.000	0.094	0.195
WN1 - 345	0.288	0.097	0.040	0.151
WN1 - 385	0.526	0.325	0.178	0.023
WN1 - 410	0.580	0.204	0.078	0.298
Standard	0.496	0.254	0.091	0.151

1,2,3: porosities of the three components
T: total porosity (sum of 1, 2 and 3)

where

D_i = intrinsic diffusion coefficient of a species diffusing through a rock sample (m^2/s)

D_o = free-water diffusion coefficient = 1.6×10^{-9} m^2/s for iodide.

The diffusivity values for samples from the WN and URL sites are presented in Table 8. The values obtained by other investigators have also been included. The mean values of diffusibilities obtained for samples from the WN and URL sites are 4.27×10^{-4} and 1.01×10^{-3}, respectively. These values are, in general, comparable to the values reported by Bradbury et al. (1982) and Skagius and Neretnieks (1985). It should be noted that a relatively small number of granite samples have been analyzed at present. Much more experimental data must be collected in order to gain a thorough understanding of diffusion processes in geologic media. Most of the experimental work on diffusion has been carried out at temperatures around 25°C. It is necessary to determine diffusion coefficients

Table 8. Diffusivities of granite samples

Rock	# of Samples	Min.	Max.	Mean	Reference
WN 1	8	2.76×10^{-4}	9.99×10^{-4}	6.12×10^{-4}	Katsube et al.
WN 2	4	2.69×10^{-5}	1.05×10^{-4}	5.79×10^{-5}	Katsube et al.
Overall WN	12	2.69×10^{-5}	9.99×10^{-4}	4.27×10^{-4}	Katsube et al.
URL 2	2	1.005×10^{-3}	1.009×10^{-3}	1.007×10^{-3}	Katsube et al.
Granite (Finnsjon)	4	2.56×10^{-5}	5.25×10^{-5}	4.16×10^{-5}	Skagius & Neretnieks, 1985
Granite (Stripa)	2	8.13×10^{-5}	1.0×10^{-4}	9.07×10^{-5}	Skagius & Neretnieks, 1985
Granite (Gidea)	4	5.63×10^{-5}	8.13×10^{-5}	6.72×10^{-5}	Skagius & Neretnieks, 1985
Granite (Svartboberget)	3	1.63×10^{-4}	4.13×10^{-4}	2.63×10^{-4}	Skagius & Neretnieks, 1985
Gossian Granite	8	3×10^{-4}	8×10^{-4}	5.5×10^{-4}	Bradbury et al. (1982)
Cornish Granite	2	1.2×10^{-5}	1.6×10^{-5}	1.4×10^{-5}	Bradbury et al. (1982)

at temperature and pressure conditions that would exist around a waste repository in order to fully assess the importance of diffusion with regards to the disposal of spent nuclear fuel. This is an area for future research.

Diffusion experiments conducted by the authors employ a single, non-sorbing tracer. Studies conducted abroad also use similar experimental conditions. Groundwater may leach a number of ionic species from spent fuel so it is essential that diffusion experiments with several ionic species in solution be carried out.

DISCUSSION

General Characteristics

One of the most commonly used methods for characterizing the rocks in relation to pore structure is the formation factor (F) vs effective porosity (ϕ_E) relationship, expressed by the Archie equation (Archie, 1942):

$$F = \frac{a}{\phi^m} \tag{23}$$

Table 9. Summary of equations relating resistivity and porosity for fully water-saturated rocks (from Parkhomenko, 1967 and Keller, 1966)

Formations for which equations are valid	Porosity Range	Number of Measurements	Equation
(1) Bradford Sand (Devonian) Woodbine Sand (Cretaceous) Wilcox Sand (Eocene)	.150-.367	30	F=.620-2.15
(2) Pennsylvanian Sandstone, Oklahoma	0.080-0.200	97	F=.650-1.91
(3) Morrison Sandstone (Jurassic) Montrose County, Colorado	0.140-.230	243	F=.620-2.10
(4) Clean Miocene Sandstone, Weeks Island, Louisiana	0.11-0.26	35	F=.780-1.92
(5) Clean Cretaceous Sandstone, Paluxy Sand, Texas	0.08-0.25	50	F=.470-2.23
(6) Clean Ordovician Sandstone, Simpson Sand, Oklahoma	0.07-0.15	44	F=1.30-1.71
(7) Shaly Sandstone (Eocene) Wilcox Formation, Texas	0.09-0.22	72	F=1.80-1.64
(8) Shaly Sandstone (Oligocene), Frio Sands, Texas	0.07-0.26	63	F=1.70-1.65
(9) Shaly Sandstone (Cretaceous) Taylor Sand, Texas	0.07-0.31	36	F=1.70-1.80
(10) Oolitic Limestone (Cretaceous), Texas	0.07-0.19	13	F=2.30-1.64
(11) Oolitic Limestone (Jurassic), Smackover Limestone, Ark.	0.09-0.26	42	F=.730-2.10
(12) Siliceous Limestone (Devonian), Texas	0.07-0.30	58	F=1.20-1.88
(13) Limestone (Cretaceous), Rodessa Limestone, Texas	0.08-0.30	37	F=2.20-1.65
(14) Weakly Cemented Detrital Rock (E.G., Sand, Sandstone and Some Limestones) usually Mesozoic in Age	.25-.45	-	F=.880-1.37
(15) Moderately Well-Cemented Sedimentary Rocks (Including Sandstones and Limestones) usually Mesozoic in Age	.18-.35	-	F=.620-1.72
(16) Well-Cemented Sedimentary Rocks Usually Paleozoic in Age	0.05-.25	-	F=.620-1.95
(17) Highly Porous Volcanic rocks (Tuff, AA, Pahoehoe)	.20-.80	-	F=3.50-1.44
(18) Dense Igneous Rocks and Metamorphosed Sedimentary Rocks (other rocks with less than 4% porosity)	.04	-	F=1.40-1.58

where a is the tortuosity factor and m is the cementation factor. There is an abundance of data on values for a and m for sedimentary rocks, but little data exists for crystalline rocks. The values for a and m are in the order of 0.6-3.5 and 1.44-2.2, respectively, as shown in Table 9. The F vs ϕ_E relationships for the WN and URL rock samples are shown in Figure 1. The values of a and m for WN and URL samples are 0.07 and 1.87, and 0.006 and 2.21, respectively. The value for m for these samples is in the same order as the reported values, but a is one or two orders of magnitude smaller than the literature values. This implies that a much larger portion of the effective porosity of these samples exists in the connecting pores, as compared to other rocks.

Another method of characterizing the rocks uses the effective porosity (ϕ_E) versus the reciprocal of the formation factor (1/F). This is based on the model proposed by Katsube et al. (1985), where the ϕ_E vs (1/F) relationship is expected to be linear:

$$\phi_E = \phi_D + \tau^2(1/F) \quad . \tag{24}$$

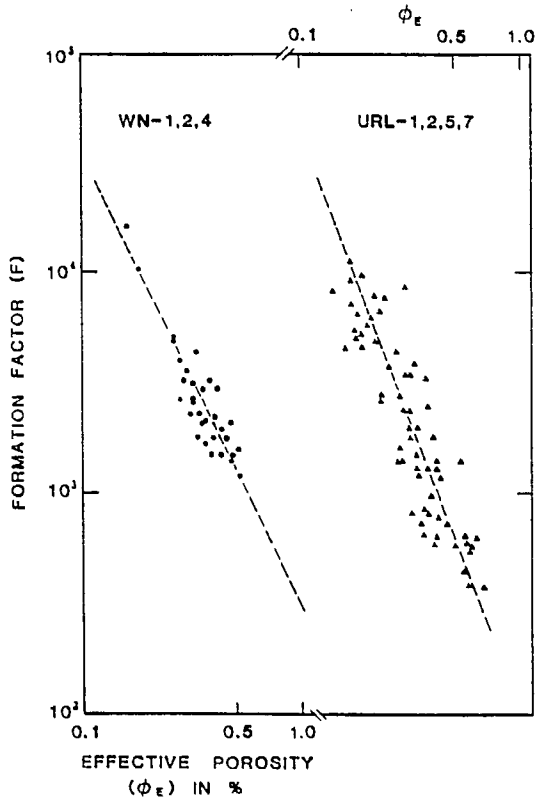

Figure 1. The Archie relationship (formation factor versus effective porosity) for samples from the WN and URL series boreholes (WN-1, 2, 4, URL-1, 2, 5).

This equation can be derived from equations 10 and 12. The results for the WN and URL samples actually indicate a linear relationship. Results of a multiple regression analysis by Agterberg et al. (1985), to determine τ and ϕ_p in equation 24, indicate that as the alteration intensity increases from 1 to 4, the tortuosity remains constant with a value of 1.36 till intensity 3, but increases to 2 at intensity 4. They also indicate that ϕ_p initially increases followed by a decrease and shows a maximum at intensity 2. Katsube et al. (1985) have suggested that these trends can be explained by leaching followed by various stages of deposition of mineral on the walls of the pores and microfractures (Figure 2).

The permeability (k) versus formation factor (F) relationship has also been used to characterize rock samples (Archie, 1942). The relationship between the two parameters for WN and URL samples is shown in Figure 3 (Katsube and Walsh, in press). The correlation is relatively good and has been used for estimating permeability values from geophysical logs (Katsube and Hume, in press).

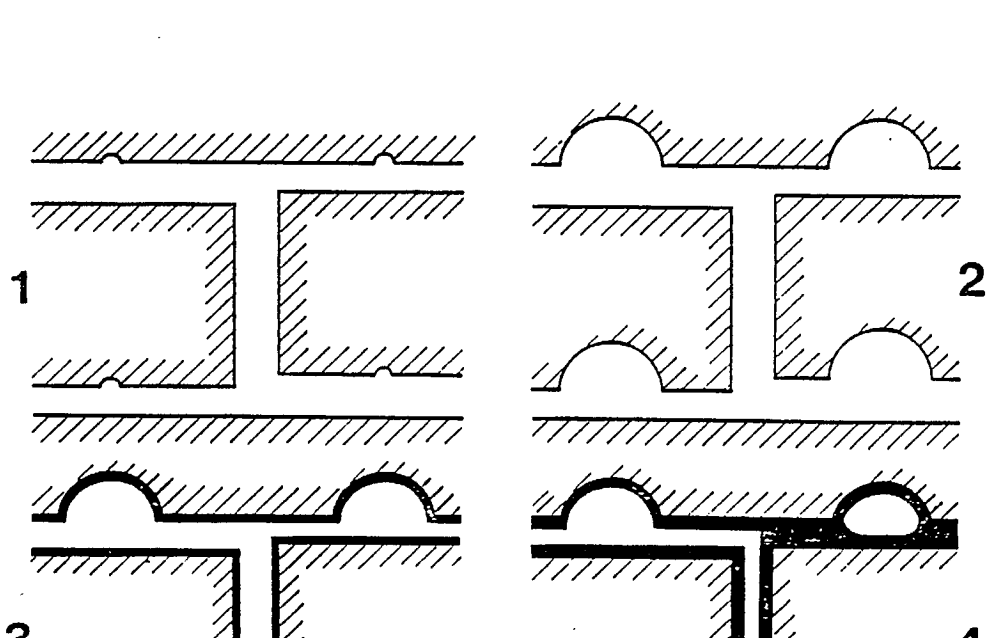

Figure 2. Effect of progressing alteration on pore structure (Katsube et al. 1985).

Diffusion measurements have been carried out to test the reliability of using pore structure parameters determined by other laboratory methods to estimate radionuclide transport rates. The results to date indicate that the formation factor is a reliable parameter, but further work is required to test the reliability of using porosity and apparent tortuosity for making these estimates.

Depth Characteristics

The effect of depth on pore structure parameters and physical properties of a rock is significant since rocks are stress released when extracted from their confined environment in the subsurface and since various physical characteristics of a rock are reflected in the pore structure parameter versus depth relationship (Katsube, 1981; Katsube and Kamineni, 1983; Annor and Katsube, 1983; Agterberg et al. 1984).

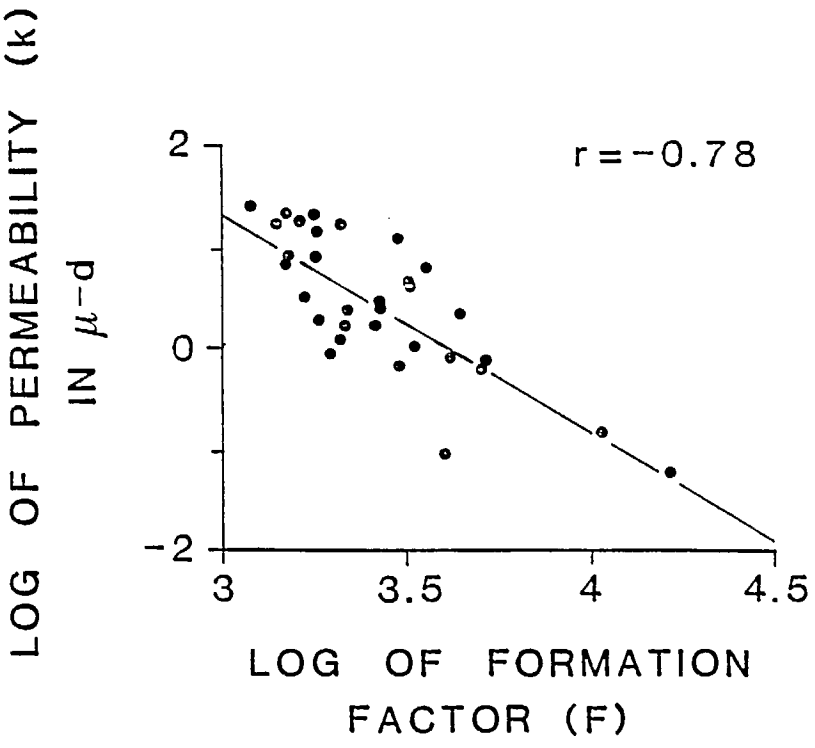

Figure 3. Permeability (k) as a function of formation factor (F) for samples from boreholes WN-1, 2 and 4. r: correlation factor (from Katsube and Walsh, in press).

The crack porosity (ε) versus depth (h) relationship is shown in Figure 4. The general relationship between the two parameters is linear, with ε being approximately 0 and 0.11% at surface and at 1000 metres, respectively. Results of a linear regression analysis of the data produces the following relationship:

$$\varepsilon = 0.049 + 0.011h \text{ (units: \%)}$$
$$r = 0.906$$

where r is the correlation factor. A more detailed relationship between the two parameters is illustrated by the broken line in the same figure. This result can be interpreted as showing changes in the ε vs h relationship at depths of 250-300 metres and 700-800 metres.

The effective porosity (ϕ_E) versus depth (h) relationship is shown in Figure 5. The general relationship is linear and can be expressed by,

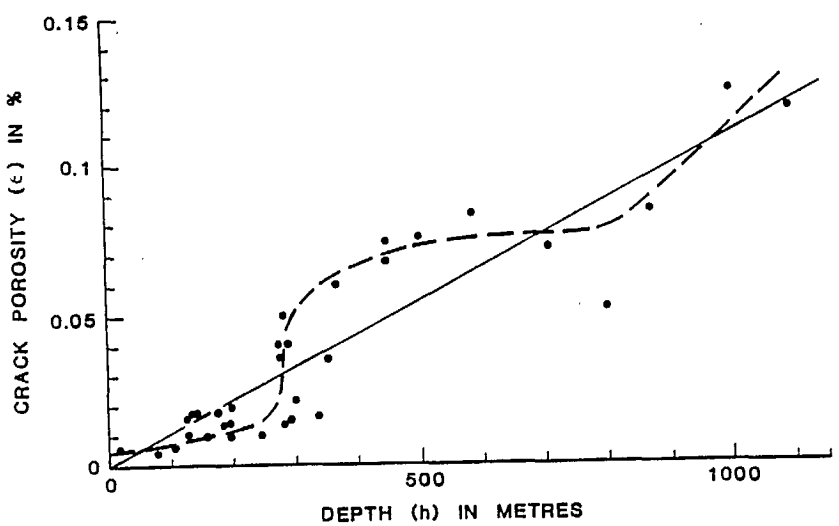

Figure 4. Crack porosity (ε) as a function of depth (h) for samples from boreholes URL-1, 2 and 5.

$$\phi_E = 0.28 + 0.00025\,h \quad \text{(units: \%)}$$
$$r = 0.65 \ .$$

According to this relationship the effective porosity at the surface and 1000 metres depth is 0.28% and 0.53%, respectively. The porosity increase over the 1000 metre depth is 0.25%. It is interesting that this is 2-3 times the crack porosity value at 1000 metres. A more detailed relationship is illustrated in the same figure by a broken line. This illustration suggests changes in the ϕ_E vs h relationship at depths of about 250 and 600 metres.

The effect of sampling depth (h) on the formation factor (F) is shown in Figure 6 on a log-log scale. The general trend is linear with two deviations. The first deviation is seen between the surface and 50-60 metres depth, where F increases with depth (broken line (1)). The second deviation starts at 250-300 metres where only the WN samples start (broken line (2)) to show higher values of F compared to other samples from the same depth. This deviation starts

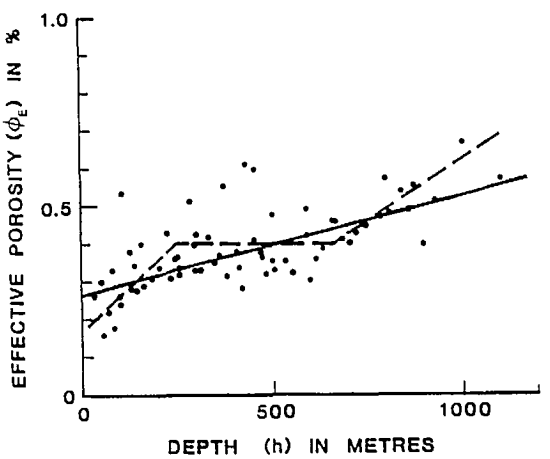

Figure 5. Effective porosity (ϕ_E) as a function of depth (h) for samples from boreholes URL-1, 2 and 5.

with an increase in F with depth (h), but then decreases (broken line (3)) with depth from about 500 metres. The linear relationship without the points that cause the two deviations can be expressed by,

$$F = \frac{6.14 \times 10^5}{h^{1.06}}$$

$$r = -0.88.$$

The permeability (k_E) versus depth (h) relationship is shown in Figure 7. Two different interpretations of the trends can be made. One (interpretation I) is a moderate increase of k with depth, with a rapid increase starting at about 50 and 600 metres for unaltered samples (alteration intensity 1) and altered (alteration intensity 2 and above) samples, respectively. The altered samples include the unaltered samples from borehole WN-4 in this case. The other interpretation (interpretation II) is a moderate increase of k to about 450 metres from which

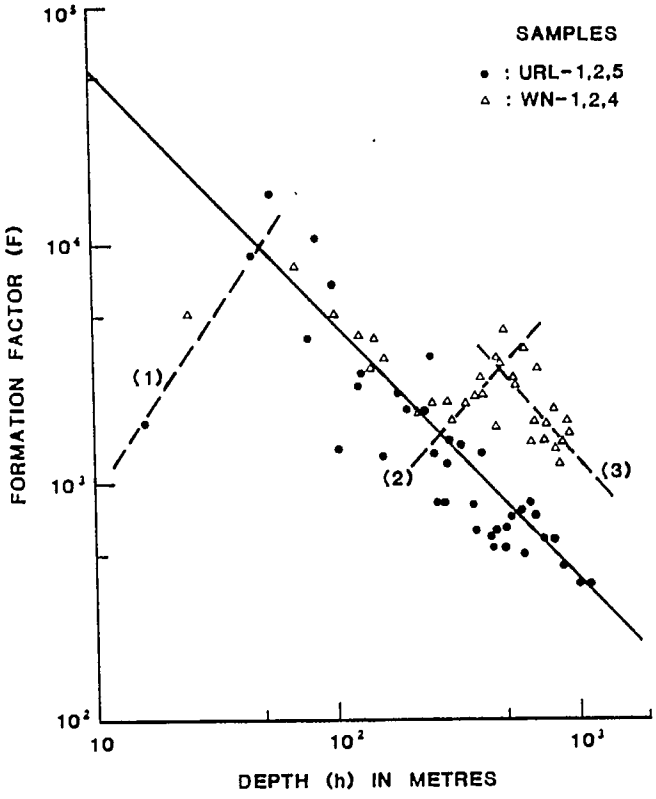

Figure 6. Formation factor (F) as a function of depth (h) for samples from boreholes URL-1, 2, 5, WN-1, 2 and 4.

depth k suddenly increases to a constant value of 20 microdarcies for unaltered samples and a moderate increase of k followed by a rapid increase from a depth of about 500-600 metres for altered samples.

Two interpretations are also possible for the aperture (d) versus depth (h) relationship (Figure 8). One (interpretation I) is a constant aperture from the surface to about 250-300 metres depth from which point d increases with depth at a constant rate. The other (interpretation II) is similar to the first to about 400 m at which point d suddenly increases to 0.4 μm for the URL samples only.

It is difficult to see any general trend for the path density coefficient (n/τ) with depth (h), as shown in Figure 9. However, when the samples from WN and URL sites are separated, different trends can be seen for the two groups of samples. For the WN samples there is an initial increase of n/τ with depth to about 250-300 m at which point it reaches a maximum. It then decreases with depth and becomes constant from about 500-600 metres. The values for n/τ generally increase with depth for the URL samples.

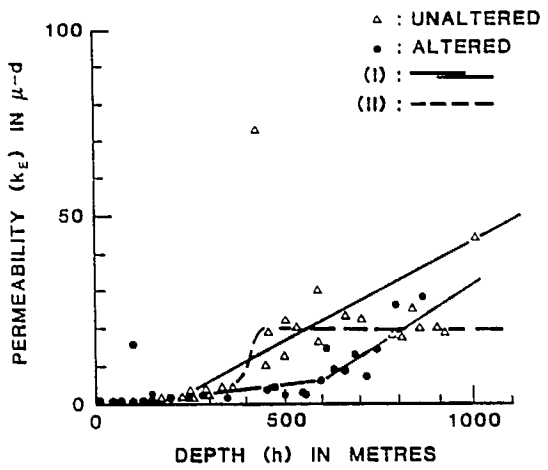

Figure 7. Equivalent rock mass permeability (k_E) as a function of depth (h) for samples from boreholes URL-1, 2, 5, WN-1, 2 and 4.

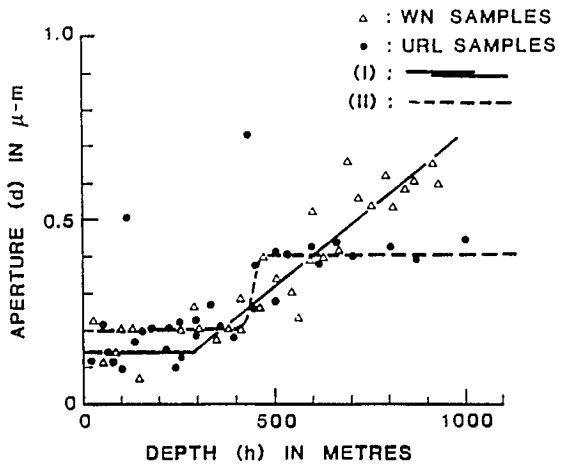

Figure 8. Aperture (d) as a function of depth (h) for samples from URL-1, 2, 5, WN-1, 2 and 4.

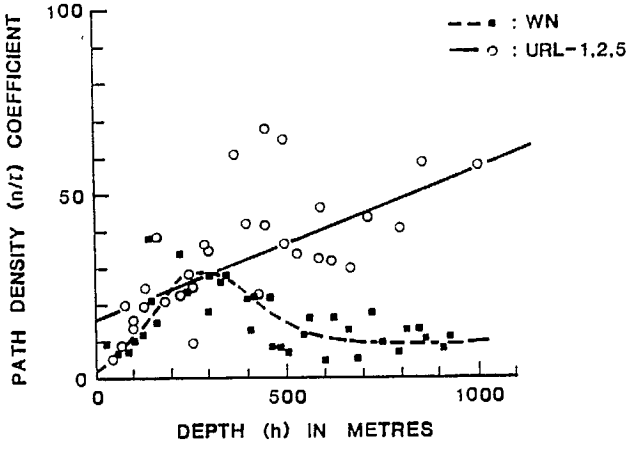

Figure 9. Path density coefficient (n/τ) as a function of depth (h) for samples from URL-1, 2, 5 and WN-1, 2 and 4.

The effects of depth on the 6 parameters: ϕ_E, F, k_o, d and n/τ, have been discussed above. There are certain depths at which changes in their trends occur. These shall be referred to as "points of inflection". The depth of these points of inflection for the 6 parameters are listed in Table 10. It is interesting to note that there are similarities between these points for different parameters. All parameters show an inflection point at about 250-300 metres depth and most show another inflection point at 500-600 metres. It is also interesting that the pore size distribution shows drastic changes at about 460 and 630 metres (Figure 10).

Petrophysical Characterization of Geological Units

The major rock types in the WN and URL boreholes are pink granite, grey granite and greenish-grey granite (Brown et al. 1985). The pink and grey granites are thought to represent the highly altered outer rim and unaltered core of the Lac du Bonnet batholith, respectively. The greenish-grey granite represents a transition zone between the pink and grey granites. The pink colouration is

Table 10. Inflection points for six parameters

Parameter	I	II	III
Crack Porosity (ε)		250-300	700-800
Effective Porosity (ϕ_E)		250	600
Formation factor (F)	50-60	250-300*	500*
Permeability (k_o)-I**		250	600
Permeability (k_o)-II**		450	500-600
Aperture (d)-I**		250-300	
Aperture (d)-II**		300-400	
Path density Const (n/T)-WN		250-300	500-600

*: only WN samples
**: interpretation I and II

considered to be due to hydrothermal alteration and weathering. At the WN and URL sites, the pink granite is generally found at the surface and the green granite in the deeper zones.

According to the interpretation of the geophysical logs from the URL site performed by von Sacken and Katsube (in prep.), the pink and grey granites generally correlate with high and low resistivity zones, respectively. The greenish-grey granite shows an intermediate resistivity range. Based on these results, it has been indicated that the depth range of the pink granite is from 0 to 200-300 m. Similarly, the grey granite starts from a depth greater than 400-500 m in the URL-1, 2 and 5 boreholes. These are the boreholes from which the standard samples have been taken. The thickness of the greenish-grey granite zone is in the order of 50-250 m.

The pink and grey granites can also be seen in boreholes WN-1, 2 and 4. The depth at which the grey granite starts in these boreholes is deeper than that of the URL boreholes. However, the grey granite in these holes does not show low

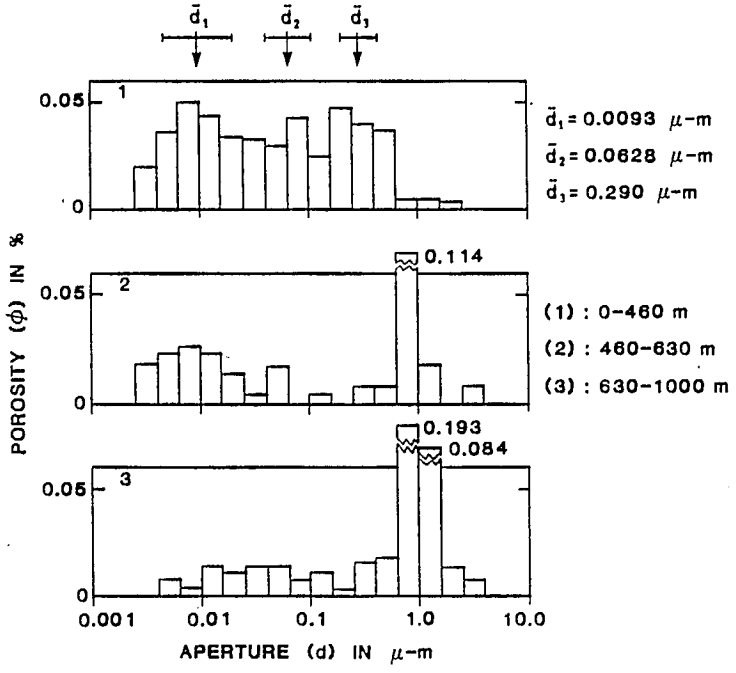

Figure 10. Average pore size distribution at different depth ranges in boreholes WN-1, 2 and 4.

resistivity as it does in the URL boreholes. The resistivity level of the grey granite is the same as the pink granite.

It is interesting to note that the depth limit of the pink granite (200-300 m) corresponds to inflection point II in Table 10 and that the depth range at which the grey granite generally starts (400-500 m) corresponds to inflection point III in the same table. That is, inflection point II indicates the lower boundary of the pink granites at URL, and inflection point III indicates the upper boundary of the grey granites at the WN site. Since the inflection points are associated with changes in petrophysical properties, the existence of relatively good correlation between the inflection points and the geological boundaries implies that the petrophysical changes are related to changes in rock type. From the petrophysical standpoint, the pink and grey granites will be considered the major rock types, or major geological units. It appears that both geologically and petrophysically the greenish-grey granite is an intermediate rock type.

Although there is no apparent difference between the pink granites from the WN and URL sites, there is for the grey granites from the two sites. The resistivity levels of the geophysical logs for the two grey granite zones are different, as stated before. Many of the petrophysical results support this difference between the two grey granites. The results of the porosity-formation factor analysis by Katsube et al. (1985) indicate that the grey granites of the WN site showed similar tortuosity characteristics to those of the pink granites. This is in contrast to the trends seen in the URL samples where the tortuosity characteristics were different for the pink and grey samples. According to Agterberg et al. (1985), the tortuosities for the pink and grey granites are 2.1 and 1.2, respectively. The formation factor versus depth characteristics of the grey granites from the WN site deviates from the others (Figure 6). There is an obvious difference between the depth characteristics of the path density-tortuosity ratio (n/τ) for the two grey granites (Figure 9). For these reasons, the two granites shall be considered separate geological units: grey granite I and II for the URL and WN sites.

Representative values for aperture (d), tortuosity (τ), equivalent rock mass permeability (k_E), effective porosity (ϕ_E) and apparent tortuosity (τ_A) have been determined for the three rock types: pink granite, grey granite I (URL) and grey granite II (WN), and are listed in Table 11. The tortuosity (τ) values were taken

from the paper by Agterberg et al. (1985). The aperture values listed under (1) in Table 11 for pink granite and grey granite I are based upon interpretation II in Figure 8. The aperture values listed under (2) for the same rocks are based upon interpretation I in the same figure. In this interpretation it is assumed that the original aperture is a constant value of 0.11 μm for the two rock types, but that it increases with depth for samples taken from depths greater than 300 m. The aperture value listed under (1) for grey granite II is based upon interpretation I but, it is assumed that the original constant value is 0.18 μm. The same values listed under (2) for that rock type is based upon interpretation I but, it is also assumed that the aperture values level off at 0.55 μm from depths greater than 600 m. Similar methods have been used to determine the values for effective porosity (ϕ_E) and equivalent rock mass permeability (k_E) shown in Figures 5 and 7. The apparent tortuosity (τ_A) values have been obtained from equation (16) using the effective porosity (ϕ_E) and formation factor (F) data in Tables 1 and 3. The values for τ_A listed under (1) are the mean values for each rock type and those listed under (2) are the range of the values.

Table 11. Petrophysical parameter values for the three rock types in the Lac du Bonnet Batholith

	Pink		Grey I (URL)		Grey II (WN)	
	(1)	(2)	(1)	(2)	(1)	(2)
d (um)	0.18	0.11	0.41	0.11	0.18	0.55
τ	2.1	-	1.2	-	2.1	-
k_E (ud)	1.4	0.4-2.4	8.6	7.6-11.6	0.8	0.4-1.2
ϕ_E (%)	0.24	0.15-0.33	0.24	0.15-0.33	0.24	0.15-0.33
τ_A	4.0	3-5	1.8	1.6-2.0	3.0	2.5-3.0

(1) = most likely values
(2) = possible values

d = aperture
τ = tortuosity
k_E = equivalent rock mass permeability
ϕ_E = effective porosity
τ_A = apparent tortuosity

CONCLUSIONS

One of the most commonly used methods for characterizing the rocks is the Archie, or the formation factor versus porosity, relationship. This relationship involves two coefficients: the tortuosity factor and cementation factor. There is an abundance of data on these coefficients for sedimentary rocks, but little for crystalline rocks. The cementation factor values for the granites from the WNRE research area are very similar to those reported in the literature, but the tortuosity coefficient values are one to two orders of magnitude smaller than those presented in the literature. This implies that a much larger portion of the effective porosity of these granites exist in the connecting pores as compared to other rocks.

The granites in the WNRE research area have been divided into three rock types from a petrophysical standpoint: pink granite, grey granite I and grey granite II. The grey granites I and II are found at the URL and WN sites, respectively, and are very different in petrophysical characteristics. The pink granite and grey granite II units can be characterized as having small pore apertures, large tortuosities and low permeabilities. The grey granite I unit has the opposite and more favourable characteristics for radionuclide transport.

The three rock types, or geological units, have been assigned representative values for aperture, tortuosity, equivalent rock mass permeability, effective porosity and apparent tortuosity, as listed in Table 11. These are some of the petrophysical parameters that are required to determine the radionuclide release rates of the host rock. As a result of data analysis and interpretation of these five parameters, a set of "most probable values" and a set of "possible values" have been assigned to these geological units. The ranges for these values have been determined mainly on the basis of differences in methods of interpretation rather than statistical distributions alone.

Diffusion studies have proven to be very useful for verifying the reliability of using the pore structure parameters for estimating radionuclide transport rates. The formation factor has proven to be a reliable parameter, but further work is required to determine the reliability of effective porosity and apparent tortuosity for these applications. Generally, little work has been done on crystalline rocks in this area, so that a considerable amount of work is required in the future.

ACKNOWLEDGEMENTS

We are grateful to M. Drury (GSC) and P. Chernis for reviewing this paper.

REFERENCES

Agterberg, F.P., Katsube, T.J., and Lew, S.N. 1984. Statistical analysis of granite pore size distribution data, Lac du Bonnet batholith, eastern Manitoba. In: Current Research, Part A, Geological Survey of Canada, Paper 84-1A, p. 29-38.

Agterberg, F.P., Katsube, T.J., and Lew, S.N. 1985. Use of multiple regression for petrophysical characterization of granites as a function of alteration. In: Current Research, Part B, Geological Survey of Canada, Paper 85-1B, p. 451-458.

Alexander, J., Hall, D.H., and Storey, B.C. 1981. Porosity measurements of crystalline rocks by laboratory and geophysical methods. Report on the Institute of Geological Sciences, ENPU81-10, 45 p.

Annor, A. and Geller, L. 1979. Dilational velocity, Young's odulus, Poisson's ratio, uniaxial compressive strength and Brazilian tensile strength for WN1 and WN2 samples. CANMET Mining Research Laboratories Technical Data 303410-M01/78, 2 p.

Annor, A. and Jackson, R. Mechanical, thermomechanical and joint properties of rock samples from the Lac du Bonnet batholith, Manitoba. Nuclear Fuel Waste Management Program Concept Assessment Document, Geotechnical Studies at Whiteshell Research Area (RA-3), Rock Properties.

Annor, A. and Katsube, T.J. 1983. Nonlinear elastic characteristics of granite rock samples from Lac du Bonnet Batholith. In: Current Research, Part A, Geological Survey of Canada, Paper 83-1A, p. 411-416.

Annor, A., Larocque, G.E., and Chernis, P.J. 1979. Uniaxial compression tests, Brazilian tensile tests and dilational velocity measurements on rock specimens from Pinawa and Chalk River. CANMET Laboratory Report MRP/MAL 79-60, 28 p.

Annor, A., Larocque, G., and Kapeller, F. 1981. Laboratory permeability measurements of granitic samples from Pinawa. Mining Research Laboratories Report ERP/MAL 81-43, 28 p.

Archie, G.E. 1942. The electrical resistivity log as an aid in determining some reservoir characteristics. Transactions of the American Institute of Mining, Metallurgical and Petroleum Engineers, v. 146, p. 54-67.

Asquith, G.B. and Gibson, C.R. 1982. Basic Well Log Analysis for Geologists. The American Association of Petroleum Geologists, Tulsa, Oklahoma, 218 p.

Bird, G.W. and Fyfe, W.S. 1982. The nuclear waste disposal problem – an overview from a geological and geochemical perspective. Chemical Geology, v. 36, p. 1-13.

Boardman, C.R. and Shrove, J. 1966. Distribution of fracture permeability of a granitic rock mass following a contained nuclear explosion. Journal of Petroleum Technology, v. 18, p. 619-623.

Boyle, R.W. 1963. Diffusion in vein genesis. Symposium on the Problems of Postmagmatics Ore Deposition, v. 1, p. 377-383.

Brace, W.F. 1965. Some new measurements of linear compressibility of rocks. Journal of Geophysical Research, v. 70, p. 391-398.

Brace, W.F., Walsh, J.B., and Frangos, W.T. 1968. Permeability of granite under high pressure. Journal of Geophysical Research, v. 73, p. 2225-2236.

Brace, W.F. 1977. Permeability from resistivity and pore shape. Journal of Geophysical Research, v. 82, p. 3343-3349.

Brace, W.F., Orange, A.S., and Madden, T.R. 1965. The effect of pressure on the electrical resistivity of water-saturated crystalline rocks. Journal of Geophysical Research, v. 70(22), p. 5669-5678.

Bradbury, M.H., Lever, D., and Kinsey, D. 1982. Aqueous phase diffusion in crystalline rock. Scientific Basis for Nuclear Waste Management V, v. 11, p. 569-578.

Brown, A., Dugal, J.J.B., Everitt, R.A., Kamineni, D.C., Lau, J.S.O., and McEwen, J.H. 1985. Advances in geology at the URL site (RA-3). Atomic Energy of Canada Limited Technical Record, TR-299, p. 253-264.

Bucker, H.P., Jr., Felsanthal, M., and Conley, F.R. 1956. A simplified pore-size distribution apparatus. Journal of Petroleum Technology, AIME, v. 8, p. 65-66.

Burleigh, E.G., Wakeham, H., Honald, E., and Skau, E.L. 1949. Pore-size distribution in textiles. Textile Research Journal, v. 19(9), p. 547-555.

Chernis, P.J. and Robinson, P.B. (this volume). Natural and stress-relief microcracks in the Lac du Bonnet batholith.

Delisle, G. 1975. Determination of permeability of granitic rocks in GT-2 from hydraulic fracturing data. Los Alamos Scientific Laboratory Informal Report LA-6169-MS, 5 p.

De Wiest, R.J.M. 1965. Geohydrology. John Wiley and Sons, Inc., New York, New York, 366 p.

de Witte, L. 1950. Relations between resistivities and fluid contents of porous rocks. Oil and Gas Journal, v. 49(16), p. 120-132.

Drake, L.C. 1949. Pore-size distribution in porous materials-application of high-pressure mercury porosimetry to crackling catalysts. Industrial and Engineering Chemistry, v. 41, p. 780-785.

Drake, L.E., and Ritter, H.L. 1945. Macropore-size distribution in some typical porous substances. Industrial and Engineering Chemistry, Analytical Edition, v. 17, p. 787-791.

Dullien, F.A.L. 1979. Porous Media: Fluid Transport and Pore Structure. Academic Press, New York, New York, 396 p.

Franklin, J.A., and Hoeck, E. 1970. Developments in triaxial testing technique. Rock Mechanics, v. 2, p. 223-228.

Freeze, R.A. and Cherry, J.A. 1979. Groundwater. Prentice Hall, New Jersey, 604 p.

Garels, R.M., Dreyer, R.M., and Howland, A.L. 1949. Diffusion of ions through intergranular space in water-saturated rocks. Bulletin of the Geological Society of America, v. 60, p. 1809-1828.

Gauvreau, C., and Katsube, T.J. 1975. Automation in electrical rock property measurements. In: Report of Activities, Part A, Geological Survey of Canada, Paper 75-1A, p. 83-86.

Grisak, G.E., and Pickens, J.F. 1980. Solute transport through fractured media: I. The effect of matrix diffusion. Water Resources Research, v. 16, p. 719-730.

Grisak, G.E., and Pickens, J.F. 1981. An analytical solution for solute transport through fractured media with matrix diffusion. Journal of Hydrology, v. 52, p. 47-57.

Hanley, E.J., Dewitt, D.P., and Roy, R.F. 1978. The thermal diffusivity of eight well-characterized rocks for the temperature range 300-1000K. Engineering Geology, v. 12, p. 31-47.

Heard, H.C., Trimmer, D., Duba, A., and Bonner, B. 1979. Permeability of generic repository rocks at simulated in-situ conditions. Lawrence Livermore Laboratory Report UCRL82609, 13 p.

Heimli, P. 1974. The porosity, permeability, swelling and capillarity of rocks. Geological Institute, Ingeniorgeologi, NTH, Rapport No. 12, 36 p.

Helander, Donald P. 1983. Fundamentals of Formation Evaluation. Oil and Gas Consultants International, Inc., Tulsa, Oklahoma, 333 p.

Hill, H.J., and Milburn, J.D. 1956. Effect of clay and water salinity on electrochemical behaviour of reservoir rocks. Transactions of the American Institute of Mining, Metallurgical and Petroleum Engineers, v. 19, p. 65-72.

Houser, F.N. 1962. Some physical property data of samples from U15A site, Nevada test site. United States Geological Survey Technical Letter, area 15-2, 4 p.

Howell, B.F. 1953. Electrical conduction in fluid-saturated rocks, Part 1. World Oil, p. 113-116.

Izett, G.A. 1960. Granite exploration hole, area 15, Nevada test site, Nye County, NV – interim report, part C. United States Geological Survey Trace Elements Memorandum Report 836-C, 37 p.

Jackson, R. 1982a. Dilational velocity Young's modulus, Poisson's ratio, uniaxial compressive strength and Brazilian tensile strength for URL-1 and URL-5 extended engineering samples. CANMET-Mining Research Laboratories Division Report ERP/MRL 82-60, 28 p.

Jackson, R. 1982b. Dilational velocity, Young's modulus, Poisson's ratio and uniaxial compressive strength for URL-2 and URL-5 samples. CANMET-Mining Research laboratories Division Report ERP/MRL 82-60, 20 p.

Jackson, R. and Paquette, D. 1984. A summary of mechanical property test data on samples from boreholes URL-7, URL-B9-1, 2&3, URL-B10-1 and URL-B26-1 at Lac du Bonnet, Manitoba. CANMET-Mining Research Laboratories Division Report ERP/MRL 84-31, 25 p.

Kapeller, F. 1981. The permeability system. Mining Research Laboratories Division Report ERP.MRL 81-29, 25 p.

Katsube, T.J. 1981. Pore structure and pore parameters that control the radionuclide transport in crystalline rocks. Proceedings of the Technical Program, International Powder and Bulk Solids Handling and Processing, Rosemont, Illinois, p. 394-409.

Katsube, T.J. and Annor, A. (this volume). Interpretation of the effect of temperature and stress on permeability for samples from the Whiteshell Research Area. Nuclear Fuel Waste Management Program Concept Assessment Document, Geotechnical Studies at the Whiteshell Research Area (RA-3), Rock Properties.

Katsube, T.J. and Walsh, J.B. (In press). Effective aperture for fluid flow in crystalline rocks. International Journal of Rock Mechanics and Mining Sciences.

Katsube, T.J., Wadden, M.M., and Chernis, P.J. 1982. Isolation of nuclear waste by the intact rock mass. Geotechnical Research: Proceedings of the Seventh Nuclear Fuel Waste Management Information Meeting, Ottawa, Ontario, May 5-6, 1980. Atomic Energy of Canada Limited, Technical Record-190, p. 115-150.

Katsube, T.J., and Kamineni, D.C. 1983. Effect of alteration on pore structure of crystalline rocks: Core samples from Atikokan, Ontario. Canadian Mineralogist, v. 21, p. 637-646.

Katsube, T.J., and Collett, L.S. 1973. Measuring techniques for rocks with high permittivity and high loss. Geophysics, v. 38, p. 92-105.

Katsube, T.J. and Hume, J.P. (in preparation). Permeability determination in crystalline rocks by standard geophysical logs

Katsube, T.J., Drury, M., and Annor, A. (this volume). Evaluation of the nuclear fuel waste containment capacity of the host rock.

Katsube, T.J., Melnyk, T.W., and Hume, J.P. 1986. Pore structure from diffusion in granitic rocks. Atomic Energy of Canada Limited Technical Record, TR-381, 28 p.

Katsube, T.J., Percival, J.B., and Hume, J.P. 1985. Characterization of the rock mass by pore structure parameters. Atomic Energy of Canada Limited Technical Record, TR-299, p. 375-413.

Keller, G.V. 1966. Electrical properties of rocks and minerals. In: Handbook of Physical Constants, Geological Society of America, Memoir 97, p. 563. Edited by S.P. Clark, Jr.

Kessler, D.W., Insley, H., and Sligh, W.H. 1940. Physical, mineralogical and durability studies on the building and monumental granites of the United States. Journal of Research of the National Bureau of Standards, v. 25, p. 161-206.

Kowalski, W.C. 1966. The interdependence between the strength and voids ratio of limestones and marls in connection with water saturation and anisotropy. In: Proceedings of the 1st International Congress on Rock Mechanics (Lisbon) Laboratorio National De Engenaria Civil, p. 118-127.

Lever, D.A., Bradbury, M.H., and Hemingway, S.J. 1985. The effect of dead-end porosity on rock-matrix diffusion. Journal of Hydrology, v. 80, p. 45-76.

Madden, T.R. 1976. Random network and mixing laws. Geophysics, v. 141, p. 1114-1125.

McKnight, T.S., Marchassault, R.H., and Mason, S.G. 1958. The distribution of pore-sizes in wood-pulp fibres and paper. Pulp and Paper Magazine of Canada, v. 59(2), p. 81-88.

Mellor, M. 1971. Strength and deformability of rocks at low temperatures. Cold Regions Research and Engineering Laboratory (Hanover, NH) Report CORREL-RR-294, 73 p.

Meyer, H.I. 1953. Pore distribution in porous media. Journal of Applied Physics, v. 4, p. 510-512.

Mogi, H. 1965. Deformation and fracture of rocks under confining pressure, elasticity of some rocks. Bulletin of the Earthquake Research Institute, v. 43, p. 349-379.

Morris, D.A., and Johnson, A.I. 1967. Summary of hydrologic and physical properties of rock and soil materials, as analyzed by the hydrologic laboratory of the United States Geological Survey. United States Geological Survey-Supply Paper 1839-D, 42 p.

Neretnieks, I. 1980. Diffusion in rock matrix: an important factor in radionuclide retardation? Journal of Geophysical Research, v. 85, p. 4379-4397.

Norton, D., and Knapp, R. 1977. Transport phenomena in hydrothermal systems: the nature of porosity. American Journal of Sciences, v. 277, p. 913-936.

Nur, A., and Simmons, G. 1969. The effect of viscosity of a fluid phase on velocity in low porosity rocks. Earth and Planetary Science Letters, v. 7, p. 99-108.

Nur, A., and Simmons, G. 1969. The effect of saturation on velocity in low porosity rocks. Earth and Planetary Science Letters, v. 7, p. 183-193.

Ohle, E.L. 1951. The influence of permeability on ore distribution in limestone and dolomite. Economic Geology, v. 46, p. 667-706.

Parkhomenko, E.I. 1967. Electrical Properties of Rocks. Plenum, New York, N.Y., p. 277.

Patnode, H.W., and Wyllie, M.R.J. 1950. The presence of conductive solids in reservoir rocks as a factor in electric log interpretation. Transactions of the American Institute of Mining, Metallurgical and Petroleum Engineers, v. 189, p. 47-52.

Pratt, H.R., Black, A.D., Brace, W.F., and Norton, D.L. 1974. In-situ joint permeability in a granite. EOS, American Geophysics Union Transactions, v. 55, p. 433.

Rasmussen, W.C. 1964. Permeability and storage of heterogeneous aquifers in the United States. International Association of Scientific Hydrology, Publication 64, p. 317-325.

Rootare, H.M. 1970. A review of mercury porosimetry. Perspectives of Power Metallurgy, v. 5, p. 225-252.

Sherwood, W.C., and Huang, J.H. 1969. Pore studies of highly indurated Appalachian rocks. The American Association of Petroleum Geologists Bulletin, v. 53(10), p. 2161-2170.

Skagius, K., and Neretnieks, I. 1986. Diffusivity measurements and electrical resistivity measurements in rock samples under mechanical stress. Water Resources Research, v. 22, No. 4, p. 570-580.

Skagius, K., and Neretnieks, I. 1985. Porosities and diffusivities of some non-sorbing species in crystalline rocks. KBS Technical Report 85-03, 62 p.

Vandergraaf, T.T., Abry, D.R.M., and Davis, C.E. 1982. The use of autoradiography in determining the distribution of radionuclides sorbed on thin sections of plutonic rocks from the Canadian Shield. Chemical Geology, v. 36, p. 139-154.

Van Genuchten, M.T. and Wierenga, P.J. 1976. Mass transfer studies in sorbing porous media. I. Analytical solutions. Journal of the Soil Science Society of America, v. 40, p. 473-480.

von Sacken, R.S., and Katsube, T.J. Relationship between focused-electrode resistivity and the geology: Lac du Bonnet Batholith, Manitoba. (In preparation).

Wadden, M.M., and Katsube, T.J. 1982. Radionuclide diffusion rates in crystalline rocks. Chemical Geology, v. 36, p. 191-214.

Walsh, J.B. 1965. The effect of cracks on the compressibility of rock. Journal of Geophysical Research, v. 70(2), p. 381-389.

Walsh, J.B., and Brace, W.F. 1984. The effect of pressure on porosity and the transport properties of rocks. Journal of Geophysical Research, v. 89, no. 811, p. 9425-9431.

Ward, S.H., and Fraser, D.C. 1967. Conduction of electricity in rocks. In: Mining Geophysics, Vol. II. Society of Exploration Geophysics, and Mining Geophysics Volume Editing Committee, Society of Exploration Geophysics, Tulsa, Oklahoma, p. 197-223.

Wardlaw, N.C. 1976. Pore geometry of carbonate rocks as revealed by pore casts and capillary pressure. The American Association of Petroleum Geologists Bulletin, v. 60(2), p. 245-257.

Washburn, E.W. 1921. Note on a method of determining the distribution of pore sizes in a porous material. Proceedings of the national Academy of Science, v. 7, p. 115-116.

Winsauer, W.O., and McCardell, W.W. 1953. Ionic double layer conductivity in reservoir rock. Transactions of the American Institute of Mining, Metallurgical and Petroleum Engineers, v. 189, p. 129-134.

Worthington, P.F. 1975. Quantitative Geophysical investigations of granular aquifers. In: Geophysical Surveys, v. 2, D. Reidel, Dordrecht, p. 313-366.

Wyllie, M.R., and Spangler, M.B. 1952. Application of electrical resistivity measurements to problems of fluid flow in porous media. Bulletin of the American Association of Petroleum Geologists, v. 36, p. 359-403.

Zurietering, P. and van Krevelen, D.W. 1954. Chemical structure and properties of coal. IV. Pore structure. Fuel, v. 33, p. 331-337.

APPENDIX

Table 12. Effective porosities (ϕ_E), Permeabilities (k_o, k_c)*, Formation Factor (F), Crack porosity (ϵ), pore aperture (d), path density coefficient (n/τ) and Alteration intensities of Standard Samples from Boreholes URL-1, URL-2, URL-5, WN-1, WN-2 and WN-4.

Sample		ϕ_E	k_o	k_c	F	ϵ	d	n/τ	Alteration
URL-1	- 46	0.30	0.44	-	8.79	77.1	0.215	5.28	4
	- 68	0.22	0.2	0.1	8.03	82.2	0.139	8.97	4
	-100	0.24	0.1	0.1	6.78	86.0	0.090	16.4	3
	-131	0.28	0.9	0.5	2.81	67.1	0.174	20.4	3
	-177	0.31	1.5	1.0	2.35	83.4	0.206	20.7	1
	-230	0.31	1.8	0.9	2.05	84.9	0.210	23.2	1
	-254	0.34	3.2	2.6	1.29	75.0	0.223	34.8	1
	-302	0.33	2.1	1.6	1.47	74.5	0.193	35.3	1
	-357	0.37	4.6	2.6	0.75	-	0.208	61.0	1
	-397	0.38	2.1	2.1	1.32	61.4	0.182	41.5	1
	-433	0.61	72.8	25.5	0.61	68.6	0.727	22.7	1
	-496	0.36	22.1	12.3	0.65	64.6	0.415	37.1	1
	-527	0.35	19.9	7.5	0.72	66.4	0.414	33.7	1
	-592	0.42	16.0	5.6	0.78	64.4	0.387	33.1	1
	-615	0.36	14.2	5.4	0.83	-	0.376	32.0	2
	-662	0.46	22.7	9.3	0.73	63.6	0.444	30.5	1
URL-2	-256	0.32	1.7	2.4	0.82	0.036	0.129	9.50	1
	-448	0.41	18.7	14.7	0.64	0.074	0.378	41.7	1
	-586	0.49	30.0	10.5	0.50	0.083	0.424	47.1	1
	-705	0.40	22.4	10.9	0.58	0.072	0.395	43.7	1
	-798	0.37	26.1	7.7	0.58	0.052	0.426	40.5	2
	-871	0.55	28.3	13.8	0.44	0.084	0.387	58.8	2
	-1001	0.67	44.0	3.0	0.38	0.124	0.451	50.3	1
	-1095	0.57	-	-	0.38	0.118	-	-	1
URL-5	- 16.5	0.40	0.71	-	1.78	0.006	0.124	44.9	2
	- 77	0.33	0.32	0.2	4.02	0.004	0.124	20.1	2
	-108	0.53	15.4	12.3	1.40	0.006	0.509	14.0	4
	-126	0.38	0.90	0.67	2.54	0.016	0.164	24.3	1
	-156	0.41	2.54	1.74	1.27	0.010	0.199	38.6	2
	-199	0.34	-	-	1.98	0.010	-	-	4
	-246	0.37	0.25	0.17	3.36	0.010	0.101	29.1	4
	-279	0.51	-	-	0.82	-	-	-	
	-289	0.43	3.76	2.85	1.17	0.040	0.233	35.8	1
	-333	0.42	4.45	2.74	1.36	0.016	0.273	26.1	1
	-370	0.56	-	-	0.64	0.060	-	-	1
	-451	0.60	10.3	5.46	0.56	0.068	0.263	67.9	1
	-497	0.58	12.4	5.76	0.54	0.076	0.284	65.3	1
WN-1	-138	0.35	0.69	0.52	3.01	0.021	0.158	21.1	4
	-160	0.29	1.09	1.04	3.31	0.017	0.208	14.6	4
	-223	0.43	0.89	0.71	1.95	0.016	0.146	34.2	3
	-245	0.36	1.74	1.39	2.14	0.019	0.209	22.7	3
	-294	0.40	2.54	0.39	2.17	0.020	0.259	17.6	4
	-303	0.33	1.39	0.90	1.83	0.012	0.202	27.5	4
	-345	0.35	1.19	0.70	2.08	0.024	0.173	27.5	3
	-384	0.31	1.39	0.76	2.30	0.020	0.196	22.2	4
	-410	0.34	1.46	0.46	2.27	0.028	0.201	21.7	4
	-460	0.37	3.37	1.45	1.67	0.036	0.262	22.4	4
WN-2	- 24	0.26	0.78	1.28	5.24	0.016	0.221	8.7	4
	- 55	0.16	0.06	0.09	16.4	0.008	0.107	5.8	1
	- 85	0.18	0.15	0.11	10.5	0.004	0.141	6.5	1
	- 98	0.26	0.65	0.34	5.02	0.008	0.198	10.1	4
	-124	0.28	0.82	0.77	4.13	0.012	0.201	12.1	4
	-145	0.28	0.09	0.09	4.00	0.028	0.066	38.0	4
WN-4	-408	0.28	2.5	1.40	2.70	-	0.285	13.0	4
	-468	0.38	4.1	0.90	3.30	-	0.403	7.5	4
	-482	0.32	4.5	-1	3.20	-	0.416	7.6	4
	-505	0.33	2.2	-1	4.40	-	0.341	6.7	3
	-551	0.32	2.8	-1	2.70	-	0.301	12.3	3
	-564	0.32	1.7	0.40	2.60	-	0.230	16.7	3
	-603	0.30	6.2	0.90	3.60	-	0.518	5.4	4
	-631	0.39	8.4	-1	1.50	-	0.389	17.1	2
	-659	0.46	8.3	0.60	1.80	-	0.423	13.1	2
	-692	0.41	12.3	1.00	3.00	-	0.665	5.0	2
	-719	0.43	7.3	-1	1.50	-	0.563	18.4	2
	-746	0.45	13.5	0.60	1.80	-	0.540	10.3	2
	-789	0.47	17.4	-1	2.10	-	0.622	7.2	1
	-809	0.48	17.3	1.50	1.40	-	0.539	13.3	1
	-840	0.54	24.5	-1	1.20	-	0.594	14.0	1
	-863	0.49	20.6	3.10	1.50	-	0.609	10.9	1
	-906	0.40	20.1	4.20	1.80	-	0.659	8.4	1
	-923	0.51	13.6	-1	1.60	-	0.598	10.5	1
Units		%	µd	µd	x10³	GPa	µm		

*k_o = permeability under confining pressures of 1.4 MPa
k_c = permeability under confining pressure equivalent to overburden pressure.

6: THERMAL PROPERTIES

THERMOPHYSICAL PROPERTIES OF ROCK SAMPLES FROM WNRE BOREHOLES

Malcolm Drury
Geological Survey of Canada
Energy, Mines and Resources Canada
1, Observatory Crescent
Ottawa, Ontario K1A 0Y3

THERMOPHYSICAL PROPERTIES OF ROCK SAMPLES FROM WNRE BOREHOLES

Malcolm Drury
Geological Survey of Canada, 1 Observatory Crescent, Ottawa, Ontario K1A 0Y3

INTRODUCTION

When the nuclear fuel waste is emplaced in a subsurface vault it will generate a considerable amount of heat and will raise the temperature of the surrounding rock. One of the fundamental problems in considering the site and design of a vault for the disposal of such material is how that heat is dissipated in the host rock. In a rock body that has been undisturbed by tectonic activity for millions of years, the principal mode of heat transfer is by conduction, although in a fractured body moving fluid can also be an effective mechanism (e.g., Drury and Lewis, 1983). The controlling physical property in this steady state is thermal conductivity, K. If a thermal disturbance occurs the transient response of the surrounding rock mass must be described in terms of the thermal diffusivity, s. It is necessary, therefore, to obtain data on such properties in statistically meaningful numbers in order to assess the concept of deep geologic burial of nuclear fuel waste. Conductivity and diffusivity of a material are related:

$$K = s/\rho C \tag{1}$$

in which ρ is the density of the material and C is its specific heat. Mathematically, the transfer of heat in the earth's crust, neglecting the effects of circulating fluids, can be expressed as:

$$\rho C \, \delta v/\delta t = \mathrm{div}(K \, \mathrm{grad} \, v) + A \tag{2}$$

in which A is the heat generated internally by decay of naturally occurring radiogenic elements and v is temperature. In the depth interval (1000 m) and time scale (10^5-10^7 a) of interest to the nuclear fuel waste management programme, the natural radiogenic heat production A can be considered to be constant.

Another fundamental problem is the mechanical response of the rock mass to temperature change. Expansion and microcrack formation must be accounted for in assessing vault stability, and in predicting potential new pathways for the flow of groundwater. The important parameters for this case are the coefficients of linear and volumetric thermal expansion of the rock. Therefore, it is also necessary to obtain linear thermal expansion data of granitic rocks for the concept assessment. The coefficient of linear thermal expansion, α, as reported here is defined as the increase in length, Δl, of a sample at a particular temperature, v, from its length, l_o, at temperature v_o

$$\alpha = \frac{1}{\ell_o} \cdot \frac{\Delta \ell}{\Delta v} \qquad (3)$$

where $\Delta v = v - v_o$ and $\Delta l = \ell - \ell_o$.

Experimental work on the measurement of thermophysical properties of rock samples was done at the former Earth Physics Branch (EPB), now amalgamated with the GSC, and Canada Centre for Mineral and Energy Technology (CANMET), both of the Department of Energy, Mines and Resources Canada. At EPB thermal conductivity and diffusivity at a single, low temperature (20-25°C) has been measured on a large number of samples in order to provide statistically significant mean values, and to permit an assessment of the validity of predicting thermal properties from mineralogical data. At CANMET, the emphasis has been on detailed measurements of small numbers of samples, at elevated temperatures and pressures, in order to predict the behaviour of a rock mass at the actual conditions to be expected in an operational vault. The two sets of data complement each other, as they permit the construction of type curves of physical property against temperature and pressure for different rock types. This paper contains a summary of all thermal property data obtained for rock samples from the Lac du Bonnet batholith, and discusses their thermal characteristics.

Data of thermal properties of crystalline rocks have been given by several authors. A summary was given by Drury et al. (1984). Table 1 is a compilation of such data for crystalline rocks of the type used in the radioactive waste disposal programme. It can be seen that there are relatively few data for thermal diffusivity. One of the aims of the EPB thermal rock properties programme has been to add substantially to a very meagre data base of diffusivity information.

Linear thermal expansion of cores was measured on samples 51 mm long by 8 mm in diameter with a commercial dilatometer, as described by Bell and Lemieux (1980) and Mirkovich (1980a). The apparatus consists of a nichrome-wound furnace having a uniform hot zone 75 mm long, a fused quartz tube closed at the bottom with a plane quartz disc set perpendicular to the longitudinal axis to support the specimen, and a fused quartz push-rod to translate expansion or contraction of the specimen directly to an Ames dial mounted rigidly on the upper end of the tube. A Pt/Pt thermocouple was used to measure temperature at the mid-point of the rock specimen. The heating rate was usually 150 mK/s, and the temperature range was 25-500°C. Later measurements, including those done on URL samples, were made over a temperature range of 25-200°C and pressure range of 1-22.5 Mpa, with a heating rate of 12 mK/s (Annor and Jackson, 1982). Tests had showed that variation of heating rate has little effect on the measured thermal expansion (Bell, 1979).

Table 1. Collected values of thermal properties of rocks. Conductivity and diffusivity at 20-25°C, and linear thermal elongation (v_o = 25°C) at 100°C

Rock type	Conductivity	Diffusivity	Ref.	$\alpha \times 10^6$	Ref.
	W/m.K	mm^2/s		/K	
Granite	1.75-3.08	1.03-1.43	1	5-11	5
	1.67-2.83	0.50-1.51	2		
	2.81-3.77		3		
Granodiorite	1.62-2.33	0.50-0.91	2		
	1.64-3.47		3		
Gabbro	1.93-2.51		3	5-9	5
		0.92	4		
Anorthosite	2.03		3		
Gneiss	2.58-4.77	1.13-1.41	1,3		
Tonalite	2.63		3		

References: 1 – Kappelmeyer and Haenel (1974); 2 – Moiseenko (1968); 3 – Clark (1966); 4 – Lindroth (1974); 5 – Skinner (1966).

EXPERIMENTAL METHODS

Thermal conductivity in the temperature range 20-25°C was measured at EPB on samples approximately 45 mm in diameter and 10 mm thick in a divided bar apparatus of the type described by Jessop (1970). The method requires the use of disks so that radial heat losses are minimised. The method gives a measurement of conductivity that is relative to a known standard, in this case fused silica. The sample is sandwiched between two disks of the reference material, and the stack inserted between a heat source and a heat sink so that heat flow is axial. Samples were measured in the water-saturated state, and were held under a uniaxial pressure of approximately 1 Mpa in order to ensure good thermal contacts in the stack. Accuracy of the measurement is approximately 3%. Thermal conductivity was measured at temperatures in the range 30-500°C at the CANMET laboratory, using a method described by Mirkovich (1980b). The method is a comparative one: a cylindrical specimen 25.4 mm in diameter and 25.4 mm thick is placed between two standards of the same dimensions, and the three cylinders are placed on a cylindrical heat stabiliser. The column of four cylinders is placed between a heat source and a heat sink. The arrangement is such that heat flow is uniaxial, so that the temperature gradient is inversely proportional to conductivity. The conductivity of the standards being known, the conductivity of the sample is easily calculated. Accuracy of measurements is approximately 5%.

Thermal diffusivity of samples at 20-25°C was measured using a system developed at EPB, described by Drury et al. (1984). The method is a modification of one first proposed by Angstrom (1863). A sinusoidal temperature wave is passed across the sample to be measured. Angstrom's original method requires that, in mathematical terms, the sample be infinitely long. In practical terms, this means a length of at least several centimetres. In order to achieve this state, a 30 cm long rod of rock similar to that being tested and of the same diameter is placed on top of the sample. A correction for thermal mismatch between sample and rod is required, although this is usually of the order ± 10% or less. The theory is given in Drury et al. (1984). Samples are placed on a flat plate that is heated by a resistor across which a very low frequency sinusoidally varying voltage is impressed. The sample and matching rod are placed in a hydraulic press and held under a pressure of approximately 1 Mpa. Temperatures at the top and bottom of the sample are measured at discrete time intervals, and the phase and amplitude of the

temperature variations at these two faces are used to calculate diffusivity according to the relationship:

$$s = \pi l^2 / T\beta \ln\delta \qquad (4)$$

in which l is the sample length, T is the period of the temperature wave, β is the phase lag and δ is the amplitude ratio. The uncertainty of this method is approximately 5%. Diffusivity at high temperatures was measured at CANMET using a method developed there (Mirkovich, 1976). Transient heat pulses are impressed on the outside of cylindrical samples and their progress monitored at the centre and at a point near the side of the cylinder. The diffusivity is calculated from analysis of the temperature difference between measurement points as a function of time and geometry.

EXPERIMENTAL RESULTS

Low temperature thermal conductivity and diffusivity

Thermal conductivity and diffusivity were measured for 227 samples from boreholes WN-1, WN-2 and WN-4, and 176 samples from holes URL-2 and URL-5 were measured. Individual data are presented hole by hole in Table 5 of the Appendix. Figures 1 and 2 are histogram distributions of the two properties, and Figures 3 and 4 are plots of the properties against depth. The mean and standard deviations for the data are given in Table 2.

It is apparent from the high standard deviation values that diffusivity varies widely. This can be seen in Figure 2. Individual values in excess of 1.8 mm^2/s were obtained. It is of interest to note that whereas the mean conductivity of URL samples is about 6% higher than that of the WN samples, mean diffusivity and specific heat are very similar between the two sets of data. Both properties are dependent on mineral content, and the mineral that has most influence is quartz. Most minerals commonly found in granitic rocks have conductivity and diffusivity of approximately 2 W/m.K and 1-1.5 mm^2/s, whereas quartz has a mean conductivity of approximately 7.7 W/m.K and a diffusivity of approximately 3.9 mm^2/s. The mean quartz content of 33 WN samples, determined by the point counting technique, is 28 ± 5%, and the mean of 173 samples from URL holes is 30 ± 7%. The mean quartz content of 108 special samples from WN-4, determined

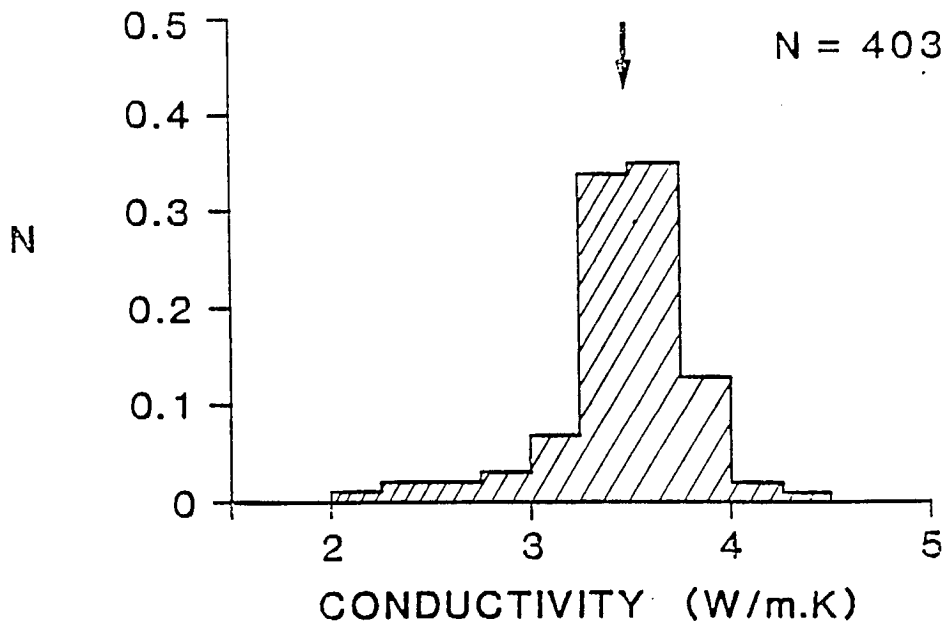

Figure 1. Histogram distribution of low temperature thermal conductivity data of Lac du Bonnet batholith samples. Arrow indicates arithmetic mean. N is number of samples. N* is the number of samples per interval normalised to N.

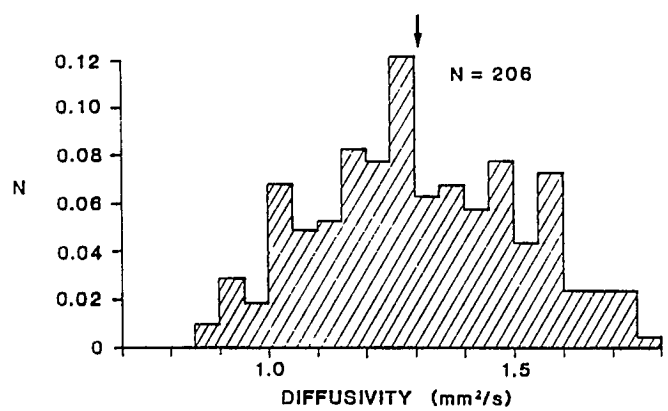

Figure 2. As Figure 1, for thermal diffusivity.

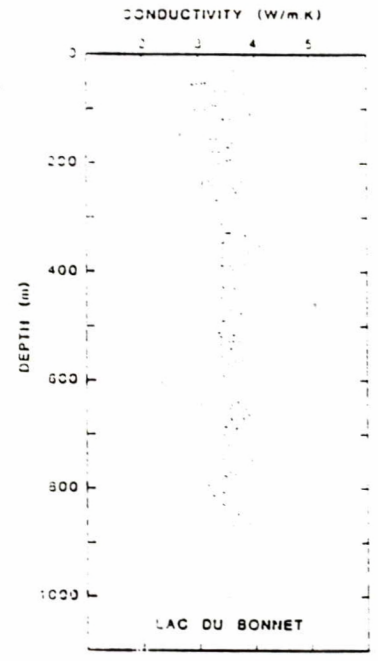

Figure 3. Variation of thermal conductivity with depth, Lac du Bonnet batholith.

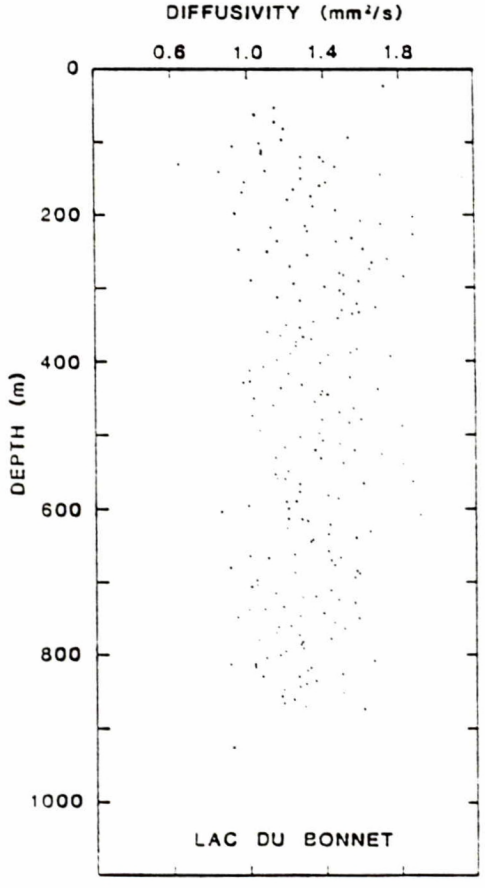

Figure 4. Variation of thermal diffusivity with depth, Lac du Bonnet batholith.

from stained sections, is 30 ± 4%. There is no apparent difference in mean quartz content between the WN and URL sample sets, and the difference in mean conductivity must be ascribed to some other factor. This will be discussed further in the next section.

There is no discernible trend of variation of either property with depth (Figures 1 and 2). A tonalitic zone in the upper 100 m is reflected in lower conductivities. Individual high or low values reflect local variations in quartz content, or basic intrusions (e.g., at 484.8 m).

High temperature thermal conductivity and diffusivity

Detailed studies of the variation of conductivity and diffusivity were made on 11 specimens from four samples from different depths in WN-1 (Mirkovich, 1980a,b). Samples and depths are 1-158.1 m, 2-156.1 m, 3-168.8 m and 4-173.2 m. Cylinders for sample 1 were cut perpendicular and parallel to the core. Sample 4 showed gneissic layering at approximately 30° to the core; cylinders were cut perpendicular to the gneissic layering and in three directions (0°, 120°, and 240°) from a common plane parallel to it. Eight to ten conductivity measurements and thirty-five to forty-five diffusivity measurements were made on each specimen in the range 25-500°C, and curves were fitted to the data by the least squares method according to the polynomial expression:

$$p = a_1 + a_2 v + a_3 v^2 \qquad (5)$$

in which p is K or s. The results are summarised in Table 3.

Thermal expansion

Linear thermal elongation data for the samples from the Lac du Bonnet batholith have been reported by Mirkovich and Bell (1978), Bell (1979), Bell and Lemieux (1979, 1980), Mirkovich (1980a), and Annor and Jackson (1982). Most measurements were made with specimens unconfined, but some were made under triaxial confining pressures of 6-23 MPa. The results were reported differently, but are summarised here using a common format – the coefficient of linear

Table 2. Mean and standard deviations of measured low temperature thermal conductivity, thermal diffusivity and the derived property specific heat for boreholes from the two sites within the Whiteshell Research Area

Conductivity:	WN	3.41 ± 0.28	W/m.K	227	samples
	URL	3.61 ± 0.40	"	176	"
	all	3.49 ± 0.35	"	403	"
Diffusivity:	WN	1.30 ± 0.19	mm^2/s	33	samples
	URL	1.33 ± 0.24	"	173	"
	all	1.32 ± 0.23	"	206	"
Specific Heat:	WN	1030 ± 160	J/kg.K	33	samples
	URL	1060 ± 206	"	173	"
	all	1060 ± 200	"	206	"

Table 3. Coefficients for the least squares polynomial fit for the dependence of conductivity and diffusivity on temperature (from Mirkovich, 1980a, 1980b). Key: a – perpendicular to core or gneissic layering; b – parallel to core or gneissic layering; c,d – parallel to gneissic layering (see text). Core orientation not specified for diffusivity samples.

	Specimen	a_1	$a_2 \times 10^3$	$a_3 \times 10^6$
Conductivity	1a	3.513	-4.039	2.251
	1b	3.507	-3.853	1.945
W/m.K	2b	3.498	-2.637	-
	3b	3.392	-2.380	-
	4a	3.657	-3.795	1.157
	4b	3.528	-4.155	2.499
	4c	3.539	-4.155	2.499
	4d	3.592	-4.282	2.473
Diffusivity	1	1.637	-3.579	3.714
	2	1.410	-2.722	2.922
mm^2/s	3	1.480	-2.610	2.539

Conductivity varies little over this short section of borehole. At 20°C it would be in the range of 3.3 to 3.5 W/m.K, in excellent agreement with measurements made near that temperature at EPB (see Fig. 1). Diffusivity is also quite uniform over the section, although quite high, ranging between 1.45 and 1.57 mm^2/s at 20°C, in good agreement with the EPB measurements (Fig. 2).

thermal expansion relative to 25°C at two or three temperatures. Owing to differences in reporting practices, the temperatures at which the coefficients were calculated are within a temperature range of ± 15 K. The data are presented in Table 4.

Curves of elongation as a function of temperature are shown by the authors cited above. All are continuous, showing that in the temperature range of 25-500°C none of the specimens undergoes sudden structural changes (Mirkovich, 1980a). Most do show an irreversible elongation of up to 0.2%. Mirkovich (1980a) noted an apparent linear relationship between thermal diffusivity and thermal elongation, but there are not enough data to verify this. As noted above, both conductivity and diffusivity are dependent to some extent on quartz content, as quartz has significantly higher conductivity and diffusivity than other common minerals of granitic rocks. Its thermal expansion is also greater (10-18 x 10^{-6}/K) than other common minerals (e.g., 0-6 x 10^{-6}/K for feldspar). An empirical relationship between thermal diffusivity and thermal elongation is therefore expected to exist.

Table 4. Coefficients of linear thermal expansion in three temperature ranges. Unc. refers to measurements made under no confining pressure. Base temperature v_o (equation 3) is 25°C

Depth m	Pressure MPa	α x 10^6 (100+/-15°C)	α x 10^6 (200+/-15°C)	α x 10^6 (500+/-5°C)
(WN-1)				
133.5	unc.	3.3	7.5	15
160.8		4.7	9.5	17
223.9		3.3	8.6	16
245.9		3.3	7.4	15
294.4		2.7	8.6	16
303.4		4.0	8.6	16
340.9	6.75	3.0	5.5	
340.9	20.20	2.3	4.5	
345.4	unc.	4.0	6.9	15
354.7		2.7	7.4	15
410.6		5.3	9.4	17
460.5		6.0	9.9	17
(WN-2)				
24.6	unc.	4.0	8.3	17
55.3		5.3	9.7	16
55.2		5.3	9.1	17
95.4		4.3	8.6	17
124.6		4.0	8.6	17
145.3		5.3	9.4	16
(WN-4)				
403.9	unc.	3.1	7.6	14.8
463.9		4.3	9.0	16.3
482.6		5.5	10.7	17.5
505.3		4.1	9.4	16.7
531.1		3.6	9.2	16.9
564.3		6.4	9.4	15.7
603.3		4.3	8.6	16.6
631.4		3.0	6.2	12.6
660.0		3.3	7.4	15.0
692.6		4.3	8.1	15.3
719.3		3.3	8.3	14.3
746.9		2.3	6.6	14.0
789.6		4.5	8.4	15.5
809.4		4.1	8.6	16.3
840.9		3.2	8.1	15.3
863.1		3.0	7.0	12.3
906.5		3.3	7.9	15.6
923.6		2.9	7.5	15.8
(URL-1)				
282.8	unc.	4.0	7.7	
283.7		3.1	7.3	
293.7	6.37	2.3	6.6	
(URL-3)				
247.7	unc.	7.0	8.4	
277.4	unc.	2.4	6.1	
277.4	6.90	3.4	5.4	
277.4	20.70	3.0	5.0	
273.8	unc.	2.0	4.8	
273.3	6.90	1.4	4.2	
273.3	20.37	1.3	6.2	

DISCUSSION AND CONCLUSION

Jessop et al. (1979) discussed the effect of quartz on thermal conductivity of some crystalline rocks, and Drury and Jessop (1983) discussed the validity of models for predicting conductivity from known mineral content. As noted earlier, the conductivity and diffusivity of quartz are substantially higher than those of other common minerals of granitic rocks. It is expected, therefore, that the thermal properties of a rock with a significant quartz fraction would be dominated by that of quartz. There clearly is a weak linear relationship. Least-squares regression of conductivity on quartz content yields:

$$K = 3.57(Qz\%) + 2.54$$

for 206 samples, with a correlation coefficient of 0.62. The intercept value is close to that expected for the conductivity of other minerals in the samples (Drury and Jessop, 1983). Linear regression of diffusivity and specific heat on quartz content yield correlation coefficients of only 0.13 and 0.18, which means that the relationship for these properties is statistically insignificant. Both mean diffusivity and specific heat are statistically equal between the WN and URL sample sets, whereas conductivity is higher for the URL set than for the WN. This may be the result of the way in which quartz and other mineral grains are interrelated. A sample with a particular quartz content would be expected to have a lower conductivity if the quartz grains were surrounded by low conductivity material than a sample in which the quartz grains were in good contact with each other. It is recommended that future petrographic work address this problem. While knowledge of quartz content would allow a rough estimate of thermal properties to be made, there is no adequate substitute for direct measurement.

The combination of high temperature data on a few samples and low temperature measurements on large numbers of samples allows the construction of type curves for thermal conductivity and diffusivity as a function of temperature. The mean parameters of equation (4) are, from Table 3:

$$\text{conductivity: } a_2 = -3.67 \times 10^{-3};\ a_3 = 2.16 \times 10^{-6}$$
$$\text{diffusivity: } a_2 = -2.97 \times 10^{-3};\ a_3 = 3.06 \times 10^{-6}$$

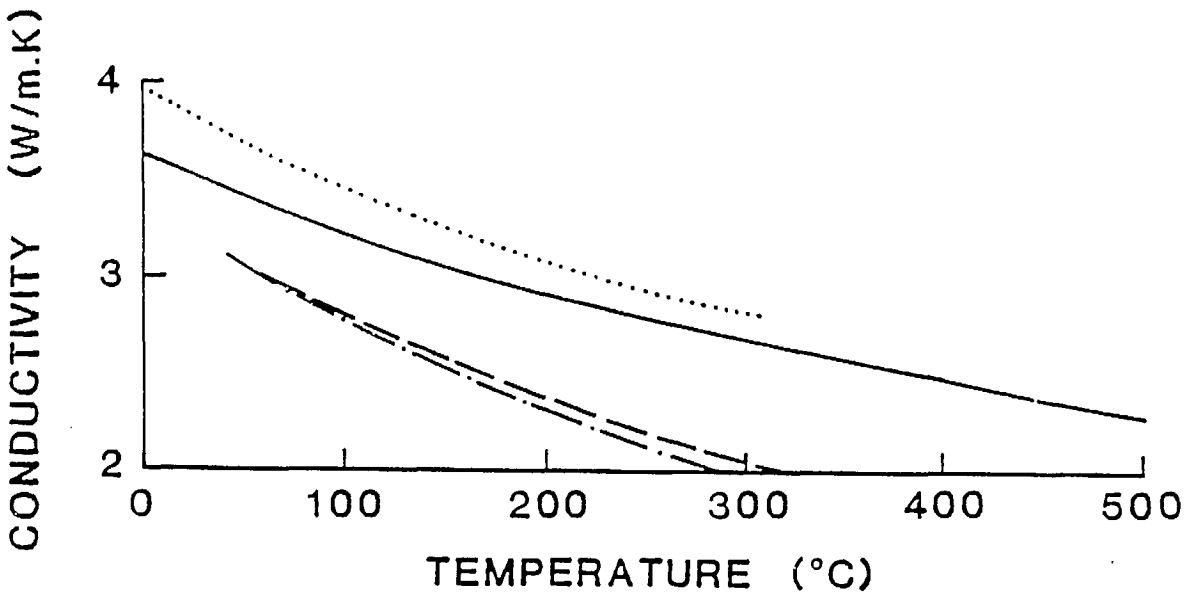

Figure 5. Variation of conductivity with temperature. Solid curve: type curve calculated from mean data of Lac du Bonnet samples. Dotted line: granite sample (conductivity x 1.15) from Kappelmeyer and Haenel (1974). Dashed line and dashed-dotted line: curves for (001) and (010) quartz (from Kappelmeyer and Haenel, 1974).

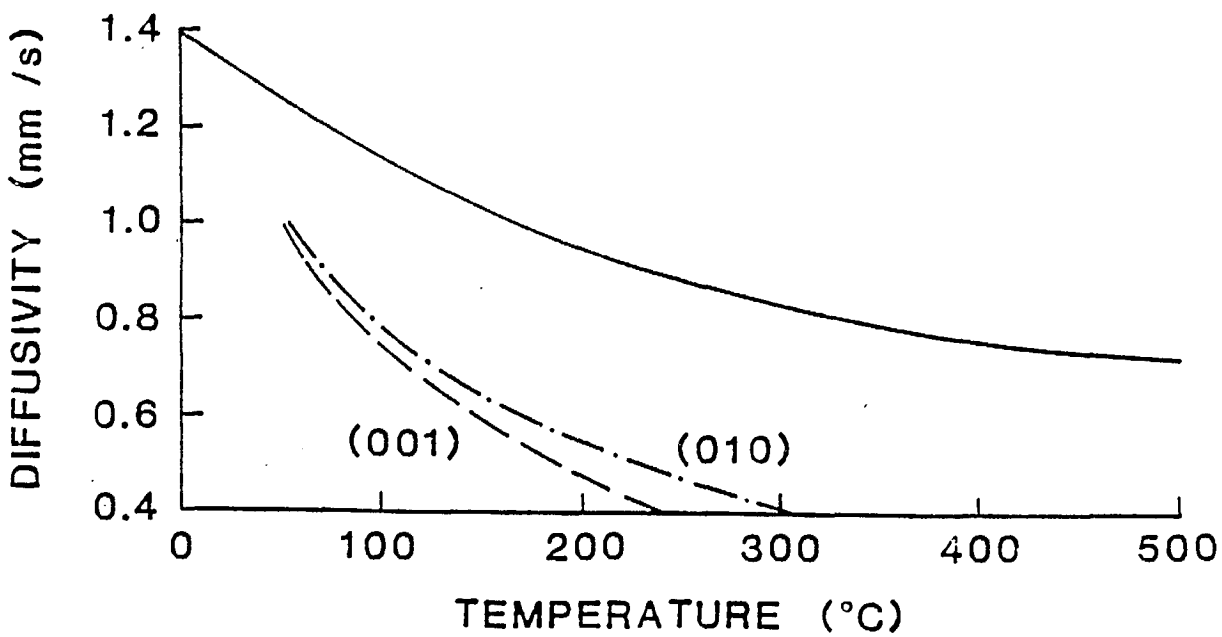

Figure 6. Variation of diffusivity with temperature. Solid line: calculated from mean of Lac du Bonnet data. Dashed lines: as for Figure 5.

Figures 5 and 6 show curves of conductivity and diffusivity as a function of temperature, using these parameters and the mean conductivity and diffusivity from Table 2. The dotted line in Figure 5 represents data for a granite sample (from Kappelmeyer and Haenel, 1974) for comparison. No comparable data for diffusivity have been found. Shown also as dashed lines are curves for (001) and (010) quartz, normalised to the value at 50°C (data from Kappelmeyer and Haenel, 1974, Table 6.4). If quartz dominates the thermal properties of the granites, the functional dependence on temperature of the whole rock should be closely parallel to that of quartz alone. Figures 5 and 6 show clearly that this is not so. Again, the conclusion is that there is no adequate substitute for direct measurement.

The mean coefficient of linear thermal elongation at 100°C (with v_0 = 25°C, equation 3) is 3.8×10^{-6}/K, which is less than the values reported in the literature. This would be a favourable conclusion with regard to rock mass stability for the vault. However, Mirkovich (1980a) has combined the thermal elongation data and high temperature diffusivity data for three rock samples from WN-1 and, on the basis of an empirical relationship among those parameters and spalling tendency, has concluded that the granite at the WN borehole sites would have a low thermomechanical stability.

ACKNOWLEDGEMENT

Rock type identifications were made by P. Chernis and W. Nuyens.

REFERENCES

Angstrom, A.J. 1863. New method of determining the conductibility of solids. Philos. Mag., v. 25, p. 130-142.

Annor, A. and Jackson, R. 1982. Summary of uniaxial elastic properties and thermal expansion data for Pinawa granite samples. CANMET Rept. ERP/MRL 82-82 (OP), 16 p.

Bell, K.E. 1979. Effect of heating rate on the thermal dilatometry of rocks. CANMET Rept. MRP/MSL 79-174 (TR), 5 p.

Bell, K.E. and Lemieux, G. 1979. Thermal expansion behaviour of thirty-three rock samples. CANMET Rept. MSL-INT 79-42, 20 p.

Bell, K.E. and Lemieux, G. 1980. Thermal expansion behaviour of eighteen rock samples from Pinawa, Manitoba. CANMET Rept. MSL-INT 79-124 (TR), 49 p.

Clark, S.P. 1966. Thermal conductivity, in Handbook of Physical Constants, S.P. Clark, ed., Geol. Soc. Am. Memoir 97, p. 459-482.

Drury, M.J. and Jessop, A.M. 1983. The estimation of rock thermal conductivity from mineral content – an assessment of techniques. Zbl. Geol. Palaeont., v. 1, p. 35-48.

Drury, M.J. and Lewis, T.J. 1983. Water movement in Lac du Bonnet batholith as revealed by detailed temperature logs of three closely-spaced boreholes. Tectonophysics, v. 95, p. 337-351.

Drury, M.J., Allen, V.S. and Jessop, A.M. 1984. The measurement of thermal diffusivity of rock cores. Tectonophysics, v. 103, p. 321-333.

Jessop, A.M. 1970. The effect of environment on divided bar measurements. Tectonophysics, v. 10, p. 39-49.

Jessop, A.M., Robertson, P.B. and Lewis, T.J. 1979. A brief summary of the thermal conductivity of crystalline rocks. AECL TR-12, 19 p.

Kappelmeyer, O. and Haenel, R. 1974. Geothermics with special reference to application. Gebruder Borntraeger, Berlin, 238 p.

Lindroth, D.P. 1974. Thermal diffusivity of six igneous rocks at elevated temperatures and reduced pressures. U.S. Bur. Mines Rept. Invest. 7954, 33 p.

Mirkovich, V.V. 1976. An apparatus for measuring thermal diffusivity in air. CANMET Rept. 77-21, 28 p.

Mirkovich, V.V. 1980a. Thermal diffusivity and linear thermal expansion of Pinawa drill core rocks. CANMET Rept. ERP/MSL 80-141 (IR), 10 p.

Mirkovich, V.V. 1980b. Thermal conductivity of Pinawa drill core rocks. CANMET Rept. ERP/MSL 80-132 (IR), 8 p.

Mirkovich, V.V. and Bell, K.E. 1978. Linear thermal elongation data for WN1 and WN2 samples. CANMET Rept. 202409-M01/78, 21 p.

Moiseenko, O.I. 1968. Warmeleitfahigkeit der Gesteine bei hohen Temperaturen. Freiberger Forschungsh., C, v. 238, p. 89-94.

Skinner, B.J. 1966. Thermal expansion, in Handbook of Physical Constants, S.P. Clark, ed., Geol. Soc. Am., Memoir 97, p. 75-96.

APPENDIX

Table 5. Individual data of each sample, showing true vertical depth of sample, rock type, conductivity (W/m.K), diffusivity (mm^2/s), specific heat (J/kg.K), density (Mg/m^3) and porosity. See Table 2 for details of rock type abbreviations. For each hole, data for standard samples are given first, followed by data for special samples.

Data for hole WN-1 – Standard samples

Depth(m)	Rock type	Cond.	Diff.	Sp.Ht.	Dens.	Por.
133.8	Granite	3.32	1.46	870	2.62	.002
155.2	Granite	3.13	1.41	850	2.62	.002
215.6	Granite	3.13	1.30	920	2.62	.001
236.6	Granite	2.89	1.15	960	2.62	.002
282.7	Granite	3.38	1.50	850	2.64	.002
291.2	Granite	3.41	1.58	820	2.62	.001
330.8	Granite	3.49	1.49	890	2.62	.002
367.6	Granite	3.05	1.29	900	2.63	.002
391.7	Granite	3.53	1.42	950	2.61	.002
438.0	Granite	3.40	1.68	770	2.62	.003

Data for hole WN-2 – Standard samples

Depth(m)	Rock type	Cond.	Diff.	Sp.Ht.	Dens.	Por.
23.8	Granite	3.50	1.72	780	2.61	.003
53.4	Tonalite	3.03	1.14	980	2.70	.002
82.0	Tonalite	3.02	1.19	930	2.73	.002
94.6	Granite	3.45	1.53	860	2.63	.002
119.7	Granite	3.50	1.28	1050	2.61	.003
139.9	Granite	3.20	1.09	1120	2.63	.002

Data for hole WN-4 – Standard samples

Depth(m)	Rock type	Cond.	Diff.	Sp.Ht.	Dens.	Por.
389.9	Granite	3.75	1.22	1175	2.62	.004
445.1	Granite	3.75	1.38	1043	2.62	.004
478.7	Granite	3.78	1.39	1038	2.62	.003
519.6	Granite	3.61	1.35	1025	2.62	.005
531.2	Granite	3.73	1.38	1027	2.63	.004
566.2	Granite	3.80	1.27	1139	2.63	.003
590.4	Granite	3.61	1.25	1129	2.62	.003
615.0	Granite	3.80	1.28	1135	2.61	.004
642.7	Granite	3.69	1.34	1047	2.62	.003
665.3	Granite	3.89	1.00	1491	2.61	.005
688.0	Granite	3.68	1.24	1125	2.63	.006
723.0	Granite	3.45	1.28	1029	2.62	.004
738.9	Granite	3.58	1.08	1263	2.64	.004
763.8	Granite	3.51	1.15	1159	2.63	.004
781.1	Granite	3.28	1.05	1208	2.59	.007
814.1	Granite	3.25	.90	1244	2.91	.007
830.6	Granite	3.62	1.07	1285	2.63	.004
830.0	Granite	3.40			2.63	.006

Table 3: continued

Data for hole WN-4 – Special samples

Depth(m)	Conductivity	Density	Porosity
36.1	3.22	2.61	.003
36.1	3.63	2.61	.003
37.6	3.81	2.62	.004
37.6	4.15	2.62	.003
48.9	3.48	2.62	.004
48.9	3.46	2.62	.003
52.3	3.14	2.45	.003
52.4	3.08	2.73	.002
55.2	2.39	2.78	.003
55.3	2.89	2.55	.005
55.3	2.92	2.56	.004
66.8	2.64	2.68	.003
66.8	2.71	2.67	.002
67.0	3.31	2.79	.003
67.0	3.50	2.73	.003
77.9	2.27	2.74	.002
77.9	2.02	2.78	.003
83.6	2.24	2.74	.002
83.6	2.34	2.78	.002
93.6	3.21	2.70	.002
93.6	3.27	2.71	.002
100.6	3.13	2.62	.003
100.6	3.43	2.62	.003
107.5	3.03	2.61	.004
107.5	3.37	2.61	.003
118.2	3.43	2.62	.004
118.2	3.59	2.62	.003
125.6	3.50	2.61	.004
125.6	3.67	2.61	.003
131.3	3.45	2.60	.003
131.3	3.70	2.60	.003
139.9	3.20	2.63	.003
139.9	3.42	2.62	.005
144.3	3.34	2.62	.003
144.3	3.57	2.61	.003
154.0	3.53	2.61	.004
154.0	3.64	2.61	.003
162.9	3.47	2.61	.004
162.9	3.61	2.61	.004
170.8	3.52	2.60	.003
170.8	3.56	2.60	.003
179.5	3.27	2.62	.003
179.5	3.38	2.63	.003
187.6	3.45	2.62	.004
187.6	3.53	2.62	.003
194.7	3.46	2.66	.003
194.7	3.53	2.64	.003
200.5	3.29	2.63	.004
200.5	3.37	2.63	.004
212.0	3.32	2.66	.004
212.0	3.52	2.63	.003
218.2	3.43	2.68	.004
218.2	3.79	2.65	.003
222.5	3.47	2.62	.004
222.5	3.66	2.62	.004
233.2	3.09	2.62	.005
233.2	3.19	2.62	.004
240.6	3.07	2.63	.003
240.6	3.07	2.69	.003
247.9	3.45	2.62	.004
247.9	3.65	2.62	.003
255.7	3.45	2.62	.003
255.7	3.65	2.61	.004
263.1	3.50	2.61	.004
263.1	3.50	2.62	.004
268.9	3.30	2.63	.005
268.9	3.35	2.63	.003
279.8	3.27	2.74	.004
279.8	3.50	2.62	.004
285.7	3.41	2.62	.003
285.7	3.57	2.62	.003
294.5	3.21	2.62	.003
294.5	3.38	2.62	.004
301.4	3.41	2.45	.004
308.6	3.38	2.62	.003
308.6	3.40	2.62	.004
315.7	3.41	2.43	.004
315.7	3.70	2.55	.003
323.8	3.44	2.62	.003
323.8	3.64	2.62	.003
331.0	3.49	2.62	.003
331.0	3.57	2.62	.003
340.6	3.50	2.61	.003
340.6	3.07	2.61	.001
348.9	3.44	2.56	.004
348.9	3.36	2.63	.006
357.1	3.55	2.64	.003
357.1	3.63	2.63	.003
361.2	2.99	2.62	.004
361.2	3.44	2.62	.003
368.5	3.50	2.64	.006
368.5	3.42	2.63	.003
375.8	3.40	2.62	.006
375.8	3.44	2.62	.003
384.0	2.81	2.63	.005
384.0	3.31	2.63	.004
390.7	3.44	2.63	.005
390.7	3.41	2.62	.003
398.1	3.42	2.62	.004
398.2	3.62	2.63	.006
404.9	3.43	2.63	.005
405.3	3.36	2.64	.004

Table 3: continued

Data for hole WN-4 – Special samples

Depth(m)	Conductivity	Density	Porosity
413.2	3.49	2.64	.006
413.2	3.37	2.62	.004
419.3	4.05	2.63	.006
419.3	3.49	2.62	.006
427.3	3.28	2.63	.005
427.3	3.52	2.63	.004
427.9	2.95	2.59	.006
427.9	3.37	2.56	.005
434.1	3.59	2.63	.009
434.1	3.35	2.62	.005
442.7	3.51	2.63	.004
442.7	3.52	2.63	.004
449.9	3.54	2.62	.004
449.9	3.42	2.62	.004
456.8	3.39	2.63	.006
456.8	3.50	2.62	.004
464.3	3.41	2.64	.008
464.3	3.41	2.64	.004
472.1	3.64	2.63	.006
472.1	3.57	2.62	.004
477.7	3.66	2.63	.005
477.7	3.59	2.62	.004
484.8	2.56	3.03	.005
484.8	2.59	3.03	.003
485.6	3.14	2.64	.004
485.6	3.32	2.64	.004
492.3	3.47	2.63	.006
492.3	3.43	2.64	.005
499.9	3.61	2.59	.006
499.9	3.63	2.61	.003
507.3	3.41	2.63	.006
507.3	3.60	2.60	.004
514.2	3.38	2.64	.003
514.2	3.36	2.64	.003
521.3	3.38	2.64	.007
521.3	3.40	2.64	.004
529.7	3.63	2.63	.005
529.7	3.55	2.63	.004
535.1	3.40	2.63	.008
535.1	3.37	2.63	.004
543.2	3.53	2.63	.008
543.2	3.58	2.63	.004
552.0	3.34	2.62	.008
552.0	3.46	2.61	.005
557.2	3.42	2.63	.006
557.2	3.49	2.62	.004
564.2	3.49	2.62	.004
564.3	3.49	2.63	.005
571.5	3.53	2.63	.005
571.5	3.46	2.63	.004
577.3	3.61	2.61	.005
585.6	3.67	2.62	.005
592.7	3.44	2.61	.006
598.7	3.53	2.62	.006
607.4	3.66	2.62	.005
612.8	3.69	2.61	.006
620.4	3.60	2.62	.005
626.3	3.58	2.61	.005
633.5	3.64	2.67	.006
639.8	3.71	2.61	.005
646.6	3.59	2.61	.005
652.6	3.56	2.61	.004
653.7	3.84	2.61	.005
661.4	3.68	2.62	.005
670.6	3.57	2.61	.006
674.1	3.59	2.62	.005
681.3	3.42	2.63	.005
687.0	3.49	2.63	.005
694.2	3.49	2.63	.006
700.2	3.44	2.63	.006
706.4	3.44	2.62	.007
713.0	3.46	2.62	.006
719.6	3.36	2.63	.006
726.0	3.34	2.64	.006
732.2	3.28	2.63	.007
738.9	3.25	2.63	.006
746.3	3.42	2.64	.006
751.7	3.30	2.64	.007
758.1	3.38	2.63	.006
764.8	3.35	2.64	.007
771.0	3.37	2.64	.005
776.8	3.44	2.64	.006
782.6	3.41	2.64	.006
789.3	3.43	2.64	.006
795.1	3.16	2.62	.007
800.9	3.27	2.63	.006
807.3	3.40	2.64	.006
813.3	3.39	2.63	.011
819.3	3.36	2.63	.003
824.8	3.37	2.63	.006
829.6	3.28	2.64	.007

Data for hole URL-2 – Standard samples

Depth(m)	Rock type	Cond.	Diff.	Sp.Ht.	Dens.	Por.
429.7	Granite	3.45	.98	1343	2.62	.005
539.4	Granite	3.80	1.19	820	2.62	.005
663.4	Granite	3.79	1.10	1315	2.62	.008
749.2	Granodiorit	3.93	.94	1578	2.65	.004
917.1	Granite	3.66	1.03	1351	2.63	.005
926.4	Granite	3.42	.91	.429	2.63	.124
1003.4	Granite	3.49			2.56	.169

Table 3: continued

Data for hole URL-2 - Special samples

Depth (m)	Rock type	Cond.	Diff.	Sp.Ht.	Dens.	Por.
332.2		3.45	1.03	1334	2.52	.002
336.4	Grndiorit	3.83	1.14	1276	2.63	.003
346.4	Granite	4.11	1.18	1332	2.62	.003
401.6	Q Mz Diort	2.95	1.06	1023	2.71	.003
426.3	Amphibolit	3.93	.92	1539	2.79	.003
441.2	Mz Granite	3.95	1.07	1405	2.62	.003
445.8	Mz Granite	3.67	1.07	1303	2.64	.003
521.0	Granite	3.87	1.38	1068	2.63	.004
525.9	Mz Granite	3.82	1.40	1048	2.61	.003
530.6	Q Mz Diort	2.16	.64	1204	2.82	.004
535.3	Q Mz Diort	2.77	1.28	796	2.71	.003
540.3	Qdiorit	2.58	.85	1127	2.70	.002
543.0	Granite	2.69	1.70	660	2.64	.004
549.6	Mz Granite	2.68	1.28	797	2.63	.001
556.7	Grndiorit	3.33	.98	1283	2.66	.002
559.8	Qsyenit	3.06	1.38	863	2.57	.004
564.3	Mz Granite	3.55	1.24	1151	2.49	.002
568.9	Grndiorit	3.85	.97	1521	2.62	.002
574.0	Granite	3.68	1.33	1062	2.61	.003
578.3	Granite	3.76	1.21	1182	2.62	.004
583.2	Grndiorit	3.80	1.34	1073	2.64	.003
593.3	Mz Granite	3.39	1.66	943	2.61	.005
598.2	Grndiorit	2.36	.93	926	2.73	.005
602.8	Mz Granite	3.86	1.37	797	2.59	.005
607.9	Mz Granite	3.50	1.39	949	2.60	.006
612.6	Mz Granite	3.68	1.70	815	2.65	.005
617.3	Mz Granite	3.60	1.12	1218	2.63	.004
622.2	Granite	3.58	1.31	1044	2.62	.003
626.9	Grndiorit	3.62	1.37	736	2.63	.003
631.7	Mz Granite	3.78	1.54	934	2.62	.005
636.3	Mz Granite	3.73	1.46	986	2.62	.005
641.4	Sy Granite	3.77			2.62	.002
646.3	Granite	3.57	1.60	847	2.63	.003
650.8	Mz Granite	3.60	1.10	1251	2.62	.005
655.6	Mz Granite	3.69	1.31	1076	2.62	.005
660.5	Grndiorit	3.61	1.73	793	2.63	.004
665.5	Mz Granite	3.64	1.65	941	2.63	.006
670.1	Mz Granite	3.99	1.22	1253	2.62	.003
674.9	Grndiorit	3.55	1.64	829	2.63	.004
679.9	Granite	3.86	1.48	993	2.62	.005
684.4	Mz Granite	4.39	1.82	921	2.62	.002
689.4	Grndiorit	3.62	1.01	1357	2.63	.002
694.2	Grndiorit	3.43	1.24	1063	2.62	.004
698.9	Grndiorit	3.52	1.40	960	2.62	.004
703.7	Mz Granite	3.53	1.48	923	2.62	.004
708.5	Granite	3.54	1.50	983	2.50	.005
713.4	Mz Granite	3.42	1.15	1181	2.52	.004
717.8	Granite	3.63	1.27	1057	2.63	.004
722.7	Mz Granite	3.65	1.57	886	2.63	.003
727.4	Granite	3.78	1.67	863	2.63	.004
733.5	Grndiorit	3.84	1.58	931	2.61	.004
736.0	Mz Granite	3.85	1.55	943	2.63	.004
742.1	Sy Granite	3.91	1.47	1028	2.59	.004
746.4	Grndiorit	3.47	1.34	931	2.65	.003
751.3	Mz Granite	3.83	1.20	1221	2.62	.004
755.0	Mz Granite	4.11	1.27	1236	2.62	.004
760.8	Mz Granite	4.12	1.10	1433	2.62	.005
765.6	Mz Granite	3.91	1.17	1279	2.61	.003
770.7	Mz Granite	4.07	1.33	1169	2.62	.004
774.6	Mz Granite	4.32	1.25	1319	2.63	.004
780.2	Granite	4.26	1.25	1303	2.62	.005
784.5	Granite	4.84	1.57	1173	2.63	.005
789.3	Granite	3.84	1.54	960	2.59	.004
794.0	Grndiorit	4.35	1.75	947	2.63	.004
798.6	Mz Granite	4.17	1.15	1401	2.59	.005
803.3	Mz Granite	3.81	1.38	1061	2.61	.004
808.3	Mz Granite	4.05	1.08	1426	2.62	.004
813.1	Grndiorit	3.43	1.01	1301	2.62	.004
817.7	Mz Granite	3.54	1.21	1107	2.64	.004
822.4	Granite	3.35	1.53	835	2.63	.005
828.0	Grndiorit	3.44	1.01	1296	2.63	.005
832.2	Granite	3.65	1.28	1052	2.63	.005
836.7	Granite	3.35	1.17	1087	2.63	.005
841.2	Grndiorit	3.64	1.39	994	2.63	.006
846.0	Granite	3.65	1.42	979	2.63	.005
850.7	Granite	3.53	1.03	1314	2.62	.006
855.1	Mz Granite	3.61	1.35	1018	2.62	.006
860.0	Mz Granite	3.44	1.13	1154	2.63	.007
864.9	Mz Granite	3.63	1.55	896	2.62	.006
869.5	Mz Granite	3.73	1.48	974	2.62	.006
874.1	Grndiorit	3.38	1.02	1249	2.63	.004
879.0	Mz Granite	3.46	1.59	831	2.62	.006
883.8	Granite	3.51	1.53	872	2.63	.006
888.5	Mz Granite	3.83	1.81	811	2.62	.006
893.2	Grndiorit	3.54	1.06	1270	2.62	.006
897.9	Grndiorit	3.48	1.37	966	2.63	.006
902.5	Mz Granite	3.73	1.27	1118	2.62	.005
907.2	Granite	3.78	1.39	1033	2.63	.005
911.7	Mz Granite	3.63	1.48	981	2.61	.006
916.3	Mz Granite	3.64	1.19	1168	2.61	.006
921.0	Mz Granite	3.65	1.56	891	2.63	.006
925.7	Mz Granite	3.90	1.70	875	2.62	.005
930.2	Mz Granite	3.83	1.14	1288	2.62	.005
937.9	Mz Granite	3.80	1.50	970	2.62	.005
939.7	Mz Granite	3.38	1.32	711	2.62	.005
944.2	Mz Granite	3.41	1.68	770	2.63	.005
948.9	Mz Granite	3.78	1.21	1196	2.61	.005
953.6	Mz Granite	3.72	1.18	1252	2.61	.006
958.2	Granite	3.91	1.15	1307	2.61	.004
962.9	Mz Granite	3.79	1.37	776	2.62	.005
965.9	Granite	3.66	1.61	866	2.62	.004
976.6	Granite	3.76	1.27	1134	2.61	.005

Table 3: continued

Data for hole URL-2 - Special samples

Depth (m)	Rock type	Cond.	Diff.	Sp.Ht.	Dens.	Por.
982.1	Granite	2.68	1.42	794	2.61	.004
985.7	Mz Granite	3.42	1.47	839	2.62	.003
990.5		3.33	1.20	1068	2.61	.004
995.1	Mz Granite	2.96	1.60	1063	2.78	.004
999.6	Grndiortt	3.18	1.21	998	2.63	.003
604.3	Bi Qzamphb	2.35	.86	995	2.74	.006
608.9	Grndiorit	3.33	1.91	660	2.64	.003
613.4	Mz Granite	3.29	1.21	1040	2.62	.004
618.1	Mz Granite	3.50	1.31	1034	2.59	.003
622.4	Grndiorit	3.84	1.43	1021	2.63	.001
626.9	Mz Granite	3.19	1.20	1019	2.62	.004
631.6	Mz Granite	3.07	1.64	714	2.62	.004
636.0	Sy Granite	3.49	1.42	953	2.58	.002
640.4	Granite	2.99	1.37	727	2.62	.003
645.3	Granite	3.04	1.33	575	2.61	.004
649.6	Mz Granite	3.18			2.62	.004
653.9	Mz Granite	3.45			2.62	.004
658.6	Mz Granite	3.15	1.42	845	2.63	.005
663.5	Mz Granite	3.79	1.24	1174	2.61	.004
667.9	Granite	3.69	1.48	951	2.63	.005
672.1	Mz Granite	3.79	1.43	1009	2.62	.004
676.9	Granite	3.66	1.45	967	2.62	.005
681.5	Granite	4.11	.90	1738	2.63	.004
686.1	Mz Granite	3.46	1.57	833	2.64	.004
689.8	Mz Granite	3.66	1.58	880	2.63	.005
695.2	Granite	3.49	1.56	851	2.63	.005
699.3	Sy Granite	4.10	1.04	1496	2.63	.004
704.6	Mz Granite	3.72	1.04	1373	2.61	.005
708.2	Granite	3.42	1.01	1234	2.63	.004
712.9	Mz Granite	3.83	1.43	1020	2.62	.005
717.2	Granite	4.29	1.43	1438	2.62	.004
721.3	Mz Granite	3.52	1.35	991	2.63	.004
725.9	Mz Granite	3.56	1.47	922	2.62	.005
730.4	Mz Granite	3.64	1.56	893	2.62	.004
735.2	Mz Granite	3.70	1.18	1194	2.62	.004
739.5	Mz Granite	3.49	1.00	1329	2.63	.005
744.1	Mz Granite	3.55	1.39	930	2.60	.005
748.3	Mz Granite	2.95	1.27	853	2.63	.004
752.0	Granite	3.49	1.58	892	2.63	.006
757.4	Mz Granite	3.75	1.45	988	2.62	.005
761.7	Granite	3.70	1.22	1162	2.61	.006
766.0	Granite	3.74	1.30	951	2.62	.005
770.6	Mz Granite	3.55	1.14	1192	2.62	.005
774.7	Mz Granite	3.63	1.26	1100	2.62	.004
779.5	Granite	3.48	1.43	929	2.62	.005
783.9	Granite	3.74	1.28	1116	2.62	.005
788.0	Grndiorit	3.71	1.27	1116	2.62	.005
792.4	Mz Granite	3.55	1.28	1072	2.60	.006
796.6	Mz Granite	3.60	1.19	1155	2.62	.006
801.4	Mz Granite	3.63	1.16	1190	2.62	.006
805.4	Mz Granite	3.68	1.09	1285	2.62	.005
809.9	Mz Granite	3.42	1.66	788	2.62	.005
814.2	Mz Granite	3.22	1.03	1185	2.63	.002
818.9	Mz Granite	3.58	1.32	1035	2.63	.005
822.9	Mz Granite	3.77	1.30	1113	2.61	.004
827.4	Mz Granite	3.57	1.49	916	2.62	.005
831.4	Mz Granite	3.42	1.26	1036	2.63	.005
836.0	Mz Granite	3.68	1.35	1042	2.61	.005
840.2	Mz Granite	3.81	1.30	1108	2.64	.006
844.2	Gabbro	3.11	1.27	824	2.97	.004
848.7	Mz Granite	3.68	1.18	1192	2.61	.005
857.3	Tonalite	3.56	1.17	1162	2.62	.006
861.7	Mz Granite	3.88	1.23	1196	2.64	.005
865.9	Mz Granite	3.85	1.18	1252	2.63	.005
870.0	Mz Granite	3.59	1.29	1055	2.63	.005
874.4	Mz Granite	3.63	1.60	855	2.65	.003

Abbreviations for rock types

Amphibilt	-	amphibolite
Bi Qzamphb	-	biotite-quartz-amphibolite
Gabbro	-	gabbro
Granite	-	granite
Grndiorit	-	granodiorite
Mz Granite	-	monzogranite
Qdiorit	-	quartz diorite
Q Mz Diorit	-	Quartz monzodiorite
Qsyenit	-	quartz syenite
Sy Granite	-	syenogranite
Tonalite	-	tonalite

CHAPTER IV

GEOPHYSICAL PROPERTIES

7. MAGNETIC PROPERTIES

MAGNETIC PROPERTIES OF LAC DU BONNET (URL) BORECORES, MANITOBA

Latham, A.G.*, Morris, W.A.** and Lapointe, P.*
Geological Survey of Canada
1 Observatory Cr.
Ottawa, Ontario K1A 0Y3

*: Geomagnetic Laboratory, Geological Survey of Canada, 601 Booth St., Ottawa, Ontario K1A 0E8
**: Morris Magnetics, R.R. No. 2, Lucan, Ontario N0M 2J0

MAGNETIC PROPERTIES OF LAC DU BONNET (URL) BORECORES, MANITOBA

A.G. Latham, W.A. Morris and P. Lapointe
Geological Survey of Canada, 601 Booth St., Ottawa, Ontario K1A 0E8

INTRODUCTION

This paper covers the magnetic properties of URL granite drillcores. The main thrust of the interpretation lies in distinguishing between fresh, unaltered granite and altered granite often associated with fracture zones. A quantitative measure of the intensity of alteration and its spatial extent is seen as essential to the Canadian Nuclear Fuel Waste Management Program in that alteration zones have the potential to provide pathways for released radionuclides while at the same time acting as potential retardation zones.

Although the interpretation of a single magnetic property may not always be strictly unique (thus requiring the use of complementary data-logs) the severity of alteration is simply due to the chemical weathering of primary magnetite whose bulk magnetic susceptibility (BMS or X) is the property most easily measured. That is, when magnetite is oxidised and/or hydrated in a fracture zone, the BMS drops from a fairly uniform high level characteristic of the fresh granite, to levels that are markedly low and variable. The recognition of degrees of alteration is greatly aided by the use of BMS and fracture histograms, and by plotting log normal distributions of BMS against its cumulative frequency (Lapointe et al. 1986).

CONCEPTS

Magnetic susceptibility is the ease with which a rock becomes magnetized in a low magnetic field, and it is a function, in the first instance, of the concentration of large-grained (titano-)magnetite in the sample. Hematite, the common weathering product of magnetite (and of other ferromagnesian minerals) has a susceptibility which is about a factor of 1000 lower than magnetite (Telford et al. 1976). Consequently, the measurement of low susceptibility values from a borehole core distinguishes the low-temperature alteration zones from the fresh, unaltered rock.

It has also been found necessary to be able to recognise levels in susceptibility which are due to lithological units or zones other than the pristine granite, and which are either of primary or high-temperature secondary type. Examples are veins, pegmatite dykes, hydrothermal alteration zones, xenoliths and zones richer in mafic minerals.

Anisotropy of magnetic susceptibility (AMS) is commonly used to find the direction of the axes of susceptibility ellipsoids. These are then commonly interpreted in terms of (primary) flow, lineations and foliations in igneous bodies. AMS was found to be of only limited use at URL, and will not be discussed further. Similarly, although natural remanent magnetization was measured on surface samples, no stable remanence was recoverable (Morris, 1980; Lapointe et al. 1982). Consequently, it is only necessary to consider the induced magnetization (and not the remanent magnetization) in the interpretation of magnetic anomaly mapping of the batholith.

INSTRUMENTATION AND METHODOLOGY

Magnetic susceptibility of URL drillcores was measured using a Bison Susceptibility bridge (Lapointe et al. 1984), with measurements taken:

(1) 0.1 m apart at 2 m intervals for cores from boreholes URL 1 to 5,
(2) at regular 0.1 m intervals (except for small missing segments) on cores from boreholes URL-6 and URL-7 (Morris, 1983),
(3) on surface outcrops (in situ), and on shallow, 15 cm cores.

The magnetic susceptibility of the standard core samples has also been measured and their BMS values are listed in Table 1 in the Appendix.

DATA ANALYSIS AND PRESENTATION

As reported in Morris (1980), Chomyn (1982), Lapointe et al. (1982), Morris (1983), and Chomyn et al. (1985), BMS has been plotted against depth:

(a) as raw data,
(b) as box-car averages, plotted;
  (i) linearly, and
  (ii) to $\log_{10}$.
(c) as histograms.
(d) as plots of $\log_{10}$ versus cumulative frequency.

We have not standardised our presentation by using $\log_{10}$ (X) in histograms, cumulative frequency plots and depth plots. Plots of $\log_{10}$ (X) versus borehole depth have been plotted along with density and fracture frequency logs to produce 2-D and 3-D diagrams of alteration correlated with lithological, density and, particularly, fracture zones.

Demarcation of Susceptibility Levels

One of the problems in assigning susceptibility levels to particular alteration zones is in deciding how significant one level is from an adjacent one: that is, in deciding how many levels there are in the range. If we choose too many levels we may trivialise the significance of some of them, whereas if we choose too few, then the distinctive susceptibility of some zones may not be recognized. This difficulty is increased if the changes in susceptibility are gradational between the zones. The first approach to this problem was the subjective recognition of patterns in the core logs, augmented by use of histograms (e.g., Chomyn and Lapointe, 1984). This approach was only partly successful. The histogram of a lithologically homogeneous rock will show a unimodal distribution indicative of a single population. However, histograms of URL data (Morris, 1980) showed that there appeared to be more than two populations of BMS which were difficult to separate. In borehole URL-1, for example, five zones were recognized with some intervals showing mixtures of populations (Lapointe et al. 1984).

The method that has been adopted for separating these populations is to plot the cumulative frequency on a probability scale against magnetic susceptibility on a logarithmic scale. The rationale for this approach is twofold:

1) the log of susceptibility has "the best stabilizing effect on the variance" (Larsson, 1977), and
2) the cumulative curve for a single population following a log-normal probability distribution gives a straight line whose position depends on the mean susceptibility and the variance. Where more than one BMS population is present in a single set of data, it may therefore be possible to separate individual populations by identifying distinct straight line segments (Folk, 1980).

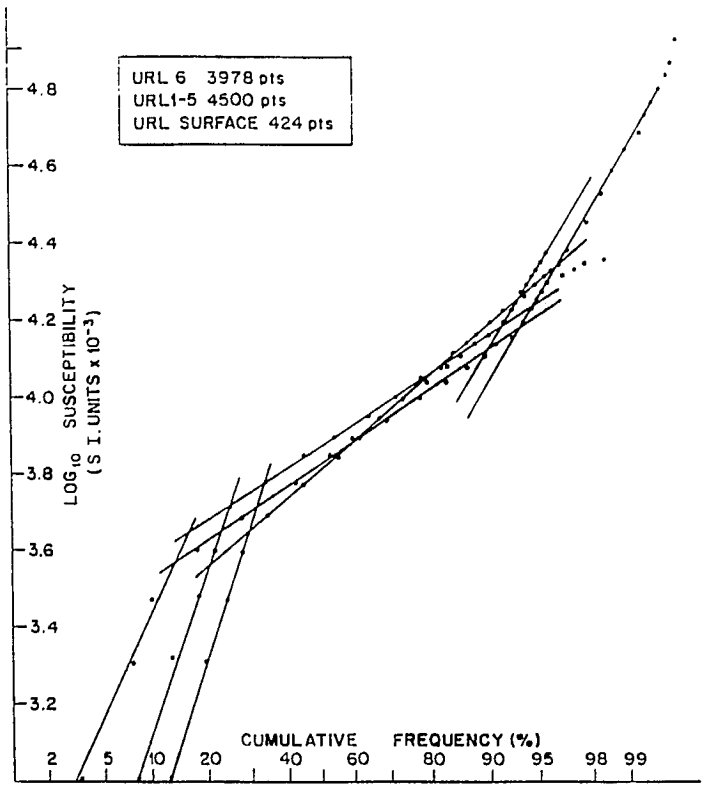

Figure 1. Log_{10} X versus cumulative frequency for URL boreholes 1-5, 6 and for surface data. X = BMS. The middle segments correspond to the fresh granite, the lower segments to the altered rock and the upper segments for the cores reflect the higher values of the mafic-rich xenolith zones.

RESULTS AND INTERPRETATION

Using the probability distribution as a means of delimiting the number and boundaries of the BMS populations (Morris, 1983), it was found that there were three distinct populations of BMS (Figure 1), and these three levels were recognisable in the combined logs of URL 1-5, in URL-6 and in the surface data (see the histogram plot, Figure 2, for comparison).

Using the boundary between the two lowest populations as the criterion for separating altered from unaltered granite gave a reasonably objective way of identifying alteration zones in the log. Figure 3 shows the URL-6 distribution (URL shaft emplacement). The fracture frequency and number of open fractures

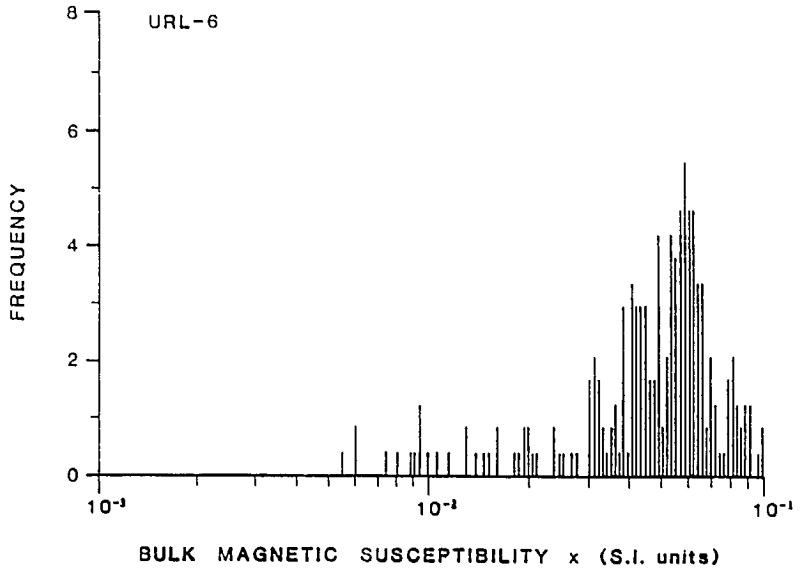

Figure 2. Frequency histogram of bulk magnetic susceptibility for URL-6 plotted on a logarithmic scale.

are also shown for comparison. Clearly there is a correlation between fracturing and the BMS values. For example, above 300 m there appears to be a one to one correlation between an increase in fracture frequency and a reduction in BMS. Furthermore, the 'texture' of the BMS values gives some indication of the type of associated fracturing: (1) narrow troughs in susceptibility at 100, 120, 230, and 270 m, each correspond to a zone of very localised high fracture frequency, and (2) broader BMS lows are associated with broad zones of uniform fracture frequency.

Below 300 m, although BMS values show at least four distinct troughs, the fracture log does not indicate the presence of any fractures in this section of the core. The troughs have been ascribed by Morris (1983) to the presence of xenoliths and xenolith-assimilation zones. It had been noted in earlier work on the core

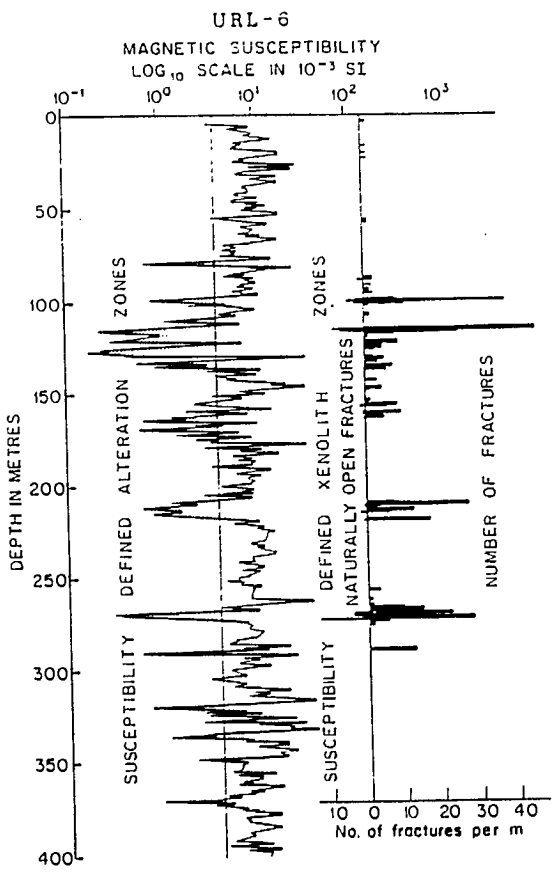

Figure 3. URL-6. Comparative logs of bulk magnetic susceptibility and fracture frequency. BMS levels (dashed lines) separate the fresh granite from the upper level xenolith-assimilation zones and the lower fracture-induced alteration zones. Note however that in the lower part of the core from 300 m downwards, low BMS corresponds to "shadow zoning" around xenoliths and not to fractures (see text). The fracture frequency data for this and subsequent diagrams is taken from Dugal and Kamineni, 1981.

(Lapointe et al. 1984) that anomalously high susceptibility levels were associated with xenoliths. The low BMS following the anomalous highs were attributed by Morris (1983) to scavenging effects of assimilation, which produced mafic-poor, susceptibility "shadow zones".

Hillary et al. (1985) used multivariate analysis on the BMS values of the Eye-Dashwa granite to determine which geological variables were the strongest factors in the BMS variations. They found that:

1) the change in BMS was most clearly correlated with alteration as judged by grades of colour from grey (fresh) to red (highly altered). This was expected since the weathering end-product of magnetite and of other ferromagnesian minerals is hematite which is red.

2) BMS was also positively correlated with the fracture frequency and the number of alteration fillings per fracture.

This, therefore, corroborates the qualitative interpretation of BMS for the URL site, and is probably applicable to other granite bodies within the Canadian Shield. It should be noted however that in the case of the URL site strict statistical analyses to correlate BMS with alteration, as determined by other methods (e.g., colour), fracture frequency, or other logs has not been done, and the expressions 'correlation' and 'significance' as used in this and other magnetic properties reports of the URL site (see references) denotes only a qualitative assessment of the susceptibility/alteration/fracture logs.

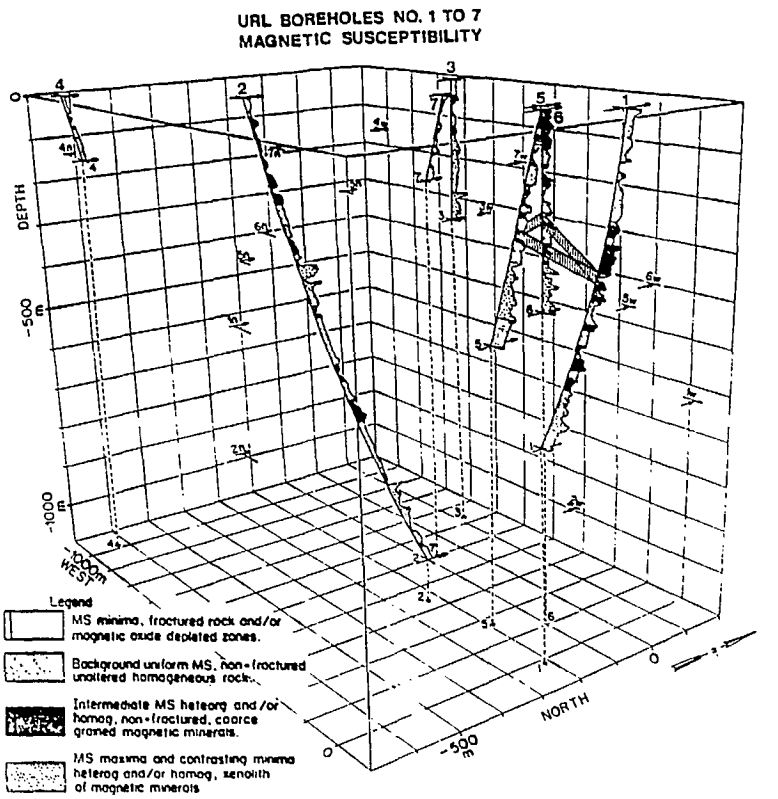

Figure 4. 3-D stereoplot of boreholes URL 1-7, and their alteration zonation (after Chomyn et al. 1985).

3-D Comparison of Logs

Figure 4 is a 3-D plot of the borehole susceptibility logs from the URL site (Chomyn et al. 1985). The BMS levels and zonations described below are after Chomyn (1982) and Chomyn et al. (1985) (Figure 5 and 6):

Depth 0-150 m: In all cores BMS minima generally correspond to fractured and/or altered rock; major fractures are common.

325-330 m in URL-1: BMS is low because of high alteration which is, in turn, due to a zone of high fracture frequency that includes open fractures.

255 and 265 m in URL-5, -6 (Figures 5 and 6): Susceptibility minima correspond to fracture frequencies from 2 up to 80 per metre.

330 m downwards: Broad susceptibility lows are associated with microfractures infilled with hematite and having a low opaque oxide content.

Elsewhere susceptibilities are high, reflecting fresh unaltered granite, or anomalously high, reflecting the presence of more mafic-rich zones and xenoliths.

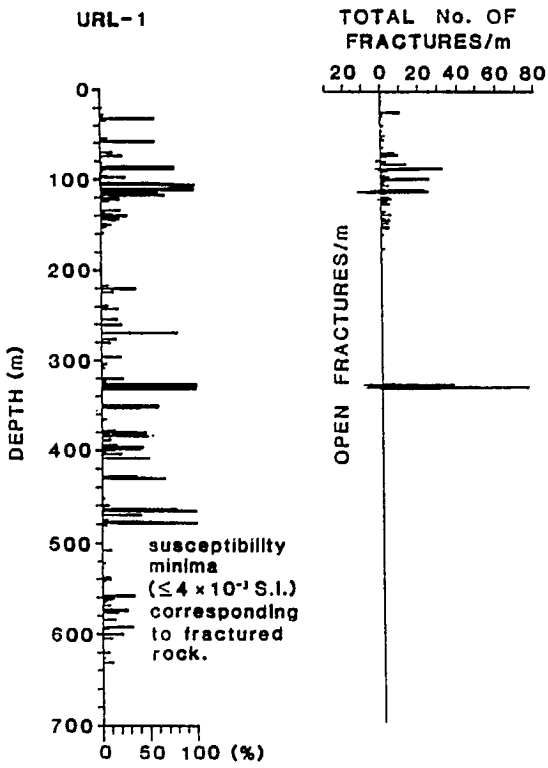

Figure 5. URL-1 log of BMS minima (2 m measurement interval) versus actual fracture log. The percentage scale is linear in which 100% coresponds to a minimum of 4.10^{-3} SI units.

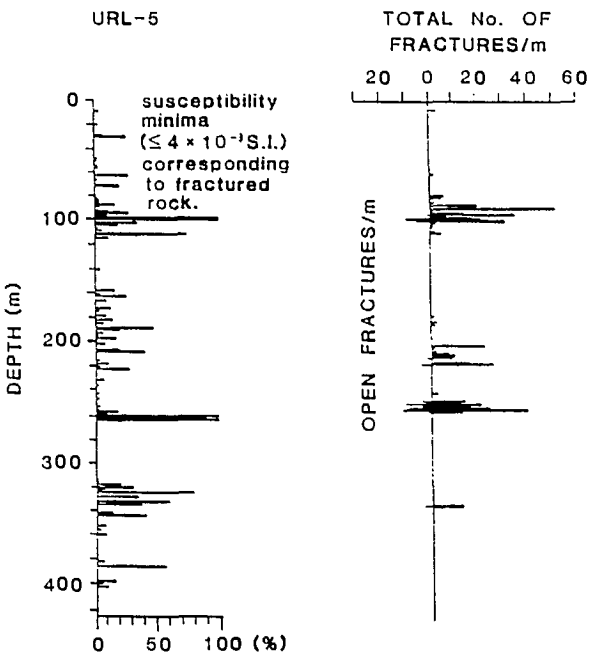

Figure 6. BMS minima (2 m measurement interval) versus actual fracture log. The percentage scale is linear in which 100% corresponds to a minimum of 4.10^{-3} SI units.

CONCLUSIONS

We conclude that:

1) Variations in the background bulk magnetic susceptibility (BMS) in the Lac du Bonnet granite are due primarily to the alteration of primary magnetite.

   Values of BMS above the characteristic level are shown to be due to mafic-rich zones associated with xenoliths.

2) There is a close visual correlation between low BMS and fracture frequency and fracture type, as seen best in URL-6. Sharp deep BMS lows are associated with zones of localised high fracture frequency and broad lows of BMS with broad zones of uniformly low fracture frequency.

3) Plots of log X versus cumulative frequency are of great value in showing the percentages of altered to unaltered granite within any given borehole. This, in turn, confirms that alteration is closely associated with fracture frequency.

4) Studies of BMS of drillcores can say little about the ages of fracturing – only that alteration to hematite is relatively late, and is of the low temperature type. Its value rather lies in indicating the extent of alteration around known fracture systems, for example around open cracks which presently act as water-carrying pathways.

5) The study of magnetic properties, especially of susceptibility, provides a proven tool for the evaluation of the homogeneity of a rock body and of (fracture-induced) rock alteration. The technique is rapid, non-destructive and inexpensive.

RECOMMENDATIONS

We stress the importance of the use of magnetic susceptibility on surface and drillcores, and on the URL galleries as a primary tool for the evaluation of rock quality and homogeneity prior to, or together with, geological and engineering mapping.

We stress the importance of the use of log X versus cumulative frequency plots; (a) section to section down the borehole, (b) borehole to borehole, and (c) granite to granite.

Such plots can obviously be applied in a variety of useful ways, in the above regard, and afford a direct measure of rock quality, of severity of alteration and of geographical extent of alteration. Other rock quality magnetic parameters are being developed presently, based on the weathering of magnetite to hematite (Chomyn et al. 1985).

It is recommended that statistical tests be carried out between fracture/fracture frequency and alteration as characterized by low BMS values. It would be preferable if expressions such as 'correlation, significance', etc. be assigned their strict statistical sense.

REFERENCES

Chomyn, B.A. 1982. A preliminary report of the magnetic susceptibility, fracture and lithological data for cores URL 1, 2, 3, 4, and 5. Internal Report, Earth Physics Branch. RW/RKP 089-82. EPB, 20 p.

Chomyn, B.A. and Lapointe, P. 1984. Magnetic susceptibility and lithological variation within the Lac du Bonnet batholith, Manitoba, Canada. In Process Mineralogy III, ed. W. Petruk, pubd. Society of Mining Engineers of the American Institute of Mining, Metallurgical and Petroleum Engineers, New York, p. 99-116.

Chomyn, B.A., Morris, W.A., Lapointe, P., and Coles, R.L. 1985. Application of magnetic susceptibility to assessing the degree of alteration of crystalline rock. The Geoscience Program – Proceedings of the Seventeenth Information Meeting of the Nuclear Fuel Waste Management Program. AECL Technical Report, TR-299, p. 609-621.

Day, R. 1977. TRM and its variation with grain size: A review. Advances in Earth and Planetary Sciences, v. 1, p. 1-33.

Dugal, J.B. and Kamineni, D.C. 1981. Fracture and lithological logs of URL boreholes, Lac du Bonnet batholith. Atomic Energy of Canada Limited, Unpublished Report. Chart Number NP-05-023.

Folk, R.L. 1980. Petrology of Sedimentary rocks. Hemphill's Pub. Inc. Texas, 175 p.

Hillary, E.M., McEwen, J.H., and Rey, N.A.C. 1985. The evaluation of fracture zones at the Atikokan drill site and their geophysical significance. The Geoscience Program – Proceedings of the Seventeenth Information Meeting of the Nuclear Fuel Waste Management Program. AECL Technical Report, TR-299, p. 609-621.

Lapointe, P., Chomyn, B.A., Morris, W.A., and Coles, R.L. 1982. Significance of magnetic susceptibility measurements from the Lac du Bonnet batholith, Manitoba, Canada. 1982 OECD workshop. RW/GPH 180U-82, 22 p.

Lapointe, P., Chomyn, B.A., Morris, W.A., and Coles, R.L. 1984. Significance of magnetic susceptibility measurements from the Lac du Bonnet batholith, Manitoba, Canada. Geoexploration, v. 22, p. 217-229.

Lapointe, P., Morris, W.A., and Harding, K.L. 1986. Interpretation of magnetic susceptibility; a new approach to the geophysical evaluation of the degree of rock alteration. Canadian Journal of Earth Sciences (in press).

Larsson, L.O. 1977. Statistical treatment of in situ measurements of magnetic susceptibility. Sveriges Geologiska Underskning, v. 71, p. 3-22.

Morris, W.A. 1980. Magnetic properties project, Lac du Bonnet (URL) study area, Final Report, 1980. RW/GPH-81-090, 32 p.

Morris, W.A. 1983. Bulk susceptibility logging of borecore URL-6. Earth Physics Branch Internal Report, 83-1, 19 p.

Telford, W.M., Geldart, L.P., Sheriff, R.E., and Keys, D.A. 1976. Magnetic susceptibilities of various minerals, table 3, in Applied Geophysics, Cambridge University Press, p. 860.

APPENDIX

Table 1. Bulk magnetic susceptibility (BMS) values for standard core samples from boreholes URL-1, -2, -5 and WN-1, -2, -4.

Sample		BMS ($\times 10^{-2}$)
URL-1	- 46	5.51
	- 68	5.77
	-100	6.71
	-131	4.91
	-177	5.56
	-230	8.16
	-254	6.14
	-302	6.16
	-357	7.06
	-397	4.15
	-433	5.07
	-496	7.16
	-527	6.25
	-592	7.76
	-615	11.58
	-662	5.98
URL-2	-256	6.92
	-448	7.35
	-586	5.35
	-705	4.83
	-798	5.37
	-871	3.66
	-1001	2.08
	-1095	-
URL-5	-16.5	6.55
	- 77	4.57
	-108	1.83
	-126	5.81
	-156	5.40
	-199	4.69
	-246	5.62
	-279	-
	-289	6.50
	-333	5.19
	-370	7.90
	-451	9.14
	-497	-

Table 1 (cont'd.)

Sample		BMS ($\times 10^{-2}$)
WN-2	- 24	-
	- 55	0.32
	- 85	0.52
	- 98	5.34
	-124	1.81
	-145	4.73
WN-4	-408	0.58
	-468	5.68
	-482	3.89
	-505	2.16
	-551	4.27
	-564	4.66
	-603	3.98
	-631	4.78
	-659	4.67
	-692	4.36
	-719	4.78
	-746	6.83
	-789	7.46
	-809	8.42
	-840	7.47
	-863	5.65
	-906	7.35
	-928	-

8. ELECTRICAL PROPERTIES

ELECTRICAL PROPERTIES OF GRANITIC ROCKS OF THE LAC DU BONNET BATHOLITH

T.J. Katsube* and J.P. Hume**
Geological Survey of Canada
601 Booth St.
Ottawa, Ontario K1A 0E8

*: Geological Survey of Canada, 601 Booth St., Ottawa, Ontario K1A 0E8
**: Atomic Energy of Canada Limited (attached to Geological Survey of Canada, Ottawa)

ELECTRICAL PROPERTIES OF GRANITIC ROCKS OF THE LAC DU BONNET BATHOLITH

T.J. Katsube and J.P. Hume
Geological Survey of Canada, 601 Booth St., Ottawa, Ontario K1A 0E8

INTRODUCTION

It is necessary to know the distribution of petrophysical, thermal and mechanical properties in a pluton because they are related to the potential radionuclide release pathways and the stability of the rock mass that would host the vault. Geophysical methods, such as electrical resistivity methods (electrical logging and surface electrical method) and subsurface radar are some of the techniques that have the potential to provide such information. However, successfully interpreting the data obtained by such techniques depends upon the available knowledge relating the geophysical parameters to physical properties. There exists a theoretical relationship between resistivity and formation factor (Katsube and Hume, this volume) and, in turn, an emperical relationship exists between formation factor and porosity and permeability. It is well known that electromagnetic (EM) waves are reflected by discontinuities in crystalline rocks and that the propagation of EM waves are influenced by its dielectric constraint of the rock. This paper provides basic data on resistivity, surface resistivity and dielectric constant of samples from the WN and URL sites in the WNRE research area, and information on the distribution of electrical resistivity in relation to rock type in this pluton.

BACKGROUND THEORY

Rocks consist mainly of mineral crystal grains that are electrical insulators, whose resistivity is in the order of 10^8-10^{14} ohm-metres. However, the actual resistivities of rocks measured in-situ or under most conditions in the laboratory are in the order of 10^3-10^5 ohm-metres for the plutonic rocks from our research areas (Katsube and Hume, in press, a,b). The reason for these rocks showing considerably lower resistivities than the constituting mineral grains is due to the fluid in the pores, which has a much lower resistivity, of the order of 10-100 ohm m. This implies that the electrical resistivity of a rock reflects the

continuity of the pores or microfractures in a rock. This is a characteristic similar to that of permeability (Katsube and Hume, this volume).

The bulk resistivity of a rock (ρ_R) is normally considered to be a function of formation factor (F) and pore water resistivity (ρ_W):

$$\rho_R = F \rho_W \quad (1)$$

The formation factor is a function of the pore structure (Katsube and Hume, this volume) and the pore water resistivity is a function of the chemical properties of the pore water in the rock. Pore water resistivity is far more sensitive to changes of chemical conditions, temperature and age of pore water compared to the formation factor. This is the reason that the formation factor is used rather than rock resistivity when studying pore structure.

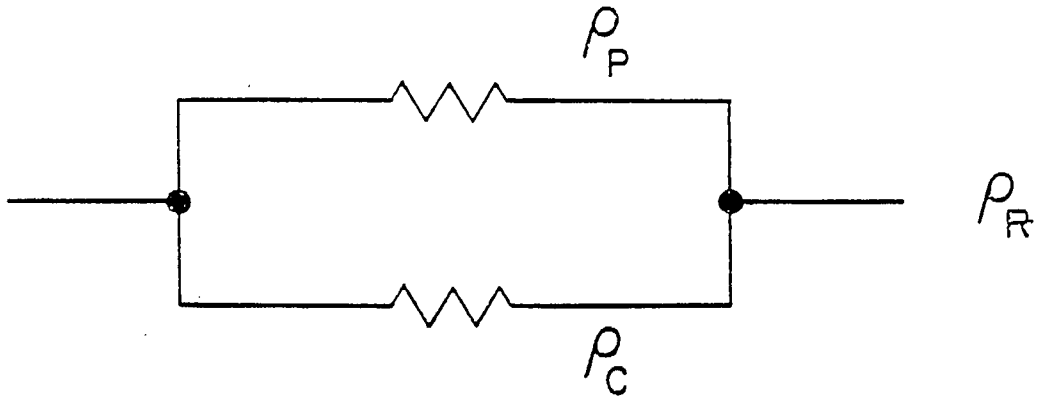

Figure 1. Equivalent circuit of the path for flow of electrical current through water saturated pores in crystalline rocks.
ρ_R = bulk rock resistivity, ρ_P = pore resistivity, ρ_C = bulk surface resistivity (after Katsube and Hume, in press-b).

Although equation (1) provides the basic concept of resistivity of rocks, there is a pore surface effect that distorts the simple relationship between the three parameters. As a number of authors (e.g., Patnode and Wyllie, 1950; de Witte, 1950; Howell, 1953) have indicated, equation (1) is often not satisfied. The effect of pore surface resistivity is to lower the bulk rock resistivity and, therefore, give an apparent formation factor which is lower than the true formation factor of a sample. Therefore, this surface resistivity enters into this model as a component parallel to $F\ \rho_W$ in equation 1 (see Figure 1). Thus, the actual equation for the resistivity of rocks is as follows:

$$\frac{1}{\rho_R} = \frac{1}{\rho_C} + \frac{1}{F\ \rho_W} \qquad (2)$$

where ρ_C is the bulk surface resistivity (Katsube and Hume, this volume). Methods for determining all four of these parameters have been discussed in Katsube and Hume (this volume) and this method has been used in our measurements.

The resistivity discussed up to this point is mainly related to the in-phase component of the electrical impedance of the rocks and applies to frequencies generally below 0.1-1.0 MHz. At frequencies higher than this, the dielectric effect becomes dominant (Katsube, 1977) and the out-of-phase component of the electrical impedance takes over. The dielectric constant (K_D) is an important characteristic of rocks at these frequencies.

The resistivity is not a very reliable parameter to represent any physical characteristics of a rock due to its dependence on the chemical properties and temperature of the pore fluids, and because the surface resistivity effects cannot be eliminated. However, electrical methods are the only geophysical techniques that respond to continuity of fractures and pores in rocks, and to hydraulically permeable conditions. Therefore, an effort must be made to relate the pore structure, or physical, characteristics of the rocks to their electrical characteristics. For example, certain relationships may be developed between the two characteristics at a specific site if it can be assumed that the pore fluid resistivity, surface resistivity and pore fluid temperature are constant.

The dielectric constant measured at 10^8 Hz is considered to be one of the parameters that characterizes the dielectric phenomena in the mineral crystals of

the rock specimen (Katsube, 1977). The dielectric constant increases with decreasing frequency mainly due to electrochemical effects of adsorbed water in wet or room dry conditions. At frequencies above 10^6-10^7 Hz and 10^9 Hz the dielectric constant (K_D) is generally independent of frequency.

GENERAL TRENDS IN ELECTRICAL PROPERTIES

Parkhomenko (1967) presented resistivity values for granites in the USSR. The resistivity value for granite from Azerbaidjan is 3.0×10^5 ohm-m. Bebro (1984) also presented resistivity data for granites. The minimum and maximum values for water saturated samples were 1.6×10^2 and 3.6×10^6 ohm-m, respectively. Olhoeft (1981) presented resistivities measured using a direct current for a number of granites from different locations in the United States. The resistivity of an aplite granite from Boulder, Colorado was 4.35×10^{11} ohm-metres. The resistivities of biotite granites ranged from 2.70×10^{10} to 8.33×10^{10} ohm-metres. The values reported for Westerly granites ranged from 3.3×10^{10} to 2.0×10^{11} ohm-metres. Resistivities of granites ranged from 3.03×10^{10} to 4.35×10^{10} ohm-metres, respectively. However, these results by Olhoeft (1981) are thought to be for dry granite samples.

Clark (1966) reported dielectric constants (measured at radio frequencies) for a number of igneous rocks. The dielectric constants of 7 dry granite samples ranged from 4.80-18.9. Repheline syenite (6 samples) gave values ranging from 6.93 to 12.7. Two diabase samples gave dielectric constants of 18.1 and 34.5.

The values of pore water resistivity obtained by other researchers are presented in Table 3. Keller and Frischknecht (1966) reported pore water resistivity values for saturated samples from various parts of the world. Pore water resistivities for igneous rocks from Europe and South Africa are 7.6 and 11.0 ohm-m, respectively. The values for metamorphic rocks from South Africa and the Australian Precambrian are 7.6 and 3.6 ohm-m, respectively.

LABORATORY METHODS OF INVESTIGATION

The resistivities of granites from the WN and URL sites were obtained using the sample impedance measuring system described by Gauvreau and Katsube (1975). The practical details of the measuring technique are described in Katsube (1981) and Katsube and Hume (this volume) and will not be repeated here.

The dielectric constant (K_D) of the sample were determined by measuring the capacitance of an oven dried specimen at 10^8 Hz using a Hewlett Packard Model 190A Q-meter:

$$K_D = \frac{C_D}{k\varepsilon_o}$$

C_D = Capicitance of the specimen

k = Geometric factor of specimen

ε_o = Permittivity of air or vacuum

Sample dimensions are measured using a Fisher Scientific micrometer caliper (0.25 mm, reads to 0.01 mm). Weights are measured using a Mettler microblance (H10TW). The technique used to obtain surface and pore-water resistivities was described in Katsube and Hume (this volume) and will not be dealt with here.

Table 1. Resistivities of Granite Samples

Rock	# of Samples	Min.	Max.	Mean	Reference
WN-1	10	1.37×10^4	8.98×10^4	4.42×10^4	Katsube et al. (1985)
WN-2	6	3.84×10^4	6.32×10^4	5.05×10^4	Katsube et al. (1985)
WN-4	18	0.063×10^4	6.83×10^4	3.71×10^4	Katsube et al. (1985)
All WN	34	0.063×10^4	8.98×10^4	4.16×10^4	Katsube et al. (1985)
URL-1	14	0.911×10^4	2.35×10^4	1.54×10^4	Katsube et al. (1985)
URL-2	8	1.57×10^4	2.27×10^4	1.99×10^4	Katsube et al. (1985)
URL-5	12	0.504×10^4	6.14×10^4	3.06×10^4	Katsube et al. (1985)
URL-7	31	1.62×10^4	4.80×10^4	2.80×10^4	Katsube et al. (1985)
All URL	65	0.504×10^4	6.14×10^4	2.48×10^4	Katsube et al. (1985)
Granite, Azerbaidjan	-	-	-	3.0×10^5	Parkhomenko, (1967)
Granites	-	1.6×10^2	3.6×10^6	-	Bebro, (1984)
Aplite Granite (Boulder, Colorado)	-	-	-	4.35×10^{11}	Olhoeft, (1981)
Biotite Granite	-	-	-	8.33×10^{10}	Olhoeft, (1981)
Granite	-	-	-	3.03×10^{10}	Olhoeft, (1981)
Rhodonite-Wollastonite-Garnet Skarn	-	-	-	1.4×10^4	Rzhevsky & Novik, (1971)
Quartz-porphyry	-	-	-	2.5×10^4	Rzhevsky & Novik, (1971)
Syenite	-	-	-	7.1×10^4	Rzhevsky & Novik, (1971)
Tremolite-Wollastonite Skarn	-	-	-	1.54×10^2	Rzhevsky & Novik, (1971)

RESULTS OF LABORATORY MEASUREMENTS

The three resistivities (bulk rock resistivity, bulk surface resistivity and pore water resistivity) of standard core samples from the WN and URL sites are listed in Table 6 in the appendix. The three resistivities are summarized in Tables 1, 2 and 3. Values obtained by other investigators are also included in these tables for the purpose of comparison. Core samples from URL-1, -2, and -5 were also divided into high-, intermediate- and low-resistivity groups based on observations made by von Sacken and Katsube (in prep.). The minimum, maximum and mean resistivities are presented in Table 4.

The dielectric constant has been measured (Wadden, 1979) for three specimens (3-directions) from each of the 16 samples from boreholes WN-1 and WN-2 (total of 48 specimens). The values are presented in Table 5. The precision of the measurements is good with the largest range being about ±2%. The range in precision for WN-2 samples is poorer with the largest being about ±6%.

ELECTRICAL RESISTIVITY DISTRIBUTION

Focused-electrode logs have been run in more than 20 boreholes at the Whiteshell Research area. This method measures the electrical resistivity of the rock surrounding the boreholes. As suggested by Katsube and Hume (1987), it is probably the method which gives the most reliable in-situ resistivity values for these rocks. The depth of measurement in these boreholes ranges from about 50 m to over 1000 m.

The background resistivity values seen in these logs generally falls within three different ranges, which allows the rocks to be categorized as either high-, intermediate-, or low-resistivity zones. According to von Sacken and Katsube (in prep.), the high resistivity zone generally covers the depth range of 0 m to 200-300 m, shows a resistivity range of 2×10^4-2.5×10^5 ohm-m and corresponds to the pink granite (Figure 2). According to the same authors, the low resistivity zone generally starts at depths ranging from about 100-400 m and continues on to depths below the depth of the boreholes. The resistivities of this zone are approximately 4×10^3 ohm-m and correspond to zones of gray granite. The intermediate resistivity zones are transitional zones between the high and low resistivity zones. They generally extend from 50-250 m and show resistivities

Table 2. Bulk Surface Resistivity Values of Rock Samples

Rock	# of Samples	Min.	Max.	Mean (Arithmetic)	Reference
Granite, WN-1	10	0.75×10^4	5.82×10^4	2.68×10^4	Katsube et al. (1985)
Granite, WN-2	6	1.91×10^4	6.31×10^4	3.52×10^4	Katsube et al. (1985)
Granite, WN-4	18	0.53×10^4	7.47×10^4	1.92×10^4	Katsube et al. (1985)
All WN	34	0.53×10^4	7.47×10^4	2.43×10^4	Katsube et al. (1985)
Granite, URL-1	14	0.34×10^4	1.32×10^4	0.76×10^4	Katsube et al. (1985)
Granite, URL-2	8	-	-	-	-
Granite, URL-5	12	0.36×10^4	2.41×10^4	1.27×10^4	Katsube et al. (1985)
Granite, URL-7	31	0.80×10^4	3.79×10^4	1.99×10^4	Katsube et al. (1985)
All URL	57	0.34×10^4	3.79×10^4	1.54×10^4	Katsube et al. (1985)
Granite, CR6	10	0.03×10^4	61×10^4	16.5×10^4	Katsube & Hume (in press)
Granite, CR7	4	1.1×10^4	1.2×10^5	4×10^4	Katsube et al. (1985)
Granite, CR8	11	1.1×10^4	11.1×10^4	4.12×10^4	Katsube et al. (1985)
Granite, CR9	15	0.3×10^4	1.8×10^4	0.29×10^4	Katsube et al. (1985)
Overall CR	40	0.03×10^4	6.1×10^4	6.8×10^4	Katsube et al. (1985)

Table 3. Pore Water Resistivities of Rock Samples

Rock	# of Samples	Min.	Max.	Mean (Arithmetic)	Reference
Granite, WN-1	10	6.40	41.38	19.08	Katsube et al. (1985)
Granite, WN-2	6	2.43	12.83	9.09	Katsube et al. (1985)
Granite, WN-4	18	0.212	45.7	19.05	Katsube et al. (1985)
All WN	34	0.212	45.7	17.29	
Granite, URL-1	14	3.47	27.2	14.27	Katsube et al. (1985)
Granite, URL-2	8	27.6	50.6	38.3	Katsube et al. (1985)
Granite, URL-5	12	9.37	43.8	20.03	Katsube et al. (1985)
Granite, URL-7	31	1.92	24.7	9.19	Katsube et al. (1985)
All URL	65	1.92	50.6	15.87	
Igneous Rocks, Europe	314	-	-	7.67	Keller and Frischknecht, 1966
Igneous Rocks, South Africa	175	-	-	11.0	Keller and Frischknecht, 1966
Metamorphic Rocks, South Africa	88	-	-	7.6	Keller and Frischknecht, 1966
Metamorphic Rocks, Australian Pre-Cambrian	31	-	-	3.6	Keller and Frischknecht, 1966

varying between 8×10^3 ohm-m and 2×10^4 ohm-meters. The rock type in the zone varies between grayish-pink, gray-pink and a greenish-gray.

Most boreholes start with a high resistivity zone in the upper part, and continue on to the transitional and low resistivity zones. However, there are some boreholes, such as WN-4 (length of 1000 m), which show resistivities in the high resistivity range and do not show any signs of intermediate- or low resistivity zones.

The low resistivity anomalies have been studied by Katsube and Hume (1987) and Radburn and Katsube (in prep.). The low resistivities range between 10 ohm-m to 10^3 ohm-m. Katsube and Hume (1987) have proposed a method for determining the transmissivity in boreholes using the focused-electrode log and density log. Radburn and Katsube (in prep.) use this method and others to identify fractured zones and to determine the transmissivity, porosity and storativity of these zones.

Table 4. Resistivities of URL-1, -2 and -5 Laboratory Samples according to the zones defined by von Sacken and Katsube

Rock	# of Sample	Min.	Max.	Mean (Arithmetic)
URL-1:				
High Resistivity Zone	6	1.33×10^4	3.44×10^4	1.97×10^4
Intermediate Resistivity Zone	6	1.22×10^4	1.86×10^4	1.42×10^4
Low Resistivity Zone	3	9.11×10^3	1.92×10^4	1.25×10^4
URL-2:				
High Resistivity Zone	-	-	-	-
Intermediate Resistivity Zone	1	2.25×10^4	2.25×10^4	2.25×10^4
Low Resistivity Zone	7	1.57×10^4	2.27×10^4	1.95×10^4
URL-5:				
High Resistivity Zone	7	2.18×10^4	6.14×10^4	3.91×10^4
Intermediate Resistivity Zone	3	2.38×10^4	3.06×10^4	2.70×10^4
Low Resistivity Zone	2	5.04×10^3	7.57×10^3	6.31×10^3

Table 5. WN-1 and WN-2 dielectric constant measurements

Sample	K
WN-1-138.15 A	5.95 ± .10
WN-1-138.15 B	5.95 ± .12
WN-1-138.15 C	5.50 ± .03
WN-1-160.45 A	5.28 ± .08
WN-1-160.45 B	4.51 ± .02
WN-1-160.45 C	4.82 ± .09
WN-1-224.05 A	4.14 ± .05
WN-1-224.05 B	5.40 ± .06
WN-1-224.05 C	5.75 ± .00
WN-1-246.00 A	4.66 ± .04
WN-1-246.00 B	4.98 ± .06
WN-1-246.00 C	5.58 ± .03
WN-1-294.05 A	4.87 ± .03
WN-1-294.05 B	5.89 ± .08
WN-1-294.05 C	5.60 ± .03
WN-1-303.15 A	5.29 ± .07
WN-1-303.15 B	4.29 ± .09
WN-1-303.15 C	4.29 ± .09
WN-1-345.05 A	5.51 ± .10
WN-1-345.05 B	5.42 ± .09
WN-1-345.05 C	4.94 ± .05
WN-1-384.35 A	5.15 ± .15
WN-1-384.35 B	5.47 ± .10
WN-1-384.35 C	4.90 ± .08
WN-1-410.20 A	4.86 ± .11
WN-1-410.20 B	4.63 ± .03
WN-1-410.20 C	5.10 ± .04
WN-1-460.25 A	4.79 ± .07
WN-1-460.25 B	5.59 ± .07
WN-1-460.25 C	5.01 ± .09
Standard	3.68 ± .02

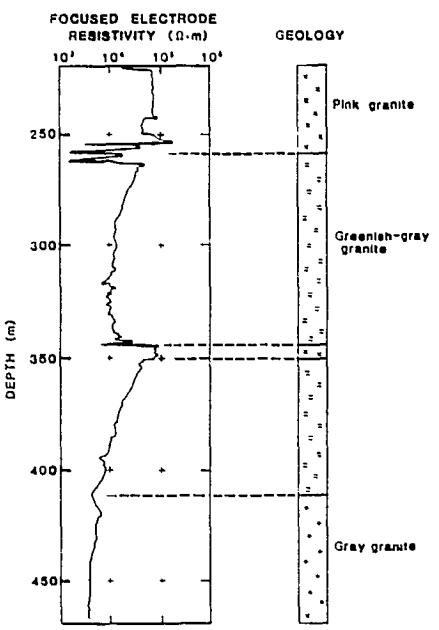

Figure 2. Typical example of focused-electrode resistivity distribution down a borehole (URL-5).

DISCUSSION AND CONCLUSIONS

The ranges of bulk rock resistivities (ρ_R) for the core samples from the Lac du Bonnet batholith are generally within the same range as those reported by others for water saturated crystalline rocks. The dielectric constant for the Lac du Bonnet core samples are in the lower range of those in the literature. In general, bulk surface resistivities are in the lower range of values reported for the crystalline rocks from Chalk River, Ontario (Katsube and Hume, in press). The pore water resistivities of the Lac du Bonnet samples are, generally, slightly higher than those reported in the literature, but are similar to the fluid resistivities (Katsube and Hume, 1987) measured in the boreholes from which these samples have been taken.

Based on the resistivities from the focused electrode log data, three zones with different resistivity ranges corresponding to different lithologies have been identified. The first zone is the high resistivity zone with resistivities in the order of 2×10^4 to 2.5×10^5 ohm-m, which corresponds to the pink granite. The depth range starts at the surface and extends to 100-400 m. The second zone is the intermediate resistivity zone with resistivities in the order of 8×10^3 to 2×10^4 ohm-m, which corresponds to grayish-pink, gray-pink to greenish-gray granites. The intermediate zone lies under the high resistivity zone and has a thickness of about 50-250 m. The third zone is the low resistivity zone with resistivities in the order of 4×10^3 ohm-m, which corresponds to the gray granite. The low resistivity zone lies under the intermediate resistivity zone.

Katsube and Hume (1987) have indicated that the in-situ formation factor values are generally about 2.5 times lower than the laboratory values for the granites in this area. This is also the case for the resistivities in the low resistivity zones which correspond to the gray granitic zone. This is thought to be mainly due to the surface resistivity effects that have not been eliminated from the in-situ rocks and to the increase in salinity at depth in the borehole fluid. In the high and intermediate resistivity zones which correspond to the pink, and greyish-pink, gray-pink and greenish-gray granites, the in-situ resistivities are, in general, either similar to or much higher than the laboratory resistivities. This is probably due to the fluid resistivity generally being high at the upper portion of the boreholes and to the stress-release effects in the laboratory samples. The stress release effects

will cause the apertures and fracture frequency of the laboratory samples to increase (Katsube and Hume, in press) and, thus, reduce the resistivities of the laboratory samples to levels below the resistivities of in-situ rocks.

Laboratory values of resistivity, surface resistivity, pore water resistivity and dielectric constant obtained for these rocks adds to the knowledge of the electrical properties of granites and aid in the interpretation of geophysical data. The observation of three fairly distinct resistivity zones will help determine the physical property distribution throughout the pluton.

REFERENCES

Beblo, M. 1982. Electrical properties. In: Landolt-Bornstein Numerical Data and Functional Relationships in Science and Technology, Physical Properties of Rocks, v. 1, Subvolume b, G. Angenheister, New York, p. 239-307.

de Witte, L. 1950. Relations between resistivities and fluid contents of porous rocks. Oil and Gas Journal, v. 49(16), p. 120-132.

Hallenburg, James K. 1984. Geophysical Logging for Mineral and Engineering Applications. Penwell Publishing Company, Tulsa, 254 p.

Howell, B.F. 1953. Electrical conduction in fluid-saturated rocks, Part 1. World Oil, p. 113-116.

Katsube, T.J. 1977. Electrical properties of rocks. Proc. Induced Polarization for Exploration Geologists and Geophysicists. Univ. of Arizona, March 14-16, 44 p.

Katsube, T.J. 1981. Pore structure and pore parameters that control the radionuclide transport in crystalline rocks. Proc. Tech. Prog., International Powder and Bulk Solids Handling and Processing, Rosemont, Ill., May 12-14, p. 394-409.

Katsube, T.J. and Hume, J.P. (1987). Permeability determination in crystalline rocks by standard geophysical logs. Geophysics, v. 52, p. 342-352.

Katsube, T.J. and Hume, J.P. (in press). Electrical resistivities of rocks from Chalk River. Submitted for publication as an Atomic Energy of Canada Limited Report.

Katsube, T.J. and Hume, J.P. (this volume). Pore structure characteristics of granitic rock samples from the Whiteshell Research Area.

Keller, G.V. 1966. Electrical properties of rocks and minerals. In: Handbook of Physical Constants, Geological Society of America Memoir 97, S.P. Clark, New York, p. 553-577.

Keller, G.V. and Frischknecht, F.C. 1966. Electrical Methods in Geophysical Prospecting. Pergamon Press, New York, 517 p.

Olhoeft, G.R. 1981. Electrical properties of rocks. In: Physical Properties of Rocks and Minerals, v. II-2, Y.S. Touloukian, W.R. Judd and R.F. Roy, New York, p. 257-329.

Patnode, H.W. and Wyllie, M.R.J. 1950. The presence of conductive solids in reservoir rocks as a factor in electric log interpretation. Transactions of the American Institute of Mining, Metallurgical and Petroleum Engineers, v. 189, p. 47-52.

Parkhomenko, E.I. 1967. Electrical Properties of Rocks. Plenum, New York, N.Y., 314 pp.

Radburn, L.K. and Katsube, T.J. Hydrogeological characteristics of granitic rocks determined from standard geophysical logs. (In preparation).

Rzhevsky, V. and Novik, G. 1971. The physics of rocks. MIA Publishers, 320 p.

von Sacken, R.S. and Katsube, T.J. Relationship between focused-electrode resistivity and the geology: Lac du Bonnet Batholith, Manitoba. (In preparation).

Wadden, M.M. 1979. Dielectric constant measurements for WN-1 and WN-2 samples. Electric-Seismic Rock Property Laboratory Technical Data 7879-07, 13 p.

APPENDIX

Table 6. Bulk rock resistivities (ρ_R), Bulk Surface Resistivities (ρ_C) and Pore Water Resistivities (ρ_W) of individual standard samples from WNRE and URL

Sample No.	ρ_R (x 10^4)	ρ_C (x 10^4)	ρ_W
WN-1 - 138.4	4.10	1.39	13.62
- 160.7	2.13	2.24	6.44
- 223.7	3.53	4.93	8.10
- 245.8	1.37	1.84	6.40
- 294.3	8.98	2.24	41.38
- 303.3	1.68	5.82	9.18
- 345.3	2.73	2.73	13.13
- 384.6	7.25	2.29	31.52
- 410.5	8.37	2.39	36.87
- 466.4	4.03	0.754	24.13
WN-2 - 24.55	6.32	3.53	12.06
- 55.25	3.84	4.85	2.34
- 85.10	4.53	6.31	4.31
- 98.30	5.39	2.52	10.74
- 124.50	5.30	1.98	12.83
- 145.65	4.92	1.91	12.30
WN-4 - 408.80	4.65	1.01	17.4
- 468.85	3.53	1.56	10.7
- 482.20	6.83	1.68	21.1
- 505.37	2.16	0.781	4.92
- 551.05	4.85	0.892	17.8
- 564.20	5.15	2.50	19.6
- 603.70	0.108	1.21	0.301
- 631.30	5.84	1.85	38.4
- 659.90	3.92	3.88	21.5
- 692.50	0.063	0.535	0.212
- 719.40	5.64	7.47	36.5
- 746.80	1.98	1.15	11.1
- 789.50	3.10	0.548	14.7
- 809.30	6.44	5.42	45.7
- 840.80	4.31	1.34	34.9
- 863.50	0.176	0.530	1.20
- 906.40	5.04	1.32	27.5
- 928.20	3.07	0.864	19.3
URL-1- 46.25	1.38	0.595	1.57
- 68.35	3.44	2.35	4.29
- 100.50	2.35	1.13	3.47
- 131.2	1.33	0.836	4.72
- 177.0	1.51	0.992	6.43
- 230.4	1.80	1.32	8.80
- 254.2	1.25	0.418	9.63
- 302.3	1.26	0.976	8.57
- 357.1	1.22	0.775	15.5
- 397.7	1.44	0.745	10.9
- 443.1	1.86	0.628	30.7
- 496.6	1.47	0.655	22.7
- 527.3	1.92	0.802	26.8
- 592.5	0.911	0.341	11.7
- 615.8	2.25	0.714	27.2
- 662.3	0.921	0.356	12.6

Table 6:- continued

Sample No.	ρ_R (x 10^4)	ρ_C (x 10^4)	ρ_W
URL-2- 256.2	2.25	-	27.6
- 448.2	2.27	-	35.7
- 586.1	1.57	-	31.4
- 705.8	2.23	-	38.5
- 798.8	2.09	-	36.1
- 871.8	1.96	-	44.6
- 1001.3	1.60	-	42.0
- 1095.0	1.91	-	50.6
URL-5- 16.5	3.59	2.41	20.1
- 77.0	5.92	1.66	14.7
- 108.2	6.14	1.9	43.8
- 126.8	3.27	2.36	12.9
- 156.9	2.18	0.671	17.2
- 199.3	2.85	1.44	14.4
- 246.8	3.40	0.750	10.1
- 289.8	2.38	1.33	20.3
- 333.9	3.06	0.984	22.5
- 370.1	2.67	0.841	41.6
- 451.1	0.757	0.537	13.40
- 497.0	0.504	0.362	3.37
URL-7- 132.00	2.52	1.47	6.60
- 134.10	2.69	1.82	7.77
- 135.40	1.91	1.81	5.48
- 137.275	1.84	1.95	4.11
- 138.40	2.64	2.05	4.77
- 139.70	2.94	2.23	2.56
- 140.66	3.07	2.46	6.87
- 143.20	3.86	3.25	4.07
- 144.00	3.38	2.60	5.00
- 145.70	3.38	3.04	6.74
- 147.50	3.67	2.10	6.92
- 147.70	4.51	3.79	9.59
- 148.15	4.80	2.93	7.33
- 150.20	1.84	1.48	3.56
- 155.80	1.67	1.46	2.65
- 157.40	2.11	1.63	2.43
- 158.25	1.62	2.72	1.92
- 159.20	3.20	2.74	3.42
- 161.70	2.88	2.47	4.95
- 161.80	2.02	1.46	4.09
- 163.74	3.84	2.54	14.5
- 166.55	3.52	2.16	15.0
- 170.70	4.22	2.88	14.7
- 174.35	2.65	1.09	17.0
- 177.60	3.53	1.22	24.7
- 181.00	2.18	1.02	22.7
- 181.80	2.52	1.32	20.2
- 184.70	2.07	1.44	17.1
- 188.00	2.16	0.884	12.3
- 192.90	1.62	0.957	11.9
- 197.80	1.88	0.806	13.2

CHAPTER V

CONCLUSIONS AND RECOMMENDATIONS

CONCLUSIONS AND RECOMMENDATIONS

A comprehensive rock property study, which is part of a generic research program on the physical properties of plutonic rocks, has been carried out on drill cores from the Whiteshell Nuclear Research Area under the auspices of the Canadian Nuclear Fuel Waste Management Program (NFWMP). The Whiteshell Nuclear Research Area consists of two sites (WN site and URL site) and is located within the boundaries of the Lac du Bonnet batholith which lies approximately 100 km northeast of Winnipeg, Manitoba. The results of this study provide some of the basic data for evaluating the radionuclide isolation capacity, vault stability and the effect of temperature on plutonic rocks.

The type of rock property data contained in this document is mineralogy, petrography, geochemistry, micromorphology (scanning electron microscope observations of microfractures in granites), mechanical properties, thermal properties, petrophysical properties (porosity, permeability, etc.), electrical properties, magnetic properties, and some geophysical data. The geological data provides a basis for the generic study, and the geophysical data can be used to determine the physical property distribution in a rock mass. This document contains 8 technical papers. The authors emphasis in two of the papers is on a summary and review of their work on rock samples from the batholith, two papers are compilations of all data obtained to date, three are on discussions and interpretation of data, and two are on geophysical results. This document contains one of the most comprehensive physical property studies of a specific rock mass.

The rock samples used in this study have been obtained from drill cores from boreholes on the two sites. The common phase of the batholith is pink porphyritic granite-granodiorite (McCrank, 1985). The major phases encountered in the boreholes are pink granite (surface), gray granite (subsurface) and green-gray granite which occurs between the pink and gray granites (Brown et al., 1985). There are no systematic mineralogical variations with depth and the average compositions of the pink and gray granites are similar (Robertson and Chernis, this volume).

The mean values of the physical properties and their ranges of the rock samples from the WNRE research area are compiled in Table 1. Most of the authors of the papers in this document have compared the physical property values

Table 1. Physical properties of Lac du Bonnet granites

Parameter	Pink Granite** URL(1), WN(1)		Green-Grey Granite		GREY** Granite I URL(2), (3)		GREY** Granite II WN(3)		Granite (All)		All Granites		Units	Reference
Major Mineral Composition														Robertson and Chemis (this volume)
Quartz											(432)	29.3 ± 6.(	(%)	
Plagioclase											(432)	36.3 ± 7.1		
Microcline											(432)	27.6 ± (0.6		
Accessories											(432)	6.3		
Major Oxides (wt%)														Percival and Hume (this volume)
SiO_2											(70)	72.3 ± 1.7	(%)	
Al_2O_3											(70)	14.4 ± 0.7		
K_2O											(70)	4.5 ± 0.8		
Major CIPW* (vol%)														Percival and Hume (this volume)
Q											(70)	31.8 ± 3.4	(%)	
OR											(70)	24.5 ± 5.8		
AB											(70)	30.9 ± 3.6		
AN											(70)	6.1 ± 1.9		
Mechanical Properties														Annor and Jackson (this volume)
Density											(579)	2.63 ± 0.05	(Mg/m^3)	
Uniaxial C**	(31)	200 ± 22	(34)	179 ± 27					(20)	(67 ± 13	(135)	190 ± 5	(MPa)	
Young's modulus	(31)	69.1 ± 5.3	(34)	61.8 ± 9.4					(20)	55.7 ± 4.9	((35)	65.3 ± 8.8	(GPa)	
Poisson's ratio	(31)	0.26 ± 0.04	(34)	0.28 ± 0.04					(20)	0.3 ± 0.007	(135)	0.27 ± 0.05		
Velocity (P-wave)											(156)	4.4 ± 0.9	(km/s)	
Uniaxial Tensile Strength	(39)	9.3 ± 1.3	(26)	10.4 ± 1.7					(14)	8.72 ± 1.98	(47)	9.56 ± 1.88	(MPa)	
Triaxial C**														
21°C											(13)	275 ± 19	(MPa)	
100°C											(8)	272 ± 8		
200°C											(10)	249 ± 22		
Triaxial Young's m.														
21°C											(13)	64.7 ± 8.5	(MPa)	
100°C											(8)	60.1 ± 10.3		
200°C											(10)	50.8 ± 8.8		
Rock Fracture Data C**	(91)	241							(174)	222	(265)	232	(MPa)	
Petrophysics*														Katsube and Hume (this volume)
Aperture (d)		0.13				0.41		0.18					(μm)	
Tortuosity (τ)		2.1				1.2		2.1						
Permeability (kg)		1.4 ± 1.0				8.6		0.8 ± 0.4					(μd)	
Porosity (Φ_E)		0.2% ± 0.09				0.2% ± 0.09		0.24 ± 0.09					(%)	
Apparent Tor. (τ_A)		4.0 ± 1				1.3 ± 0.2		3.0						
Thermophysics														
Conductivity											(403)	3.49 ± 0.35	W/m.K	
Diffusivity											(206)	1.32 ± 0.23	mm^2/s	
Specific Heat											(206)	1060 ± 200	J/Kg.K	
Thermal Elongation											(46)	1.4-7.0	($x10^{-6}$)	
Magnetics BMS**		(2+3/-2)x(10^3							(3.9+11.1/-4.9)x10^{-3}		(4.0 ± 0.2)x10^3		SI Units	Morris (1983) in Latham et al. (this volume)
Electrical Properties														Katsube and Hume (this volume)
Dielectric Constant											(30)	5.1 ± 0.5		
Resistivity (log)	(log)	(0.2-2.5)x10^9	(log)	(0.8-2)x10^9					(log)	4x10^3	(log)	4x10^3	(Ω•m)	
Resistivity (lab)	(10)	4.4x10^9	(10)	2.(2x10^9	(12)	1.28x10^9	(18)	3.7x10^9			(99)	3.66x10^9	(Ω•m)	
Surface Resistivity	(10)	2.7x10^9					(18)	1.92x10^9			(91)	1.87x10^9	(Ω•m)	
Pore Water Res.	(10)	19.1			(3)	38.3	(18)	19.1			(99)	(6.4	(Ω•m)	

*: Major C.I.P.W. normative mineral composition.
**: Compressive strength.
•: Results of data interpretation.
••: Bulk magnetic susceptibility.
(): Number inside brackets indicate number of samples
: Rock units
•••: Rock unit WN(2) is included in Gray Granite II for the mechanical properties, and in Pink Granite for the petrophysical and electrical properties.

for the rocks from the WNRE research area with the values for granitic rocks reported in the scientific literature. The values of bulk density, uniaxial compressive strength, Young's modulus and Poisson's ratio for the WNRE rocks is consistent with those reported in the literature (Annor and Jackson, this volume). The uniaxial tensile strength of the WNRE rocks is slightly lower than the reported values. The measured values for effective porosity and permeability for the WNRE samples are consistent with the reported values (Katsube and Hume, this volume - a). The interpreted values for porosity are also consistent, but the interpreted values for permeability are at the lower end of the reported values. It is the interpreted values that are listed in petrophysics section of Table 1. The formation factor values of the WNRE samples are generally lower than the reported values (Katsube and Hume, this volume - a). The thermal conductivity, thermal diffusivity and thermal elongation (coefficient of linear thermal elongation between 25-100°C) values for the WNRE samples are all consistent with the results reported in the scientific literature (Drury, this volume). The resistivity values for the rock sample from WNRE are consistent with the reported values, but the pore water resistivity values are generally larger than the reported values (Katsube and Hume, this volume - b). In general, the physical properties of the rocks from WNRE are consistent with those reported in the scientific literature for granitic rocks. The major conclusions and topics of this document are summarized below:

1. General Topics

The existence of an effect of alteration on many of the physical properties, the existence of a distinct relationship between certain physical properties and depth or degree of stress release, and the existence of a division in rock types based on physical properties are some of the significant scientific and technological findings that are common to more than one discipline in the rock property studies of rocks from the WNRE research area. These divisions in rock type are not necessarily geologically recognizable.

(1) Effect of Alteration

Alteration due to hydrothermal activities and weathering exists in these rocks. The degree of pinkish colour increases as alteration intensity increases.

An excellent relationship exists between the bulk magnetic susceptibility (BMS) and the alteration intensity (Latham et al., this volume). Annor and Jackson (this volume) have noted a difference between the uniaxial compressive strength and Young's modulus values for the pink and gray granites. Although stress release may play a significant role in the existence of these differences, it is possible that alteration is also a contributing factor. Katsube and Hume (this volume - a) have also observed a difference in the permeability behaviour with depth for altered and unaltered rock samples. These facts indicate that alteration has a significant effect on certain physical properties.

(2) Rock Type Differentiation Based on Physical Properties

A significant division of the properties of surface and subsurface rocks occurs at a depth of about 300 ± 50 m at both the WN and URL sites, and another subdivision of subsurface rocks occurs at about 600 ± 50 m at both sites. These divisions will be represented by Rock Units WN(1), WN(2), WN(3), URL(1), URL(2) and URL(3). Units WN(1) and URL(1) are the surface rocks, and WN(3) and URL(3) are the deeper of the subsurface units. These divisions have been pointed out by Katsube and Hume (this volume - a) as a result of analysing the petrophysical data for effective porosity, permeability, formation factor and some other petrophysical parameters. Based on the petrophysical data, units WN(1) and URL(1) appear similar, but the two subsurface units, WN(2), WN(3), URL(2) and URL(3), appear to be different. Therefore, WN(1), WN(2) and URL(1) are grouped as pink granite, URL(2) and URL(3) as gray granite I, and WN(3) as gray granite II. Drury (this volume) notes differences in thermal conductivity between granites from the WN and URL sites. This fact can be considered supportive of these rock type divisions.

Chernis and Robertson (this volume) note the existence of stress cracks in WN core samples collected at depths below approximately 450 m. A considerable difference in resistivity is noticed in the focused electrode logs at the URL site. This difference starts at a depth of about 100-400 m. According to the alteration intensity determined by the method proposed by Kamineni and Dugal (1982), altered rocks extend from the surface to a depth of about 100-300 m at the URL site, and to about 750 m at the WN site. These geological and geophysical observations appear to be related and can be considered to support the proposed physical property divisions of the rocks at WN and URL sites. These divisions must be taken into consideration when evaluating isolation capacity and vault stability in the Lac du Bonnet batholith.

(3) Effect of Depth and Stress Release

As depth increases the overburden stress on the rock increases. Therefore, there is a direct correlation between core sample depth and stress release effects. This stress release has various effects on the physical properties of rock samples measured in the laboratory. Porosity and permeability increase, and formation factor decreases with depth (Katsube and Hume, this volume - a). Chernis and Robertson (this volume) noted an increase of stress crack density with depth in WN samples. Compressive strength, compressive wave velocity and Young's modulus decrease and Poisson's ratio increases with an increase in depth (Annor and Jackson, this volume). This stress release has to be considered when estimating the true in situ values of many of the rock properties. A certain amount of knowledge about the characteristics of this stress release has been obtained and this has enabled the interpretation of most of the petrophysical data (Katsube and Hume, this volume - a). The interpreted results are listed in Table 1 for these parameters. Knowledge of this effect will be very useful when using the mechanical property values in vault design studies.

2. Geological Topics

(4) The average mineral composition by model analysis of all WN and URL samples (432) that have been examined by Chernis and Robertson (in press) is: quartz 29.3 ± 6.1 (%), plagioclase 36.8 ± 7.1 (%), microcline 27.6 ± 10.4 (%) and 6.3% of accessories. The average composition of these samples is monzogranite (Robertson and Chernis, this volume).

(5) Grain boundary cracks preferentially occur around quartz grains and account for 50% of the total natural porosity of the samples. Stress cracks due to stress release are present in core samples collected from depths below approximately 450 m vertical depth at WN, and their density increases with depth. They are developed at grain boundaries (particularly around quartz) and within plagioclase and microcline feldspars. Therefore, rock properties measured in the laboratory under ambient conditions are not necessarily representative for the rock mass in situ. The number and size of natural microcracks in candidate plutons may be kept to a minimum by selecting quartz-poor lithologies. The relationship between grain size and microcracks has not been fully investigated,

but preliminary SEM observations indicate that fine-grained rocks, despite having more grain boundaries, may possess fewer microcracks and may make more favourable repository sites (Chernis and Robertson, this volume).

(6) The C.I.P.W. normative mineral composition shows that the samples used in this study are predominantly granite with a few granodiorites (from Percival and Hume, this volume).

3. Mechanical Properties

Eight different types of mechanical tests and measurements have been carried out: density measurements, uniaxial compressive strength, Young's modulus, Poisson's ratio, velocity (P-wave) and tensile strength tests, triaxial compressive strength tests at 3 different temperatures, and triaxial Young's modulus measurements at 3 different temperatures.

(7) The unconfined mechanical behaviour of the Lac du Bonnet granitic samples show trends of decreasing compressive strength, compressive wave velocity and Young's modulus and increasing Poisson's ratio with increasing depth. While this trend can be attributed to changes in rock alteration with increasing depth, it also suggests some significant effects of stress relaxation of the core samples. In-situ stress release at vault depth could result in slabbing of the walls (Annor and Jackson, this volume).

(8) The Lac du Bonnet granitic samples can be classified as a high strength to very high strength rock, with a medium modulus ratio. The strength, deformation and acoustic velocity values of the Lac du Bonnet rock compare favourably with literature data on granitic rocks with similar mineralogical compositions (Annor and Jackson, this volume).

(9) Temperature levels of up to 100°C do not have any pronounced effects on the strength and deformational properties of Lac du Bonnet granitic samples. However, a significant reduction in these properties occurs at 200°C (Annor and Jackson, this volume).

(10) Studies should be carried out to establish the effects of scale on the mechanical behaviour of both intact and fractured rock samples. The mechanical behaviour of jointed samples as a function of temperature and the effects of stress and temperature paths on the mechanical properties should be investigated (Annor and Jackson, this volume).

4. Petrophysics

(11) Although the porosity of the Lac du Bonnet granites is much smaller than that of sedimentary rocks (usually larger than 5%), the formation factor versus porosity relationship suggests that a much larger portion of the porosity in the granites is in connecting pores compared to sedimentary rocks. This indicates that smaller porosities do not necessarily imply smaller radionuclide transport rates (from Katsube and Hume, this volume - a).

(12) The grey granites I and II are found in the URL and WN sites, respectively, and are very different in petrophysical characteristics. The rock units WN(1), URL(1), WN(2) and WN(3), that are grouped as pink granites and gray granite II can be characterized as having small apertures, large tortuosities and low permeabilities. The rock units URL(2) and URL(3), that are grouped as grey granites I, have the opposite characteristics. This implies that the grey granite at the URL site has the most unfavourable radionuclide transport characteristics (Katsube and Hume, this volume - a).

(13) Aperture, tortuosity, equivalent rock mass permeability, effective porosity and apparent tortuosity are the five petrophysical parameters that control the radionuclide transport (advection and diffusion) rates (velocity and flux) in granites. Most of these parameters are sensitive to stress release. A method has been developed to eliminate this effect and only the results without stress release effects are listed in Table I. However, in some cases there is more than one possible interpretation of the data. This causes serious uncertainties in the estimate of radionuclide transport rates. Further work must be carried out to establish the effect of stress release on these parameters, and on the variation of these parameters with variation in rock type (Katsube and Hume, this volume - a).

5. Thermal Properties

(14) The thermal conductivity and thermal diffusivity of quartz is substantially higher than those of other common minerals in granitic rocks. However, a correlation between these parameters and the quartz content does not necessarily exist. In addition, a conductivity difference exists between the granites from the WN and URL sites, although the quartz content is very similar. The type curves for thermal conductivity as a function of temperature for the Lac du Bonnet granites differ substantially from those for quartz. These facts suggest that factors other than quartz minerals contribute to the thermal properties of granites. It is thought that rock texture and way in which quartz is distributed in the rock are factors to be considered. It is important to pursue this subject in the future (Drury, this volume).

(15) The mean coefficient of linear thermal elongation at 100°C is less than the values reported in the literature. This would be a favourable conclusion with regard to rock mass stability for the vault. However, an empirical relationship between thermal elongation and high temperature diffusivity parameters and spalling tendency, indicates that the granite at the WN borehole sites would have a low thermomechanical stability (Drury, this volume).

6. Geophysical Properties

(16) Background bulk magnetic susceptibility (BMS) measurements have proven to be an excellent method of identifying altered zones in the rock, particularly the alteration associated with water carrying pathways. Variation in BMS in the Lac du Bonnet granite is due primarily to the alteration of primary magnetite. A quantitative estimate of the degree and percentage of alteration is possible using this method. Identification of mafic-rich zones is also possible by this method (from Latham et al., this volume).

(17) Results of analysis of the focused electrode log indicates that background resistivities determined by this tool can be used to identify three distinctly different resistivity zones which correspond to the pink granite, green-grey granite and grey granite lithologies. A high resistivity zone (2×10^4-

2.5×10^5 ohm.m), an intermediate resistivity zone (8×10^4-2×10^4 ohm.m) and a low resistivity zone (4×10^3 ohm.m) are the three zones which correspond to the three lithologies. There is a contrast of about a factor of 10 between the resistivities of the pink and grey granites. Laboratory and in situ resistivities show slight differences that are thought to be due to stress release and pore surface conduction effects. These resistivity levels indicate that all micropores and microcracks are continuous throughout the rock mass (Katsube and Hume, this volume - b).

REFERENCES

Annor, A. and Jackson, R. (in prep.). Mechanical, thermomechanical and joint properties of rock samples from the Lac du Bonnet batholith, Manitoba. In The Canadian Nuclear Fuel Waste Management Program Concept Assessment Document: Geotechnical Studies at the Whiteshell Research Area, AECL 8410-3.

Brown, A., Dugal, J.J.B., Everitt, R.A., Kamineni, D.C., Lau, J.S.O. and McEwen, J.H. 1985. Advances in geology at the URL site (RA-3). Atomic Energy of Canada Limited Technical Record, TR-299, p. 253-264.

Chernis, P.J. and Robertson, P.B. (in prep.). Natural and stress-relief microcracks in the Lac du Bonnet granite. In The Canadian Nuclear Fuel Waste Management Program Concept Assessment Document: Geotechnical Studies at the Whiteshell Research Area, AECL 8410-3.

Drury, M. (in prep.). Thermophysical properties of rock samples from WNRE and URL boreholes. In The Canadian Nuclear Fuel Waste Management Program Concept Assessment Document: Geotechnical Studies at the Whiteshell Research Area, AECL 8410-3.

Kamineni, D.C. and Dugal, J.J.B. 1982. A study of rock alteration in the Eye-Dashwa Lakes pluton, Atikokan, northwestern Ontario, Canada. Chemical Geology, v. 36, p. 35-57.

Katsube, T.J. and Hume, J.P. (in prep. - a). Pore structure characteristics of granitic rock samples from the Whiteshell research area. In The Canadian Nuclear Fuel Waste Management Program Concept Assessment Document: Geotechnical Studies at the Whiteshell Research Area, AECL 8410-3.

Katsube, T.J. and Hume, J.P. (in prep. - b). Electrical properties of the granitic rocks in the Lac du Bonnet batholith. In The Canadian Nuclear Fuel Waste Management Program Concept Assessment Document: Geotechnical Studies at the Whiteshell Research Area, AECL 8410-3.

Latham, A.G., Morris, W.A. and Lapointe, P. (in prep.). Magnetic properties of Lac du Bonnet (URL) borecores, Manitoba. In The Canadian Nuclear Fuel Waste Management Program Concept Assessment Document: Geotechnical Studies at the Whiteshell Research Area, AECL 8410-3.

McCrank, G.F.D. 1985. A geological survey of the Lac du Bonnet batholith, Manitoba. Atomic Energy of Canada Limited, Report AECL-7816, 63 p.

Percival, J.B. and Hume, J.P. (in prep.). Geochemical analysis of standard core samples from the Whiteshell research area. In The Canadian Nuclear Fuel Waste Management Program concept Assessment Document: Geotechnical Studies at the Whiteshell Research ARea, AECL 8410-3.

Robertson, P.B. and Chernis, P.J. (in prep.). General geology of the Lac du Bonnet batholith and petrography of core samples from the WNRE research area. In The Canadian Nuclear Fuel Waste Management Program Concept Assessment Document: Geotechnical Studies at the Whiteshell Research Area, AECL 8410-3.